Performance and Stability of Electron-Accepting Boron Subphthalocyanines in Organic Photovoltaics

by

David Scott Josey

A thesis submitted in conformity with the requirements
for the degree of Doctor of Philosophy

Department of Chemical Engineering and Applied Chemistry
University of Toronto

Performance and Stability of Electron-Accepting Boron Subphthalocyanines in Organic Photovoltaics

David Scott Josey

Doctor of Philosophy

Chemical Engineering and Applied Chemistry
University of Toronto

2019

Abstract

Boron subphthalocyanine (BsubPc) is a promising organic material with favourable optical and electronic properties for application in organic photovoltaics (OPVs). These properties can be tuned by chemically modifying the peripheral and axial substituents of the BsubPc. In this thesis, the influence of different substituents on the OPV performance of BsubPc as an electron acceptor was assessed using a standardized OPV configuration. Substitution of the BsubPc peripheral hydrogens with chlorines is used to adjust the voltage output of OPVs, but the ability to tune the voltage output using pure BsubPc is quantized based on the number of peripheral positions. Mixtures of compounds with different degrees of peripheral chlorination were found to behave as electronic alloys, providing infinite degrees of material tunability. The effects of axial substitution with phenyl and phenoxy groups were also explored and showed promising time-zero OPV performances. Phenoxy-BsubPcs provided a unique platform to study halogen bonding within OPVs, which were observed to influence molecular orientation and significantly impact OPV performance. The stability of the most promising BsubPcs was assessed and compared in OPVs. Outdoor testing revealed that peripheral chlorination and the addition of benzene rings (boron subnaphthalocyanine) have minimal impact on stability, but axial phenylation and phenoxylation dramatically reduce stability. Given the freedom to peripherally halogenate a BsubPc without

impacting stability, these conclusions lay the foundation for the development of new BsubPcs and BsubPc alloys. Through strategic halogen placement, energy levels and molecular orientation can be controlled simultaneously to achieve the ideal materials for OPVs.

Acknowledgments

First, I would like to express my sincere gratitude to Professor Tim Bender for inviting me into his group. His supervision, timely observations, and encouragement to pursue my ideas are what made this research possible. I am grateful for all his assistance navigating unexpected device results and equipment setbacks, and patience whenever my coding projects took longer than anticipated. His consistent excitement around new device data was a great source of motivation. Professor Bender, thank you for making my Ph.D. such an enjoyable experience.

I am grateful to my original device engineering mentors: Jeffrey, Trevor, and Benoit, for teaching me everything I know about being a *voidsmith*. Their commiseration and assistance were invaluable every time I discovered something else that could break in a vacuum chamber. To our next *voidsmith* Ph.D. student (-to-be), Adam, thank you for quickly absorbing all information thrown you and for assuming my vacuum chamber responsibilities, allowing me to focus on completing this thesis. To my labmates who put up with me for more than half of my time in the Bender lab: Katie, Hasan, Anjuli, Jeremy, Jess, Steph, Aleksa, Devon, Esmeralda, Cynthia, Richard, and Trevor, and to all other past and present Benderites, thank you for your encouragement; for making all the materials I needed; for helping troubleshoot broken equipment; for running HPLC samples time after time; for brainstorming figures and critiquing my colour choices; for always being available to discuss research ideas, results, or TV shows; for exercising, playing squash, and running with me; for pushing me to participate in social activities; for teaching me new games/board games; for all the entertaining desk pranks; for being great friends; and for contributing to an all-around wonderful graduate experience.

To my committee members, Professor Dwight Seferos and Professor Zheng-Hong Lu, thank you for your constructive criticisms, encouragement, and for keeping me pointed in the right direction.

I would like to thank my parents, Pauline and Ronnie Josey, my sister, Dr. Maria Josey, and my Nana, Dona Armstrong, for all their love and encouragement as I buried myself in studies over the years. Mom, thank you for reading and editing this entire thesis. Dad, thank you for keeping me up to date on all the sports news that I was too busy to follow. Maria, thank you for demonstrating how to get a Ph.D. faster than your older brother. I am also grateful to my parents-in-law, Ann and Quoc Hau, and siblings-in-law, Annita and Benjamin Horsley, for dealing with my constant

traveling back and forth to Oshawa, for allowing me to eat all your food, and for supporting my research by providing quiet spaces to work and welcome distractions whenever I needed them.

Finally, I would not be the researcher or person I am today without the constant love and support of my incredible wife, Dianna. Her willingness to listen to me explain my research, sharp eye for graphic design, ability to recognize when I should keep working or take a break, delicious home-cooked meals, encouragements through my disappointments, and celebrating with me in my successes, were the support I needed to stay productive and balanced throughout my degree. Dianna, I love you, I am so thankful God brought us together, and I am excited to see what He has planned for us next.

Table of Contents

List of Tables

List of Figures

List of Abbreviations

246F_3PhO-BsubPc	2,4,6-trifluorophenoxy-boron subphthalocyanine
35F_2PhO-BsubPc	3,5-difluorophenoxy-boron subphthalocyanine
4-FPh-BsubPc	4-fluorophenyl-boron subphthalocyanine
4-MePh-BsubPc	4-tolyl-boron subphthalocyanine
A	area
AM1.5	air mass coefficient of 1.5
aryl-BsubPc	aryl-boron subphthalocyanine
α-6T	alpha-sexithiophene
α-NPD	N,N'-Bis(naphthalen-1-yl)-N,N'-bis(phenyl)-2,2'-dimethylbenzidine
BCP	bathocuproine
BHJ	bulk heterojunction
BSTV	(E)-Bis-1,2-(5,5''-Dimethyl-(2,2':3',2''-terthiophene)vinylene
BsubNc	boron subnaphthalocyanine
BsubPc	boron subphthalocyanine
C_{60}	C_{60} fullerene
C_{70}	C_{70} fullerene
CdTe	cadmium telluride
CIGS	copper indium gallium diselenide
Cl-AlPc	chloro-aluminum phthalocyanine
Cl-BsubNc	chloro-boron subnaphthalocyanine
Cl-BsubPc	chloro-boron subphthalocyanine
Cl-$^{\beta}Cl_2$BsubPc	chloro-beta-dichloro boron subphthalocyanine
Cl-$^{\beta}Cl_{2n}$BsubPc	chloro-beta-$(chloro)_{2n}$ boron subphthalocyanine
Cl-$^{\beta}Cl_4$BsubPc	chloro-beta-tetrachloro boron subphthalocyanine
Cl-$^{\beta}Cl_6$BsubPc	chloro-beta-hexachloro boron subphthalocyanine
Cl-$^{\beta}Cl_6{}^{\alpha}Cl_2$BsubPc	chloro-beta-hexachloro alpha-dichloro boron subphthalocyanine
Cl-$^{\beta}Cl_6{}^{\alpha}Cl_{2n}$BsubPc	chloro-beta-hexachloro alpha-$(chloro)_{2n}$ boron subphthalocyanine
Cl-$^{\beta}Cl_6{}^{\alpha}Cl_4$BsubPc	chloro-beta-hexachloro alpha-tetrachloro boron subphthalocyanine
Cl-Cl_{12}BsubPc	chloro-dodecachloro boron subphthalocyanine
Cl-Cl_4BsubPc	chloro-tetrachloro boron subphthalocyanine
Cl-Cl_6BsubPc	chloro-hexachloro boron subphthalocyanine
Cl-Cl_nBsubNc	chloro-$(chloro)_n$ boron subnaphthalocyanine
Cl-F_{12}BsubPc	chloro-dodecafluoro boron subphthalocyanine
Cl-F_3BsubPc	chloro-trifluoro boron subphthalocyanine
Cl-F_6BsubPc	chloro-hexafluoro boron subphthalocyanine
Cl_nBsubNc	$(chloro)_n$ boron subnaphthalocyanine
CuPc	copper phthalocyanine
D	diffusivity
DCB	dichlorobenzene
DIP	diindenoperylene

DNTT	dinaphthothienothiophene
E_F	Fermi energy level
EJ	exajoule (1 x 10^{18} joule)
EL	electroluminescence
ELI	electroluminescence imaging
EQE	external quantum efficiency
F-$(CN)_3$BsubPc	fluoro-tricyano boron subphthalocyanine
F-F_{12}BsubPc	fluoro-dodecafluoro boron subphthalocyanine
F_4ZnPc	tetrafluoro zinc phthalocyanine
F_5-BsubPc	pentafluorophenoxy-boron subphthalocyanine
F_5-Cl_nBsubPc	pentafluorophenoxy-(chloro)$_n$ boron subphthalocyanine
FF	fill factor
F_nPhO-BsubPc	(fluoro)$_n$ phenoxy-boron subphthalocyanine
GaAs	gallium arsenide
HOMO	highest occupied molecular orbital
HPLC	high-performance liquid chromatography
I	current
IE	ionization energy
IR	infrared
ISOS	international summit on organic photovoltaic stability
ISOS-O1	basic-level protocols for outdoor testing
ISOS-O2	intermediate-level protocols for outdoor testing
ISOS-O3	advanced-level protocols for outdoor testing
ITO	indium tin oxide
J	current-density
J_M	current-density at the maximum power point
J_{SC}	short-circuit current density
LED	light-emitting diode
LUMO	lowest unoccupied molecular orbital
m-BrPhO-BsubPc	meta-bromophenoxy-BsubPc
m-ClPhO-BsubPc	meta-chlorophenoxy-BsubPc
m-IPhO-BsubPc	meta-iodophenoxy-BsubPc
m-XPhO-BsubPc	meta-halogenated phenoxy-BsubPc
MoO_X	molybdenum oxide
MPC	metal phthalocyanine
MPP	maximum power point
OLED	organic light-emitting diode
OPV	organic photovoltaic
P	power
P3HT	poly(3-hexylthiophene-2,5-dily)
PbPc	lead phthalocyanine

PbS	lead sulphide
Pc	phthalocyanine
PCE	power conversion efficiency
PEDOT:PSS	poly(3,4-ethylenedioxythiophene) polystyrene sulfonate
Ph-BsubPc	phenyl-boron subphthalocyanine
PHJ	planar heterojunction
PhO-BsubPc	phenoxy-boron subphthalocyanine
PhO-Cl_nBsubNc	phenoxy-$(chloro)_n$ boron subphthalocyanine
PL	photoluminescence
PLI	photoluminescence imaging
P_M	maximum power
PV	photovoltaic
Q	insolation
R_a	axial substituent
R_{MPP}	resistance at the maximum power point
R_p	peripheral substituent
SD	standard deviation
SiPc	silicon phthalocyanine
T_0	time zero
T_{50}	operation time at which the device reaches 50% of the initial measurement
T_{80}	operation time at which the device reaches 80% of the initial measurement
Tc	tetracene
μ-oxo-$(BsubPc)_2$	oxygen-bridged dimer of boron subphthalocyanine
UPS	ultraviolet photoelectron spectroscopy
UV	ultraviolet
V	voltage
VIS	visible
V_M	voltage at the maximum power point
V_{OC}	open-circuit voltage
WF	work function
ZnPc	zinc phthalocyanine
ZrAcac	zirconium acetylacetonate

Chapter 1
Introduction

1.1 Photovoltaics (PVs)

Within the next hour, and every hour after that, enough solar energy will reach the earth (624.7 EJ) to meet global energy demands for an entire year (571.3 EJ).[1-2] Capturing just 0.02% of that energy would eliminate the need for fossil fuels and provide endless energy supply for all future generations. Photovoltaic (PV) solar panels could be the answer to the large-scale harnessing of solar energy and could power electrical grids worldwide.[3] PV solar panels produce electrical power whenever the sun is shining, release zero greenhouse gasses during operation, have no moving parts, are noiseless, and require no cooling water. Other advantages of solar panels include the scalability, minimal safety concerns, and the ability to locate PV solar panels almost anywhere. While the intermittent nature of solar power generation does present challenges, PV solar panels have the potential to produce electricity at extremely low-costs.[4] Lower electricity costs will motivate and accelerate the development of energy storage technologies, eventually solving the intermittency challenges.

PVs rely on semiconducting materials to convert light into electricity.[5] The definition of a material as a conductor, semiconductor, or insulator depends on the distribution of electrons in that material. Electrons will only adopt specific, discrete energies; for each energy, a mathematical function called an "orbital" describes a region of space that is most probably occupied by that electron.[6] Electrons that occupy higher energy orbitals are less tightly bound to the material. In some materials, there is a gap (called a "bandgap") between the highest energy orbital normally occupied by an electron and the lowest energy orbital normally unoccupied by an electron.[7] The size (energy difference) of this gap defines whether a material is a conductor, semiconductor, or insulator: materials without a gap are conductors, materials with a small gap are semiconductors, and materials with a large gap are insulators (**Figure 1.1**).

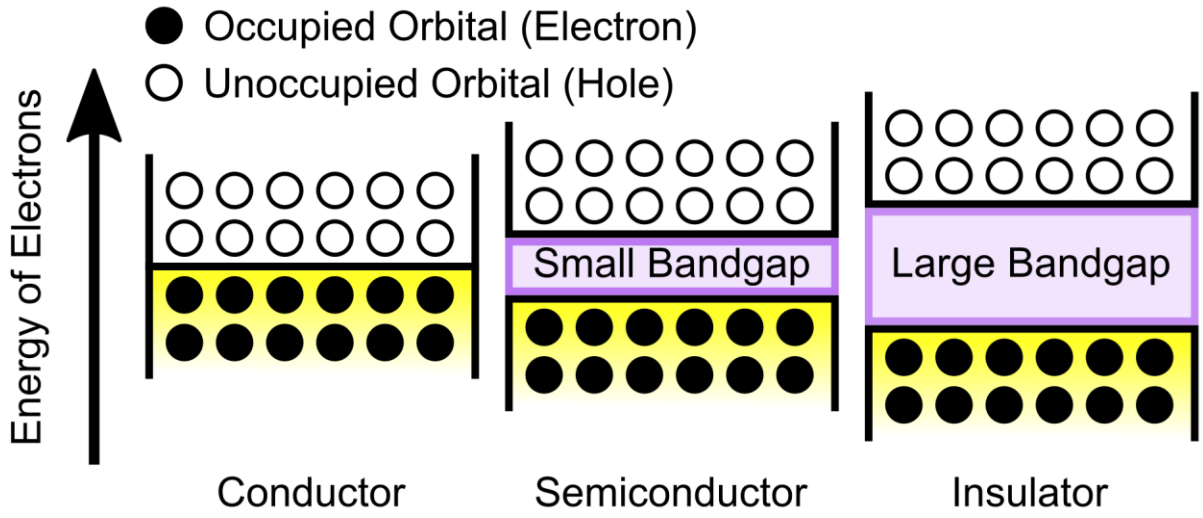

Figure 1.1. Approximate energy of the bandgap between the highest normally occupied and lowest normally unoccupied orbitals of a conductor, semiconductor, and insulator.

Semiconductors and insulators can only absorb photons that have energies larger than their bandgap. When a semiconductor or insulator absorbs a sufficiently energetic photon, the energy of the photon transfers to an electron. The increase in energy promotes the electron across the bandgap to a higher energy orbital, leaving behind a hole (empty state) in the lower energy orbital it used to occupy. The electron and hole are both considered charge carriers; the electron has a negative charge, and the hole represents a corresponding positive charge. Directly extracting these charge carriers from the material would result in direct current electricity with a voltage proportional to the energy difference between the electron and hole, and a current proportional to the number of charge carriers extracted.

Sunlight consists of many photons, each with a discrete energy. Semiconductors generally have bandgaps that correspond to the energy of light in the visible spectrum (1.8 – 3.1 eV). Given that much of the energy in sunlight is visible light, semiconductors are an obvious choice for harvesting solar energy. Solar PV panels traditionally employ crystalline silicon as the semiconducting material, the most common material found in commercial solar panels.[8] Newer generations use other semiconducting materials such as amorphous silicon, cadmium telluride (CdTe), copper indium gallium diselenide (CIGS), gallium arsenide (GaAs), lead sulphide (PbS), perovskite, and

organic.[8-11] Each semiconductor possesses unique benefits, and the current PV applications of these semiconductors range between pure research to already commercialized.

1.2 Organic Photovoltaics (OPVs)

1.2.1 Organic Semiconductors

Organic photovoltaics (OPVs) are a class of PV technology that employs organic molecules as semiconductors. Molecules are groupings of atoms bonded together by sharing electrons. Organic molecules are broadly defined as molecules that contain carbon atoms. The bonding of atoms within a molecule results in an overlap between some of the individual atomic orbital, creating a shared set of molecular orbitals.[12] The energy of electrons that occupy each molecular orbital depends on atomic composition and molecular structure. The energy of the highest occupied molecular orbital (HOMO), the lowest unoccupied molecular orbital (LUMO), and the corresponding bandgap (LUMO – HOMO = bandgap) are important parameters for the application of organic molecules in OPVs.[7] Most organic molecules are electronic insulators due to a large energy bandgap. However, the bandgap of organic molecules can be reduced with conjugation, a term that describes linking double bonds. In general, higher degrees of conjugation (linking more double bonds) result in smaller bandgaps. Enough conjugation results in organic molecules with semiconducting properties.[13]

A major difference between organic and inorganic (e.g. Si, CdTe, GaAs) semiconductors involves the overlap of atomic orbitals. In layers of inorganic semiconductors, atomic orbitals overlap throughout the layer. The widespread orbital overlap results in bands that provide charge carriers with high mobility throughout the layer (band transport).[14] In organic semiconductors, the overlap between orbitals is more localized within each molecule. Charge carriers must hop between these localized molecules (hopping transport) to move through a layer.[15] Another major difference between organic and inorganic semiconductors is the nature of electron excitation across the bandgap. The HOMO and LUMO of some inorganic semiconductors (e.g. Si) are misaligned (indirect bandgap), requiring the cooperation of atomic vibrations (phonon) and photons to excite an electron across the bandgap. Organic semiconductors have direct bandgaps, facilitating excitation across the bandgap by eliminating the necessity for cooperative phonons. Increasing the

temperature improves charge carrier mobility in organic semiconductors due to a corresponding increase in vibrational energy that can help charge carriers overcome these energy barriers.[16] A voltage applied across a layer will tilt the energy bands, encouraging charge carriers to flow in one direction.

When an organic semiconductor absorbs a photon, the energy from the photon can promote an electron across the bandgap (excitation, **Figure 1.2a**). However, this electron remains coulombically bound to the positively charged hole left behind in the HOMO. This electron/hole pairing is called an exciton. An exciton can transfer from molecule to molecule, travelling through the semiconductor layer (**Figure 1.2b**). Eventually, the electron will fall back to the HOMO, recombining with the hole and shedding the excess energy as heat or by emitting a slightly less energetic photon (**Figure 1.2c**).

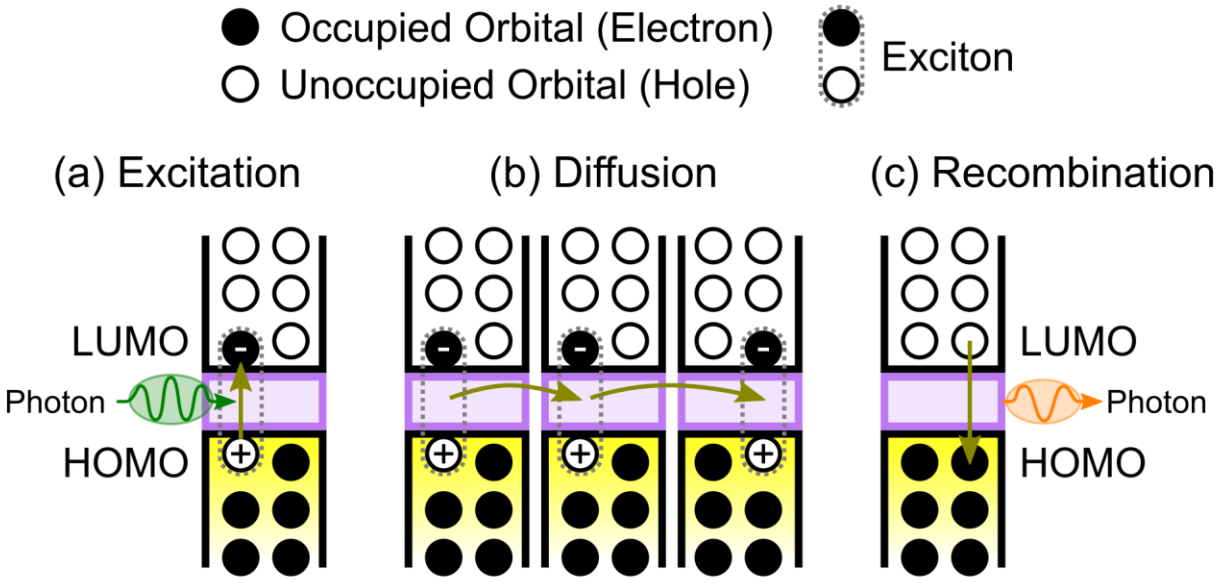

Figure 1.2. (a) Excitation of an electron across the bandgap through the absorption of a photon, forming an exciton. (b) Diffusion of an exciton from molecule to molecule. (c) Recombination of the exciton and the corresponding emission of a less energetic photon.

1.2.2 Operating Principles

OPVs are designed to capture the energy in excitons before recombination by using organic semiconductors with different affinities for electrons (**Figure 1.3**). An interface is created between these different semiconductors so that an exciton diffusing through one semiconductor layer may encounter an interface/heterojunction with a second semiconductor layer (**Figure 1.3,** step 2). If the second semiconductor has a stronger electron affinity than the first semiconductor, the electron may be pulled into the second semiconductor layer while remaining coulombically bound to the hole in the first semiconductor (**Figure 1.3,** step 3).[17] Due to their roles in this process, the first and second semiconductor layers are called the electron donor (D) and the electron acceptor (A), respectively. The presence of an exciton on an electron donor or acceptor molecule is denoted as D* or A*, respectively. The coulombically bound charge transfer state is denoted $[D^+A^-]$. From this charge transfer state the electron and hole may then either recombine or achieve complete separation (D^+ and A^-, **Figure 1.3,** step 3).[18] Dissociating the exciton into a free hole and free electron in this way preserves an energy difference between them (energy of acceptor LUMO – energy of donor HOMO). The holes and electrons are then free to travel through their respective semiconducting layers (**Figure 1.3,** step 4). In OPVs, conductors are located on both sides of the semiconductors as electrodes to collect these free charge carriers as electricity (**Figure 1.3,** step 4). The rate that charge carriers reach the electrodes is proportional to the direct electrical current generated by the OPV, with a voltage proportional to the energy difference between the acceptor LUMO and donor HOMO.[19]

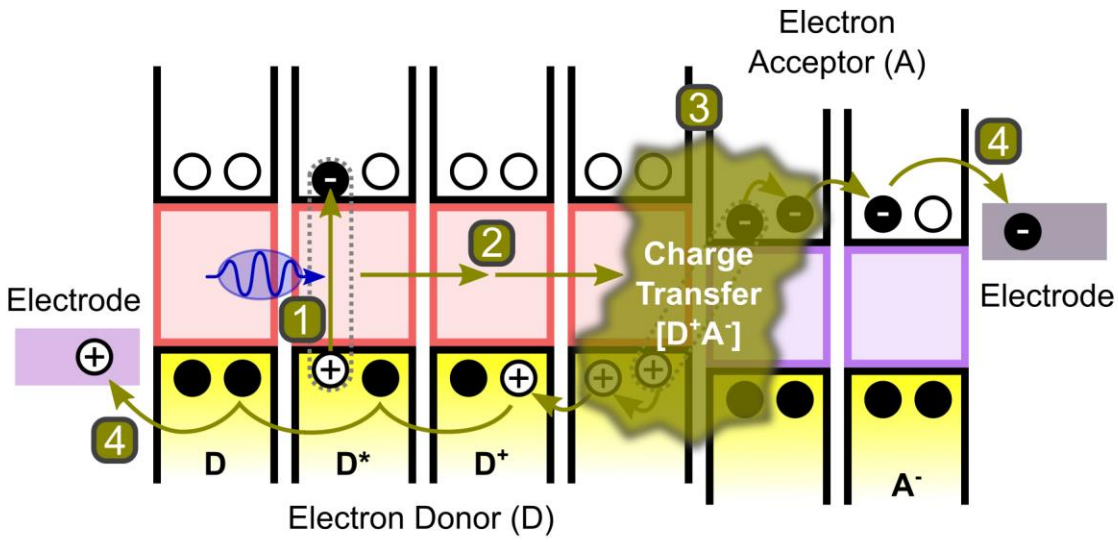

Figure 1.3. Operating principles of an OPV, combining an electron donor (D) with an electron acceptor (A). Additional occupied and unoccupied orbitals omitted for clarity. Step 1: Absorption and excitation, forming an exciton (D* or A*). Step 2: Exciton diffusion to an electron donor / electron acceptor heterojunction. Step 3: Charge transfer ($[D^+A^-]$) and exciton dissociation (see **Figure 1.4**). Step 4: Charge carrier (D^+ and A^-) migration to electrodes, where they are collected as electricity.

The mechanisms involved in the exciton charge transfer and ensuing exciton dissociation at the electron donor / electron acceptor heterojunction (**Figure 1.3**, Step 3) have been explained in detail by Savoie et al.[20] **Figure 1.4** outlines the combined energy of a donor and acceptor molecule (D + A) through the various states of photoexcitation (D* + A), charge transfer ($[D^+A^-]$), and free charge carriers ($D^+ + A^-$) recombine to reach a lower energy state (D or A).

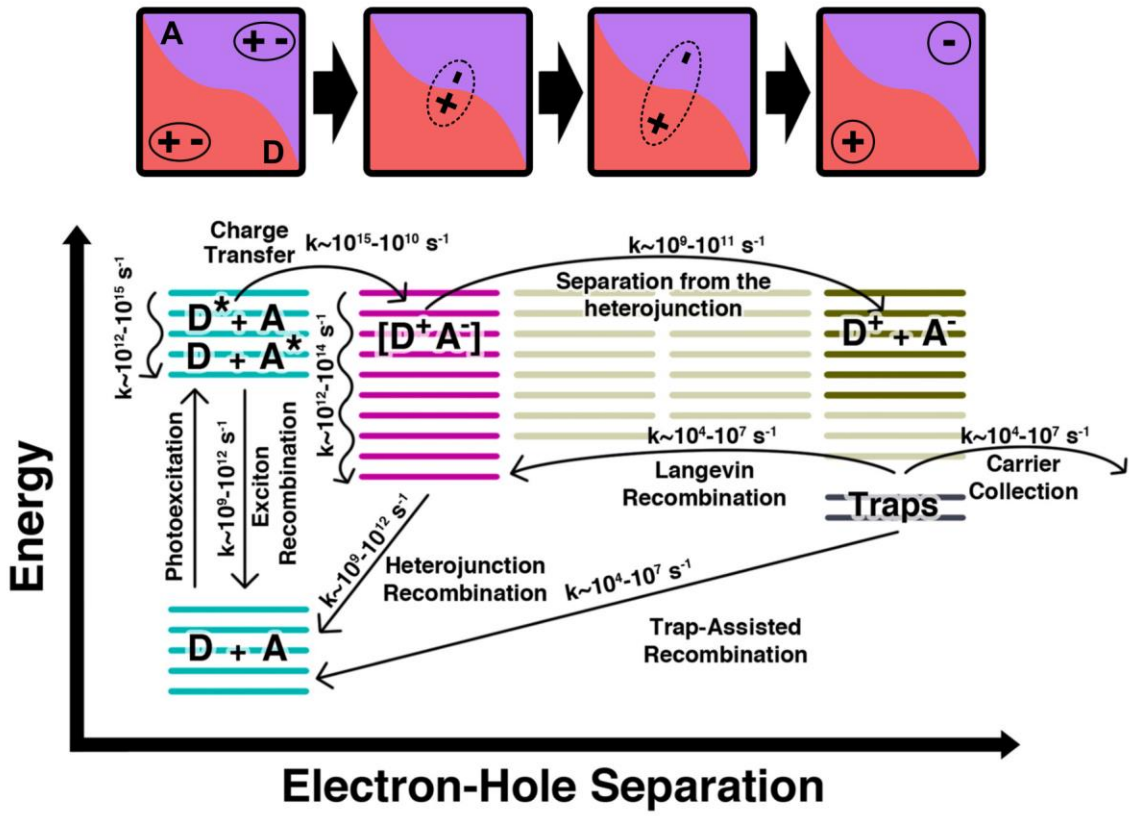

Figure 1.4. Outline of the recombination and charge generation processes of an organic electron donor / electron acceptor heterojunction. Energy levels represent the combined energy of a donor (D) molecule and an acceptor (A) molecule at various states. D* and A* depict photoexcited electron donor and electron acceptor, respectively. $[D^+A^-]$ depicts a charge transfer state. D+ and A- depict a free hole residing on an electron donor and a free electron residing on an electron acceptor, respectively. Representative rates (k) of each process are included. Triplets are omitted for clarity. Adapted with permission from Savoie et al.[20] Copyright 2014 American Chemical Society.

When an exciton (D* + A) diffuses to a heterojunction between an electron donor and an electron acceptor, lower-energy states can be accessed through exciton recombination or the transfer an electron from the donor to acceptor. An electron transfer results in a charge transfer state ($[D^+A^-]$) that can either undergo heterojunction recombination or spatially separate into free charge carriers. Once separated, free charge carriers can be collected at the electrode as electricity, unless they encounter traps or recombine at the heterojunction. The relative rate at which each process occurs

dictates the efficiency of charge generation within an OPV, where higher efficiencies result from higher separation rates and lower recombination rates.

A simple OPV structure consists of four, thin (<100 nm) layers: one electron donor layer and one electron acceptor layer, sandwiched between two electrodes (**Figure 1.5a**).[21] An even simpler structure with only one organic layer is called a Schottky diode, which still functions as an OPV but with much lower performance. Together, the donor and acceptor layers are commonly known as the photoactive region due to their role in absorbing and converting photons into charge carriers. In more advanced OPV designs, additional layers of organic semiconductors are applied between the electrodes and photoactive region to assist with charge carrier extraction and to contain excitons within the photoactive region (**Figure 1.5b**).[22-25]

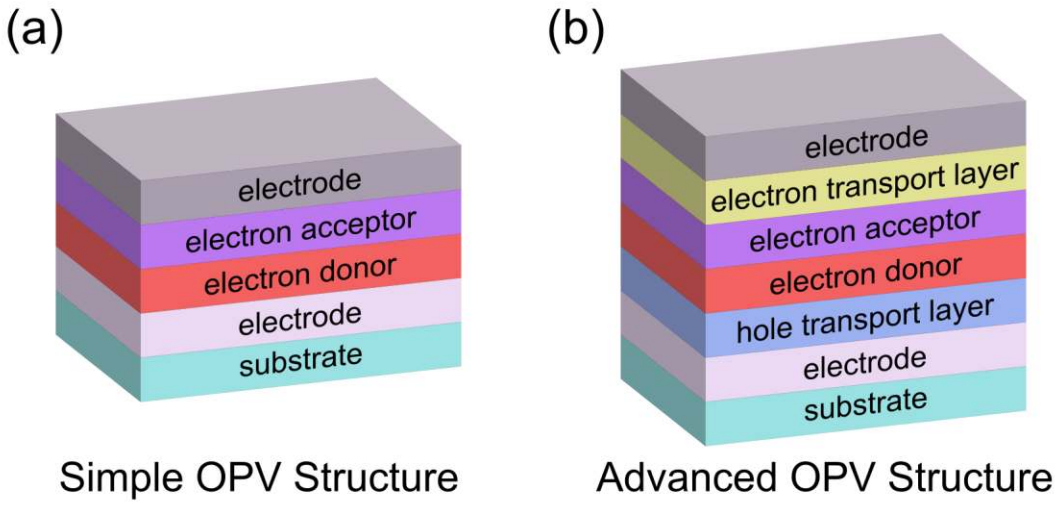

Figure 1.5. (a) Simple and (b) advanced combinations of layers that form an OPV. Layer thicknesses are not shown to scale.

1.2.3 Fabrication Techniques

The OPV multilayer stack can be fabricated using two types of techniques: solution casting and vacuum deposition. Solution casting requires that the material is soluble enough to be dissolved in a solvent. The solution is cast onto a surface and then dried to remove the solvent, depositing a thin layer of the material on the surface (**Figure 1.6a**). There are many known techniques to perform the casting and spreading of the solution onto a surface, including spin coating, blade

coating, slot die coating, spray coating, flexographic printing, gravure printing, screen printing, and inkjet printing. Vacuum deposition requires that the organic materials are small enough to sublime (undergo a direct phase transition from solid to gas). The material is placed in a crucible, then heated to sublimation in vacuum. The sublimed material then deposits (desublimes) onto any cooler surface placed above the crucible, creating a thin layer of the material on that surface (**Figure 1.6b**). Either or both techniques can be applied sequentially to build the multilayer stack of an OPV. However, caution must be exercised if solution-casting onto other layers, as the underlying layers may be re-dissolved while casting the next solution.[26-27]

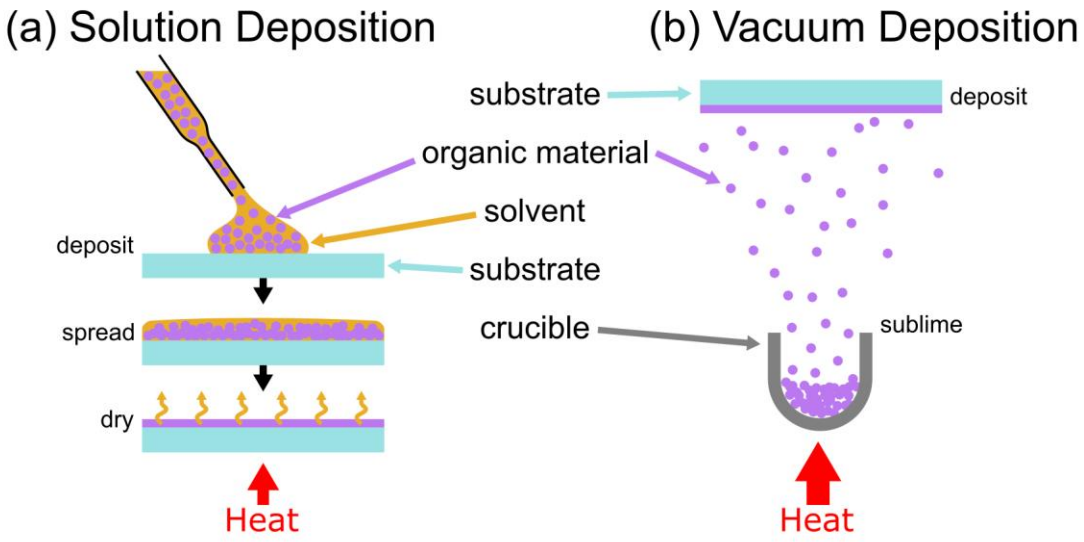

Figure 1.6. Illustration of the fabrication of thin organic films using (a) solution deposition and (b) vacuum deposition.

The configuration of the donor and acceptor heterojunction (also known as a heterojunction) can significantly influence exciton dissociation and charge carrier extraction within OPVs. Within the field of OPVs, there are two main heterojunction configurations: bulk heterojunction (BHJ) and planar heterojunction (PHJ).[21, 28] The donor and acceptor layers in BHJ OPVs are deposited simultaneously, resulting in an intermixed photoactive region. This process increases the interfacial area between the donor and acceptor but results in more complex pathways for charge carrier extraction. PHJ OPVs are fabricated by depositing the donor and acceptor layers sequentially, resulting in two planar layers and a planar heterojunction. This configuration has a

reduced interfacial area between donor and acceptor but simplifies the charge carrier extraction pathways. Most solution-cast OPVs have BHJ configurations, and most vacuum-deposited OPVs have PHJ configurations. However, it is possible to make solution-cast PHJ OPVs and vacuum-deposited BHJ OPVs.[27, 29]

1.3 Performance and Stability

1.3.1 Initial Characterization

PVs are first assessed immediately after fabrication (time zero). Usually, the first characterization is a voltage sweep (**Figure 1.7**), performed while illuminating the PV with one sun intensity of simulated sunlight. A sourcemeter applies a set of voltage (V) biases while measuring the corresponding current (I). Since the current output from the PV will be higher for a larger area, the current output is normalized to current density (J) by dividing by the current by the area (I/A = J).

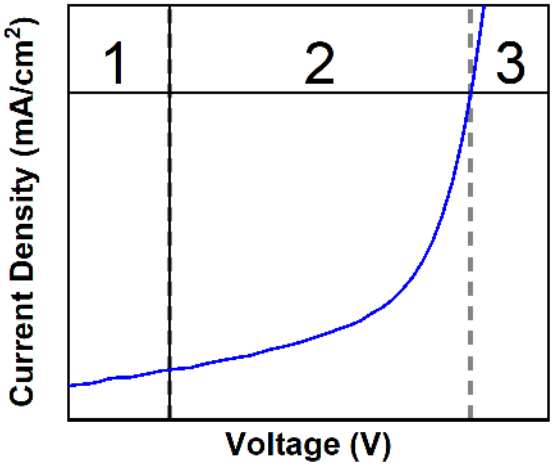

Figure 1.7. The three regions of a typical current density-voltage (J–V) curve of an OPV. Region 1: reverse bias. Region 2: small forward bias. Region 3: large forward bias.

The voltage sweep produces a J–V curve with three different regions. The first region occurs when the PV is under reverse bias, or when a negative voltage is applied. Reverse bias increases the current output from the PV, but the applied voltage requires more energy input than output. Therefore, this is a region of negative power generation. As the voltage applied switches from

negative to positive, the PV enters forward bias. Small forward biases simulate the application of a resistive load to the PV. Small forward bias is the region of positive power generation. Further increasing the forward bias eventually reverses the output of the PV, with current flowing in the direction of the forward bias. In the large forward bias region, more energy is input than extracted, effectively resulting in negative power generation.

Under large forward bias, charge carriers are injected into the device rather than extracted from the device. The injected electrons eventually find and recombine with the injected holes, shedding their excess energy in the form of light or heat.[30] A PV can be optimized to have this energy preferentially converted to light instead of heat. However, the optimizations required for light emission in large forward bias mode usually compete with the optimizations required for power generation in small forward bias mode. PV layer stacks optimized for light emission in large forward bias mode are instead called light-emitting diodes (LEDs), which are commonly used in displays for televisions, smartphones, and lighting. Likewise, OPVs and organic LEDs (OLEDs) have very similar structures but differ in their optimizations for different functions and operation in different regions of the J–V curve.

Typically, four J–V curve parameters are reported (**Figure 1.8**): short-circuit current density (J_{SC}), open-circuit voltage (V_{OC}), fill factor (FF), and power conversion efficiency (PCE). These parameters are used to assess and compare the performance of different PV. The application of zero bias (the point between reverse bias and small forward bias) is equivalent to short-circuiting the PV with a zero resistance load. The current-density at short-circuit (J_{SC}) is the highest possible current-density that is extractable from a PV without external assistance. The application of a bias that halts all current flow (the point between small forward bias and large forward bias) means the PV is effectively an open-circuit, equivalent to loading the PV with infinite resistance. The voltage at open-circuit (V_{OC}), is the highest possible voltage that is extractable from a PV without external assistance.

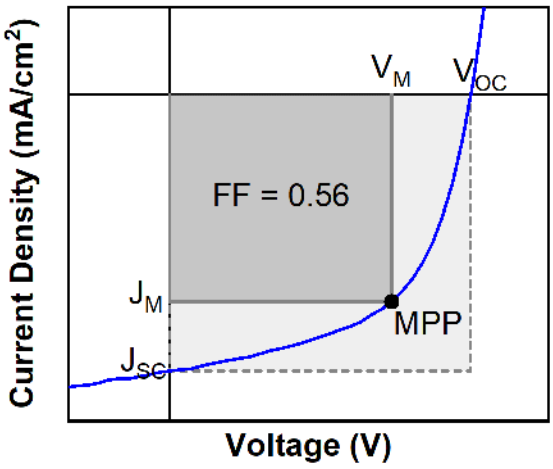

Figure 1.8. Parameters extracted from a sample current density-voltage (J–V) curve of an OPV: open-circuit voltage (V_{OC}), short-circuit current density (J_{SC}), maximum power point (MPP), voltage at MPP (V_M), current-density at MPP (J_M), and fill factor (FF). The FF = 0.56 in this example.

During the voltage sweep of the small forward bias region, increasing voltage reduces the current density. Since power (P) is the product of voltage and current, there exists a maximum power point (MPP) between J_{SC} and V_{OC} with maximum power (P_M). The P_M is a product of the voltage and current at that point (V_M and $J_M \cdot A$). An ideal PV would have a V_M and J_M equivalent to the V_{OC} and J_{SC}, resulting in a perfectly rectangular J–V plot. Real PVs have a curved J–V plot (J–V curve), such that the V_M and J_M are less than the V_{OC} and J_{SC}. Fill factor (FF) is a parameter used to quantify this non-ideality.[31] FF is the ratio between V_M x J_M and V_{OC} x J_{SC}. The FF of a perfectly rectangular J–V would have a value of 1, and a straight line would have a value of 0.25. PVs with charge carrier imbalance can produce "S-kinked" J–V curves,[32] which result in FF values even lower 0.25. PCE is calculated by taking the maximum power (P_M) output from the PV and dividing it by the amount of solar power input into the OPV (100 mW/cm^2). PCE can be improved by increasing the amount of current or voltage input from the cell, or by achieving a higher fill factor.

Another common PV characterization that is performed immediately after fabrication (time zero) are wavelength sweeps while short-circuiting the device. A monochromator is used to illuminate

the PV with one wavelength (colour) of light at a time. At each wavelength, the amount of current produced is measured and compared to the amount of light received. The ratio of electrons output vs photons input provides a measure of how efficiently the PV converts various wavelengths of light into electricity (**Figure 1.9**).

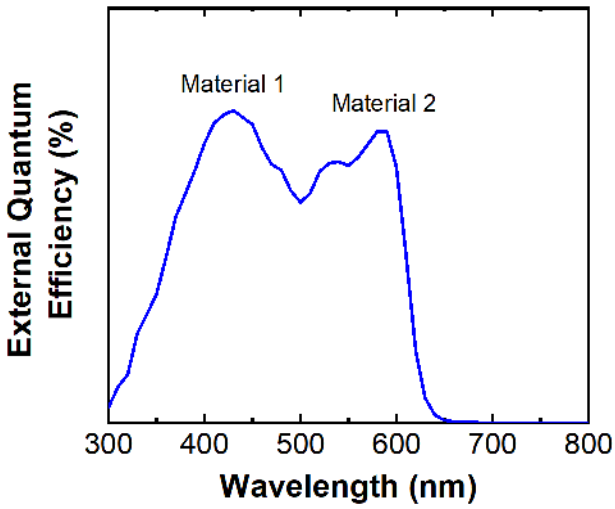

Figure 1.9. An external quantum efficiency (EQE) curve of a sample OPV, showing the peak contributions of two materials in different regions of the EQE curve.

The area under an EQE curve is proportional to the J_{SC}, so a higher and broader EQE curve represents a higher extractable current when comparing between different OPVs. The shape of the EQE curve is approximately the combined absorbance profiles of each semiconducting material. Knowledge about the individual material absorbance profiles can be applied to strategically select materials to cover a broader portion of the solar spectrum. EQE curves can be used to identify materials in the photoactive region that are not significantly contributing to the current output of the OPV. The integration of these EQEs with the solar spectrum provides an estimate of the expected short-circuit current density under one sun illumination. The "EQE J_{SC}" and "J–V J_{SC}" should theoretically be very similar and can be compared for validation of both measurements.[33]

1.3.2 Long-term durability

What happens to the performance of PVs after time zero? Silicon PVs have been established and implemented for decades, demonstrating lifetimes of 20 to 30 years.[34] For OPVs, a significant

amount of work has focused on improving the time-zero performance; relatively little research has been conducted to investigate OPVs beyond the initial measurements. Improvements in time-zero performance are increasingly achieved through the development of synthetically complex organic semiconductors.[35-37] Increased complexity increases the number of synthetic steps, compounding any energy inefficiencies and the production of toxic waste.[38] Increasing the embodied energy of a material used for photovoltaics is counterproductive to the goal of power generation. Also, materials with high performances at time zero are quickly adopted by other research groups and often reach commercial availability prior to any stability testing. An unstable material is effectively useless for commercial application in OPVs. Scaling up the use of organic semiconductors without knowledge of their stability could waste significant resources.

Consensus protocols for testing the stability of OPVs were established in 2011 at the international summit on OPV stability (ISOS).[39] These protocols describe many different types of OPV stability testing: dark storage, laboratory weathering, thermal cycling, solar-thermal-humidity cycling, and outdoor testing. The outdoor testing protocols include instructions about how to mount and orient the OPVs outdoors, what parameters to track, how frequently to measure those parameters, and how to report the data. Using these protocols enables direct comparisons between the reported results and data from other groups around the world, where the outdoor conditions are inevitably different. Unfortunately, so far only 24 studies have cited these protocols while reporting outdoor stability testing of OPVs.[40]

Stability is a critical parameter to consider before OPVs can achieve widespread industrial relevance. Silicon PVs have become competitive in energy markets around the world due to the ability to annualize costs over their 20 to 30-year lifetimes. While the costs to fabricate and install OPVs have the potential to be much lower than for silicon PVs,[41] the annualized costs of OPVs will not be competitive until the achievement of longer lifetimes.

1.4 Boron Subphthalocyanine (BsubPc)

Boron subphthalocyanines (BsubPcs, **Figure 1.10**) are a class of small organic molecules of special interest for OPVs. The peak absorption of BsubPcs is around 590 nm, conveniently near

the peak intensities of the solar spectrum (**Figure 1.10**).[42] BsubPcs also have a nonplanar "bowl" structure, which enables unique packing in solid-state films and desirable electronic properties for application in organic photovoltaics. A major attraction of BsubPcs is that many properties can be easily tuned through the chemical addition or modification of substituents.[43-48] BsubPc substituents are categorized based on their position: axial and peripheral (R_a and R_p, **Figure 1.10**).

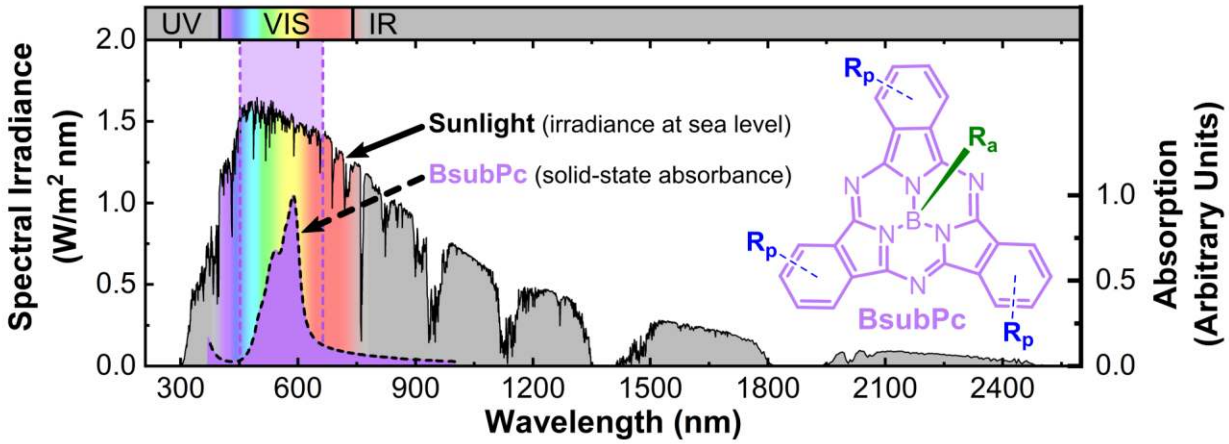

Figure 1.10. Spectral irradiance of the sun at sea level overlaid with the solid-state absorption of boron subphthalocyanine (BsubPc), and the chemical structure of a BsubPc depicting the axial (R_a, green) and peripheral (R_p, blue) substituent locations. Indications for ultraviolet (UV), visible (VIS), and infrared (IR) wavelengths (top).

The Bender lab has a wealth of chemical experience synthesizing new BsubPcs and modifying BsubPc substituents.[43, 49-53] The most significant difference between axial and peripheral substituents is their influence on the HOMO and LUMO of a BsubPc. Axial substituents are generally considered to have minimal effect on molecular orbitals, whereas peripheral substituents often strongly influence the molecular orbitals.[46, 54] Substituents can also influence the orientation and packing density of the molecules in a solid-state film,[50, 55] charge carrier/exciton transfer and dissociation between molecules,[56-59] and stability (**Chapter 4**). BsubPcs provide a platform to study the effects of different substituents and their influence on OPV performance and stability.

1.5 Electron-Accepting BsubPcs in OPVs

This thesis follows a "staple thesis" format, a compilation of the work I have published during my doctorate studies. This section (**Section 1.5**) is adapted from my section of a review article published in *The Chemical Record*. I am a co-first author of the manuscript, which is adapted here with permission from "*Grant, T.M., *Josey, D.S., *Sampson, K.L., Mudigonda, T., Bender, T.P, Lessard, B.H. (**2019**). *Boron Subphthalocyanines and Silicon Phthalocyanines for use as Active Materials in Organic Photovoltaics.* The Chemical Record, 19: 1-21. *co-first authors"[60]

This section describes the evolution of vacuum-deposited boron subphthalocyanine (BsubPc) applied as an electron acceptor in organic photovoltaics (OPVs). Parts of the published manuscript that also appear elsewhere in my thesis are omitted from this chapter. I conducted the exhaustive literature search, structured the existing literature into categories, and wrote every section except for **Section 1.5.4**. The first draft of **Section 1.5.4** was written by Thanmayee Mudigonda, which I then edited and incorporated into my other sections. Trevor Grant and Katie Sampson wrote separate sections on silicon phthalocyanine and soluble, solution-casted boron subphthalocyanines, respectively. Trevor also merged our three sections into the final manuscript. Professor Bender and Professor Lessard supervised and provided guidance and editing throughout the development of this review article.

1.5.1 Introduction

When BsubPcs first appeared in OPVs, they were exclusively applied as electron-donating materials paired with C_{60} fullerene.[61-63] The vast amount of research and progress made towards advancing the application of BsubPcs as electron donors was recently reviewed by Torres *et al.*[64] With BsubPcs well-established in the electron donor space, recent efforts have been more focused on using BsubPcs to replace fullerene as electron acceptors. Fullerenes have a low absorption coefficient but have excelled as electron acceptors in OPVs due to their high electron mobility and electron affinity. The capability to tune the electronic properties of fullerenes is limited compared to other organic semiconductor molecules. A strong absorption coefficient near the peak intensity of the solar spectrum and highly tunable electronic properties make BsubPcs excellent candidates to improve on the shortcomings of fullerenes and surpass their performance as electron acceptors

in OPVs.[42] Indeed, several studies in the last decade have reported remarkable progress and success replacing fullerenes with BsubPcs. Herein, an exhaustive review presenting of every instance of BsubPc application as an electron-accepting material in vacuum-deposited OPVs.

1.5.2 All BsubPc / BsubNc OPVs

Fabricating OPVs with similar molecular structures can simplify the development process of OPVs. The ability to apply discoveries about specific molecules to the entire set of materials accelerates the achievement of high performance, high stability OPVs. BsubPc and boron subnaphthalocyanine (BsubNc, **Figure 1.11b**) derivatives offer a collection of chemically similar materials with widely differing electronic properties, such as complimentary absorption, that can be effectively paired together as active materials within OPVs.

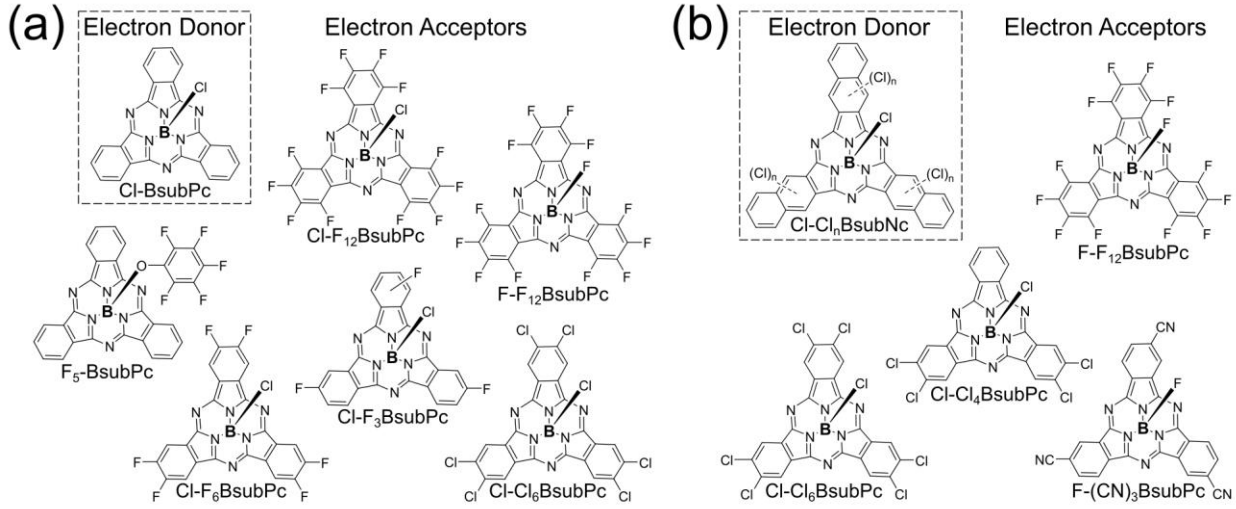

Figure 1.11. Chemical Structures of the electron-accepting BsubPcs that have been paired with electron-donating (a) chloro-BsubPc (Cl-BsubPc) and (b) chloro-(chloro)$_n$ BsubNc (Cl-Cl$_n$BsubNc).

BsubPc / BsubPc Pairing

One previously explored OPV configuration is the direct pairing of BsubPcs, one as an electron donor and one as an electron acceptor (**Figure 1.12a**). In this case, each BsubPc has an overlapping absorption spectrum with its paired BsubPc counterpart.

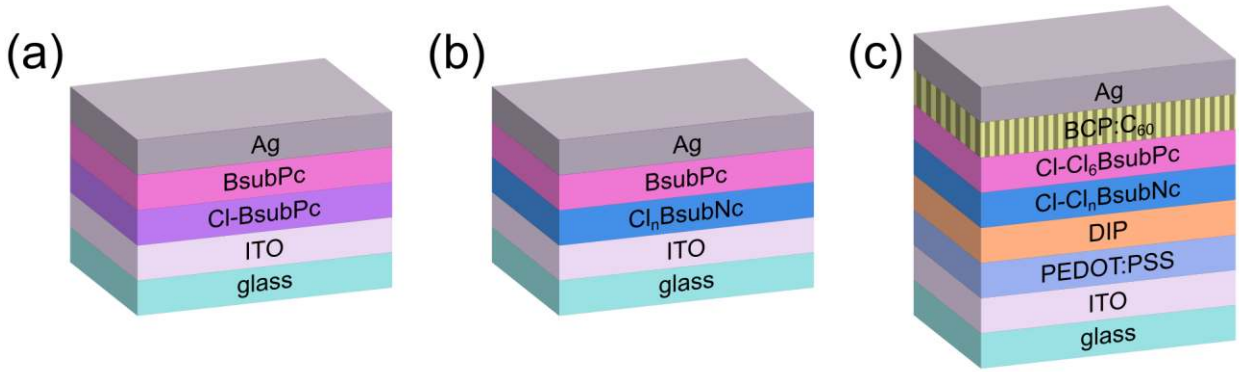

Figure 1.12. Device schematic illustrating the layer stack of (a) BsubPc/BsubPc, (b) Cl_nBsubNc / BsubPc and (c) Cl-Cl_nBsubNc / chloro-hexachloro BsubPc (Cl-Cl_6BsubPc) OPVs.

Peripheral fluorination significantly increases the ionization energy and electron affinity of the BsubPc molecule. In 2009, Gommans *et al.* exploited this energy level tuning to produce the first-ever examples of a BsubPc used as an electron acceptor: two all-BsubPc OPVs of Cl-BsubPc / fluoro-dodecafluoro BsubPc (F-F_{12}BsubPc) and Cl-BsubPc / chloro-dodecafluoro BsubPc (Cl-F_{12}BsubPc) (**Figure 1.11a**).[65] The PCEs of these two OPVs (F-F_{12}BsubPc: 0.96%, Cl-F_{12}BsubPc: 0.52%) were still significantly lower than the 3.0% PCE of their Cl-BsubPc / C_{60} baseline. The low PCEs were primarily attributed to the complete peripheral fluorination of the electron-accepting BsubPcs, which shifted their energy levels excessively deep for pairing with Cl-BsubPc.

BsubPcs with only partial fluorination and chlorination were explored by Sullivan *et al.* to optimize the energy level offset with Cl-BsubPc and improve on these first OPV results.[48] The derivatives chloro-trifluoro (Cl-F_3), chloro-hexafluoro (Cl-F_6), and chloro-hexachloro (Cl-Cl_6) BsubPc (**Figure 1.11a**) were all assessed as electron acceptors paired with Cl-BsubPc. The energy level offset between Cl-BsubPc and Cl-F_3BsubPc was demonstrated to be too slight for efficient exciton dissociation, and Cl-BsubPc / Cl-F_6BsubPc displayed OPV functionality with a high V_{OC} (1.22 V) and PCE of 0.80%. Most significantly, this study reported substantial performance gains by employing Cl-Cl_6BsubPc as the electron acceptor. The Cl-BsubPc / Cl-Cl_6BsubPc OPV produced a record V_{OC} of 1.31 V, in addition to a FF of 0.58 and a J_{SC} of 3.53 mA/cm^2. A promising step towards replacing fullerene, the corresponding PCE of 2.68% nearly matches that of their Cl-BsubPc / C_{60} baseline (PCE=2.97%). In a follow-up study, Sullivan *et al.* sought to fully exploit

the Cl-BsubPc / Cl-Cl_6BsubPc structure by combining several Cl-BsubPc / Cl-Cl_6BsubPc and Cl-BsubPc / C_{60} heterojunctions in tandem OPVs.[59] Despite the negligible improvement in PCE, the resulting OPVs did produce extremely high V_{OC}s of up to 7.04 V. These tandem OPVs also exhibited a reduced sensitivity to spectral changes due to their sole reliance on green light.

Further work on Cl-BsubPc / Cl-Cl_6BsubPc examined inversion of the device structure. Hancox *et al.* demonstrate that ITO / MoOx / Cl-BsubPc / Cl-Cl_6BsubPc / BCP / Ag could be inverted simply by flipping the device fabrication order (ITO / BCP / Cl-Cl_6BsubPc / Cl-BsubPc / MoOx / Ag) with minimal PCE losses.[66] Replacing BCP with solution coated ZrAcac improves the performance of the inverted stack and reaches an approximately equivalent PCE as compared to the traditional stack.

The most recently reported BsubPc / BsubPc pairing was an axially substituted, pentafluorophenoxy-BsubPc (F_5-BsubPc, **Figure 1.11a**). In contrast to the peripherally substituted BsubPcs, the five fluorines around the axial phenoxy result in only slightly deeper energy levels compared to Cl-BsubPc. Morse *et al.* report the pairing of Cl-BsubPc / F_5-BsubPc to produce an OPV with a V_{OC}, J_{SC}, and FF of 1.06 V, 2.06 mA/cm^2, 43.2, respectively.[44] Ultimately this OPV achieves a similar PCE (0.94%) as the original Cl-BsubPc / F-F_{12}BsubPc pairing.[65] Together, these two OPVs establish an approximate upper and lower boundary for the LUMO of a BsubPc electron acceptor to be effectively paired with Cl-BsubPc.

BsubNc / BsubPc Pairing

As noted in the previous section, a limitation of all-BsubPc OPVs is the near-perfect overlap in the absorption spectra of the electron donor and acceptor. One approach to circumvent these limitations while maintaining the advantages of similar chemical composition is to pair the BsubPc electron acceptors with BsubNc electron donors (**Figure 1.12b**). BsubNc possesses a complementary absorption to BsubPcs and shares similarly tunable energy levels. Our group has established that "BsubNc" material has random amounts of bay position chlorination.[67] We, therefore, abbreviate BsubNc as Cl_nBsubNc to indicate the consideration of those chlorines.

The first Cl_nBsubNc / BsubPc pairings were explored in the original 2009 BsubPc acceptor paper, where Gommans *et al.* pair Cl-Cl_nBsubNc with F-F_{12}BsubPc (**Figure 1.11b**). As with the Cl-BsubPc / F-F_{12}BsubPc OPV, the V_{OC} (0.70 V) and PCE (0.63%) of Cl-Cl_nBsubNc / F-F_{12}BsubPc suffers from the excessively deep energy levels of F-F_{12}BsubPc. However, this OPV established a baseline for future work.

In 2014, after Cl-Cl_6BsubPc was demonstrated to perform exceptionally well with Cl-BsubPc, Verreet *et al.* advanced the performance of electron-accepting BsubPcs even further by pairing Cl-Cl_6BsubPc with Cl-Cl_nBsubNc (**Figure 1.11b**).[68] In addition to this novel active layer pairing, they also demonstrate significant performance enhancements through the selection of new hole transport and electron transport layers (**Figure 1.12c**). The insertion of diindenoperylene (DIP) between PEDOT:PSS / Cl_nBsubNc serves as a hole transport layer with improved exciton blocking properties, radically enhancing the extracted current and overall PCE. Using a co-deposited layer of BCP:C_{60} as the electron transport layer slightly outperforms sequentially deposited C_{60} / BCP cascade layers, despite the former's lack of C_{60} photocurrent contribution. The improvements made by using BCP:C_{60} are attributed to higher conductivity, which enables the use of thicker layers for optical optimization.

A year later, Cnops *et al.* investigated the Cl_nBsubNc / BsubPc device structure in even more detail. They compared pairings of Cl-Cl_nBsubNc with four different BsubPc derivatives as electron acceptors: chloro-tetrachloro (Cl-Cl_4), Cl-Cl_6, fluoro-tricyano (F-$(CN)_3$), and Cl-F_{12}BsubPc (**Figure 1.11b**). Hole transport layers (MoO_X and DIP) and electron transport layers (BCP:C_{60} and BCP:Yb) were also compared for each of these architectures. The optimal hole transport layer was determined to be DIP in all cases. The optimal electron transport layer was shown to depend on the electron acceptor. For the deep energy levels of Cl-F_{12}BsubPc, an electron transport layer of BCP:Yb produced the best results. The study showed that BCP:C_{60} is the optimal electron transport layer for Cl-Cl_6BsubPc. A fully optimized device stack of ITO / PEDOT:PSS / DIP / Cl_nBsubNc / Cl-Cl_6BsubPc / BCP:C_{60} / Ag (**Figure 1.12c**) achieves a PCE of over 6%.[46, 68] Though it still employs C_{60} within the electron transport layer, this efficiency is well-beyond any bilayer stack that incorporates fullerene in the active layer.

With the improvements in extracted current when using DIP attributed to improved exciton blocking, Chandran *et al.* report a phenomenon that could provide a potential explanation for why those performance gains are so substantial.[69] They demonstrate significant free carrier generation within the Cl-BsubPc and Cl-Cl$_n$BsubNc layers, even without the presence of a dissociating interface. By reducing the potential quenching pathways for excitons through the application of DIP, even excitons that are far from a rectifying interface can generate free carriers. Excitons within the Cl-Cl$_n$BsubNc layers that may have been quenched by a different hole transport layer are therefore potentially able to contribute to the overall photocurrent.

1.5.3 Singlet Fission Materials

Singlet fission is a process that converts one singlet exciton into two triplet excitons. Singlet fission occurs in a limited number of materials, the most popular of which are linear acenes such as tetracene, pentacene, and rubrene (**Figure 1.13**). Harnessing singlet fission for application in OPVs has attracted interest due to the unique potential of extracting two electrons per incident photon. Harvesting triplet excitons can be challenging, which requires the use of materials with sufficiently deep LUMO levels. Fullerene is capable of harvesting triplets from pentacene,[70] so an early question in the pursuit of replacing fullerene as an electron acceptor was whether BsubPcs could replace the ability to harvest triplets.

Figure 1.13. Chemical structures of the electron-donating, singlet fission materials that have been paired with BsubPcs.

Tetracene

A BsubPc pairing with tetracene (**Figure 1.13**) was reported for the first time in 2011.[71] The tetracene / Cl-BsubPc OPV produces a very high V_{OC} of 1.24 V and a PCE of 2.89%. This device was later replicated with some device optimization, yielding a slightly higher PCE of 3.09%.[72]

Minor photocurrent contribution was detected from tetracene in the EQEs, likely the dissociation of singlets given the relatively shallow LUMO level of Cl-BsubPc.[56] The singlet fission process in tetracene is considered slow compared to materials like pentacene, where singlets are rapidly converted to triplets before dissociation can occur.[70, 73-74] This report represents the first occurrence in literature where the performance of an OPV containing BsubPc as the electron acceptor (tetracene / Cl-BsubPc) exceeded that of the equivalent fullerene-containing OPV (tetracene / C_{60}, PCE: 1.83%).

V_{OC} tunability of tetracene / BsubPc OPVs was demonstrated by comparing two BsubPcs with different amounts of peripheral chlorination (Cl-BsubPc and Cl-Cl_6BsubPc) as electron acceptors.[75] The V_{OC} decreases from Cl-BsubPc (1.18 V) to Cl-Cl_6BsubPc (0.89 V), consistent with the deepening of the LUMO level. However, the modest 15% gain in J_{SC} from Cl-BsubPc to Cl-Cl_6BsubPc is insufficient to offset the V_{OC} losses.

Pentacene

Pentacene was one of the many donor materials Gommans *et al.* reported pairing with F-F_{12}BsubPc in 2009.[65] The full layer stack of ITO / pentacene / F-F_{12}BsubPc / BCP / Al yielded the lowest-performing OPV (PCE=0.03%) of any electron donor used in that study. The LUMO of F-F_{12}BsubPc was likely sufficiently deep to extract photocurrent contribution from pentacene via triplet harvesting, but pentacene contribution is only suggested in the text without a reported EQE for the device.

Morse *et al.* reported the next example of a pentacene / BsubPc pairing, applying F_5-BsubPc as the electron acceptor.[44] This OPV exhibited negligible photocurrent contributions from pentacene, but the improvement in energy level offset did increase the overall PCE approximately 10-fold (0.3%) as compared to the original pentacene / F-F_{12}BsubPc device. Still, the performance of these BsubPc OPVs is far lower than comparable to pentacene / C_{60} OPVs.

As with tetracene, V_{OC} tunability of pentacene / BsubPc OPVs was demonstrated through variation of the BsubPc peripheral chlorination, comparing Cl-BsubPc, Cl-Cl_6BsubPc, and Cl-Cl_{12}BsubPc as electron acceptors (**Figure 1.14**).[75-76] For the first time with BsubPcs, triplet harvesting became

evident when pairing pentacene with Cl-Cl_6BsubPc and Cl-Cl_{12}BsubPc. Pentacene / Cl-Cl_{12}BsubPc achieved a substantial photocurrent contribution from the pentacene layer, even higher than what C_{60} extracts from pentacene. This study marks the first indication that the triplet harvesting ability from C_{60} can be completely replaced with a BsubPc, even if the pentacene / C_{60} OPV still slightly outperforms the pentacene / Cl-Cl_{12}BsubPc OPV (PCE=1.4% vs 1.2%) due to a lack of absorption in the 400--450 nm range.

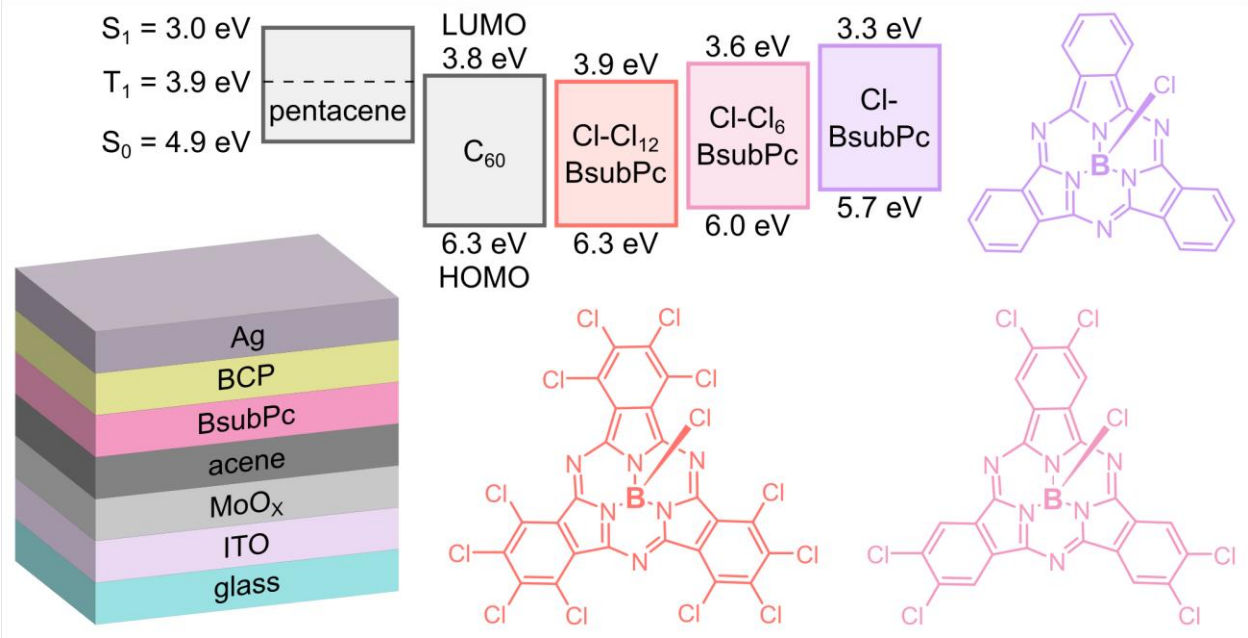

Figure 1.14. HOMO/LUMO energy level diagram of electron-donating pentacene, and electron-accepting materials: C_{60} fullerene, Cl-Cl_{12}BsubPc, Cl-Cl_6BsubPc, and Cl-BsubPc. Schematic illustrating the OPV layer stack and chemical structures of the electron-accepting BsubPcs. Adapted from Castrucci *et al.*[76]

Rubrene

Rubrene has only recently been explored as an electron donor with BsubPc as an electron acceptor. In 2017, Lin *et al.* reported pairing rubrene with Cl-BsubPc. They take advantage of the large rubrene bandgap to produce OPVs with the highest V_{OC} (up to 1.44 V) ever reported for a single junction OPV, and PCEs of up to 2.52%. However, the exceptionally high V_{OC} and shallow LUMO levels of Cl-BsubPc suggest that triplet harvesting is unlikely to be occurring in this device.[77]

One other unique occurrence in literature was the application of rubrene as an interlayer in an OPV applying Cl-Cl_nBsubNc and Cl-BsubPc as electron acceptors. Nikolis *et al.* inserted rubrene as an interlayer between the alpha-sexithiophene (α-6T) / Cl-Cl_nBsubNc layers in an α-6T / Cl-Cl_nBsubNc / Cl-BsubPc device developed by Cnops *et al.* (discussed in next section).[78-79] The insertion successfully achieved their goal of improving the V_{OC}, and it also slightly increased the BsubNc contribution to the photocurrent. However, even the inclusion of the thinnest layer of rubrene significantly reduced all other device parameters, negating the other gains.

1.5.4 α-Sexithiophene

Many recent studies have incorporated BsubPc and BsubNc derivatives as electron acceptors with an α-sexithiophene (α-6T, **Figure 1.15**) electron-donating layer. Compared to other, fullerene-optimized electron donors, α-6T is better suited for pairing with BsubPc electron acceptors due to its broad, complementary absorbance (350 – 550 nm) with BsubPc and BsubNc derivatives, and shallower energy levels.[56, 80] The inherent surface roughness of α-6T also facilitates charge dissociation at the donor / acceptor interface.[79] The following section reviews every publication that pairs electron-donating α-6T with electron-accepting BsubPcs or BsubNcs.

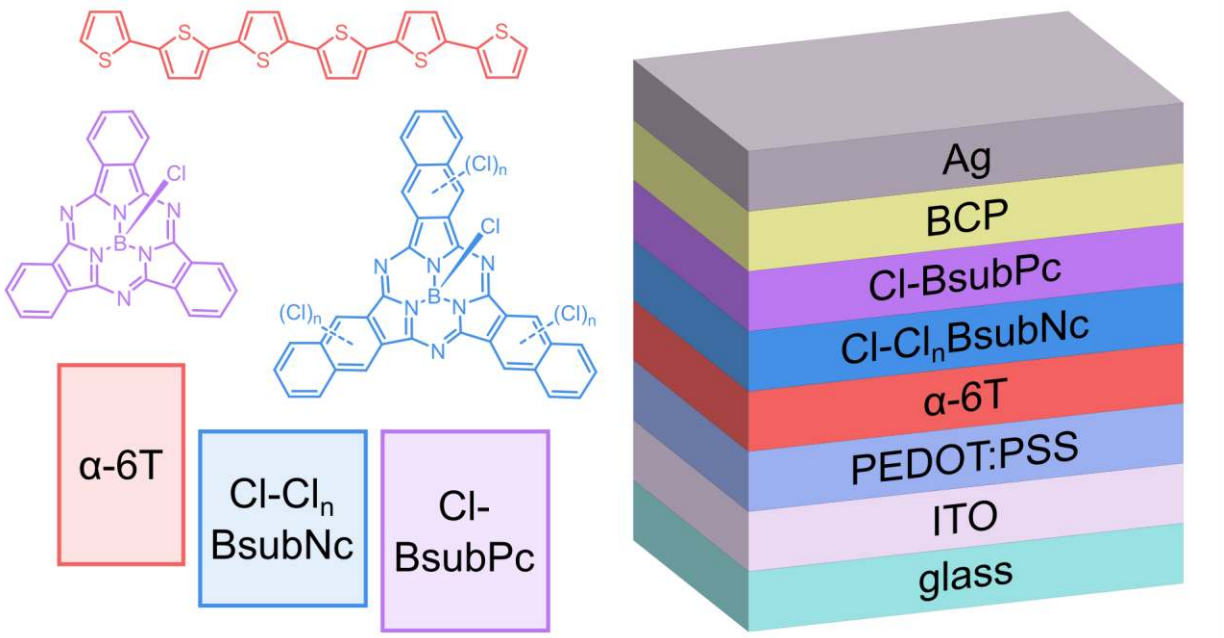

Figure 1.15. Chemical structures and HOMO/LUMO energy level diagram of electron-donating α-sexithiophene (α-6T), and electron-accepting materials: Cl-Cl$_n$BsubNc and Cl-BsubPc. Schematic illustrating the OPV layer stack. Adapted from Cnops *et al.*[79]

Trilayer Energy Cascade

In 2014, Cnops *et al.* demonstrated the validity and high performance of a three-layer energy cascade device architecture (**Figure 1.15**),[79] which became the basis of several follow-up studies.[67, 78, 81] They apply Cl-Cl$_n$BsubNc and Cl-BsubPc as dual electron acceptors paired with α-6T, whereby exciton dissociation follows a two-step process. Excitons generated in the Cl-BsubPc layer are transferred to Cl-Cl$_n$BsubNc via long-range Förster energy transfer, followed by diffusion to the α-6T / Cl-Cl$_n$BsubNc interface for dissociation. The broad, complementary absorption of three materials with efficient charge and exciton transfer resulted in a record vacuum-deposited planar heterojunction (PHJ) OPV, achieving a PCE of 8.4%.[79]

A subsequent study aimed to reduce losses in V_{OC} by introducing an interlayer at the α-6T / Cl-Cl$_n$BsubNc interface.[78] The interlayer materials investigated were DIP, phenoxy BsubPc (PhO-BsubPc), and the previously mentioned rubrene. These materials were selected to have HOMO energy levels similar to the HOMO of Cl-Cl$_n$BsubNc. Insertion of the three interlayers resulted in

an increase in V_{OC} in all cases, with an 8 nm interlayer of rubrene representing the most significant increase (0.98 V to 1.16 V). The increase in V_{OC} was attributed to inhibition of nonradiative recombination losses due to reduced contact between donor and acceptor interfaces. A 2 nm interlayer of PhO-BsubPc was the only interlayer that achieved any improvement in PCE, with an increase in V_{OC} and J_{SC} barely compensating for the drop in FF of a rubrene interlayer.

Bilayers

Castrucci and Garner *et al.* explored the integration of the oxygen linked BsubPc dimer, μ-oxo-$(BsubPc)_2$, a novel BsubPc derivative, into OPV devices as an electron acceptor paired with α-6T.[82] μ-oxo-$(BsubPc)_2$ yielded a very low PCE of 0.37%, potentially due to unfavourable interfacial arrangement onto the α-6T layer.

Huang *et al.* conducted a study of BsubPc and Cl_nBsubNc OPVs paired with α-6T, which outperformed the corresponding fullerene OPVs. They also determined that the V_{OC} is mostly influenced by charge transport through the device. Insertion of molybdenum trioxide as an anode buffer layer improves the surface roughness and work function.[80] Carrier injection dynamics were also investigated in α-6T / Cl-BsubPc OPVs and found to be very slow, attributed to the migration of excitons in α-6T.[83]

Morozan *et al.* proceeded in a different direction and explored the construction of a hydrogen evolving noble metal-free photocathode.[84] They found an α-6T / Cl-BsubNc bilayer PHJ solar cell to be effective for H_2 evolution, because donor and acceptor absorb at different wavelengths of the solar spectrum, therefore allowing for large photocurrent generation.[84]

Stability

Improving durability and lifetime of OPVs is a well-known challenge in the field but has received comparatively little attention in literature. Ageing experiments were conducted on the α-6T / BsubNc / BsubPc energy cascade solar cell that was first demonstrated by Cnops *et al.*[81] An indoor climate chamber with a mounted solar simulator was used to age the OPVs and compare different encapsulation architectures. α-6T was identified as the main degrading component because a

reduction in α-6T thickness led to increased device lifetimes. This degradation was attributed to potential rearrangement of α-6T under illumination.

1.5.5 Phthalocyanines

A significant motivation to pair phthalocyanines (Pcs) with BsubPcs is their complementary absorptions. Pcs also exhibit many chemical similarities as BsubPcs, giving the Pc / BsubPc OPV architecture (**Figure 1.16a**) similar advantages as the all BsubNc / BsubPc OPVs.

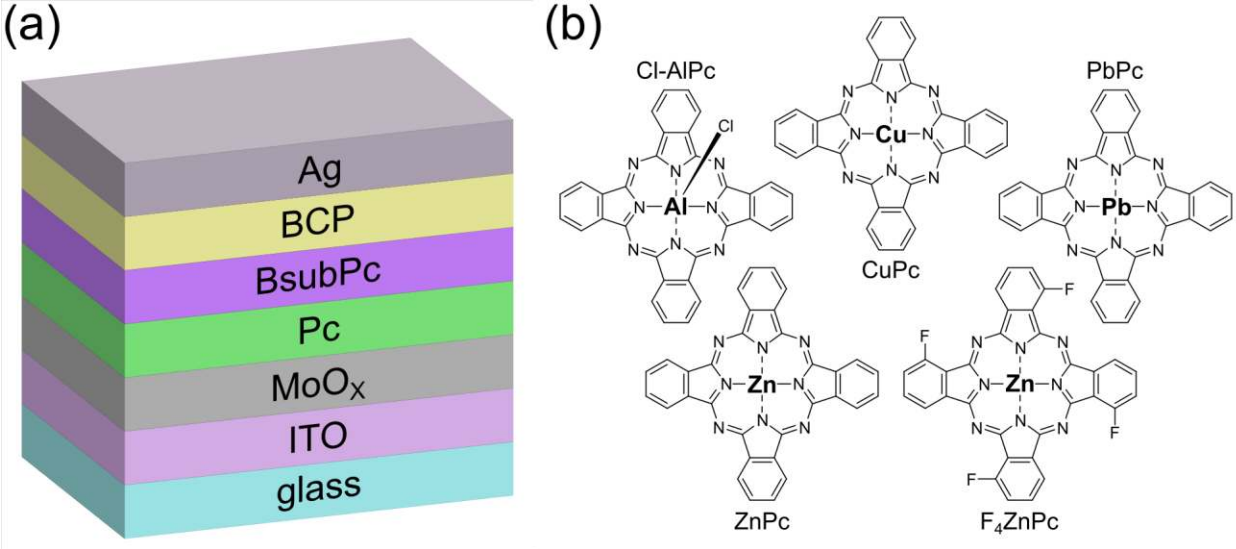

Figure 1.16. (a) Device schematic illustrating the layer stack of a Pc / BsubPc OPV. (b) Chemical structures of the electron-donating Pcs that have been paired with electron-accepting BsubPcs in OPVs.

The initial 2009 report by Gommans *et al.* investigated Cl-AlPc, and CuPc (**Figure 1.16b**) as electron donors paired with F-F_{12}BsubPc and Cl-F_{12}BsubPc.[65] Cl-AlPc / F-F_{12}BsubPc did reach a V_{OC} of 0.66 V, but neither electron donor produced an OPV with a PCE over 0.2%. It was six years before the report of another pairing of Pc electron donors and BsubPc electron acceptors. Cnops *et al.* studied a wide range of donor and acceptor materials:[46] They paired PbPc, ZnPc, and F_4-ZnPc (**Figure 1.16b**) with electron acceptors Cl-Cl_4BsubPc, Cl-Cl_6BsubPc, F-$(CN)_3$BsubPc, and Cl-F_{12}BsubPc. They also acquired HOMO/LUMO energy level measurements for every

material, enabling the demonstration of linear dependence between the interfacial energy gap and V_{OC}.

Of all the combinations tested, ZnPc / Cl-Cl_6BsubPc achieved the best PCE of 2.23%, a more than 10-fold increase over the 2009 Pc / BsubPc OPVs. Other OPV combinations achieved impressive individual parameters: a J_{SC} of 6 mA/cm^2 for PbPc / F-$(CN)_3$BsubPc, a FF of 53.9 for PbPc / Cl-Cl_6BsubPc, and a V_{OC} of 0.87 V for F_4ZnPc / Cl-Cl_6BsubPc, but all with corresponding parameters that resulted in PCEs of less than 1%. Despite achieving improvements in OPVs that pair Pcs as electron donors with BsubPcs, the OPV performance is not yet competitive with electron donors such as Cl_nBsubNc or α-6T.

1.5.6 Miscellaneous Electron Donors

The following three electron donor pairings with BsubPcs each only appear once in literature.

In 2013, α-NPD (**Figure 1.17**) was paired with Cl-BsubPc, a transparent exciton dissociation layer. The OPV does exhibit an exceptional V_{OC} of 1.34 V, but poor J_{SC} and FF result in a PCE of only 0.53%. However, the main objective of the OPV was accomplished, proving that dissociation did occur at the α-NPD / Cl-BsubPc interface.[85] This study establishes the application of α-NPD as a hole transport layer with Cl-BsubPc, which doubles as a second dissociating interface in the OPV.

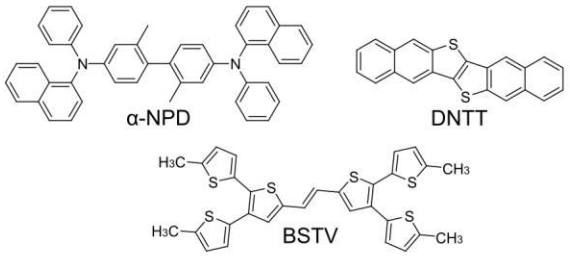

Figure 1.17. Chemical structures of the other three electron-donating materials that have been paired with electron-accepting BsubPcs in OPVs.

Zheng *et al.* reported the use of dinaphthothienothiophene (DNTT, **Figure 1.17**) as a wide band gap electron donor paired with Cl-BsubPc. Cl-BsubPc outperforms C_{60} in bilayer OPVs made with DNTT due to a higher V_{OC} (0.82 V to 0.54 V) and J_{SC} (2.73 mA/cm^2 to 2.29 mA/cm^2), resulting

in a PCE difference of 0.98% compared to 0.60%.[86] Cl-BsubPc doped into DBP as the electron-accepting layer increases the overall OPV performance, raising the V_{OC} and PCE to 1.24 V and 1.18% respectively for the optimized ratio of DBP:Cl-BsubPc (7:3). Adding a neat, 5 nm BsubPc layer on top (DNTT / DBP:Cl-BsubPc (7:3) / Cl-BsubPc) further improves the PCE to 1.32%, but the performance of these OPVs is not yet competitive with OPVs that use sexithiophene or Cl_nBsubNc as the electron donor.

Finally, a very recent study in 2018 reported the use of a branched sexithienylene vinylene oligomer (E)-Bis-1,2-(5,5"-Dimethyl-(2,2':3',2"-terthiophene)vinylene (BSTV, **Figure 1.17**) as an electron donor paired with Cl-BsubPc in an OPV. Despite displaying an exceptionally high V_{OC} of 1.35 V, the Cl-BsubPc OPV is still outperformed by BSTV / C_{60} (PCE of 2.28% vs 1.50%).[87]

1.5.7 BsubPc as Ambipolar Interlayer

Given the proven capability of BsubPcs as an electron donor paired with C_{60}, along with its electron-accepting capabilities as discussed above, there have been OPVs reported that add C_{60} (or C_{70}) onto the donor / BsubPc layer stack. The resulting OPV (donor / BsubPc / C_{60} or C_{70}) creates a charge cascade OPV (**Figure 1.18**), where there are two dissociating interfaces within the active layer: the donor / BsubPc interface and the BsubPc / C_{60} or C_{70} interface.

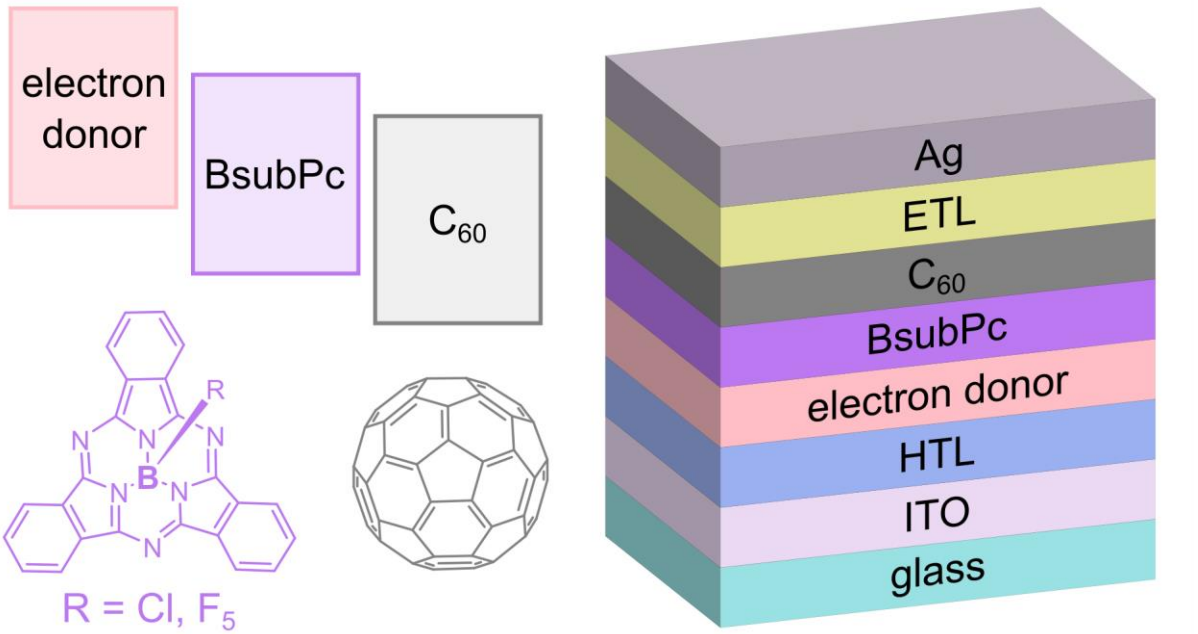

Figure 1.18. HOMO/LUMO energy level diagram of a typical charge cascade OPV, applying a BsubPc as the ambipolar interlayer and C_{60} fullerene as the electron acceptor. Chemical structures of C_{60} and the BsubPcs interlayers. Device schematic illustrating the typical layer stack of a charge cascade OPV.

The first example of a charge cascade OPV with a BsubPc as the ambipolar layer was reported in 2012 by Cnops *et al.* The device structure of tetracene / Cl-BsubPc / C_{60} achieved improvements in J_{SC} but ultimately produced a lower overall performance compared to OPVs consisting of the individual bilayer components: Tc / Cl-BsubPc and Cl-BsubPc / C_{60}.[72]

Similarly, most subsequent charge cascade OPVs that used BsubPc as an interlayer fail to outperform OPVs consisting of their bilayer components. Charge cascade OPVs consisting of pentacene / F_5-BsubPc / C_{60} and Cl-BsubPc / F_5-BsubPc / C_{60},[44] DNTT / Cl-BsubPc / C_{60},[86] and Cl-AlPc / Cl-BsubPc / C_{60}[88] are all outperformed by least one of their corresponding bilayer components.

The first example of a charge cascade that exceeds its bilayer components was a Cl-BsubPc / μ-oxo-BsubPc / C_{70} OPV developed by Castrucci *et al.*[82] Cattin *et al.* also managed to take advantage of the charge cascade architecture to produce a BSTV / Cl-BsubPc / C_{60} OPV achieving a PCE of

5.18% compared to their Cl-BsubPc / C_{60} bilayer reference of (PCE=4.66%).[87] Dissociation at the BSTV / Cl-BsubPc interface is questionable given the similar HOMOs, but a BSTV / Cl-BsubPc device did function as an OPV.

In a unique approach to applying BsubPc as an interlayer in a charge cascade OPV, Nikolis *et al.* inserted varying thicknesses of PhO-BsubPc at the α-6T / Cl-Cl_nBsubNc interface of the α-6T / Cl-Cl_nBsubNc / Cl-BsubPc OPV developed by Cnops *et al.*[78] Slight increases in performance were observed, but only for the 2 nm layer of PhO-BsubPc. All other thicknesses studied hindered the overall OPV performance.

1.5.8 Conclusions

Organic photovoltaics (OPVs) are a promising energy harvesting technology that has the potential for inexpensive large-scale fabrication. Metal phthalocyanines (MPcs) are inexpensive conjugated macrocycles utilized in a plethora of applications ranging from commercial dyes and pigments to photoresists and organic electronics. This review highlights the use of boron subphthalocyanines (BsubPcs) as a class of MPcs that is showing tremendous potential for use in OPVs. These materials require few steps to synthesize, resulting in low embedded energy and a reduced environmental footprint. The molecules can easily be modified to include axial groups that can be used to tune the solubility and solid-state stacking of the molecules. Unlike fullerene, BsubPcs have impressive molar extinction coefficients, which facilitate the absorption of photons in the orange/red part of the solar spectrum and make them ideal candidates to be paired with conjugated polymers. Unlike the classically thought of MPcs, BsubPcs have been demonstrated to successfully replace fullerene in high performing OPVs. Axial functionalization of BsubPcs can be used to direct the solid-state arrangement of the chromophore in a thin film obtained by thermal evaporation. These versatile molecules have been successfully incorporated into many different planar heterojunction OPVs.

This review highlights the potential of these emerging materials and illustrates the development of structure-property relationships that lead to improved device performance. Future studies are required to develop these structure-property relationships further and guide researchers in the

development of high-performance fullerene-free OPVs. However, these materials are worthy of further investigation.

1.6 Thesis Statement

The goal of my research is to strengthen the fundamental understanding of how substituents influence the performance and stability of a vacuum deposited BsubPc within an OPV and to apply this understanding to develop improved BsubPcs for OPVs. For this thesis, BsubNc derivatives are considered as BsubPc derivatives with peripheral benzene ring substituents. The pursuit of better-performing BsubPcs with higher stabilities leads to the following thesis statement:

Novel combinations of substituents can improve the performance and stability of electron-accepting boron subphthalocyanines in organic photovoltaics.

My thesis contains four focal points to address this thesis statement. The first focal point of my thesis is the establishment of a screening method that was then used to assess the OPV performance of a wide array of new BsubPc derivatives. Each new BsubPc derivative possesses a unique combination of substituents, categorized according to their locations: axial or peripheral. The second focal point centres on the exploration of alloyed mixtures. The third focal point centres on the influence of halogen bonding in OPVs. The final focal point addresses the stability aspect of the thesis statement. This focal point includes the development of outdoor stability testing protocols and stability assessments of the best derivative candidates from the screening stages.

Chapter 2
Peripheral Substituents

In this chapter, I examine the influence of peripheral substituents on the time-zero performance of BsubPcs in OPVs. This chapter is adapted from my contributions to three published manuscripts and one manuscript in preparation for submission to ACS Omega. I am the first author of the first manuscript (**Section 2.1**), which is adapted with permission from "Josey, D.S., Castrucci, J.S., Dang, J.D., Lessard, B.H., Bender, T.P. (**2015**). *Evaluating thiophene electron donor layers for the rapid assessment of boron subphthalocyanines as electron acceptors in organic photovoltaics; solution or vacuum deposition?* ChemPhysChem, 16(6): 1245-1250."[89] Copyright 2015 Wiley-VCH GmbH & Co. KGaA, Weinheim.

In this manuscript, I performed all device fabrication, conducted most of the data analysis, and wrote the manuscript. Jeffrey Castrucci contributed some valuable insights on device thickness optimizations. Jeremy Dang synthesized the chloro-BsubPc and chloro-hexachloro BsubPc and purified these materials by train sublimation. Some of the ideas in this manuscript were born from discussions with Benoit Lessard and Professor Bender. Professor Bender also supervised and provided guidance throughout the research and publication stages of this manuscript.

I am the second author of the second manuscript, which was adapted with permission from "Castrucci, J.S., Josey, D.S., Thibau, E., Lu, Z.-H., Bender, T.P. (**2015**). *Boron subphthalocyanines as triplet harvesting materials within organic photovoltaics.* J. Phys. Chem. Lett., 6(15): 3121-3125."[76] Copyright 2015 American Chemical Society. The data for α-sexithiophene / chloro-dodecachloro BsubPc OPVs in this manuscript was integrated into the figures and discussion of **Section 2.1**.

The fabrication of these devices was my main contribution to this manuscript. Jeffrey Castrucci wrote the manuscript and fabricated OPVs with pentacene and chloro-dodecachloro BsubPc. Emmanuel Thibau performed the ultraviolet photoelectron spectroscopy on chloro-dodecachloro BsubPc under the supervision of Professor Lu. Professor Bender supervised and provided guidance throughout the research and publication stages of this manuscript.

I am the second author of the third manuscript (**Section 2.2**), which is adapted from "Dang, J.D., Josey, D.S., Lough, A.J., Li, Y., Sifate, A., Lu, Z.-H., Bender, T.P. (**2016**). *The mixed and alloyed chemical composition of chloro-(chloro)$_n$ boron subnaphthalocyanines dictates their physical properties and performance in organic photovoltaics.* J. of Mater. Chem. A, 4(24): 9566-9577."[67] with permission from the Royal Society of Chemistry

Jeremy Dang synthesized and characterized most of the boron subnaphthalocyanines (BsubNcs). I performed all device fabrication and analysis. I designed and created all the figures and wrote the device sections of the paper. Yiying Li performed UPS and wrote that section of the paper under the supervision of Professor Lu. Jeremy wrote all the other sections of the paper. Alan Lough performed X-ray diffraction on crystals that Jeremy procured via train sublimation. Alaa Sifate synthesized some of the BsubNcs. Professor Bender supervised and provided guidance throughout the research and publication stages of this manuscript.

I am the first author of the final manuscript (**Section 2.3**), which is being prepared for submission to ACS Omega. I performed all the device fabrication and analysis. Katie Sampson and I performed the initial Cl-$^{\beta}$Cl$_{2n}$BsubPc synthesis, and then Katie and Ross Phillips performed all subsequent syntheses. Siena Wong and Devon Holst conducted some additional HPLC analysis. Peicheng Li performed all the UPS characterization for the BsubPcs, under the supervision of Professor Lu. Professor Bender has supervised and provided guidance throughout the research stages and initial writing of this study.

Appendix A includes all experimental details about materials, substrates, layer deposition, and characterization.

2.1 Evaluating Thiophene Electron Donor Layers for the Rapid Assessment of Boron Subphthalocyanines as Electron Acceptors in Organic Photovoltaics; Solution or Vacuum Deposition?

In this study, the choice of a standard electron donating material is considered for pairing with boron subphthalocyanines (BsubPcs) to rapidly assess the viability of new BsubPc derivatives as

electron-accepting materials within organic photovoltaic devices (OPVs). Specifically, the effectiveness of solution-cast poly(3-hexylthiophene-2,5-dily) (P3HT) as an electron donor paired with BsubPc derivatives is evaluated relative to vacuum-deposited sexithiophene (α-6T). Using fullerene (C_{60}), chloro-boron subphthalocyanine (Cl-BsubPc), and chloro-hexachloro BsubPc (Cl-Cl_6BsubPc) as electron acceptors, the devices made with α-6T are found to outperform those with P3HT. Chloro-dodecachloro (Cl-Cl_{12}BsubPc) is also applied as an electron acceptor with α-6T. However, the two thiophene-based materials show the same performance trends. Given the preservation of these trends, either option can be recommended for assessing the potential of new BsubPc derivatives; P3HT as a solution-cast electron donor layer or α-6T as a vacuum deposited alternative.

2.1.1 Discussion

The active components of an organic photovoltaic (OPV) cell consist of multiple organic semiconductor materials. The performance of the cells hinges on how well these materials work together to absorb light and convert it into electricity. An efficiency of 4.69% has recently been achieved using BsubPc chloride (Cl-BsubPc, **Figure 2.1**) as an electron acceptor when paired with sexithiophene (α-6T, **Figure 2.1**).[79] Cl-BsubPc has also been used in cascade OPV architectures, where one or more interlayer capable of dissociating excitons at both interfaces between the electron donor and electron acceptor layers.[72]

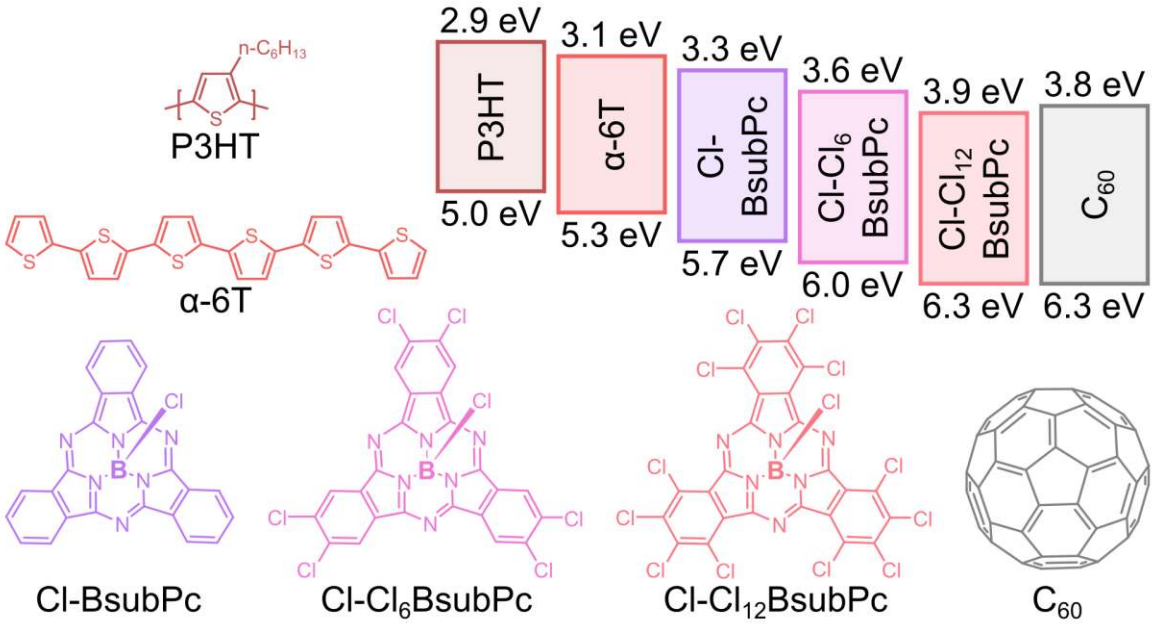

Figure 2.1. Chemical structures of poly(3-hexylthiophene-2,5-diyl) (P3HT), α-sexithiophene (α-6T), C_{60} fullerene, chloro-boron subphthalocyanine (Cl-BsubPc), chloro-hexachloro BsubPc (Cl-Cl_6BsubPc), and chloro-dodecachloro BsubPc (Cl-Cl_{12}BsubPc) and their reported frontier molecular orbital energy levels.[48, 61, 76, 90-91]

Our laboratory has been interested in the synthesis of new BsubPc derivatives for some time now.[43, 49-53, 55, 92-94] For the most part, the derivatives we have synthesized are amenable to vacuum processing and fabrication into OPVs using sublimation. For example, we have recently shown that a derivative other than Cl-BsubPc, pentafluoro phenoxy BsubPc (F_5-BsubPc), can function within a planar heterojunction OPV as either an electron acceptor or electron donor material.[44] We have also determined the electron mobility of F_5-BsubPc.[58]

When evaluating new BsubPc derivatives as electron donor materials, a pairing with fullerene (C_{60}) and comparison against the well-established Cl-BsubPc / C_{60} planar heterojunction OPV cell[48, 95] using vacuum processing entirely is a logical approach. However, as the use of a BsubPc as an electron acceptor material is a relatively new area of research[48, 71, 75, 79] there is no equally well-established OPV device structure for pairing BsubPc with an electron donor material. Pentacene, a very well established material in organic electronics,[96-98] has been demonstrated as

an effective electron donor to BsubPcs.[75] However, the process of singlet fission is known to occur in pentacene (the generation of two triplet excitons per photon absorbed). The proportion of harvested triplet excitons is known to vary significantly with slight differences in the energy of the electron acceptor lowest unoccupied molecular orbital (LUMO).[75, 99-100] Given that we want to select an electron donor that will allow for rapid screening, avoiding the variable of triplet harvesting and its impact upon short circuit current density is strongly preferred. Therefore, it would be of interest to select and establish a standard electron donor material that pairs well with a variety of BsubPcs while purposefully avoiding the singlet fission process and its considerations.

Constructing a PHJ OPV device is preferable for evaluating basic functionality of new OPV materials, as it avoids consideration of the morphological issues associated with solution fabricated bulk heterojunction OPVs.[101-102] Thus, it would also be idyllic for a standard electron donor being used for BsubPc evaluation to be solution castable thereby reducing the number of materials requiring vacuum deposition. A solution castable electron donor may be of interest to researchers with vacuum deposition systems having a limited number of sublimation sources. Alternatively, a standard electron donor that can be solution cast would also enable direct comparisons between vacuum-deposited BsubPcs and solution-processable BsubPcs within an established device structure. Finally, establishing a standard solution-cast electron donor layer may lay the groundwork for the study of new combinations of BsubPc electron acceptors and with a wide variety of electron-donating polymers available commercially and in the literature.[103]

Despite the recent establishment of α-6T as an electron donor layer for pairing with Cl-BsubPc,[79] this oligomeric thiophene is not easily solution-cast.[104] On the other hand, poly(3-hexylthiophene-2,5-dily) (P3HT, **Figure 2.1**) is an easily solution-cast polymeric thiophene.[105] P3HT has been a standard organic electronic material for a long time. P3HT has seen significant application in bulk heterojunction (BHJ) OPVs as an electron donor material paired with $PC_{61}BM$.[101-102, 106] P3HT has also been paired in bilayer structures with C_{60}, achieving efficiencies of ~0.24% to 0.33% for non-annealed devices.[107-110] Given its past success in BHJ OPVs[106] and chemical similarity to α-6T, P3HT is a good candidate to investigate as a solution-cast alternative to α-6T as an electron donor in PHJ OPVs with BsubPcs as electron acceptors.

In this section, we directly compare vacuum-deposited α-6T and solution-cast P3HT layers as electron donors when paired with relatively established BsubPc electron acceptors: Cl-BsubPc, and chloro-hexachloro BsubPc (Cl-Cl_6BsubPc, **Figure 2.1**), and chloro-dodecachloro BsubPc (Cl-Cl_{12}BsubPc, **Figure 2.1**).[48, 71, 75] C_{60} is used as a general baseline as is the pairing of α-6T and Cl-BsubPc.[79, 107] Cl-Cl_6BsubPc and Cl-Cl_{12}BsubPc were chosen to begin to explore whether α-6T is an effective electron donor for all BsubPcs or just Cl-BsubPc. We discuss the roles that crystallinity likely plays between α-6T and P3HT. We show that P3HT, while not as well-performing as α-6T, can still provide a solution-cast alternative to vacuum-deposited electron donors for the evaluation of electron acceptor BsubPc derivatives.

We began our study by replicating the work of Cnops *et al.* using α-6T (**Figure 2.1**) as a vacuum deposited electron donor paired with Cl-BsubPc (**Figure 2.1**) as an electron acceptor in a planar heterojunction device.[79] Devices were constructed with the following architecture: ITO / poly(3,4-ethylenedioxythiophene) poly(styrenesulfonate) (PEDOT:PSS) / α-6T (55 nm) / C_{60} (40 nm), Cl-BsubPc (20 nm), Cl-Cl_6BsubPc (20 nm), or Cl-Cl_{12}BsubPc (20 nm) / bathocuproine (BCP, 10 nm) / Ag (80 nm). The α-6T thickness was chosen to be close to that used by Cnops *et al*.[79] The P3HT thickness was chosen to match the thickness of α-6T. The thickness of the C_{60} and BCP layers was selected to match the thickness in the P3HT / C_{60} devices demonstrated by Stevens *et al.*,[107] allowing for direct comparisons to P3HT devices. BsubPcs thicknesses were optimized to half that of C_{60} to maximize the power conversion efficiency (PCE). Current density-voltage (J–V) characteristics (**Figure 2.2a**) and characteristic parameters (**Table 2.1**) of these devices were measured under 100 mW/cm^2 of simulated solar illumination. External quantum efficiency (EQE) measurements are shown in **Figure 2.2b**.

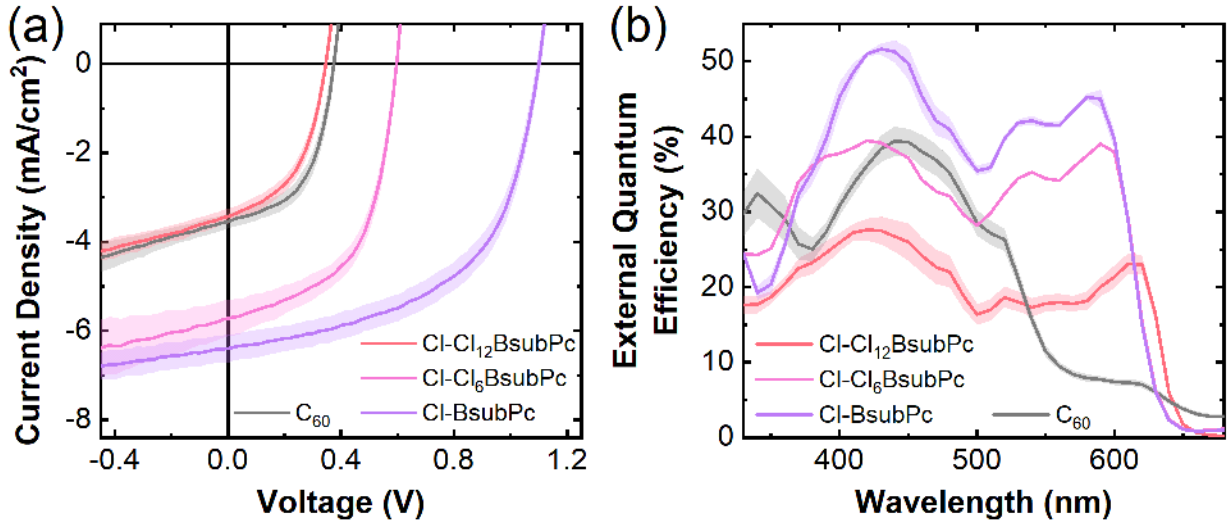

Figure 2.2. (a) J–V characteristics and (b) measured EQE spectra of α-6T / C_{60}, Cl-Cl_{12}BsubPc, Cl-Cl_6BsubPc, and Cl-BsubPc devices. Shading indicates ± one standard deviation.

Table 2.1. Average device parameters of α-6T / C_{60}, Cl-Cl_{12}BsubPc, Cl-Cl_6BsubPc, and Cl-BsubPc devices. The standard deviation (SD) is indicated in brackets next to each parameter. At least 15 devices were used to determine these values.

Acceptor	**Voc**[a] (V)	**Jsc**[b] (mA/cm^2)	**FF**[c]	**PCE**[d] (%)
C_{60}	0.38 (0.01)	3.54 (0.17)	0.53 (0.03)	0.71 (0.06)
Cl-Cl_{12}BsubPc	0.35 (0.01)	3.40 (0.17)	0.49 (0.02)	0.58 (0.05)
Cl-Cl_6BsubPc	0.60 (0.01)	5.72 (0.42)	0.56 (0.03)	1.89 (0.12)
Cl-BsubPc	1.10 (0.01)	6.40 (0.32)	0.55 (0.02)	3.86 (0.27)

[a]Open-circuit voltage. [b]Short-circuit current density. [c]Fill factor. [d]Power conversion efficiency

In our laboratory, the PCE of α-6T / C_{60} and α-6T / Cl-BsubPc devices are not quite as high as those achieved by Cnops *et al.*[79], which is mostly due to a lower measured short-circuit current (J_{SC}). We attribute the lower J_{SC} to our less extensive optimization of the layer thicknesses. Pairing Cl-Cl_6BsubPc with α-6T mostly compares well to Cl-BsubPc with just 10% less J_{SC} and the same FF, but an open-circuit voltage (V_{OC}) of about half as much. The drop in V_{OC} is even more dramatic for α-6T and Cl-Cl_{12}BsubPc pairings, which also experience significant losses in J_{SC} and FF. The V_{OC} losses are expected, considering the deeper LUMOs of Cl-Cl_6BsubPc and Cl-Cl_{12}BsubPc (**Figure 2.1**). The deeper LUMOs, together with the highest occupied molecular orbital (HOMO)

of the electron donor, is thought to be, to a first approximation, the principal determinant of the V_{OC}.[19] The Cl-Cl_{12}BsubPc OPVs exhibit much lower photocurrent contributions from both α-6T and BsubPc (**Figure 2.2b**), suggesting poor exciton dissociation or significant recombination at the electron donor / acceptor interface. Cl-Cl_6BsubPc still outperforms C_{60} as an electron acceptor paired with α-6T in all aspects; α-6T is therefore likely an excellent donor to pair with BsubPc derivatives, provided the HOMO/LUMO levels are no deeper than those of Cl-Cl_6BsubPc

We then moved to the construction of devices using solution cast P3HT as an electron donor layer. Devices using P3HT as the electron donor were constructed using the same device architecture as for the α-6T devices, replacing the vacuum-deposited α-6T with spin-coated P3HT of the same thickness: ITO / PEDOT:PSS / P3HT (55 nm) / C_{60} (40 nm) or Cl-BsubPc (20 nm) or Cl-Cl_6BsubPc (20 nm) / BCP (10 nm) / Ag (80 nm). J–V characteristics (**Figure 2.3a**) and device parameters (**Table 2.2**) of these devices were measured under 100 mW/cm^2 of simulated solar illumination. EQE measurements are shown in **Figure 2.3b**.

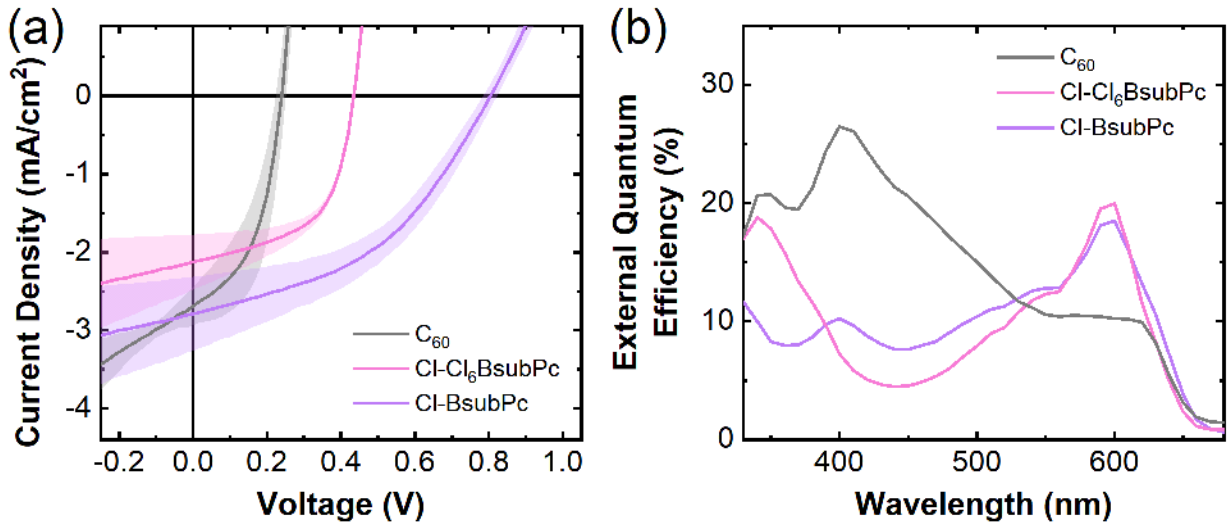

Figure 2.3. (a) J–V characteristics and (b) measured EQE spectra of P3HT / C_{60}, Cl-Cl_6BsubPc, and Cl-BsubPc devices. Shading indicates ± one standard deviation.

Table 2.2. Average device parameters of P3HT / C_{60}, Cl-Cl_6BsubPc, and Cl-BsubPc devices. The standard deviation (SD) is indicated in brackets next to each parameter. At least nine devices were used to determine these values.

Acceptor	V_{OC}[a] (V)	J_{SC}[b] (mA/cm2)	FF[c]	PCE[d] (%)
C_{60}	0.24 (0.02)	2.69 (0.24)	0.47 (0.07)	0.31 (0.09)
Cl-Cl_6BsubPc	0.44 (0.01)	2.13 (0.35)	0.57 (0.09)	0.52 (0.05)
Cl-BsubPc	0.80 (0.02)	2.79 (0.47)	0.44 (0.06)	0.98 (0.11)

[a]Open-circuit voltage. [b]Short-circuit current density. [c]Fill factor. [d]Power conversion efficiency

The performance characteristics for P3HT / C_{60} devices fabricated in our laboratory surpassed those achieved by Stevens *et al.* with non-annealed devices,[107] possibly due to incorporating a thicker P3HT layer. Pairing C_{60}, Cl-BsubPc and Cl-Cl_6BsubPc with P3HT results in the same trends in V_{OC} and PCE seen with α-6T. The fill factor (FF) for P3HT / Cl-Cl_6BsubPc devices is much better than for the P3HT / C_{60} and P3HT / Cl-BsubPc devices. The J_{SC} shows a different trend when compared with α-6T, with C_{60} having essentially the same J_{SC} as Cl-BsubPc. The EQEs suggest that the photocurrent is dominated by the electron acceptor contributions in all devices, with relatively minimal P3HT contribution. Annealing reportedly causes C_{60} to diffuse into the amorphous regions around the crystalline domains of an underlying P3HT film, increasing the J_{SC} up to 6.6 mA cm^{-2} due to the increased effective interfacial area.[107] If C_{60} slightly intermixes with P3HT during vacuum deposition, at least to a greater extent than the BsubPcs, then this would explain the higher than expected J_{SC} for C_{60} with P3HT. This idea would also be consistent with other work showing that α-6T vacuum-deposited films are polycrystalline,[111] making penetration on vacuum deposition more demanding and explaining why C_{60} might intermix with P3HT but not α-6T.

In all cases, devices made with α-6T perform better than the corresponding P3HT devices. The V_{OC}s for α-6T devices are about 30% higher, the J_{SC}s are up to 2.5 times higher, and the FF is either as good or better. The increase in V_{OC} correlates with the lower HOMO of α-6T. Crystallinity is known to have a significant impact on charge transport,[112] and α-6T films are known to have a much higher degree of crystallinity than P3HT.[111, 113] This is likely the main factor behind the

decrease in J_{SC} from α-6T to P3HT. Despite the lower performance of P3HT devices, the same trend emerges for BsubPcs as when using α-6T as the electron donor. In our opinion, this leaves open the opportunity of using solution-cast P3HT as an electron donor to evaluate new BsubPc derivatives as electron acceptors.

We have not yet investigated the effects of annealing, which has been shown to improve the performance of P3HT / C_{60} PHJ devices through crystallization of the P3HT layer[114] and blending of the P3HT / C_{60} interface.[107-108, 110] This method allows for more morphological control of the interface than co-depositing the materials from the same solution. However, for rapid screening purposes, we recommend avoiding the variables associated with morphological engineering until after the identification of viable electron acceptor candidate BsubPcs.

2.1.2 Conclusions

In summary, by pairing C_{60} and Cl-BsubPc with α-6T, we have shown that we can replicate similarly performing devices as Cnops *et al.* to use as baseline devices in our laboratory. We have demonstrated further evidence that α-6T is an appropriate electron donor to pair with BsubPc derivatives beyond Cl-BsubPc, with Cl-Cl_6BsubPc outperforming C_{60} as an electron acceptor. However, alternative electron donors should be explored for BsubPcs with deeper HOMO/LUMO levels (Cl-Cl_{12}BsubPc). Aside from a higher than expected J_{SC} for C_{60}, which is thought to be due to intermixing, we obtained the same trend for the electron acceptors when replacing the vacuum-deposited α-6T with solution-cast P3HT. The devices made with α-6T ultimately do perform much better than those made with P3HT, hypothesized to be due to the higher crystallinity in the α-6T films. We, therefore, consider α-6T to be the best electron donor for screening new BsubPcs. However, considering that the trends observed for BsubPcs in α-6T devices also held in P3HT devices, we feel P3HT is still a good solution-cast alternative to vacuum-deposited electron donors to assess the effectiveness of new BsubPc derivatives as electron acceptors.

2.2 The Mixed and Alloyed Chemical Composition of Chloro-(Chloro)$_n$ Boron Subnaphthalocyanines Dictates Their Physical Properties and Performance in Organic Photovoltaics

Chloro-boron subnaphthalocyanine (Cl-BsubNc) has recently attracted significant interest as a light-harvesting and charge transporting material in organic photovoltaics (OPVs) by enabling an 8.4% efficient planar heterojunction OPV cell.[79] Whether Cl-BsubNc is synthesized via literature methods, our in-house methods, or purchased commercially, we determined that it is actually an alloyed mixture of Cl-BsubNcs with random amounts of chlorination at the bay positions of the BsubNc structure.[67] Therefore, we will hereafter refer to Cl-BsubNc as Cl-Cl_nBsubNc. This peripheral chlorination could not be eliminated, but new synthetic processes resulted in varying amounts of peripheral chlorination. The amount of chlorination was reduced by using a new *p*-cymene process and increased by using a new nitrobenzene process.[67] This section describes the exploration of these different Cl_nBsubNc samples in OPVs. Samples with lower and higher amounts of bay position chlorination resulted in performance differences within planar heterojunction OPVs; the mixture of Cl-Cl_nBsubNc with lower amounts of chlorination produced less efficient OPVs (albeit with a higher open-circuit voltage) compared to the mixture with higher amounts of chlorination. Additionally, the sample of Cl-Cl_nBsubNc with the highest level of bay position chlorination yielded the best performing OPVs through an improved fill factor.

2.2.1 Discussion

Although recent efforts of our group[44, 75] and others[48, 61-62, 65] have shown that a variety of boron subphthalocyanines (BsubPcs) can have application in OPVs, the majority of the applications have focused on the use of the prototypical derivative chloro-BsubPc (Cl-BsubPc, **Figure 2.4**).[42] Boron subnaphthalocyanines (BsubNcs) are structurally similar to boron subphthalocyanines and, as a result of the more-extended π-conjugation system compared to BsubPc, BsubNc has an absorption that is significantly red-shifted to 686 nm in the solid-state.[115] Therefore, BsubNc can capture regions of red light for OPV applications, as has been demonstrated with the chloro-BsubNc (Cl-BsubNc, **Figure 2.4**) derivative.[21, 65, 68, 79, 115-119]

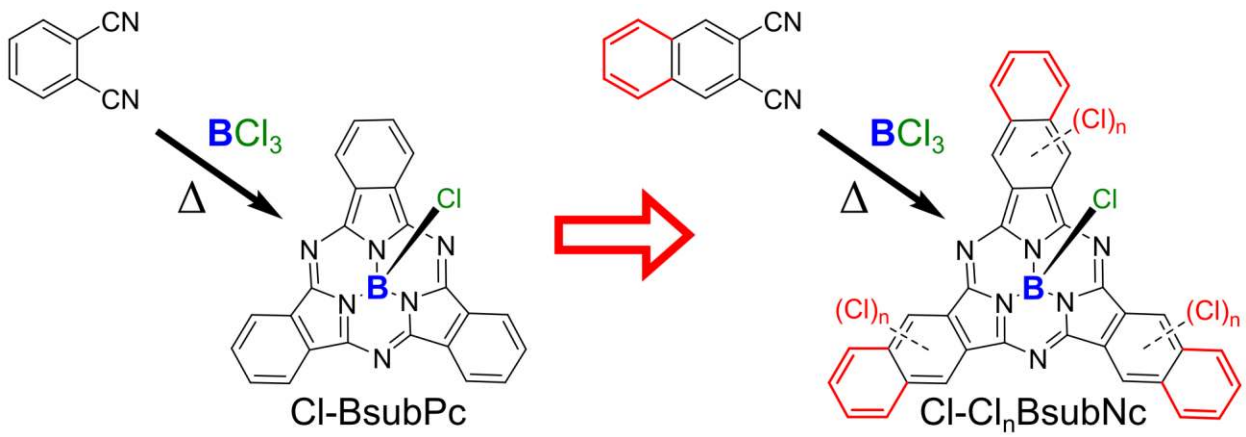

Figure 2.4. Chemical structures of boron subphthalocyanine chloride (Cl-BsubPc) and boron subnaphthalocyanine chloride with random peripheral chlorination (Cl-Cl$_n$BsubNc).

The first examples of Cl-BsubNc in OPVs showed that its substitutions for Cl-BsubPc as an electron-donating and charge generating material paired with fullerene (C_{60}) resulted in small improvements in photocurrent generation.[21, 115-116, 118] This substitution reduced the spectral overlap between the donor and acceptor but lost the photocurrent contributions in the 500-600 nm region from the Cl-BsubPc. Gommans *et al.* were the first to pair a BsubPc with Cl-BsubNc, reclaiming the BsubPc region of the spectrum but losing the blue region contributions from C_{60}.[65]

Recently, Cheyns and Cnops *et al.* demonstrated that the inclusion of Cl-BsubNc into a planar heterojunction (PHJ) OPV enables power conversion efficiencies (PCEs) as high as 6.4%[68] and 8.4%[79]. These measured efficiencies are amongst the highest achieved for PHJ OPVs. Cheyns, Cnops *et al.* show evidence that the high PCEs are attributable to the complementary absorption profiles of BsubPc and BsubNc, broadening the overall absorption range of the OPV. The 8.4% efficiency is achieved using an energy-relay cascade with a single exciton dissociating interface. Using a single dissociating interface avoids the drop in V_{OC} seen in other 3-layer OPVs where multiple dissociating interfaces are incorporated.[79]

We determined that, regardless of the synthesis and purification methods, Cl-BsubNc always consists of a mixture of Cl-BsubNc compounds with random amounts of bay-position chlorination (**Figure 2.4**).[67] Although we could not purify any of our synthetic samples to a single Cl-BsubNc compound, newly developed synthesis processes resulted in three Cl-Cl$_n$BsubNc samples with

different degrees of chlorination: p-cymene-Cl-Cl_nBsubNc (less bay-position chlorination), literature-Cl-Cl_nBsubNc (traditional amount of bay-position chlorination), and nitrobenzene-Cl-Cl_nBsubNc (more bay-position chlorination). Growth and diffraction of solid-state crystals from the literature- and nitrobenzene-Cl-Cl_nBsubNc samples demonstrate that the mixture samples form a single crystal structure and behave more like an alloy than a heterogeneous mixture. The performance of each sample was examined within a PHJ OPV to determine if there are any performance differences attributable to the differing amounts of peripheral chlorination. Given the consistency between the diffractable crystals grown via sublimation and X-ray photoelectron spectroscopy results obtained from sublimed films,[67] we were not concerned with any alteration of the chemical composition on the fabrication of PHJ OPVs. In this study, we assess the differently chlorinated Cl_nBsubNc samples in OPVs. We also incorporate the "commercial-Cl-Cl_nBsubNc" into OPVs as an additional point of comparison, which has nearly identical amounts of bay position chlorination as the literature-Cl-Cl_nBsubNc sample.

Four sets of OPV devices were therefore fabricated, pairing each sample of Cl-Cl_nBsubNc as the electron acceptor with sexithiophene (α-6T) as an electron donor, with the following device configuration: indium tin oxide (ITO) / poly(3,4-ethylenedioxythiophene):poly(styrenesulfonate) (PEDOT:PSS) / sexithiophene (α-6T, 55 nm) / Cl-Cl_nBsubNc (25 nm) / bathocuproine (BCP, 10 nm) / silver (Ag, 80 nm). These devices mimic our previous work using Cl-BsubPc paired with α-6T[89] and are consistent with and comparable to the PHJ OPVs fabricated by Cnops *et al*.[79] Current density-voltage (J–V) characteristics (**Figure 2.5a**) were measured under 100 $mW \cdot cm^{-2}$ of simulated solar illumination (AM1.5). The measured external quantum efficiency (EQE) spectra are shown in **Figure 2.5b**. Average parameters and standard deviations of at least six PHJ OPV devices are also presented (**Table 2.3**).

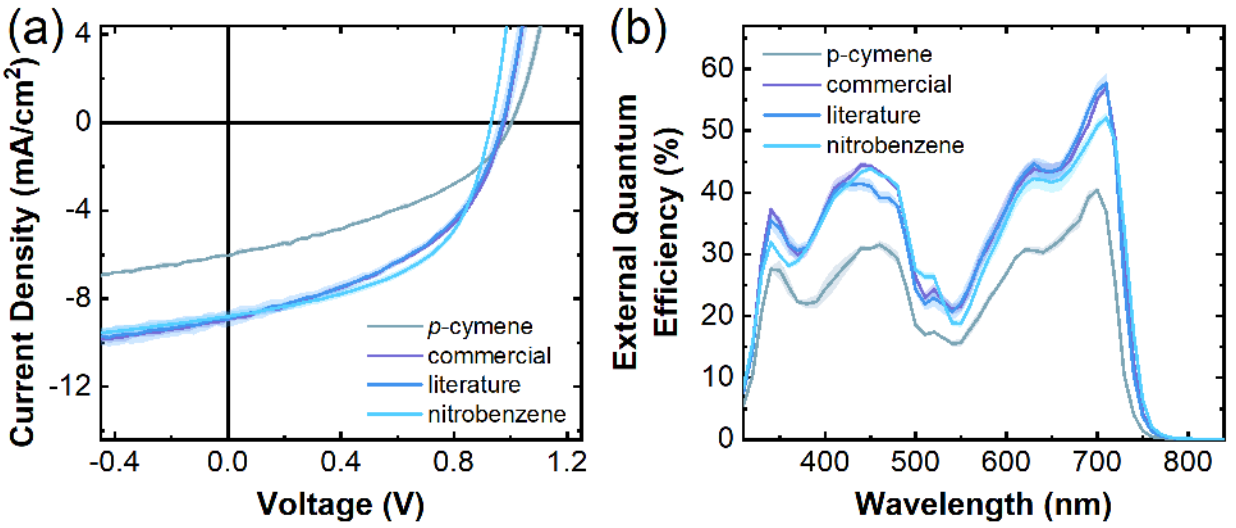

Figure 2.5. (a) J–V characteristics and (b) external quantum efficiency (EQE) spectra of PHJ OPVs of the following configuration: ITO / PEDOT:PSS / α-6T (55 nm) / Cl-Cl$_n$BsubNc (25 nm) / BCP (10 nm) / Ag (80 nm), where the Cl-Cl$_n$BsubNc layer is made of *p*-cymene-Cl-Cl$_n$BsubNc, commercial-Cl-Cl$_n$BsubNc, literature-Cl-Cl$_n$BsubNc, or nitrobenzene-Cl-Cl$_n$BsubNc. Shading indicates ± one standard deviation.

Table 2.3. Average device parameters of PHJ OPVs of the following configuration: ITO / PEDOT:PSS / α-6T (55 nm) / Cl-Cl$_n$BsubNc (25 nm) / BCP (10 nm) / Ag (80 nm), where the Cl-Cl$_n$BsubNc layer is made of *p*-cymene-Cl-Cl$_n$BsubNc, commercial-Cl-Cl$_n$BsubNc, literature-Cl-Cl$_n$BsubNc, or nitrobenzene-Cl-Cl$_n$BsubNc. The standard deviation is indicated in brackets next to each parameter. Each parameter is a result of the measurement of at least six devices.

Acceptor	**Voc**[a] (V)	**Jsc**[b] (mA/cm^2)	**FF**[c]	**PCE**[d] (%)
***p*-cymene-Cl-Cl$_n$BsubNc**	1.004 (0.009)	6.05 (0.07)	0.40 (0.01)	2.44 (0.13)
commercial-Cl-Cl$_n$BsubNc	0.976 (0.005)	8.92 (0.37)	0.45 (0.01)	3.90 (0.12)
literature-Cl-Cl$_n$BsubNc	0.972 (0.018)	8.91 (0.13)	0.46 (0.01)	3.96 (0.07)
nitrobenzene-Cl-Cl$_n$BsubNc	0.930 (0.002)	8.80 (0.19)	0.53 (0.01)	4.32 (0.11)

[a]Open-circuit voltage. [b]Short-circuit current density. [c]Fill factor. [d]Power conversion efficiency

The performances of OPVs made with literature-Cl-Cl_nBsubNc and commercial-Cl-Cl_nBsubNc samples are nearly identical. The performance of these devices fabricated in our laboratory is not quite as high as for those made by Cnops *et al*.[79], but the losses can be attributed to a less extensive optimization of the layer thicknesses undertaken in our fabrication system. Devices made with the *p*-cymene-Cl-Cl_nBsubNc (less bay position chlorination) produce significantly lower short-circuit current (J_{SC}) and fill factor (FF) compared to OPVs derived from Cl-Cl_nBsubNcs with more bay position chlorination. Conversely, a small yet statistically relevant increase in V_{OC} was observed, as was suggested by Khan *et al*.[56] Now considering nitrobenzene-Cl-Cl_nBsubNc, while we saw an equally small reduction in the V_{OC} of the PHJ OPV and a small reduction in the J_{SC}, a notable increase in the fill factor, therefore, resulted in the highest PCE. The observed small changes in V_{OC} are in line and proportional to the measured HOMO by UPS.

These results suggest that inclusion of the bay position chlorinated Cl-Cl_nBsubNc derivatives in a mixture with Cl-BsubNc improves the overall performance of the layer in OPVs. This finding is conceptually similar to the work of Fleetham *et al*. who showed an enhancement in OPV performance using a mixture of peripherally chlorinated zinc phthalocyanine (ZnPc) and pure ZnPc.[120-121]

Traditionally, impurities in organic semiconductors are believed to always act as traps, hindering device performance.[122-123] Street *et al*. have recently challenged that notion, demonstrating that different materials, specifically fullerene derivatives, can be blended together to achieve an alloying effect of their electronic properties, so long as their size allows them to easily intermix without disrupting the local order of one another.[124-125] The crystal structure of literature-Cl-Cl_nBsubNc shows co-crystallization of the different bay position chlorinated Cl-BsubNc compounds, indicating that the presence of bay position chlorination does not disrupt the local order. Therefore, an alloying effect similar to what Street *et al*.[124-125] observed for fullerenes in bulk heterojunction OPVs could be occurring. Alloying could explain why the performance of a Cl-Cl_nBsubNc mixture in OPVs is improved instead of crippled by impurity trap states. While a comparison between Cl_nBsubNc mixtures and pure Cl-BsubNc was not possible, and may never

be possible, the strong performance in OPVs utilizing "Cl-BsubNc" reported in literature may be caused by the alloying together of slightly different electronic states.

2.2.2 Conclusions

Among three Cl-Cl_nBsubNcs and a commercial sample, the photo- and electro-physical change in properties was found to translate to differing performances in PHJ OPVs when applied as an electron-accepting material paired with α-6T as an electron donor material. PHJ OPVs made from Cl-Cl_nBsubNc with lower amounts of chlorine (*p*-cymene-Cl-Cl_nBsubNc) was found to perform poorly in contrast to PHJ OPVs made from Cl-Cl_nBsubNc with higher/highest amounts of chlorination (nitrobenzene-Cl-Cl_nBsubNc). Ultimately nitrobenzene-Cl-Cl_nBsubPc was found to perform moderately better than Cl-Cl_nBsubNc made via the literature procedure (literature-Cl-Cl_nBsubNc) or a commercially-available Cl-Cl_nBsubNc sample (commercial-Cl-Cl_nBsubNc). However, we feel these rather small differences do not call into question the 8.4% efficient PHJ OPV results of Cnops *et al.*,[79] rather it offers a cautionary note as to the actual chemical composition of the "Cl-BsubNc" used previously in their study, other studies presented in the literature, and any moving forward.

2.3 Intentional Mixtures of Peripherally Chlorinated Boron Subphthalocyanines and Their Application in Organic Photovoltaics

Using mixtures of materials in organic photovoltaics (OPVs) has traditionally been avoided due to the assumption that one of the materials will act as a charge carrier trap. From this perspective, the high performance of boron subnaphthalocyanine (BsubNc) in OPVs was surprising. BsubNc was discovered to be a mixture of differently chlorinated BsubNc derivatives, termed "Cl_nBsubNc". Rather than act as traps, the derivatives form an electronically alloyed material. The high performance of Cl_nBsubNc suggests that a similar BsubPc mixture may also yield a higher performance material. BsubPc mixtures are synthesized by intentionally mixing different phthalonitriles to produce a mixture of BsubPcs with varying amounts of peripheral chlorination. The mixtures are characterized by high-performance liquid chromatography and ultraviolet

photoelectron spectroscopy, then assessed within OPVs as electron acceptors. The application of such mixtures in OPVs is validated, and promising future pathways are outlined.

2.3.1 Discussion

The performance of organic photovoltaics (OPVs) and the purity of materials comprising those OPVs are generally considered to have a direct relationship: higher purity materials result in higher performance OPVs.[122-123] Impurities within the organic layers typically have undesirable impacts on OPVs, such as trapping charge carriers or excitons and reducing the overall current extracted from the device.[126-127] Small molecules like oxygen, water or residual solvent molecules are common charge-trapping impurities, and OPVs are typically fabricated under inert gas or vacuum conditions to minimize the introduction of such molecules.[128-130] Larger organic molecules impurities, such as synthesis byproducts or residual starting materials, can also affect OPV performance.[131] Depending on the molecular structure, these larger impurities can act as traps, interfere with charge transfer, or dilute the concentration of target molecules in the layer.[132] Significant effort is usually made to ensure only the target molecule remains in the material, with the initially synthesized batch undergoing various purification steps like column chromatography, Soxhlet extraction, or multiple train sublimations.[133-134]

The use of dopants is an exception to targeting layers that consist of only one type of molecule. Dopants are molecules that are intentionally added to a layer of host molecules and are commonly used in organic light-emitting diodes (OLEDs).[135] In OLEDs, dopants are applied as emitters that take advantage of their inherent charge trapping to collect holes and electrons from the host, forming excitons and emitting that excitonic energy as light. Dopants are less commonly found in OPVs but have been applied to encourage long-range exciton transfer to another layer and to convert singlet excitons to triplet excitons for longer exciton diffusion lengths.[57, 136] Dopant and host molecules are typically quite different, each design to perform different roles.

Mixtures of organic molecules with similar structures into the same layer were traditionally always avoided. This notion was challenged by Street et al., who demonstrated an electronic alloying effect in mixtures of different materials.[124-125] In a mixture of fullerene derivatives, the OPV

parameters interpolate based on the ratio of each derivative, so long as the different fullerenes sizes did not disrupt the crystallinity of one another. Fleetham et al. then demonstrated that mixing partially chlorinated zinc phthalocyanine (ZnPc) with pure ZnPc can enhance open-circuit voltage (V_{OC}).[120-121] Analogously, we discovered that boron subnaphthalocyanine (BsubNc) consists not of a single pure compound but a mixture of compounds with different degrees of peripheral chlorination (Cl_nBsubNc).[67] Surprisingly, the presence of Cl_nBsubNc derivatives with more chlorination was found to result in better OPV performance compared to less chlorination. However, a compositionally pure Cl-BsubNc could not be produced for comparison. Boron subphthalocyanines (BsubPcs) and Cl_nBsubNcs are structurally similar, but compositionally pure BsubPc derivatives can be readily synthesized. The improved performance of Cl_nBsubNc mixtures suggests that "Cl_nBsubPc" mixtures may achieve similar enhancements in performance.

In this study, varied ratios of differently chlorinated phthalonitriles are used to synthesize BsubPc mixtures. The BsubPc mixtures were characterized by high-performance liquid chromatography (HPLC), mass spectroscopy, and ultraviolet photoelectron spectroscopy (UPS). OPVs were fabricated using BsubPc mixtures that had similar amounts of peripheral chlorination as the compositionally pure chloro-BsubPc (Cl-BsubPc) and chloro-hexachloro BsubPc (Cl-$^{\beta}Cl_6$BsubPc or Cl-Cl_6BsubPc, **Figure 2.6**). We examined correlations between OPV voltages, chemical composition, and UPS data. We also demonstrated a voltage tunability that has been de-quantized, due to the ability to synthesize mixtures at any desired ratio of phthalonitriles. The OPV performances will be used to direct future applications of new BsubPc mixtures.

BsubPcs mixtures were synthesized according to previously reported synthesis methods for Cl-BsubPc[137] and Cl-$^{\beta}Cl_6$BsubPc[54], but using mixtures of phthalonitrile:4,5-dichlorophthalonitrile or 4,5-dichlorophthalonitrile:3,4,5,6-tetrachlorophthalonitrile as the starting materials. This procedure produces a mixture of four differently chlorinated BsubPcs, where the relative amounts of each BsubPc are dependent on the ratio of phthalonitriles (**Figure 2.6**). The starting materials determine the nomenclature assigned to each mixture: phthalonitrile and 4,5-dichlorophthalonitrile make "Cl-$^{\beta}Cl_{2n}$BsubPc", and 4,5-dichlorophthalonitrile and 3,4,5,6-tetrachlorophthalonitrile make "Cl-$^{\beta}Cl_6{}^{\alpha}Cl_{2n}$BsubPc", where n = 0, 1, 2, and 3 (see **Table B.1** for a complete list). The alpha

positions around phthalonitrile are the 3,6 positions, and the beta positions are the 4,5 positions. The ratio of starting materials is indicated in square brackets following the name, with the amount of the least chlorinated phthalonitrile listed first (ex. a BsubPc mixture synthesized using 80% 4,5-dichlorophthalonitrile and 20% 3,4,5,6-tetrachlorophthalonitrile is: Cl-$^{\beta}Cl_6{}^{\alpha}Cl_{2n}$BsubPc [80:20]).

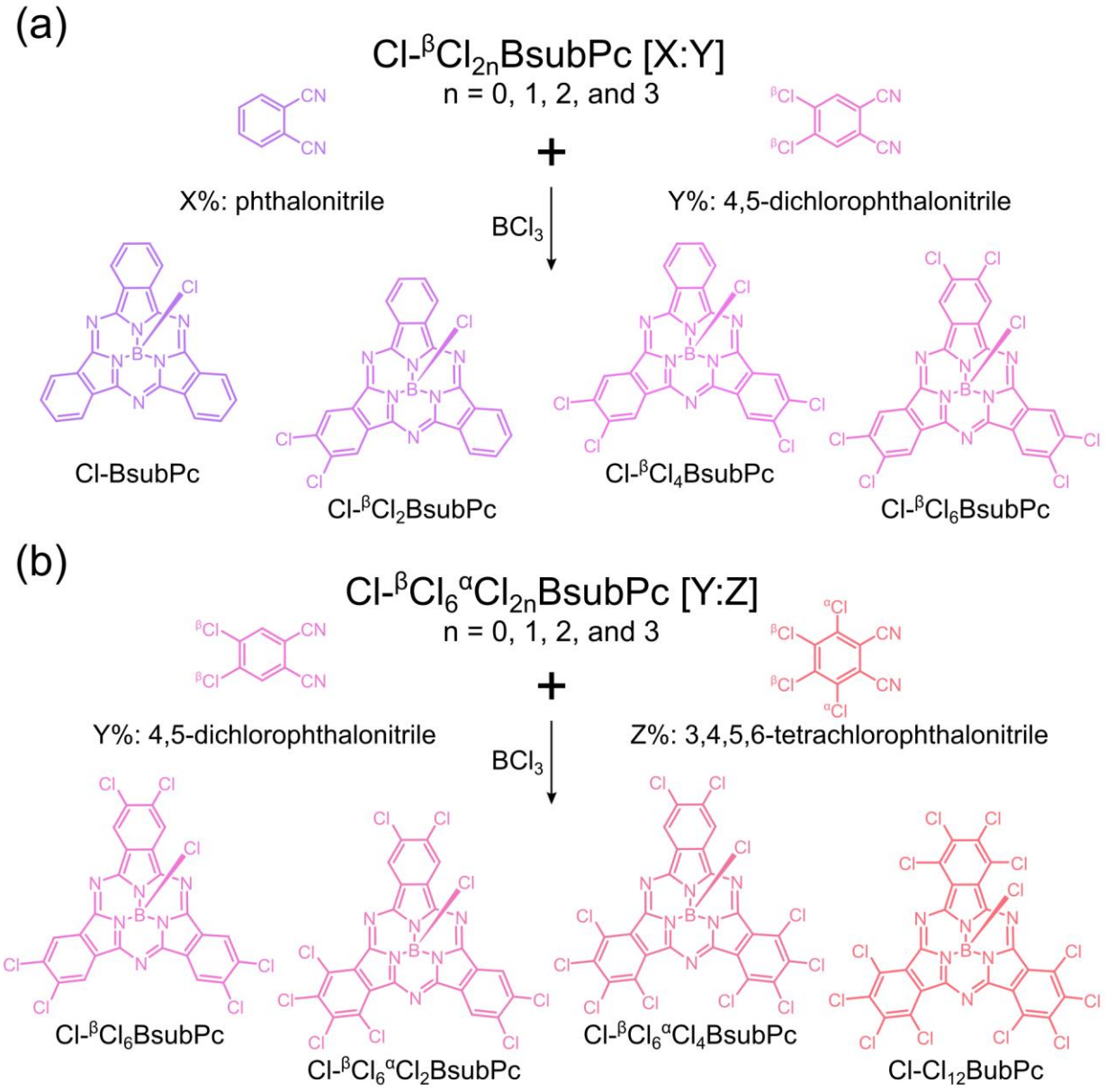

Figure 2.6. Composition of chlorinated BsubPc mixtures synthesized using (a) phthalonitrile and 4,5-dichlorophthalonitrile, and (b) 4,5-dichlorophthalonitrile and 3,4,5,6-tetrachlorophthalonitrile.

BsubPc mixtures were synthesized with ratios of 80:20, 60:40, 40:60, 20:80 phthalonitrile:4,5-dichlorophthalonitrile for Cl-$^{\beta}Cl_{2n}$BsubPc, and a ratio 80:20 4,5-dichlorophthalonitrile:3,4,5,6-tetrachlorophthalonitrile for Cl-$^{\beta}Cl_6{}^{\alpha}Cl_{2n}$BsubPc. The synthesis and ensuing purifications of Cl-$^{\beta}Cl_6{}^{\alpha}Cl_{2n}$BsubPcs with higher ratios of 3,4,5,6-tetrachlorophthalonitrile were too low yielding to be considered in this study. BsubPc mixtures synthesized in this way can contain up to four chlorinated species, but the amount of each species depends on the ratio of phthalonitriles. Composition of each mixture (**Figure 2.7**) was quantified using HPLC analysis of the crude and sublimed materials, and vacuum-deposited films. The average number of peripheral beta-chlorines and alpha-chlorines were calculated from these HPLC measurements (**Table 2.4**).

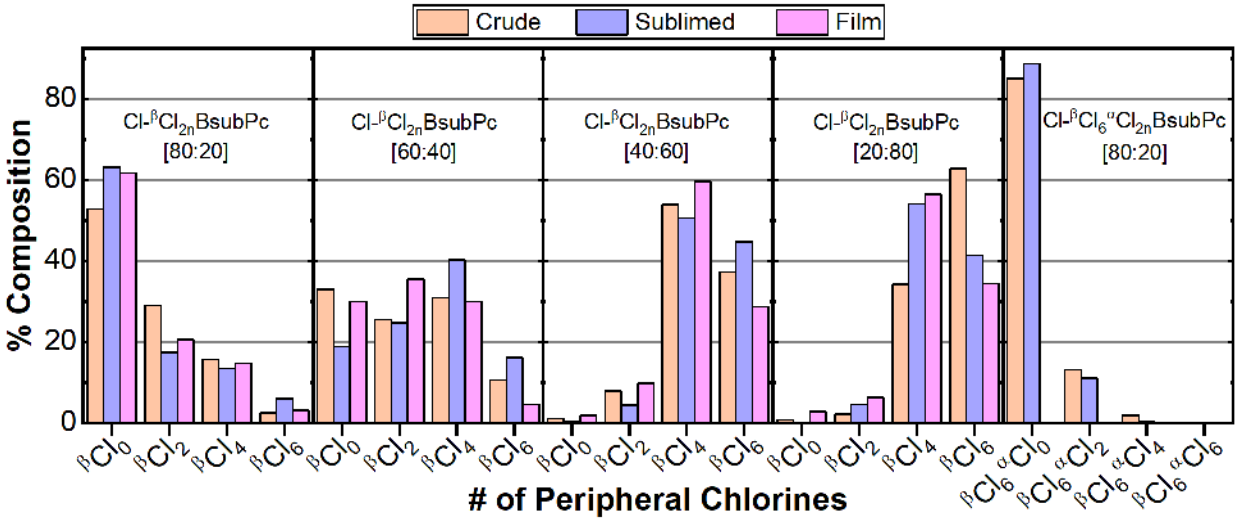

Figure 2.7. Percent compositions of the four BsubPc derivatives in each BsubPc mixture as measured by HPLC at crude, sublimed, and film stages of processing. The composition of Cl-$^{\beta}Cl_6{}^{\alpha}Cl_{2n}$BsubPc [80:20] was not measured as a film.

Table 2.4. The average number of peripheral beta-position and alpha-position chlorines in each BsubPc mixture at each stage of synthesis and purification processing.

BsubPc	Starting Material		Crude		Sublimed		Film	
	# $^{\beta}$Cls	# $^{\alpha}$Cls	# $^{\beta}$Cls	# $^{\alpha}$Cls	# $^{\beta}$Cls	# $^{\alpha}$Cls	# $^{\beta}$Cls	# $^{\alpha}$Cls
Cl-BsubPc	0	0	0	0	0	0	0	0
Cl-$^{\beta}Cl_{2n}$BsubPc [80:20]	1.20	0	1.36	0	1.25	0	1.19	0
Cl-$^{\beta}Cl_{2n}$BsubPc [60:40]	2.40	0	2.39	0	3.08	0	2.18	0

Cl-$^{\beta}Cl_{2n}$BsubPc [40:60]	3.60	0	4.55	0	4.80	0	4.30	0
Cl-$^{\beta}Cl_{2n}$BsubPc [20:80]	4.80	0	5.18	0	4.74	0	4.45	0
Cl-$^{\beta}Cl_6$BsubPc	6	0	6	0	6	0	6	0
Cl-$^{\beta}Cl_6{}^{\alpha}Cl_{2n}$BsubPc [80:20]	6	1.20	6	0.34	6	0.23	6	-

The composition of BsubPc mixtures skew toward the Cl-BsubPc derivative when made with a higher ratio of phthalonitrile, and mixtures made with a higher ratio of 4,5-dichlorophthalonitrile skew towards the Cl-$^{\beta}Cl_6$BsubPc derivative. Relative to the starting materials, the average number of peripheral chlorines in the crude BsubPc mixtures is approximately constant for Cl-$^{\beta}Cl_{2n}$BsubPc [80:20] and [60:40], increases for Cl-$^{\beta}Cl_{2n}$BsubPc [40:60] and [20:80], and decreases for Cl-$^{\beta}Cl_6{}^{\alpha}Cl_{2n}$BsubPc [80:20]. In general, proportionally more of the 4,5-dichlorophthalonitrile incorporates into the synthesized product than phthalonitrile or 3,4,5,6-tetrachlorophthalonitrile. These proportions suggest that the BsubPc reaction is more favourable with 4,5-dichlorophthalonitrile than the other phthalonitriles. Subsequent purification processes reduce the amount of peripheral chlorination in all cases except for a slight increase observed in the Cl-$^{\beta}Cl_{2n}$BsubPc [40:60] mixture after train sublimation. Molecules with higher molecular weights are generally more difficult to sublime, supporting the observed reduction upon sublimation of BsubPcs with more peripheral chlorination.

The mixtures were analyzed by UPS in three separate experiments, with Cl-$^{\beta}Cl_6$BsubPc and Cl-$^{\beta}Cl_{2n}$BsubPc [20:80] each rerun as inter-experiment controls. These controls were used to slightly adjust each set of measurements for plotting the UPS spectra together (**Figure 2.8**). The secondary electron cut-off and valence band regions of the UPS spectra are used to calculate work function and the highest occupied molecular orbital (HOMO) with respect to the Fermi energy level (E_F, **Table 2.5**). The sum of the work function and HOMO-E_F is equal to the ionization energy (IE, **Table 2.5**), which is equivalent to the HOMO.

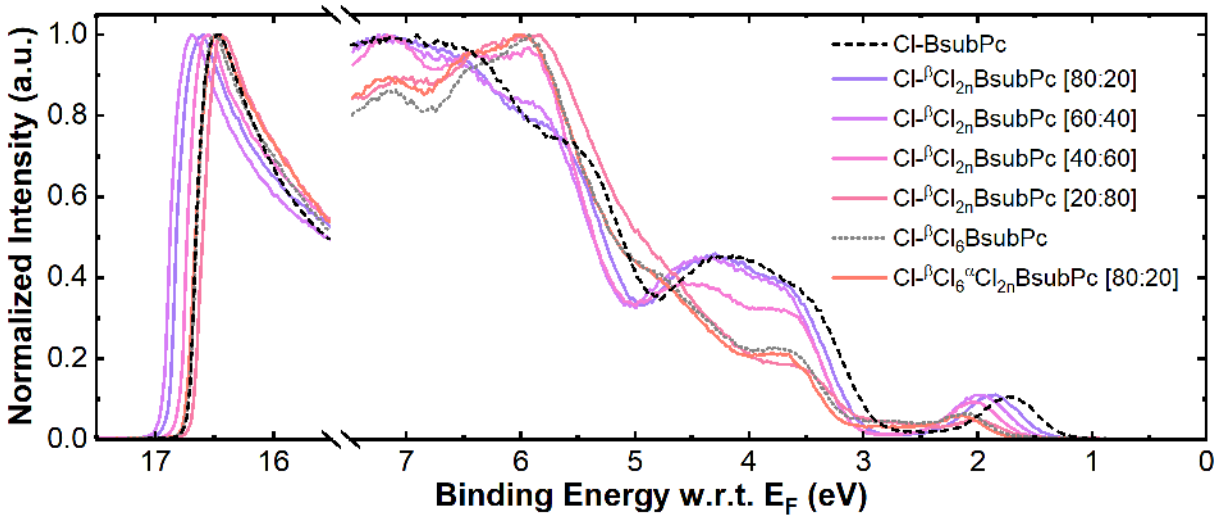

Figure 2.8. Ultraviolet photoelectron spectroscopy (UPS) He Iα ($h\nu$ = 21.22 eV) spectra of: Cl-BsubPc, Cl-$^{\beta}Cl_{2n}$BsubPc [80:20], Cl-$^{\beta}Cl_{2n}$BsubPc [60:40], Cl-$^{\beta}Cl_{2n}$BsubPc [40:60], Cl-$^{\beta}Cl_{2n}$BsubPc [20:80], Cl-$^{\beta}Cl_6$BsubPc, Cl-$^{\beta}Cl_6{}^{\alpha}Cl_{2n}$BsubPc [80:20]. Secondary electron cut-off region shown on the left (17.5 – 15.5 eV), highest occupied molecular orbital (HOMO) regions shown on the right (7.5 – 0 eV). Measurements were performed in three experiments (**Table 2.5**) and plotted together using the HOMO values as controls.

Table 2.5. Ultraviolet photoelectron spectroscopy (UPS) characteristics of the BsubPc mixtures. Measurements were performed in three experiments, with Cl-$^{\beta}Cl_6$BsubPc and Cl-$^{\beta}Cl_{2n}$BsubPc [20:80] measured twice as inter-experiment controls.

Experiment	BsubPc	WF[a] (eV)	HOMO-E_F[b] (eV)	IE[c] (eV)
1	Cl-BsubPc	4.38	1.38	5.76
1	Cl-$^{\beta}Cl_6$BsubPc	4.45	1.85	6.30
2	Cl-$^{\beta}Cl_{2n}$BsubPc [80:20]	4.40	1.34	5.74
2	Cl-$^{\beta}Cl_{2n}$BsubPc [60:40]	4.35	1.44	5.79
2	Cl-$^{\beta}Cl_{2n}$BsubPc [40:60]	4.50	1.52	6.02
2	Cl-$^{\beta}Cl_{2n}$BsubPc [20:80]	4.47	1.55	6.02
3	Cl-$^{\beta}Cl_{2n}$BsubPc [20:80]	4.53	1.62	6.15
3	Cl-$^{\beta}Cl_6$BsubPc	4.50	1.73	6.23
3	Cl-$^{\beta}Cl_6{}^{\alpha}Cl_{2n}$BsubPc [80:20]	4.47	1.77	6.24

[a]Work Function. [b]Highest Occupied Molecular Orbital (HOMO) with respect to the Fermi energy level. [c]Ionization Energy (IE = WF + HOMO-Fermi)

The materials repeated in separate experiments demonstrate a small degree of variability, which has been controlled for in **Figure 2.8** based on the HOMO-E_F measurements. The HOMO-E_F, WF, and IE of the compositionally pure materials (Cl-BsubPc and Cl-$^{\beta}Cl_6$BsubPc) all increase with the number of peripheral chlorines. For the mixtures, this trend only holds for the HOMO-E_F and IE. Any correlation between WF and peripheral chlorines in the mixtures is too subtle, with too much measurement variability to extract a trend. WF measurements are highly surface sensitive, so this WF variability may imply that vacuum-deposited mixtures have a uniquely variable surface composition or roughness. Given that IE is the sum of HOMO-E_F and WF, the WF variability introduces some noise into the correlation between peripheral chlorination and IE. The bandgap (the difference between the IE, or HOMO, and the lowest unoccupied molecular orbital, LUMO) is assumed to remain constant across each of these materials, which means any changes in HOMO are considered to correlate to changes in LUMO directly.

OPVs were fabricated to explore the mixtures with compositions closest to Cl-BsubPc and Cl-$^{\beta}Cl_6$BsubPc: Cl-$^{\beta}Cl_{2n}$BsubPc [80:20], Cl-$^{\beta}Cl_{2n}$BsubPc [20:80] and Cl-$^{\beta}Cl_{2n+6}$BsubPc [80:20]. The BsubPcs were paired with α-6T (**Figure 2.9**, **Table 2.6**), following the established procedure for screening the performance of BsubPcs as electron acceptors in OPVs.

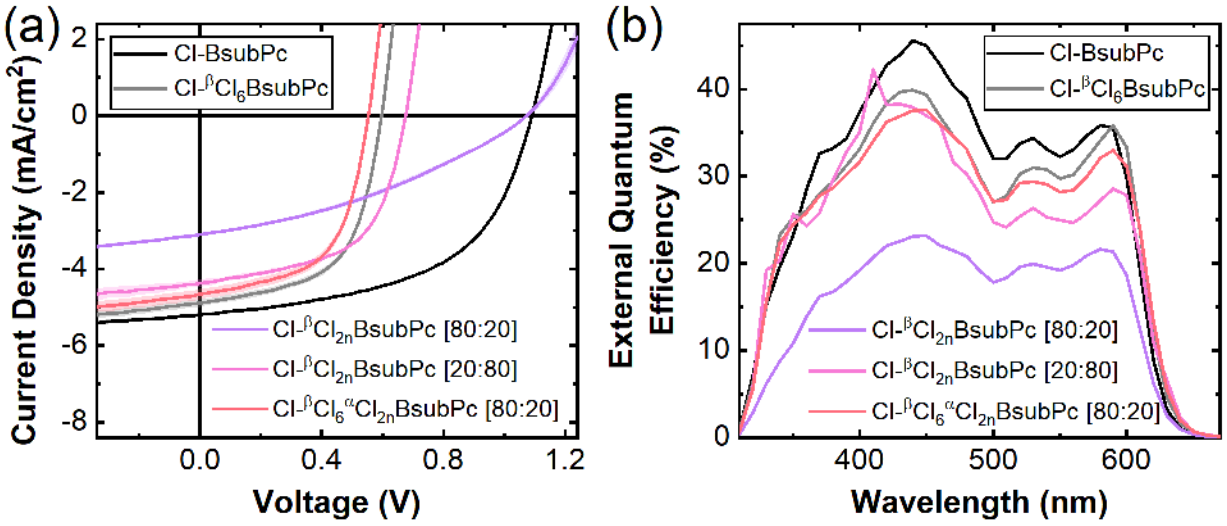

Figure 2.9. (a) J–V characteristics and (b) measured EQE spectra of α-6T / Cl-BsubPc, Cl-Cl_6BsubPc, Cl-$^{\beta}Cl_{2n}$BsubPc [80:20], Cl-$^{\beta}Cl_{2n}$BsubPc [20:80], and Cl-$^{\beta}Cl_6{}^{\alpha}Cl_{2n}$BsubPc [80:20]. Shading indicates ± one standard deviation.

Table 2.6. Average device parameters of α-6T / Cl-BsubPc, Cl-Cl_6BsubPc, Cl-$^{\beta}Cl_{2n}$BsubPc [80:20], Cl-$^{\beta}Cl_{2n}$BsubPc [20:80], and Cl-$^{\beta}Cl_6{}^{\alpha}Cl_{2n}$BsubPc [80:20]. The standard deviation (SD) is indicated in brackets next to each parameter.

Acceptor	**V_{OC}[a]** (V)	**J_{SC}[b]** (mA/cm^2)	**FF[c]**	**PCE[d]** (%)
Cl-BsubPc	1.091 (0.002)	5.19 (0.04)	0.54 (0.01)	3.07 (0.03)
Cl-$^{\beta}Cl_{2n}$BsubPc [80:20]	1.074 (0.009)	3.10 (0.04)	0.35 (0.01)	1.18 (0.04)
Cl-$^{\beta}Cl_{2n}$BsubPc [20:80]	0.675 (0.003)	4.37 (0.09)	0.57 (0.01)	1.68 (0.02)
Cl-$^{\beta}Cl_6$BsubPc	0.596 (0.002)	4.89 (0.10)	0.58 (0.01)	1.70 (0.04)
Cl-$^{\beta}Cl_6{}^{\alpha}Cl_{2n}$BsubPc [80:20]	0.553 (0.002)	4.66 (0.14)	0.57 (0.01)	1.48 (0.05)

[a]Open-circuit voltage. [b]Short-circuit current density. [c]Fill factor. [d]Power conversion efficiency

An apparent trend of decreasing V_{OC}s with increased peripheral chlorination of the BsubPc is observed, consistent with previous reports with compositionally pure BsubPcs. The observation of the same trend for mixtures indicates that an electronic alloying effect is occurring like the one observed for Cl_nBsubNc. If electronic alloying did not occur, a V_{OC} approximately pinned to the lowest level would have been expected instead of interpolation. Given their application as electron acceptors, the decreases in V_{OC} are consistent with deeper LUMOs with increased peripheral

chlorination. Cl-$^{\beta}Cl_{2n}$BsubPc [80:20] and Cl-$^{\beta}Cl_6{}^{\alpha}Cl_{2n}$BsubPc [80:20] both resulted in OPVs with lower performance across all OPV device characteristics compared to the closest compositionally pure BsubPc (Cl-BsubPc and Cl-$^{\beta}Cl_6$BsubPc, respectively). However, Cl-$^{\beta}Cl_{2n}$BsubPc [20:80] exhibited approximately equivalent performance compared to Cl-$^{\beta}Cl_6$BsubPc with a similar fill factor (FF), higher V_{OC}, and proportionally lower short-circuit current (J_{SC}). This type of trade-off between V_{OC} and J_{SC} is consistent with a change in energy offset between the HOMO of the electron donor and the LUMO of the electron acceptor.

The distinct performance differences between the 80:20 ratios and the 20:80 ratio can be explained based on their composition and their application as an electron acceptor. The 80:20 ratio mixtures consist mostly of shallow energy level BsubPc derivatives. The minority derivatives are unlikely to participate in electronic alloying, with HOMO/LUMO levels that are much deeper than the majority derivatives. During electron transport through the mixture, the minority derivatives with deep energy levels act as traps, significantly reducing the J_{SC} and potentially creating a charge imbalance that could harm the FF. The reduction in performance is more significant for the Cl-$^{\beta}Cl_{2n}$BsubPc [80:20] mixture, likely because that mixture has a higher concentration of minority derivatives. For Cl-$^{\beta}Cl_{2n}$BsubPc [20:80], the minority derivatives have much shallower HOMO/LUMO levels. Though the shallow energy levels of the minority derivatives present in the layer are unable to participate in charge transport through electronic alloying, they are also unable to act as electron traps. This trend should reverse if applying the mixtures as electron donors, with the 80:20 ratios no longer containing charge trapping derivatives. Given the similar OPV performances of Cl-$^{\beta}Cl_{2n}$BsubPc [20:80] and Cl-$^{\beta}Cl_6$BsubPc, the application of BsubPc mixtures in OPVs appears to be promising for energy level tuning in OPVs.

It would be convenient if the OPV V_{OC}s could be predicted based on a relatively quick HPLC analysis of the material composition rather than UPS analysis. The ability to rely on a direct correlation between V_{OC} and composition would also facilitate the targeting of mixtures with specifically tuned energy levels. UPS analysis may also be unreliable for predicting the HOMO values of mixtures due to the WF variability. The V_{OC}s measured in the OPVs of this study are compared to the UPS calculated IE/HOMO. Another comparison between the HOMO-E_F values

and the V_{OC}s eliminates the WF measurement variability. Finally, the OPV V_{OC}s are compared to chemical composition, in terms of the average number of peripheral chlorines in the sublimed mixtures (**Figure 2.10**). A coefficient of determination (R^2) is calculated, and a linear regression is plotted for each comparison.

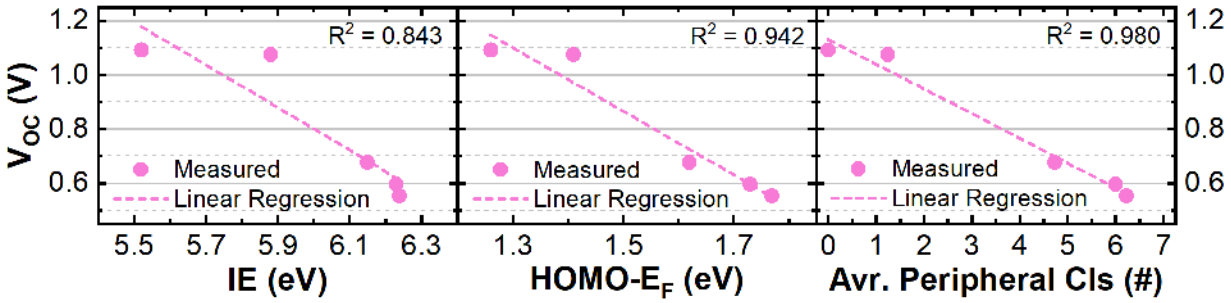

Figure 2.10. Correlations between open-circuit voltage (V_{OC}) vs ionization energy (IE, left), V_{OC} vs HOMO with respect to the Fermi energy level (HOMO-Fermi, middle), and V_{OC} vs the average number of peripheral chlorines in each mixture (right). The coefficient of determination (R^2) of each correlation is shown in the top right corners.

With the variability of the WF measurement incorporated into the IE calculation, the correlation of V_{OC} vs IE is the weakest of the three comparisons. The correlation improves from an R^2 of 0.84 to 0.94 by eliminating the WF variability and comparing HOMO-E_F directly to the V_{OC}. A less variable mixture WF measurement may enhance the correlation between V_{OC} and IE but achieving such a precise measurement may be unnecessary. The number of peripheral chlorines has the strongest correlation with V_{OC}, resulting in an R^2 value of 0.98. Such a strong correlation between composition and V_{OC} is promising for the predictive value of HPLC analysis of mixtures.

2.3.2 Conclusions

The OPV applications of intentionally mixed materials have been validated with a mixture demonstrating approximately the same OPV performance as a compositionally pure material. Interpolated V_{OC}s instead of pinned V_{OC}s across the different mixture ratios indicate that electronic alloying occurs between at least some of the derivatives in the BsubPc mixtures, analogous to Cl_nBsubNc. However, the design of intentional BsubPc mixtures must prevent minority derivatives from acting as traps. Avoiding minority derivative traps can be achieved by choosing

an application where the energy levels of the minority carriers too shallow to trap electrons or too deep trap holes. Alternatively, the development of singly or triply chlorinated phthalonitriles could produce BsubPc mixtures with tighter electronic alloys, enabling all derivatives to participate in the alloying. The tuning of alloyed mixture energy levels can be much more precise than for compositionally pure materials. When the same molecule comprises a material, energy level tuning is limited to the quantized number of substituents that can be added or removed from that molecule. The tuning precision limit of alloyed mixtures is the ratio that can be measured out during synthesis. Variability in WF reduces the reliability of UPS measurements to predict and target a specific energy level tuning, but chemical composition can be used instead because it is shown to correlate better to the corresponding V_{OC}s in an OPV. Future studies will investigate BsubPc mixtures with deeper HOMO/LUMO levels, for applications in triplet harvesting other electron donor pairings.

Chapter 3
Axial Substituents

In this chapter, I examine the influence of axial substituents on the time-zero performance of BsubPcs in OPVs. This chapter is adapted from my contributions to three published manuscripts and one manuscript in preparation for submission to ACS Applied Materials & Interfaces. I am a co-first author of the first manuscript (**Section 3.1**), which is adapted from "*Bonnier, C., *Josey, D.S., Bender, T.P. (**2015**). *Aryl-substituted boron-subphthalocyanine and their application in organic photovoltaics.* Aust. J. Chem., 68(11): 1750-1758. *co-first authors"[138].

I performed all the device fabrication and data analysis for this manuscript and wrote the sections related to the device work. The other co-first author, Catherine Bonnier, synthesized and purified all the phenyl-BsubPc compounds, performed all analytic characterization and wrote the synthetic and chemical analysis component. Professor Bender supervised and compiled the synthetic and chemical analysis components into the final manuscript during submission.

I am the second author of the second manuscript (**Section 3.2**), which is adapted with permission from "Sampson, K.L., Josey, D.S., Li, Y., Virdo, J.D., Lu, Z.-H., Bender, T.P. (**2018**). *Ability to Fine-Tune the Electronic Properties and Open-Circuit Voltage of Phenoxy-Boron Subphthalocyanines through Meta-Fluorination of the Axial Substituent.* J. Phys. Chem. C., 122(2): 1091-1102."[139] Copyright 2018 American Chemical Society.

I performed all device fabrication and data analysis for this manuscript and wrote the sections related to the device work. Yiying Li performed the UPS experiments under the supervision of Professor Lu. Jessica Virdo achieved an X-ray diffractable crystal of $3F_1PhO$-BsubPc. Professor Bender supervised and provided guidance throughout the research and publication stages of this manuscript. The first author, Katie Sampson, edited some of my device sections and performed all other experiments, analysis, and writing for this manuscript.

I am the second author of the third manuscript (**Section 3.3**), which is adapted with permission from "Dang, J.D., **Josey, D.S.**, Dang, M.T., Bender, T.P. (**2018**). *Phenoxy-(chloro)$_n$ boron subnaphthalocyanines; alloyed mixture, electron-accepting functionality, enhanced solubility for*

bulk heterojunction organic photovoltaics. ACS Omega, 3(2): 2093-2103."[140]

Jeremy Dang performed all the synthesis and chemical characterization and wrote that section of the manuscript. I completed the planar heterojunction (PHJ) device fabrication, device analysis, wrote the PHJ device sections of the manuscript and designed and created all the figures. Minh-Trung Dang performed the device fabrication of the bulk heterojunction (BHJ) and wrote the initial draft of the BHJ section of the manuscript. In addition to supervising, Professor Bender also revised the BHJ section and compiled the different sections of the manuscript together during publication.

I am the first author of the final manuscript (**Section 3.4**), which is being prepared for submission to ACS Applied Materials & Interfaces. Jessica Virdo performed all the synthesis and purification, crystal growth and analysis, Fourier-transform infrared spectroscopy, AFM, and made most of the OPV devices pairing the *m*-XPhO-BsubPcs as electron donors with fullerene. Thomas Howells fabricated some *m*-XPhO-BsubPc / fullerene OPV devices, under the supervision of Professor Jones. I developed the interlayer halogen bonding hypothesis, fabricated many additional OPVs sets, and wrote the manuscript. Professor Bender supervised and provided guidance throughout the research and writing of this thesis section and manuscript.

Appendix A includes all experimental details about materials, substrates, layer deposition, and characterization.

3.1 Aryl-Substituted Boron Subphthalocyanines in Organic Photovoltaics

A family of three axial aryl-substituted boron subphthalocyanine (BsubPc) derivatives bearing a hydrido, methyl, or fluoro substituent at the *para* position of the aryl were synthesized.[138] On incorporation of these derivatives into organic photovoltaic (OPV) devices, the methyl and fluoro derivatives produced similar results. Both derivatives, however, were significantly outperformed by the hydrido derivative. The uniqueness of the hydrido derivative is only realized once incorporated into OPVs as it shares the same basic physical properties as the other derivatives.

Given these findings, we identify the hydrido derivative as the aryl-BsubPc with the most promise for future work in OPVs.

3.1.1 Discussion

In this section, we revisit an understudied class of BsubPcs with an aryl axial substituent, incorporating them directly into photovoltaic cells. The resulting cells demonstrate the high potential of this class of BsubPcs within this area. Three of the aryl-BsubPcs, i.e. phenyl-BsubPc, 4-tolyl-BsubPc, and 4-fluorophenyl-BsubPc (**Figure 3.1**) were selected to be examined further in OPVs as electron donors and electron acceptors. These three aryl-BsubPcs were selected for the following reasons: (1) they all have robust reduction electrochemistry; (2) phenyl-, and 4-tolyl-BsubPc have similar solid-state arrangements; (3) phenyl-, and 4-tolyl-BsubPc differ in the presence of a mild electron-donating group (CH_3) in the *para* position of the aryl moiety; and (4) 4-fluorophenyl-BsubPc has a very different solid-state arrangement and has a mild electron-withdrawing group (F) in the *para* position of the aryl moiety.[138]

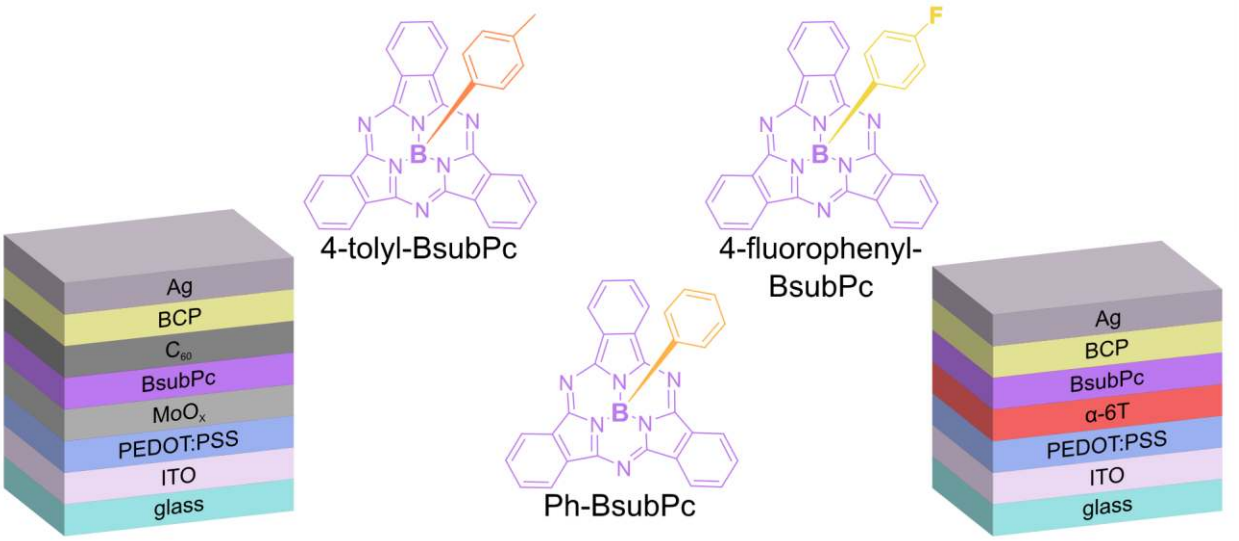

Figure 3.1. Chemical structures of phenyl- (Ph-), 4-tolyl- (4-MePh-), and 4-fluorophenyl- (4-FPh-) BsubPc. Device schematics illustrating the layer stacks pairing the BsubPcs with C_{60} and α-6T.

Six sets of OPV devices were fabricated to investigate these aryl-BsubPcs as both electron donors and acceptors. The first three sets were made by pairing each aryl-BsubPc with C_{60} to scope their

potential as electron-donating materials within the following device configuration: indium-tin oxide (ITO) / poly(3,4-ethylenedioxythiophene)-poly(styrenesulfonate) (PEDOT:PSS) / aryl-BsubPc (10 nm) / fullerene (C_{60}, 30 nm)/bathocuproine (BCP, 10 nm) / silver (Ag, 80 nm). The device thicknesses were selected to be close to those used for a previously published Cl-BsubPc / C_{60} device by Sullivan et al.[59] The other three sets were made by pairing each aryl-BsubPc with sexithiophene (α-6T) to evaluate their potential as electron acceptors within the following device configuration: ITO / PEDOT:PSS / α-6T (55 nm) / aryl-BsubPc (20 nm) / BCP (10 nm) / Ag (80 nm), following our previously published method for screening BsubPcs as acceptors.[89] Current density-voltage (J–V) characteristics (**Figure 3.2a** & **Figure 3.3a**) and characteristic parameters (**Table 3.1**) were measured under 100 mW/cm^2 of simulated solar illumination. External quantum efficiency (EQE) measurements are shown in **Figure 3.2b** & **Figure 3.3b**.

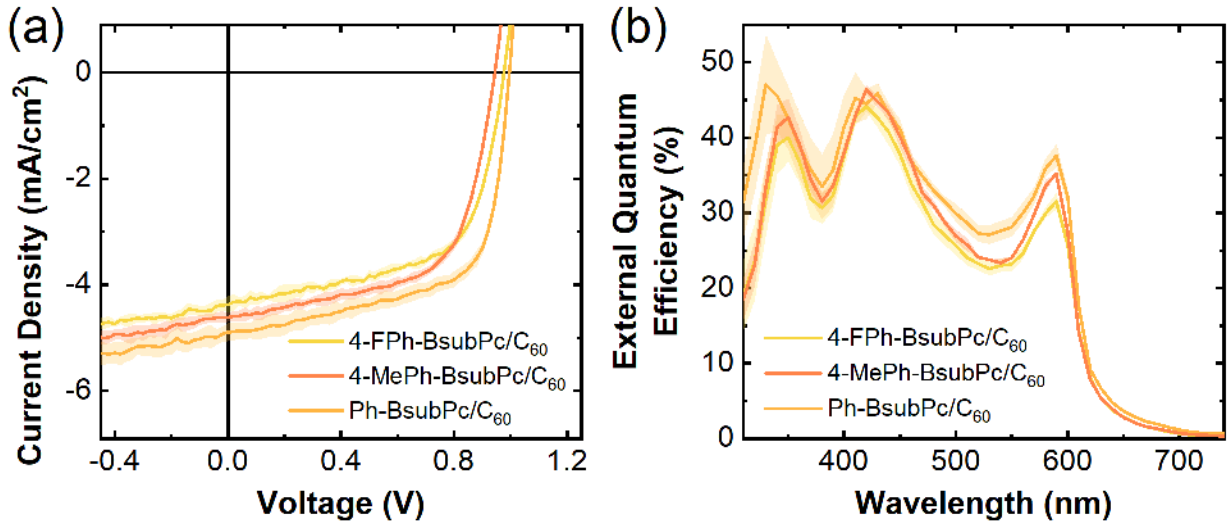

Figure 3.2. (a) Current density versus voltage characteristics and (b) measured external quantum efficiency spectra of phenyl- (Ph-), 4-tolyl- (4-MePh-), and 4-fluorophenyl- (4-FPh-) BsubPc / C_{60} fullerene devices. Shading indicates ± one standard deviation.

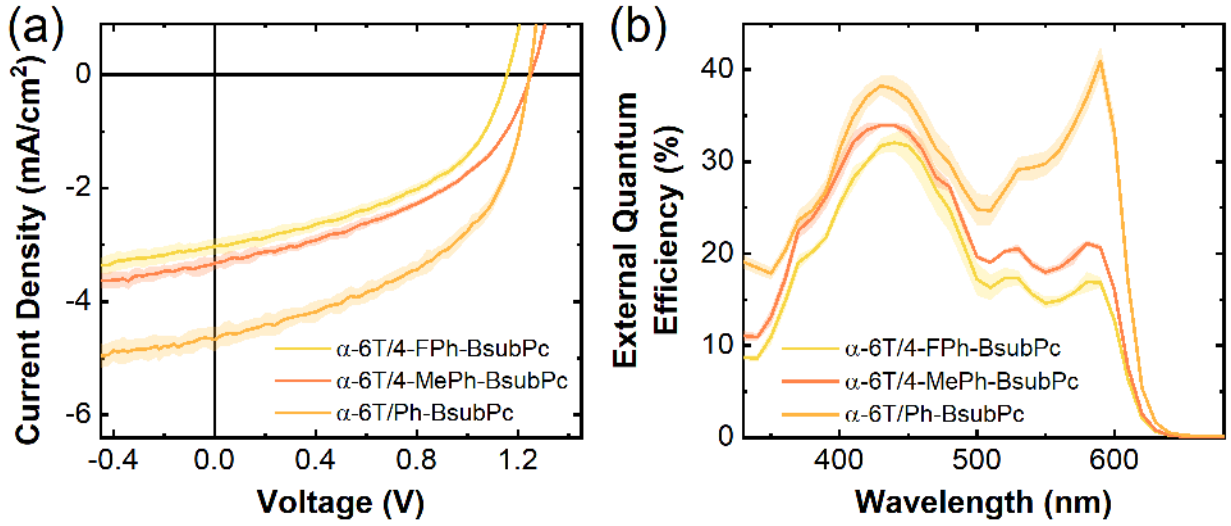

Figure 3.3. (a) Current density versus voltage characteristics and (b) measured external quantum efficiency spectra of α-sexithiophene / phenyl- (Ph-), 4-tolyl- (4-MePh-), and 4-fluorophenyl- (4-FPh-) BsubPc devices. Shading indicates ± one standard deviation.

Table 3.1. Average parameters of all devices. The standard deviation is indicated in brackets next to each parameter. At least eight devices were tested to determine these values.

Acceptor	**V_{OC}[a]** (V)	**J_{SC}[b]** (mA/cm^2)	**FF[c]**	**PCE[d]** (%)
phenyl-BsubPc / C_{60}	1.00 (0.003)	4.90 (0.17)	0.65 (0.01)	3.18 (0.12)
4-tolyl-BsubPc / C_{60}	0.94 (0.004)	4.62 (0.08)	0.62 (0.01)	2.70 (0.06)
4-fluorophenyl-BsubPc / C_{60}	0.98 (0.003)	4.38 (0.15)	0.62 (0.03)	2.66 (0.05)
α-6T / phenyl-BsubPc	1.24 (0.004)	4.67 (0.22)	0.50 (0.02)	2.89 (0.14)
α-6T / 4-tolyl-BsubPc	1.25 (0.002)	3.33 (0.11)	0.45 (0.01)	1.87 (0.05)
α-6T / 4-fluorophenyl-BsubPc	1.16 (0.003)	3.03 (0.14)	0.47 (0.02)	1.64 (0.06)

[a]Open-circuit voltage. [b]Short-circuit current density. [c]Fill factor. [d]Power conversion efficiency

As an electron donor material paired with C_{60}, phenyl-BsubPc outperforms 4-tolyl-BsubPc and 4-fluoro-BsubPc. With only a slightly higher open-circuit voltage (V_{OC}) and short-circuit current density (J_{SC}), when compared with those of the other derivatives, the main increase in power conversion efficiency (PCE) comes from a higher fill factor (FF = 0.65). This device matches the FF of the Cl-BsubPc / C_{60} device reported by Sullivan et al. and almost matches their 3.29 % PCE.[59] The EQE spectra (**Figure 3.2b**) show that the BsubPc contribution to the photocurrent

(~550 nm to ~650 nm) is highest for the phenyl-BsubPc device and lowest for the fluorophenyl-BsubPc device, although only by a slight margin and consistent with the small J_{SC} differences.

As an electron acceptor material paired with α-6T, all the aryl-BsubPcs generate very high V_{OC}s. The V_{OC} of 1.25 V produced by the 4-tolyl-BsubPc device represents the highest reported V_{OC} for any single-junction OPV to date using a BsubPc as the acceptor, with one exception of an OPV fabricated by Sullivan et al.; the latter device uses BsubPcs as both an electron donor and electron acceptor in an all BsubPc OPV.[48] Overall, phenyl-BsubPc once again outperforms the other two aryl-BsubPcs, this time by a wider margin. The phenyl-BsubPc-containing device still produces a higher FF and this time with a significant increase in J_{SC}. The α-6T / phenyl-BsubPc device produces a higher J_{SC} (corresponding to an increase of more than 35 %) than either of the other two devices, with most of this difference coming from a significantly higher BsubPc contribution to the photocurrent (**Figure 3.3b**). However, the PCE of the α-6T / phenyl-BsubPc device falls short of the PCE from our previously reported α-6T / Cl-BsubPc device.[89]

The differences in the measured J_{SC} could be due to differences in exciton diffusion length or dissociation rate of the corresponding aryl-BsubPcs.[141] Considering the aryl-BsubPc thickness when applied as an acceptor is double the thickness when used as a donor, the effect of different exciton diffusion lengths within the aryl-BsubPcs would be exaggerated in the acceptor devices.[141] This could explain why the acceptor devices have significantly different J_{SC}s, whereas the donor devices all have similar J_{SC}s. If true, the corresponding J_{SC}s from the devices using aryl-BsubPcs as electron acceptors suggest that phenyl-BsubPc may have the longest exciton diffusion length, whereas 4-tolyl-BsubPc and 4-fluorophenyl-BsubPc may have similar and relatively shorter exciton diffusion lengths.[141]

The electrochemical data outlined that the HOMO and LUMO levels of all the studied aryl-BsubPcs are the same.[138] Hence, in both the donor and acceptor cases, the small changes in V_{OC} (less than 10 %) are unlikely to be due to differences in the HOMO/LUMO gap at the interface.[19] Therefore, the small changes are likely due to subtle differences in carrier recombination or dielectric effects.[142] The improvement in FF for the phenyl-BsubPc devices suggests better charge balance, possibly due to a better charge carrier mobility or better charge carrier extraction.[31] It may

be possible to improve the FF of the 4-tolyl- and 4-fluorophenyl-BsubPc devices through rigorous optimization, but for this study, we adhere to the rapid screening method outlined previously[89] to determine which aryl-BsubPcs hold the most promise as electron-accepting or electron-donating materials in OPVs. Based on our results, we can conclude that phenyl-BsubPc shows the most promise in both applications. Conveniently, phenyl-BsubPc is also the easiest of the group to synthesize.

3.1.2 Conclusions

A novel family of BsubPcs bearing various aryl ligands at the axial position of boron were assessed in OPVs. By integrating phenyl-, 4-tolyl, and 4-fluorophenyl-BsubPc in OPV devices, we have demonstrated their dual functionality as electron donors and electron acceptors and identified the aryl-BsubPc with the most promise in future OPVs. Phenyl-BsubPc exhibits better performance in all aspects when compared with the other derivatives. The higher performance is hypothesized to be mainly due to a longer exciton diffusion length. All derivatives have the same basic physical properties, including electrochemical behaviour, and phenyl-, and 4-tolyl-BsubPc share the same solid-state arrangement. The distinction of phenyl-BsubPc was only found once incorporated into OPVs. Combined with the additional advantage of having the easiest synthesis when compared with the other derivatives, we feel that phenyl-BsubPc has significant potential for further investigation.

3.2 The Ability to Fine-Tune the Electronic Properties and Open-Circuit Voltage of Phenoxy-Boron Subphthalocyanines through Meta-Fluorination of the Axial Substituent.

Four different boron subphthalocyanines with fluorophenoxy axial substituents were applied as electron acceptors in planar heterojunction organic photovoltaic devices. The categorization of these “buckets” was confirmed by the fine change in open-circuit voltage between 1.15 V and 1.21 V, which are exceptionally high values for OPVs. This degree of fine-tuning of properties and device metrics is a unique handle enabled by the phenoxy axial substituent of BsubPcs.

3.2.1 Discussion

The energy level alignment of the organic semiconductor materials has an important role in converting light into electrical current within organic photovoltaic (OPV) devices.[46] The dissociation of excitons (electron-hole pairs) generated within the active layer of an OPV is dependent on the energetic spacing of the highest occupied molecular orbital (HOMO) and lowest unoccupied molecular orbital (LUMO) of the electron-donating and electron-accepting materials, respectively.[143-144] Therefore, the ability to fine-tune these energy levels is a potential handle to engineer efficient charge transfer and improve device performance.

A previously explored derivative of boron subphthalocyanine (BsubPc), pentafluorophenoxy-BsubPc (F_5-BsubPc), has a pentafluorophenoxy group in the axial position (**Figure 3.4**).[54] We outlined how the HOMO and LUMO energy levels are less sensitive to modification of the substituents on the axial phenoxy ligand than the same modifications around the periphery of the BsubPc molecular fragment.[54] F_5-BsubPc was found to be an exception, whereby it did change the HOMO and LUMO energy levels of the BsubPc chromophore likely due to the five strong electron-withdrawing fluorines present on the phenoxy group. Compared to a representative phenoxy-BsubPc (PhO-BsubPc, **Figure 3.4**), the HOMO and LUMO energy levels of F_5-BsubPc were measured to be notably deeper by ~0.4 eV.[54]

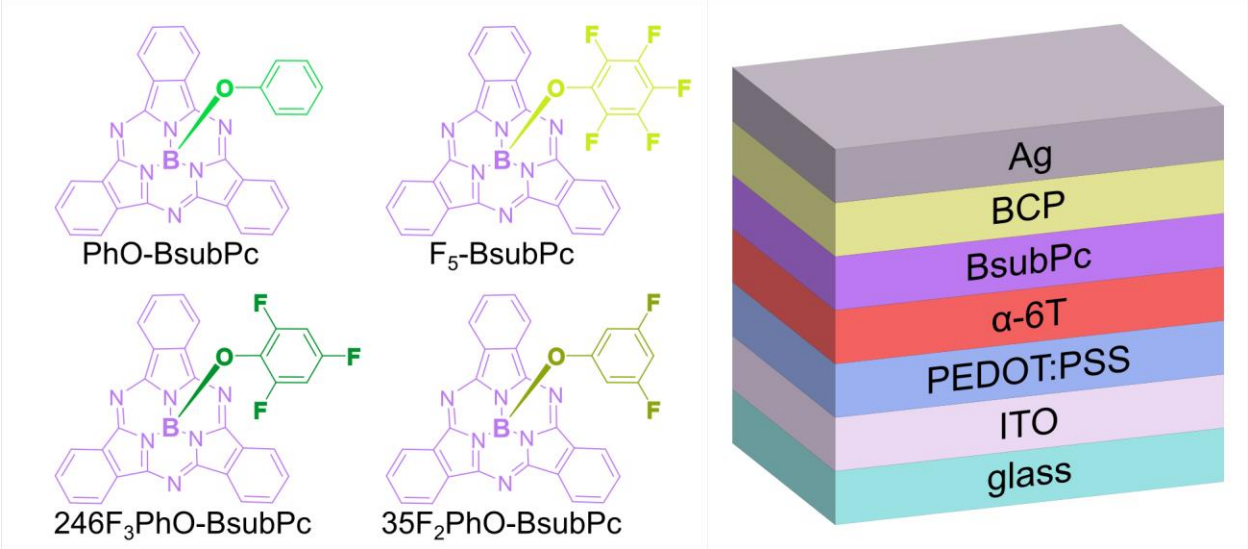

Figure 3.4. Chemical structures of phenoxy- (PhO-), 2,4,6-trifluorophenoxy- ($246F_3$-), pentafluorophenxoy- (F_5-) and 3,5-difluorophenoxy- ($35F_2PhO$-) BsubPc. Device schematics illustrating the layer stack used to pair the BsubPcs with α-6T.

In this study, we were able to determine the root cause of the unique properties of F_5-BsubPc. We also demonstrate that the electronic properties can be fine-tuned by systematically reducing the number of fluorine groups on the fluorophenoxy substituent. This observed ease of energy level tuning of an electron acceptor material, compared to that of fullerene acceptors, is ideal for improving charge extraction and achieving high V_{OC} in an OPV device.

Changing the HOMO and LUMO levels of active materials in OPVs is known to result in a corresponding change in the open-circuit voltage (V_{OC}).[145-147] To determine whether the V_{OC}s also fall into two "buckets", as per our conclusion above, F_nPhO-BsubPcs were incorporated into OPVs as electron acceptors using the following device structure: ITO / PEDOT:PSS / sexithiophene (α-6T, 50nm) / BsubPc (20nm) / bathocuproine (BCP, 7nm) / silver (Ag, 80 nm). This device structure mimics our previously published baseline for screening BsubPcs as electron acceptors.[89] PhO-BsubPc and $246F_3$PhO-BsubPc were chosen from the non-meta fluorines "bucket". F_5-BsubPc and $35F_2$PhO-BsubPc were chosen from the meta fluorine "bucket". Voltage sweeps (J–V curves) were performed to determine the V_{OC} resulting from each F_nPhO-BsubPc (**Figure 3.5a**), and external quantum efficiencies (EQEs) were measured to assess the spectral performance (**Figure 3.5b**).

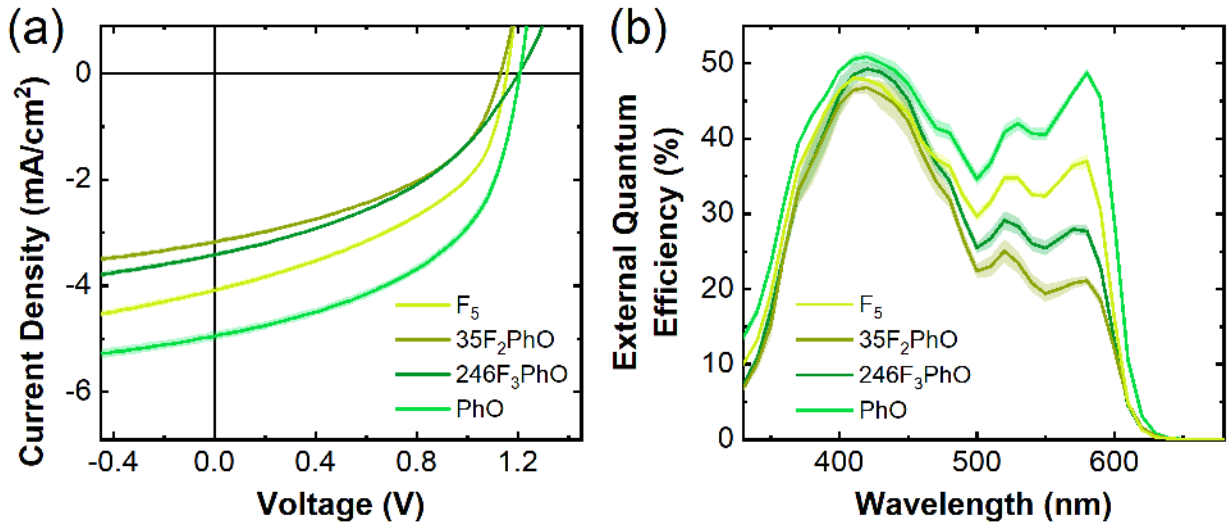

Figure 3.5. (a) Current density versus voltage characteristics and (b) measured external quantum efficiency spectra of α-sexithiophene / BsubPc devices. Shading indicates ± one standard deviation.

The best performing OPVs, based solely on power conversion efficiency (PCE), were achieved using the F_nPhO-BsubPcs with a non-fluorinated or fully fluorinated phenoxy group (**Table 3.2**). This result may be due to the concave-ligand stacking in F_5BsubPc and lack of hydrogen-fluorine bonds in the PhO-BsubPc crystal structure. However, the strong hydrogen-to-fluorine bonds and π-π stacking in the 246F_3PhO-BsubPc appears to improve the solid-state arrangement and short-circuit current (J_{SC}). Also, the voltage sweeps confirm that the "buckets" trend still holds in devices, with regards to V_{OC}. The OPVs made using F_nPhO-BsubPcs with meta fluorines (F_5-BsubPc and 35F_2PhO-BsubPc) have V_{OC}s of around 1.15 V, while the OPVs using F_nPhO-BsubPcs without meta fluorines (PhO-BsubPc and 246F_3PhO-BsubPc) have V_{OC}s of approximately 1.21 V. This change of 0.06 V is both fine-tuned and statistically valid. Also, the V_{OC} of 1.20 V is remarkably high for both BsubPcs and electron acceptors in general in vacuum-deposited planar heterojunction OPVs. Other examples include Bartynski *et al.* reaching a high V_{OC} of 1.27 V in a single-junction OPV with α-6T as the donor and a non-BsubPc small molecule acceptor.[148] Typical V_{OC}s for devices with BsubPc electron acceptors range from ~0.9 to 1.1 V, with the highest report of 1.3 V achieved by Sullivan *et al.*[46, 48, 138] The higher V_{OC}s for the F_nPhO-

BsubPcs from the "non-meta fluorine bucket" are consistent with their shallower HOMO and LUMO levels, as measured by electrochemistry and UPS.

Table 3.2. Average parameters of devices with α-6T as the electron donor and one of the four F_nPhO-BsubPcs as the electron acceptor material (F_5-BsubPc, 246F_3PhO-BsubPc, 35F_2PhO-BsubPc, and PhO-BsubPc. The standard deviation is listed in the brackets next to each parameter

Acceptor	**V_{OC}**[a] (V)	**J_{SC}**[b] (mA/cm^2)	**FF**[c]	**PCE**[d] (%)
α-6T / F_5-BsubPc	1.16 (<0.01)	4.08 (0.06)	0.46 (<0.01)	2.16 (0.04)
α-6T / 35F_2PhO-BsubPc	1.13 (<0.01)	3.17 (0.05)	0.45 (<0.01)	1.63 (0.03)
α-6T / 246F_3PhO-BsubPc	1.20 (<0.01)	3.42 (0.05)	0.41 (0.01)	1.68 (0.03)
α-6T / PhO-BsubPc	1.21 (<0.01)	4.96 (0.09)	0.50 (0.01)	3.02 (0.08)

[a]Open-circuit voltage. [b]Short-circuit current density. [c]Fill factor. [d]Power conversion efficiency

The study by Shin *et al.* also observed an increase in V_{OC} from 0.83 to 0.96 V with the addition of fluorine in the meta position of the phenoxy side chain on an electron-donating polymer.[149] As well, other studies that explored the addition of fluorine on semiconducting materials also observed an increase in V_{OC} due to the electron-withdrawing fluorines.[150-151] Our group also found that for OPV devices that integrate silicon phthalocyanine with a 2,4,6-trifluorophenoxy substituent, the axial group with the least amount of electron-withdrawing capabilities also stood out with a high V_{OC}, which is similar to our finding.[152] In a similar fashion to our study, Cnops *et al.* tuned the LUMO energy levels and were able to optimize the interface energy gap and produce an OPV with a V_{OC} over 1.0 V.[46]

3.2.2 Conclusions

An array of fluorophenoxy-BsubPc compounds with various number and position of fluorines was assessed in OPVs. By varying the position of fluorines in the phenoxy axial substituent of BsubPc, specifically by placing fluorines in the meta positions, the electronic properties of the BsubPc can be uniquely fine-tuned to generate OPVs with high V_{OC}s. We found no correlation between the number of fluorines and electronic properties, but the presence of fluorine in the meta position decreased the V_{OC} by an average of 0.06 V in planar heterojunction organic photovoltaic devices.

With the ability to fine-tune the electronic properties and energy levels, we can enhance the extraction of charge and overall performance of organic electronic devices. Given the overall performances, we believe the PhO-BsubPc derivative is an excellent candidate for future investigation in OPVs.

3.3 Phenoxy-(Chloro)$_n$ Boron Subnaphthalocyanines: Alloyed Mixture, Electron-Accepting Functionality, Enhanced Solubility for Bulk Heterojunction Organic Photovoltaics

The first set of phenoxy BsubNc compounds, PhO-Cl$_n$BsubNc and F$_5$-Cl$_n$BsubNc, were synthesized.[140] Like their precursor, the products were found to be an alloyed mixture of phenoxylated Cl$_n$BsubNcs situated randomly in the solid-state yet consistent in the frequency of bay position chlorination. Phenoxylation yielded differences in organic photovoltaic (OPV) device metrics. Specifically, a significant increase in open-circuit voltage (V_{OC}) was observed, ultimately exceeding 1.0 V when phenoxylated Cl$_n$BsubNcs were paired with alpha-sexithiophene (α-6T) in planar heterojunction (PHJ) OPVs.

3.3.1 Discussion

In our previous work, we demonstrated that Cl-BsubNc, whether synthesized via literature methods or our in-house developed processes or purchased from a commercial vendor, is a mixture of Cl-BsubNc products with random amounts of chlorination at the bay positions of the BsubNc structure.[67] As a result of this mixture and chlorination format, we appropriately refer to the compound as Cl-Cl$_n$BsubNc (**Figure 3.6**).[67] The conclusion of our study was consistent with the study of Endres *et al.*,[56] published at approximately the same time. We were unable to develop a chemical process to produce a pure, non-peripherally-chlorinated sample of Cl-BsubNc. However, we were able to develop chemical processes to produce Cl-Cl$_n$BsubNcs with either lower or higher amounts of peripheral chlorination relative to the literature or commercial Cl-Cl$_n$BsubNc samples. PHJ OPV device characteristics were found to be different among the Cl-Cl$_n$BsubNc samples with varying amounts of chlorination. Our findings strongly suggest that the Cl-BsubNc samples used in all previously reported OPV studies are likely not pure, consisting of a mixture of Cl-Cl$_n$BsubNcs with bay position chlorination.[67]

Though a pure, non-peripherally chlorinated Cl-BsubNc cannot be obtained, its mixture of chlorinated species collectively shows excellent promise as a light-harvesting and charge transporting material in OPVs.[67] Given this performance appeal and the absence of reports on any BsubNcs in OPVs besides Cl-BsubNc/Cl-Cl$_n$BsubNc, we were motivated to examine other derivatives of this class. We were interested in adopting axial phenoxylation chemistry. We have shown that displacing the axial halide with a phenoxy group(s) leads to improvements or benefits on several different levels: (1) open-circuit voltage (V_{OC}) output stemming from a better solid-state arrangement for Pcs,[152-153] (2) charge transport properties for BsubPcs,[58] (3) solubility in organic solvents for BsubPcs[45, 93] and Pcs[154], and (4) ambipolar (*i.e. n*- and *p*-type) characteristics for BsubPcs[44] and SiPcs.[152-153]

Herein, we first describe an examination of phenoxy-Cl$_n$BsubNc (PhO-Cl$_n$BsubNc, **Figure 3.6**) and pentafluorophenoxy-Cl$_n$BsubNc (F$_5$-Cl$_n$BsubNc, **Figure 3.6**) within PHJ OPVs. Comparison of the device properties is then made to those of Cl-Cl$_n$BsubNc. Again, we emphasize that this work not only augments the small collection of known BsubNc derivatives, but it marks the first set of examples of BsubNcs other than the prototypical Cl-BsubNc as the organic photoactive material in OPVs.

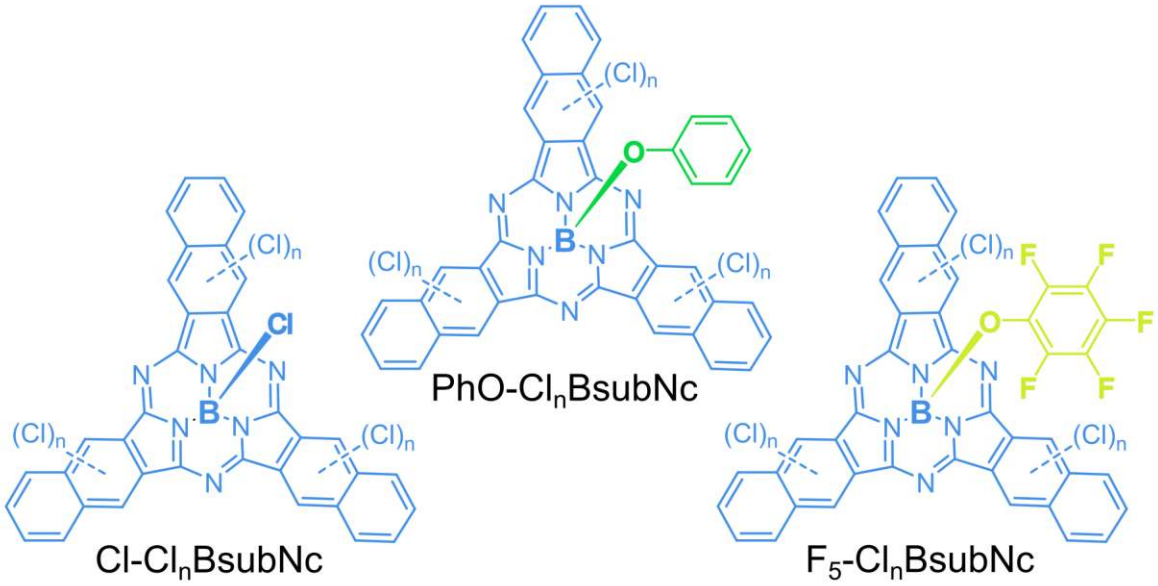

Figure 3.6. Chemical structures of Cl-, PhO-, F$_5$-Cl$_n$BsubNc.

Given the similar photophysical properties to literature-Cl-Cl$_n$BsubNc and the reversible electrochemical nature of phenoxy Cl$_n$BsubNcs, the performance of PhO-Cl$_n$BsubNc and F$_5$-Cl$_n$BsubNc were examined as electron acceptors within PHJ OPV devices. Each compound was paired with sexithiophene (α-6T) using the following device structure: indium tin oxide (ITO) / poly(3,4-ethylenedioxythiophene) poly(styrenesulfonate) (PEDOT:PSS) / α-6T (55 nm) / Cl-Cl$_n$BsubNc (25 nm) / bathocuproine (BCP, 10 nm) / silver (Ag, 80 nm). This configuration replicated the one adopted for the Cl-Cl$_n$BsubNc-based PHJ OPV cells in our previous study,[67] allowing for a direct point of comparison. Current density-voltage (J–V) characteristics (**Figure 3.7a**) were measured under 100 mW·cm^{-2} of simulated AM 1.5G solar illumination. The measured external quantum efficiency (EQE) spectra are shown in **Figure 3.7b**. The performance characteristics (**Table 3.3**) are derived from the measurement of at least 16 PHJ OPV devices.

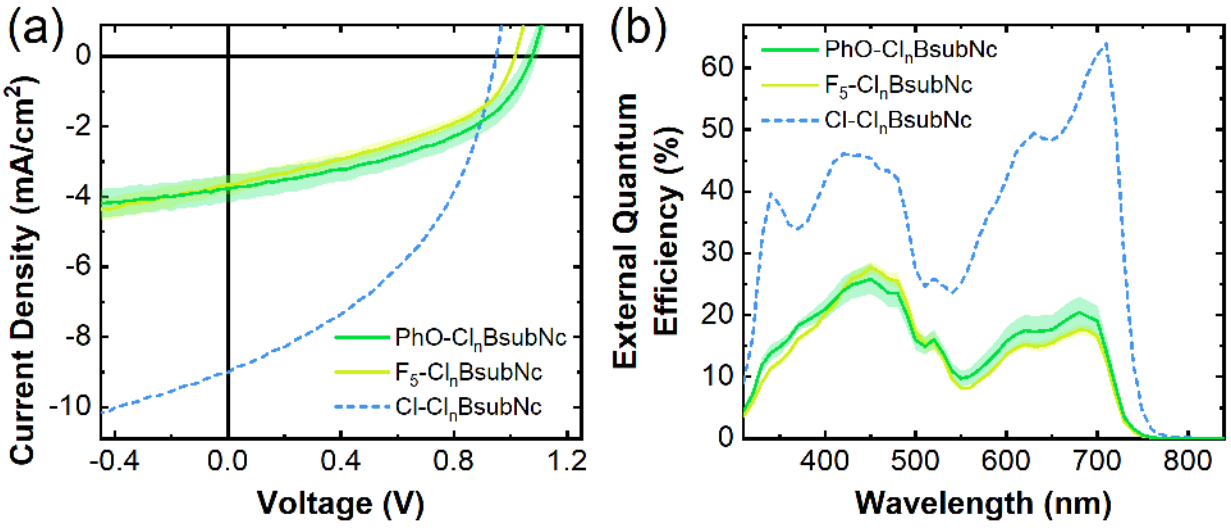

Figure 3.7. (a) J–V characteristics and (b) EQE spectra of PhO-Cl$_n$BsubNc and F$_5$-Cl$_n$BsubNc. PHJ OPVs of the following configuration: ITO / PEDOT:PSS / α-6T (55 nm) / Cl$_n$BsubNc (25 nm) / BCP (10 nm) / Ag (80 nm) whereby the Cl$_n$BsubNc layer is either PhO-ClnBsubNc or F$_5$-Cl$_n$BsubNc. Shading indicates ± one standard deviation.

Table 3.3. Average device parameters of PHJ OPVs of the following configuration: ITO / PEDOT:PSS / α-6T (55 nm) / Cl$_n$BsubNc (25 nm) / BCP (10 nm) / Ag (80 nm) whereby the Cl$_n$BsubNc layer is either PhO-Cl$_n$BsubNc or F$_5$-Cl$_n$BsubNc. The standard deviation is indicated

in brackets next to each parameter. Each parameter is a result of the measurement of at least 16 devices.

Acceptor	V_{OC}[a] (V)	J_{SC}[b] (mA/cm^2)	FF[c]	PCE[d] (%)
PhO-Cl$_n$BsubNc	1.073 (0.024)	3.76 (0.39)	0.46 (0.01)	1.87 (0.24)
F$_5$-Cl$_n$BsubNc	1.016 (0.006)	3.67 (0.28)	0.42 (0.02)	1.57 (0.11)
literature-Cl-Cl$_n$BsubNc	0.962 (0.026)	8.96 (0.72)	0.45 (0.02)	3.88 (0.21)

[a]Open-circuit voltage. [b]Short-circuit current density. [c]Fill factor. [d]Power conversion efficiency

PHJ OPV cells made with PhO-Cl$_n$BsubNc outperform the devices made with F$_5$-Cl$_n$BsubNc in all aspects (*i.e.* V_{OC}, J_{SC}, FF), producing an average PCE of 1.87% for the former and 1.57% for the latter. The V_{OC}s are higher than those based on literature-Cl-Cl$_n$BsubNc and are consistent with a steric shielding effect,[155] observed with sterically bulky groups (*i.e.* phenoxy groups) in small molecule-[156-158] and polymer[159]-based OPVs. This effect is due to an increase in the distance between the donor and acceptor materials induced by steric hindrance. This increase in separation distance causes the potential energy of electron-hole pairs at the donor-acceptor interface to increase, leading to an enhancement in the V_{OC}.[155]

While these cells had higher V_{OC}s than those based on literature-Cl-Cl$_n$BsubNc, their PCEs were more than two times lower. The significant loss for both sets of devices was the result of much lower extracted J_{SC}s. Given that the photophysical properties of the phenoxy Cl$_n$BsubNcs are similar to literature-Cl-Cl$_n$BsubNc, it is unlikely that the origin of this loss is due to the efficiency behind the photon absorption and exciton generation process. It is more likely that the lower J_{SC}s are attributed to a decrease in the efficiency behind the exciton dissociation step, whereby the barrier for electron transfer from the α-6T to the BsubNc layer is higher as evident in the higher reduction potentials (*i.e.* weaker electron-accepting ability). The drop in the J_{SC}s could be the result of a steric shielding effect (as described above) due to the higher potential energy of electron-hole pairs at the donor-acceptor interface, making it more difficult to separate and collect the individual charge carriers.[155] Overall, these results imply that contrary to BsubPcs,[44] adding phenoxy groups at the axial position of Cl$_n$BsubNc mixtures is detrimental to PHJ OPV device performance. These

results also suggest that there could be a better electron-donating material than α-6T for pairing with the phenoxy Cl_nBsubNcs, a point of future work.

3.3.2 Conclusions

Phenoxylation significantly impacts the application of Cl_nBsubNc in OPVs. Contrary to BsubPcs, the axial derivatization of Cl_nBsubNcs has a pronounced effect on the PHJ OPV performance. Phenoxylation resulted in a significant performance drop compared to Cl-Cl_nBsubNc. However, the inclusion of the phenoxy molecular fragment did improve the V_{OC}s, suggesting that a steric shielding effect between the donor and acceptor is influencing the OPV. Higher efficiencies could be afforded with better electron-donating materials than α-6T to see the ultimate potential of BsubNcs as electron-accepting materials.

3.4 The Influence of Halogen Bonds Within Organic Electronics

3.4.1 Discussion

The relationship between molecular structure and supramolecular structure in organic electronic devices has attracted interest for its influence on device performance.[160-161] Introducing or tuning intermolecular interactions can modify the supramolecular structure of a material (intermolecular orientation and spacing). The influence of aromatic π-π interactions on solid-state arrangements of organic electronic materials are well known.[162-163] A less considered interaction is the relative strength and directionality of halogen bonds.[164] Halogen bonds are the net attraction between a covalently-bound halogen (R-X) and the lone pair of an atom (Y), typically denoted "R-X···Y" and close to 180°.[165] The net attraction between X and Y will typically reduce the interatomic distance to less than the sum of their Van der Waals radii. Y donates electrons to the electrophilic region of the electrophilic region of the halogen, forming the halogen bond (**Figure 3.8**). The electrophilic region of R-X is defined as the halogen bond donor and the nucleophilic region of Y is defined as the halogen bond acceptor. This definition is applied throughout this section, although it is noted to be opposite to the convention normally applied in organic electronics.

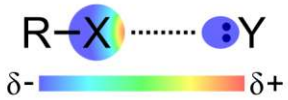

Figure 3.8. Illustration of the molecular electrostatic potential (not to scale) of a halogen bonding interaction, where X is chlorine, bromine, or iodine, and Y is an atom with at least one lone pair.

Unless sterically hindered, halogen bonding could occur between any material containing a halogen bond donor (chlorine, bromine, or iodine) and any other material containing a halogen bond acceptor (nitrogen, oxygen, sulphur, or any other atom with lone pairs). Halogen bonding interactions have been employed to increase the photovoltages of dye-sensitized solar cells[166-167], and for surface passivation of organic-inorganic halide perovskite photovoltaics,[168] but there are no reported applications in organic electronic devices. If halogen bonds are formed within the thin layers that comprise organic electronic devices, then strategic placement of the halogen bond donor and acceptor could provide a handle to control molecular orientation. Halogen bonding can theoretically occur both within a layer and at the interface between layers. Proving the presence of halogen bonds within organic electronic devices could significantly advance solid-state engineering as well as the ability to achieve higher performance organic electronic devices.

Nitrogen in boron subphthalocyanines (BsubPcs) has been previously demonstrated to be a reliable halogen bond acceptor (Y).[94] The axial position of BsubPcs can be readily substituted with halogenated phenoxy moieties. A set of three meta-halogenated phenoxy-BsubPcs (*m*-XPhO-BsubPcs, where X = Cl, Br, or I, **Figure 3.9a,b,c**) provides the perfect platform to study halogen bonding within organic electronic devices.[94] All three derivatives form identical solid-state crystal structures (**Figure 3.9d**).[94] All three exhibit very similar optical, electrochemical, or electronic properties.[54] Within the crystal structures, halogen bonding has been previously identified with calculated bond strengths of 0.8, 0.5, and 3.9 kcal/mol for C-Cl···N, C-Br···N, and C-I···N, respectively. The crystals were obtained through train sublimation, which approximates the vacuum deposition conditions used in the fabrication of OPVs.[169] While crystals are not representative of the thin layers that comprise vacuum-deposited organic electronic devices, the halogen bonding in the solid-state crystals proves that there are circumstances in which *m*-XPhO-BsubPcs will form halogen bonds.

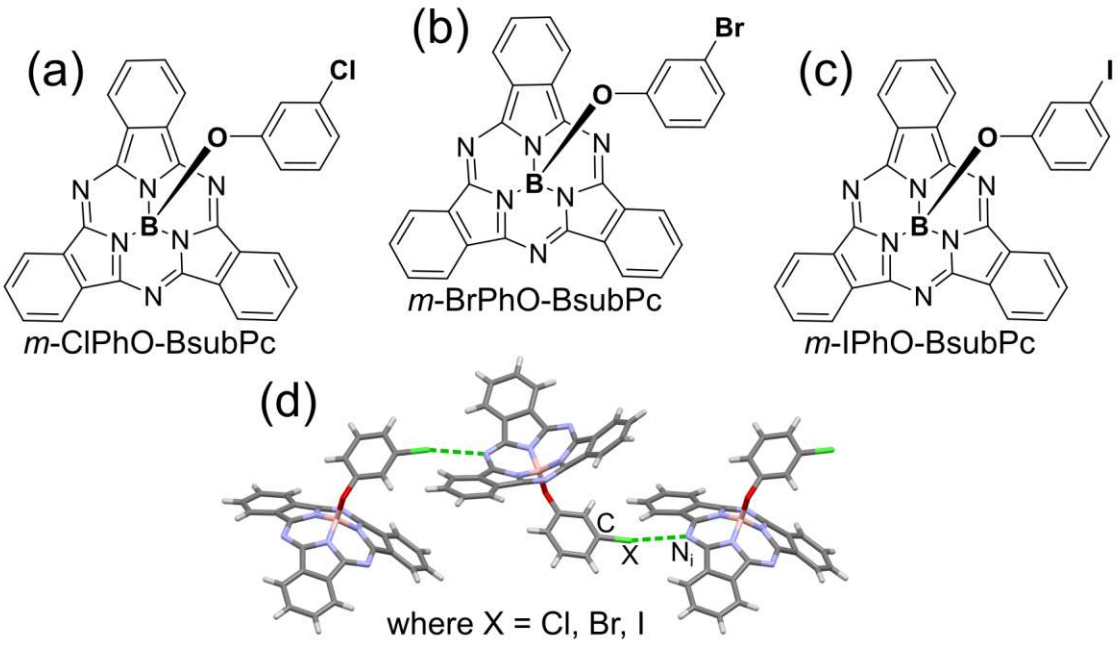

Figure 3.9. Chemical structures of (a) meta-chlorophenoxy-boron subphthalocyanine (*m*-ClPhO-BsubPc), (b) meta-bromophenoxy-BsubPc (*m*-BrPhO-BsubPc), and (c) meta-iodophenoxy-BsubPc (*m*-IPhO-BsubPc). (d) Solid-state arrangements of the *m*-XPhO-BsubPc demonstrating the C-X···N halogen bonds crystal structure, redrawn using *m*-ClPhO-BsubPc from Virdo et al.[94] Key: carbon = grey, nitrogen = light purple, oxygen = red, boron = light pink, chlorine = green.

In this study, we use planar heterojunction (PHJ) OPVs to probe for the potential presence and influence of halogen bonding within organic electronic devices. We use carefully selected layer combinations to examine and decouple the effects of potential intralayer and interlayer halogen bonding on OPV performance. We find that changing the halogen has a minimal intralayer effect on device performance. Changes to device performance, however, are observed when introducing different interfacial halogen bond acceptors. The differences in device performance correlate with the strength of the potential halogen bond or the size of the halogen, depending on the location of the interface within the device.

Three sets of OPVs were made for every layer stack, each containing a *m*-XPhO-BsubPc. Materials without any potential halogen bond acceptors were selected to surround the *m*-XPhO-BsubPc layer, isolating any intralayer effects. We adopted a layer stack previously developed by Cnops et

al. for chloro-BsubPc[72] where tetracene (Tc) and fullerene (C_{60}) surround the BsubPc layer: ITO / PEDOT:PSS / MoO_X (5 nm) / Tc (60 nm) / *m*-XPhO-BsubPc (10 nm) / C_{60} (30 nm) / BCP (7 nm) / Ag (80 nm). Tc and C_{60} contain only carbon atoms, eliminating the possibility of halogen bonding at those interfaces. Any change observed in OPV performance between the *m*-XPhO-BsubPcs would, therefore, be attributed to intralayer differences. Given the similarities in material properties, such differences could only be due to the strength of the potential halogen bonds or other effects related to the presence of different halogens. Current density-voltage (J–V) characteristics were measured under simulated AM1.5G (**Figure 3.10**).

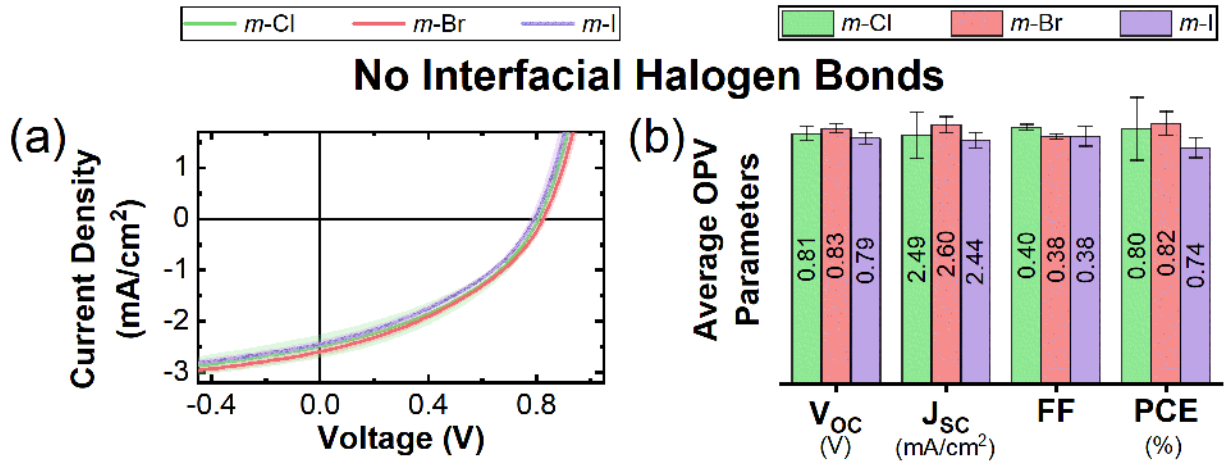

Figure 3.10. (a) J–V data and (b) the corresponding device performance characteristics of OPVs with no potential to form interfacial halogen bonds (ITO / PEDOT:PSS / MoO_X / Tc / *m*-XPhO-BsubPc / C_{60} / BCP / Ag, where X = Cl, Br, or I).

Aside from a slight translation, the shape of the J–V curves for each *m*-XPhO-BsubPc is virtually identical; the strength of the potential intralayer halogen bonds and the presence of different halogen atoms within the film appear to have minimal effect on OPV performance. Open-circuit voltage (V_{OC}) and short-circuit current (J_{SC}) (*m*-I < *m*-Cl < *m*-Br) may slightly, inversely correlate with C-X···N halogen bonding strength (C-Br···N < C-Cl···N < C-I···N), but the differences are within measurement error. This minimal impact on OPV performance does not indicate whether halogen bonding occurs within the film. Each material could be forming no halogen bonds, an equivalent amount of halogen bonds, or a variable amount of halogen bonds. However, this set of

OPVs provides an important control for the minimal intralayer influence on OPV performance. In other OPV configurations, any significant differences to the J–V curves or performance characteristics that emerge as a result of changing the *m*-XPhO-BsubPc can now be attributed to interfacial effects.

The layers surrounding *m*-XPhO-BsubPc in the OPVs were sequentially substituted with materials containing halogen bond acceptors. Three sets of OPVs were made to separately introduce three different materials with potential halogen bond acceptors to the *m*-XPhO-BsubPc interfaces: bathocuproine (BCP), molybdenum oxide (MoO_X), and α-sexithiophene (α-6T). The nitrogen (BCP), oxygen (MoO_X) and sulphur (α-6T) atoms present in these materials could all potentially act as halogen bond acceptors. The following three-layer stacks comprise the sets of OPVs used to examine these interfaces: the first was ITO / PEDOT:PSS / MoOx (5 nm) / tetracene (60 nm) / *m*-XPhO-BsubPc (20 nm) / BCP (7 nm) / Ag (80 nm), the second was ITO / MoOx (5 nm) / *m*-XPhO-BsubPc (15 nm) / C_{60} (40 nm) / BCP (8 nm) / Al (100 nm), and the third was ITO / PEDOT:PSS / MoOx (5 nm) / α-6T (60 nm) / *m*-XPhO-BsubPc (10 nm) / C_{60} (30 nm) / BCP (7 nm) / Ag (80 nm), where X = Cl, Br, or I for each layer stack. Current density-voltage (J–V) characteristics were measured under simulated AM1.5G (**Figure 3.11**).

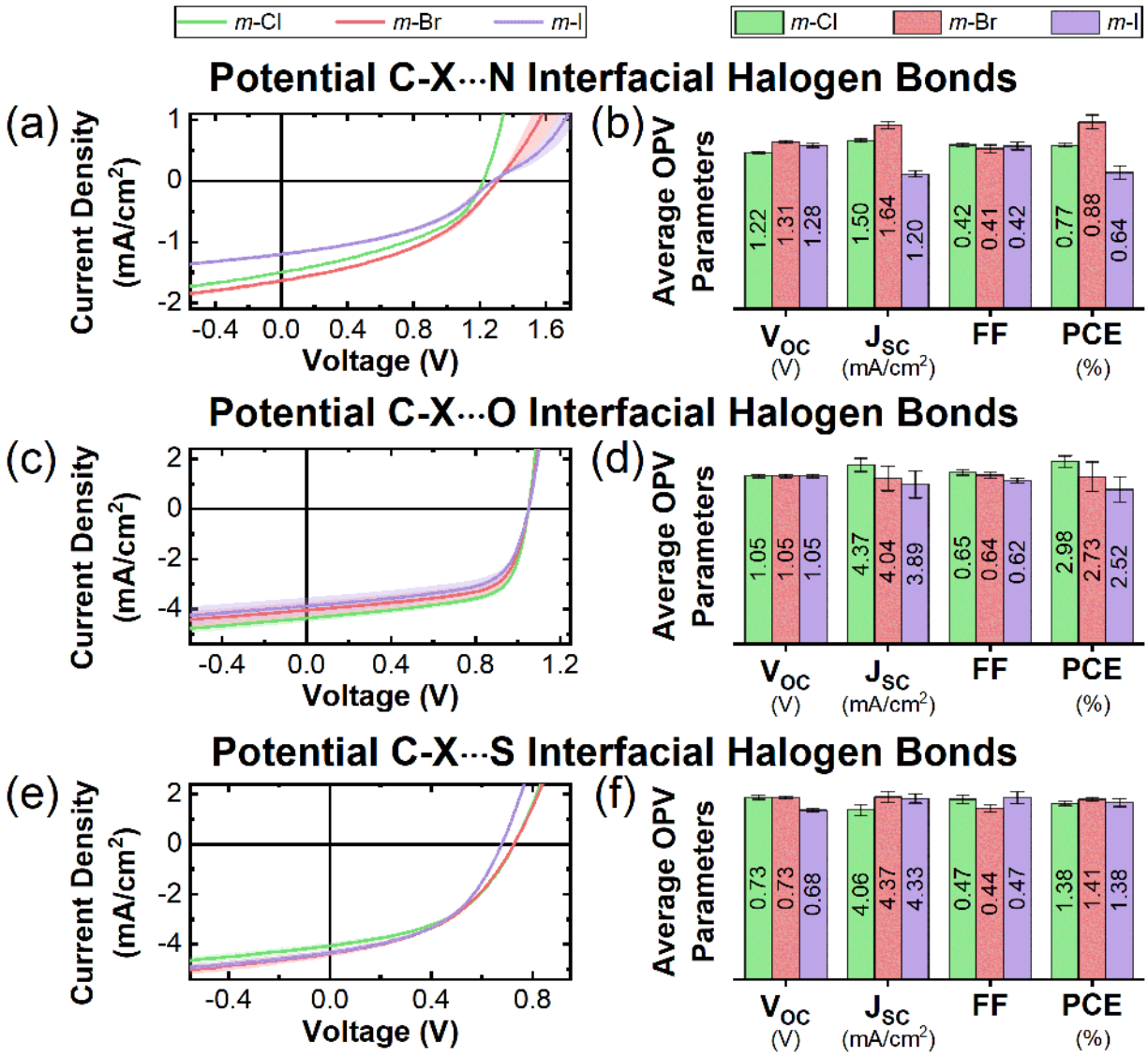

Figure 3.11. (a) J–V data and (b) the corresponding device performance characteristics of OPVs with the potential to form interfacial X···N halogen bonds (ITO / PEDOT:PSS / MoO_X / Tc / *m*-XPhO-BsubPc / BCP / Ag, where X = Cl, Br, or I). (c) J–V data and (d) the corresponding device performance characteristics of OPVs with the potential to form interfacial X···O halogen bonds (ITO / MoO_X / *m*-XPhO-BsubPc / C_{60} / BCP / Al, where X = Cl, Br, or I). (e) J–V data and (f) the corresponding device performance characteristics of OPVs with the potential to form interfacial X···S halogen bonds (ITO / PEDOT:PSS / α-6T / *m*-XPhO-BsubPc / C_{60} / BCP / Ag, where X = Cl, Br, or I).

When introducing materials with potential halogen bond acceptors (atoms with lone pairs) to interfaces of the *m*-XPhO-BsubPc layer, the J–V characteristics suddenly depend on which halogen is present. Variation in J–V characteristics is most dramatic for the set of OPVs with a *m*-XPhO-BsubPc / BCP interface. BCP contains two nitrogen atoms that could be forming halogen bonds with the *m*-XPhO-BsubPcs. A noticeable decrease in J_{SC} (*m*-Br > *m*-Cl >> *m*-I) is observed with the increasing halogen bond strength calculated between the halogen and nitrogen atoms in a m-XPhO-BsubPc solid-state crystal (C-Br···N < C-Cl···N << C-I···N).[94] Beyond J_{SC}, each OPV in this set has a distinctly shaped J–V curve. In particular, the *m*-IPhO-BsubPc OPV exhibits a dramatic "s-kink" beyond the V_{OC}. The trend in J_{SC} and differently shaped J–V curves strongly suggest that halogen bonds are forming at the *m*-XPhO-BsubPc / BCP interface and influencing the device performance. The orientation between halogen-bonded BCP and *m*-XPhO-BsubPc may impede electron transfer relative to non-halogen-bonded molecular orientations. If more halogen bonds form at the interface when halogens that form stronger halogen bonds are present, this would be consistent with the inverse correlation between J_{SC} and halogen bond strength.

For the set of OPVs containing the MoO_X / *m*-XPhO-BsubPc interface, the J_{SC} once again varies depending on which halogen is present. In this set, decreasing short-circuit current density (J_{SC}) correlates with increasing halogen atom size. Any significant variation in device performance suggests that halogen bonding occurs between MoO_X and *m*-XPhO-BsubPc. This correlation is different than for the *m*-XPhO-BsubPc / BCP OPVs, but similarities should not necessarily be expected; MoO_X and BCP are different materials, the order of deposition is opposite (BsubPc onto MoO_X vs BCP onto BsubPc), and the functions that occur at each interface are different (hole transfer vs electron transfer). Strengths of the purported C-X···O halogen bonds have not previously been calculated, so the bond strengths may happen to correlate with the observed trend in J_{SC} inversely. Alternatively, if MoO_X and *m*-XPhO-BsubPc form halogen bonds with the same frequency independent of the halogen, the dipoles of the larger halogens might increase exciton recombination at that interface, explaining the reduction in J_{SC}.

There are subtle differences in the J–V characteristics of the OPVs containing the α-6T / *m*-XPhO-BsubPc interface. The V_{OC} of the *m*-IPhO-BsubPc OPVs is about 7% lower than the similar V_{OC}s

of the *m*-ClPhO- and *m*-BrPhO-BsubPc OPVs. The J_{SC} of the *m*-ClPhO-BsubPc OPVs is about 7% lower than the similar J_{SC}s of the *m*-BrPhO- and *m*-IPhO-BsubPc OPVs. The fill factor (FF) of the *m*-BrPhO-BsubPc OPVs is about 6% lower than the similar FFs of the *m*-ClPhO- and *m*-IPhO-BsubPc OPVs. Together, these differences result in nearly identical power conversion efficiencies (PCEs). The lack of clear performance trends makes it difficult to determine whether the sulphur atoms in α-6T are not forming any halogen bonds with the *m*-XPhO-BsubPc, or if halogen bonding at that interface does not have a strong influence on OPV performance.

3.4.2 Conclusions

In summary, the similar performances of the Tc / *m*-XPhO-BsubPc / C_{60} OPVs combined with significant performance differences observed in the other OPVs strongly implies that halogen bonding occurs between vacuum-deposited organic layers and that halogen bonds can have a substantial influence on OPV performance. The availability and theoretical strength of C-X···N halogen bonding at the *m*-XPhO-BsubPc / BCP interface noticeably affect the OPV performance characteristics. The availability of C-X···O halogen bonding at the MoO_X / *m*-XPhO-BsubPc interface in OPVs results in an inverse correlation between halogen atom size and the J_{SC}. Evidence for C-X···S halogen bonding at the α-6T / *m*-XPhO-BsubPc interface is inconclusive due to the minimal impact on OPV performance. Despite the speculative nature of our explanations behind the OPV performance correlations with interfacial halogen bond acceptors, we believe the mere presence of any difference in device performance is enough to evidence to infer that interfacial halogen bonding occurs within OPVs. Whether the influence of halogen bonding on device performance is due to molecular orientation or due to other mechanisms will be explored in future work. This work also validates the application of crystal structure engineering for organic electronic applications, despite the differences in scale between crystals and thin films. Halogen bonds are presumably already affecting the molecular orientation in many current organic electronic devices unintentionally. Any organic electronic device that incorporates organic materials containing halogens and halogen bond acceptors has the potential to form halogen bonds. Intentional implementation of halogen bonding could provide a versatile tool to manipulate intermolecular interactions and orientations, enable better control over solid-state morphologies of organic thin films, and ultimately lead to higher performing organic electronic devices.

Chapter 4
Outdoor Stability

In this chapter, I examine the influence of peripheral and axial substituents on the stability of BsubPcs in OPVs. This chapter is adapted from my contributions to three manuscripts. The first section (**Section 4.1**) describes the development of protocols for outdoor stability testing.

I pioneered the development of outdoor testing in our laboratory, and I led the first three summers of outdoor experiments. I collaborated with Jeffrey Castrucci during the initial planning for the required equipment and encapsulation method. I led the design of the sample holders and mounting modules. Stephanie Nyikos assisted with the design and sketched the original drawings (**Figure A.3**). John Ford (Machine Shop Supervisor, Chemistry, University of Toronto) and I continued to develop the design while John translated the drawings into CAD software (**Figure A.4**). Johnny Lo (Machine Shop Craftsperson, Chemistry, University of Toronto) constructed all the components. With my help, Richard Garner led an improvement in the experimental design in 2016. Richard wrote one of the MATLAB scripts, and I wrote most of the other MATLAB code, with some assistance from Richard, Aleksa Dovijarski, and Stephanie Nyikos. Jonathan Wang provided weather monitoring.

I am the first author of the first manuscript (**Section 4.2**) which is adapted with permission from "Josey, D.S., Nyikos, S.R., Garner, R.K., Dovijarski, A., Castrucci, J.S., Wang, J.M., Evans, G.J., Bender, T.P. (**2017**). *Outdoor Performance and Stability of Boron Subphthalocyanines Applied as Electron Acceptors in Fullerene-free Organic Photovoltaics.* ACS Energy Lett., 2(3): 726-732."[170] Copyright 2019 American Chemical Society.

Stephanie Nyikos and Jeffrey Castrucci assisted me with the design of our new outdoor testing apparatus and experimental design. Stephanie assisted me with device fabrication and daily testing. Stephanie, Richard Garner, and Aleksa Dovijarski each played a role in assisting me with the data processing and analysis. Jonathan Wang collected the weather data required to comply with the protocols established by the International Summit on OPV Stability (ISOS), while under the supervision of Professor Evans. Professor Bender supervised and provided guidance throughout

the research and publication stages of this manuscript. I wrote the manuscript and performed all the other work not listed above.

I am the first author of the second manuscript (**Section 4.3**), which is adapted with permission from "Josey, D.S., Ingram, G.L., Garner, R.K., Wang, J.M., Evans, G.J., Lu, Z.-H., Bender, T.P. (**2019**). *Outdoor Stability of Chloro-(Chloro)$_n$ Boron Subnaphthalocyanine and Chloro-Boron Subphthalocyanine as Electron Acceptors in Bilayer and Trilayer Organic Photovoltaics.* ACS Applied Energy Materials, 2(2): 979-986."[40] Copyright 2019 American Chemical Society.

This study was a collaboration with Grayson Ingram under the supervision of Professor Lu. Richard Garner and I performed all the device fabrication and initial testing. I performed daily testing with assistance from Richard. Grayson performed photoluminescence and electroluminescence, during which he captured photographs and emission spectra. Grayson, Richard, and I all performed various roles in the data processing. Jonathan Wang collected the weather data required to comply with the protocols established by the International Summit on OPV Stability (ISOS), while under the supervision of Professor Evans. I wrote the entire manuscript with some assistance from Grayson. Professor Bender supervised and provided guidance throughout the research and writing stages.

I am the second author of the third manuscript (**Section 4.4**), which has been prepared for submission to *ACS Applied Electronic Materials*.

Much of this study was managed and performed by Hasan Raboui, including the optical measurements and some of the device fabrication. Jonathan Wang collected the weather data required to comply with the protocols established by the International Summit on OPV Stability (ISOS), while under the supervision of Professor Evans. I carried out the device fabrication of α-6T / Cl-BsubPc and Cl-Cl$_6$BsubPc OPVs and led the outdoor testing with the assistance of Hasan Raboui and Yin Jin. Only the α-6T / Cl-Cl$_6$BsubPc lifetime data appears in the manuscript, but α-6T / Cl-BsubPc was tested simultaneously. I have written an adaption of the manuscript to put this section in the context of the rest of my thesis, where I compare and discuss the stability of only the α-6T / Cl-BsubPc and α-6T / Cl-Cl$_6$BsubPc OPVs.

Appendix A includes all experimental details about materials, substrates, layer deposition, characterization, and stability testing.

4.1 Design of Outdoor Testing Protocols

4.1.1 ISOS Protocols

Researchers in the field of organic photovoltaic (OPV) stability recognized that the current protocols for more mature PV technologies might not apply to the challenges and degradation mechanisms involved in OPVs. Guidelines for conducting OPV stability tests were established through discussions at the first three International Summit on OPV Stability (ISOS) meetings (2008, 2009, and 2010).[39] These guidelines were introduced to enable comparisons between stability data collected different laboratories around the world. In order to maximize the number of laboratories able to adapt and use the protocols, three different levels of procedures were established for each type of testing: Basic (Level 1), Intermediate (Level 2), and Advanced (Level 3). Procedures were outlined for five different types of stability testing: dark, outdoor, laboratory weathering testing, thermal cycling, and solar-thermal humidity cycling.

The OPV stability tests conducted in this chapter were designed based on the procedures for the most advanced level of outdoor testing (ISOS-O3). The ISOS-O3 procedures specify the amounts of exposure to direct sunlight, ambient temperatures, and ambient relative humidity. The ISOS-O3 procedures permit static mounting (front side oriented towards the equator, tilted at latitude angle) and passive electrical loading (resistor). ISOS-O3 testing protocols also specify to monitor and report the ambient temperature, ambient relative humidity, irradiance, accumulated irradiance (insolation), substrate temperature on the backside, wind speed and direction. According to the ISOS-O3 protocols, the frequency at which the OPV outdoor output is to be monitored is every fifteen minutes to hourly. Indoor characterizations should be performed weekly to monthly. The report should also include the latitude, longitude, date of testing, J_{SC}, V_{OC}, FF, PCE/MPP, and stability performance parameters. Including full JV characterization in the report is optional.

4.1.2 Experimental Design

The standard design used for the OPVs made for non-stability studies consists of patterned ITO as the bottom electrode and silver strips as the top electrode (**Figure 4.1a**, **Figure A.1**). Silver is also coated on top of the ITO electrode for enhanced contact. For every type of electronic testing, contact must be made to each electrode on either side of the substrate while the device is held in precisely the correct position and orientation. A substrate holder and corresponding mounting modules for outdoor, indoor, and glove box testing were designed to facilitate this process (**Figure 4.1**). More detailed drawings of the components can be found in **Section A.7**.

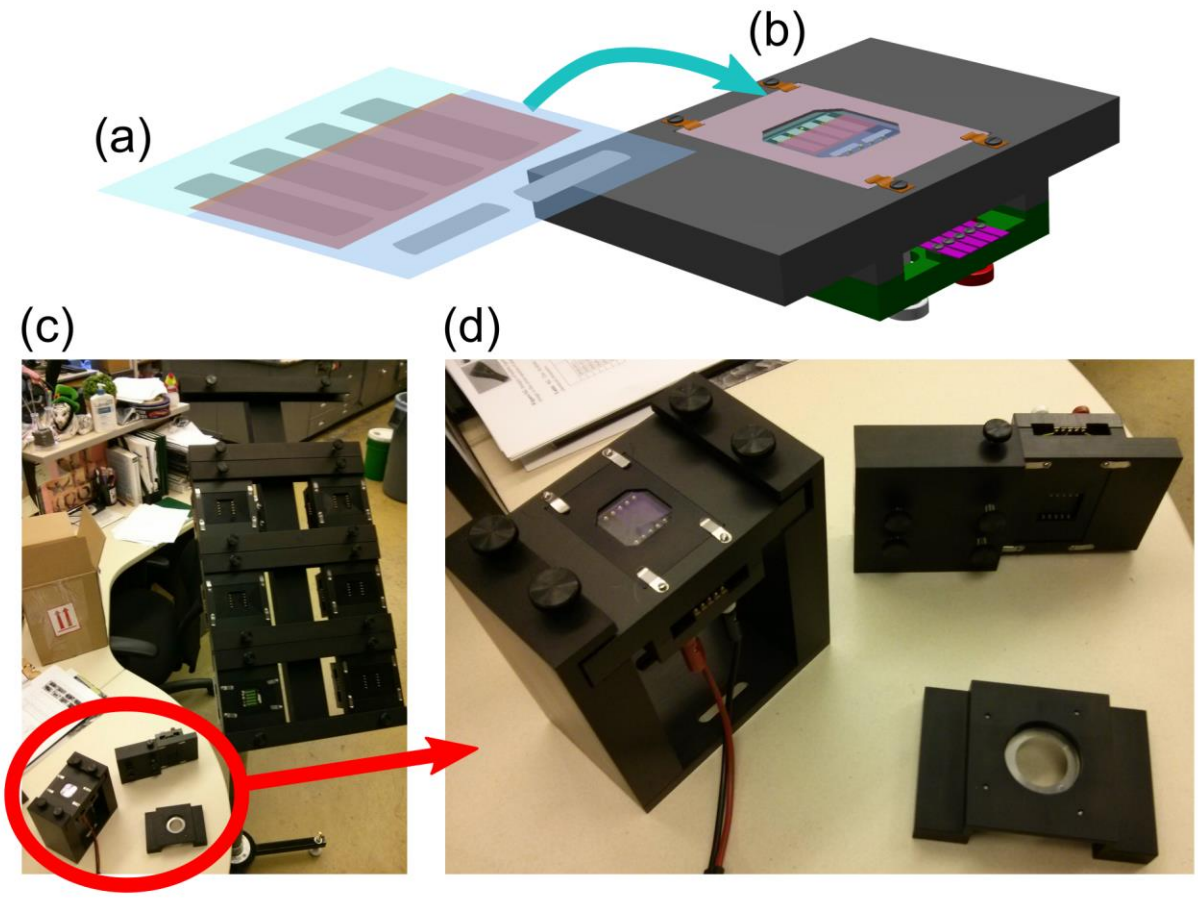

Figure 4.1. (a) A substrate with the approximate layout of the organic and metal layers of OPVs. The OPVs are inserted into a (b) custom-designed OPV substrate holders. Contact to metal layers is made with spring-loaded gold-coated pins that are wired to banana sockets installed on the bottom of the holder. The substrate holder can be mounted in the (c) outdoor testing module, (d)

left: indoor testing module, and top right: glove box testing module. A holder was also designed to hold the photodiode used for calibration (bottom right).

The substrate holders are made from black plastic (Delrin) and black anodized aluminum to minimize reflections. The substrate is secured onto the top of the substrate holder (**Figure 4.1b**), and each electrode is contacted with spring-loaded gold-coated pins. The pins are wired to banana sockets that are located on the bottom of the sample holder. The substrate holder enables quick electrical connections to be made to individual OPVs using banana plugs. The sides of the substrate holder are designed to fit into each of the three mounting modules (**Figure 4.1c,d**). Up to eight substrate holders can be loaded onto the outdoor testing module (**Figure 4.1c**), which ensures each holder is in the same plane. The outdoor testing module can be tilted to orient that plane to comply with the ISOS-O3 static mounting requirements. The indoor testing module (**Figure 4.1d**, left) secures one substrate holder horizontally for testing underneath a small area solar simulator (LCS-100, Newport). The glove box testing module (**Figure 4.1d**, top right) secures one substrate holder vertically in front of a liquid light guide, which feeds simulated solar light into the glove box for testing. A holder was also designed to locate the reference photodiode in the same plane as the substrates (**Figure 4.1d**, bottom right). The cross-compatibility of the substrate holders with each type of holder module enables OPVs to be rapidly moved between different methods of characterization, significantly reducing the amount of time spent conducting the daily measurements.

For outdoor stability testing, the outdoor testing module was placed outdoors on the roof of the Wallberg Building, University of Toronto, Ontario, Canada (latitude = 43.7°, longitude = -79.4°). OPVs were made using identical layer structures, other than which BsubPc was incorporated into the device. The OPVs were loaded into individual sample holders. Indoor JV characterization was performed on each day without precipitation (compared to the ISOS-O3 recommendation of weekly/monthly indoor measurements), and then the OPVs were brought outdoors (**Figure 4.2**, **Table C.1**, **Table D.1**, and **Table E.1**). The OPV output and temperature were monitored throughout each day, along with various weather conditions.

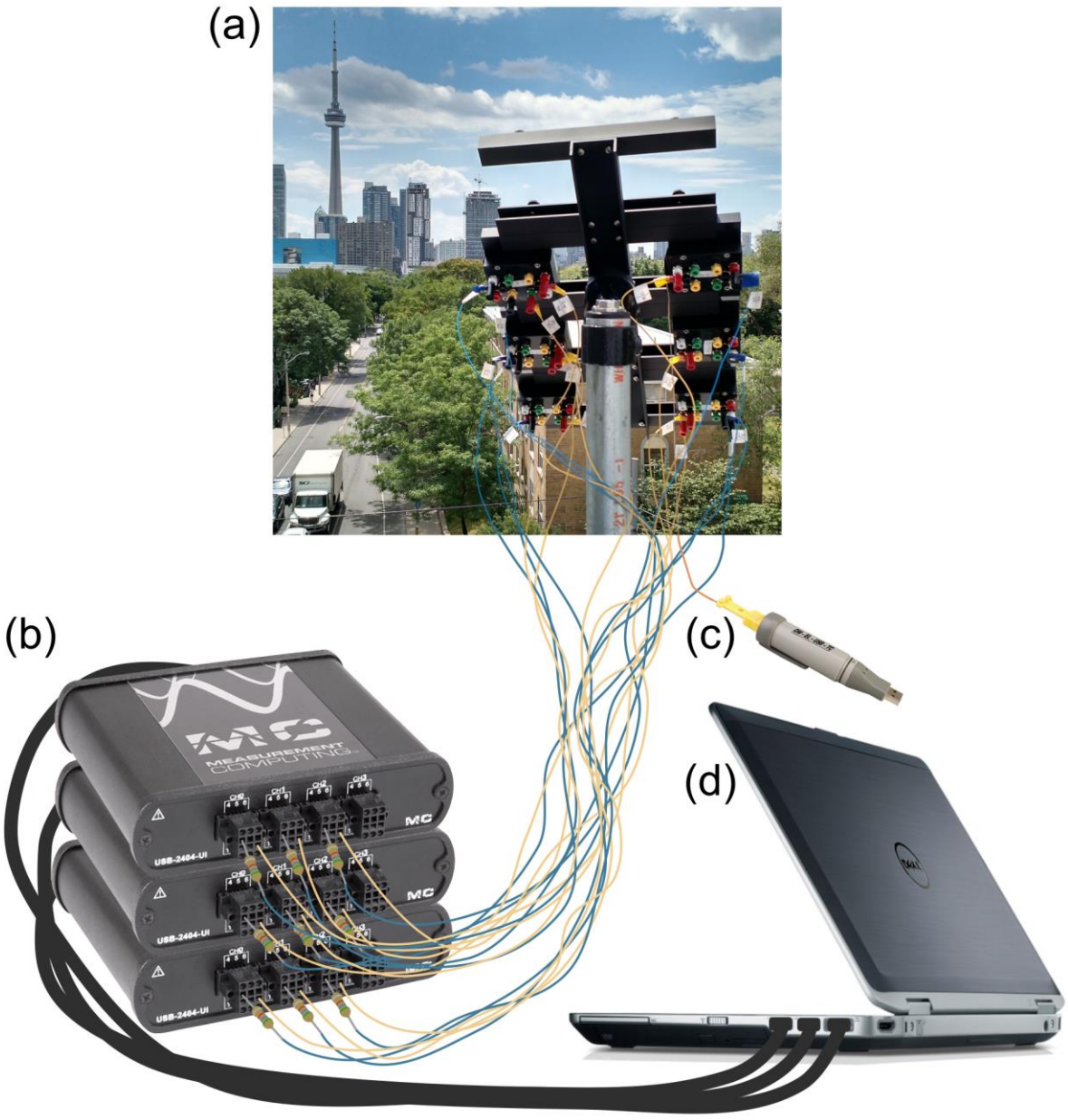

Figure 4.2. Outdoor testing set up used for **Section 4.2**. (a) A photo of the outdoor testing module on the roof of the Wallberg Building, University of Toronto, Ontario, Canada (latitude = 43.7°, longitude = -79.4°) with the front side oriented towards the equator, tilted at 43.7°. The outdoor testing module is loaded with substrate holders that contain encapsulated OPVs. Selected OPVs from each substrate are wired through a resistor to (b) Measurement Commuting USB-2404-UI data acquisition devices to monitor the currents produced throughout the day. A thermocouple

contacting the back of one of the substrates is used to monitor the temperature with a (c) battery-powered thermocouple data logger (OM-EL-USB-TC). OPV current data was displayed and saved directly to the (d) laptop computer. Temperature data was downloaded to the computer daily.

To comply with the ISOS-O3 protocols, the outdoor testing module with the OPV plane facing south, tilted at the ~43.7° latitude angle (**Figure 4.2a**). The exact southern direction was determined by using shadows at the calculated time of solar noon, and the tilt was set using a level and a protractor. The output of selected OPVs from each substrate was measured at 2 Hz (well above ISOS-O3 recommendations of 1/15 min to 1/1 hour) through resistors used to load the OPVs to their maximum power points passively. For the first study in **Section 4.2**, three Measurement Computing USB 2404-UI data acquisition devices were used to measure the current of the OPVs, a battery-powered thermocouple data logger was used to monitor temperature on the back of one substrate, and a horizontally mounted pyranometer was used to measure irradiance.

For subsequent studies, the laptop and data acquisition devices were located indoors, and the OPV outputs were connected indoors through 15 m radio-shielded cable. Instead of the USB 2404-UI data acquisition devices, a National Instruments 32-channel potentiometric NI-9205 data acquisition device was employed. The increased number of channels enabled the simultaneous monitoring of more OPVs. The USB 2404-UI devices were repurposed to monitor temperature on the back of two substrates. Instead of the horizontally mounted pyranometer, a Hukseflux LP02 pyranometer was installed onto the outdoor testing module and tilted in the same plane as the OPVs (**Figure A.2**). The voltage output from the pyranometer was monitored on one of the NI-9205 channels. With all the measurement devices inside, data acquisition was run continuously (24 hours a day), even when the OPVs were not connected outdoors.

In all studies, weather data (air temperature, relative humidity, and wind speed) was collected from a weather station located within approximately 6 m of the outdoor testing module. The location of the wind speed monitoring device (optional for ISOS-O1 and ISOS-O2) is therefore slightly farther than the distance recommended in ISOS-O3 (1.2 m). ISOS-O3 specifies that the passive loads must stay within 10% of the resistance at maximum power point. This specification was

maintained for every stability test in this chapter except for the phenoxy- and phenyl-BsubPc stability tests in **Section 4.2**, which deviated by more than 10%.

4.1.3 Analysis

The continuous collection of voltage data at 2 Hz amounted to daily text files over 15 MB in size. Temperature data was collected at 2 Hz only while the OPVs were connected, resulting in text files typically over 3 MB in size. MATLAB code was written to convert the raw voltage data into current density, irradiance, and insolation to minimize the time required to process this data. MATLAB code was also written to sync the time component of this data with the time of the temperature data and with the indoor JV characterizations. This automation of data processing enabled rapid assessment of the OPV state of degradation, ensuring that additional characterizations (such as external quantum efficiencies) were measured at the appropriate stages of degradation.

In the 2015 study (**Section 4.2**), irradiance was monitored using a horizontally mounted sensor. In order to appropriately compare the measured irradiance to the irradiance received by the OPVs, the tilted irradiance was estimated using correlations developed by Erbs et al.[171] MATLAB code was once again written to facilitate the conversion of horizontal irradiance to tilted irradiance for the entire dataset.

The use of resistors to passively load the OPVs to their maximum power points (MPPs) will always be less precise than using active maximum power point tracking. Calculations were performed using data from the 2016 study to estimate the difference in precision between passive loading and active tracking (**Section 4.3**). These calculations used the daily JV characterizations made indoors under simulated light, the outdoor OPV output while loaded with resistors, and the assumption that the open-circuit voltage and fill factor remain approximately constant under the solar irradiances incurred. The difference in precision between passive and active tracking was assessed based on total energy conversion, which implicitly emphasizes the loading accuracy under high levels of solar irradiation and deemphasizes loading inaccuracy under low levels of solar irradiation. The

full equations (**Equation D.1**), graphical illustrations (**Figure D.1**), and a detailed explanation of the calculations can be found in **Appendix D**.

4.2 Influence of Axial Substituents on Outdoor Lifetime

The outdoor lifetime and performance of organic photovoltaics (OPVs) using boron subphthalocyanine (BsubPc) derivatives as electron-accepting materials are presented. The protocols followed are based on the most advanced level of outdoor testing established by the International Summit on OPV Stability (ISOS). The stability of each BsubPc is compared using three different sets of encapsulated planar heterojunction OPVs, with each set containing a different BsubPc as the electron-accepting layer. The performance and stability of each set are tested outdoors using epoxy glue and a glass coverslip as protection from the ambient environment. Outdoor testing continued until the OPVs reached 80 or 50% of their original power conversion efficiency, as determined by frequent indoor characterization. OPVs utilizing chloro-BsubPc exhibit the highest stability and performance, while the stability of the other two BsubPc derivatives is reduced presumably as a result of their phenoxy or phenyl functionalization in the molecular axial positions. The established structure-property relationship and guidance for the design of future compounds for application in planar heterojunction OPVs are contrary to, and could not have been anticipated from, time zero laboratory testing.

4.2.1 Discussion

The prospect of renewable energy in the form of a flexible, low-cost solar cell with low energy-payback time has motivated a vast amount of effort on improving organic photovoltaic (OPV) technology.[172-176] The majority of this effort is spent on the synthesis of new materials and the optimization of device architectures to produce high power conversion efficiencies (PCEs) immediately after fabrication, as characterized at time zero (T_0) by “one sun” of simulated sunlight.[177-178] The performance of these new materials in the outdoor ambient environment over the time scale of a device lifetime is just as critical to the pursuit of high-performance, commercially feasible OPVs and their industrial production.[179-180]

Protocols have been developed through the International Summit on OPV Stability (ISOS) to establish standards for lifetime testing.[39] OPV lifetime studies that adhere to these protocols have been conducted to investigate encapsulation,[181-184] electrodes,[185-188] charge transport layers,[189-197] and active layers.[198-203] All of these cited studies use solution-processed bulk heterojunction (BHJ) OPV architectures, whereby performance is strongly dependent on active layer morphology.[204] To decouple individual material performance from potentially complex morphological degradation mechanisms, vacuum deposition techniques can be used to fabricate planar heterojunction (PHJ) OPV architectures. The performance of each material in a PHJ OPV can be studied and directly compared to that of other materials via substitution, without changing or needing to engineer the active layer morphologies within the device.

A class of materials that have been shown to perform well as electron acceptors in OPVs are boron subphthalocyanines (BsubPcs).[44, 46, 68, 75, 79, 89] The tuneability of their electronic and physical properties through straightforward chemical modifications have been well documented, with reported syntheses of many new BsubPc derivatives in recent years.[205] The most common BsubPc derivative is chloro-BsubPc (Cl-BsubPc). A PHJ OPV recently developed by Cnops et al. incorporated Cl-BsubPc to achieve a record PHJ OPV PCE of 8.4%.[79] Their wide range of accessible properties allows BsubPcs to be adjusted to suit a variety of applications. BsubPc derivatives have been used in BHJ OPVs to reach PCEs of up to 4%[47, 206] and have been shown to harvest pentacene-generated triplets successfully.[76] Cl-BsubPc has also been shown to be applicable as an injection layer in perovskite-based solar cells.[207] To date, however, only the Cl-BsubPc variant has been tested for stability in OPVs.[81, 208-209] The most recent report examined an OPV structure similar to the one developed by Cnops et al. within a laboratory under AM1.5G illumination at 38 °C and 50% relative humidity.[81] While this study did not adhere to ISOS protocols, it did identify alpha-sexithiophene (α-6T) as the main degrading component within the OPV. The two previous studies focused on an OPV with Cl-BsubPc as an electron donor material paired with C_{60} fullerene,[208-209] which limited the possible insight regarding BsubPc stability due to convolution with the faster degradation and burn-in effects of the C_{60} fullerene.

One of the fullerene-free PHJ OPV baselines identified by Cnops et al. incorporates α-6T as an electron-donating material with Cl-BsubPc as an electron acceptor.[79] We have demonstrated our ability to replicate this baseline and have shown that it is suitable to explore other BsubPc derivatives,[89] such as phenoxy-BsubPc (PhO-BsubPc) and phenyl-BsubPc (Ph-BsubPc) (**Figure 4.3**).[54, 138] In terms of time zero (T_0, day of fabrication) performance in PHJ OPVs, PhO- and Ph-BsubPcs do not yet match Cl-BsubPc (Table 4.1). Both compounds do produce higher open-circuit voltages (V_{OC}s) than Cl-BsubPc, a parameter of interest that is known to be linked directly to material properties.[61, 210] Improvements in the short-circuit current (J_{SC}) and fill factor (FF) could likely be achieved through further device engineering, but their outdoor stability should first be assessed to determine whether that additional effort is warranted.

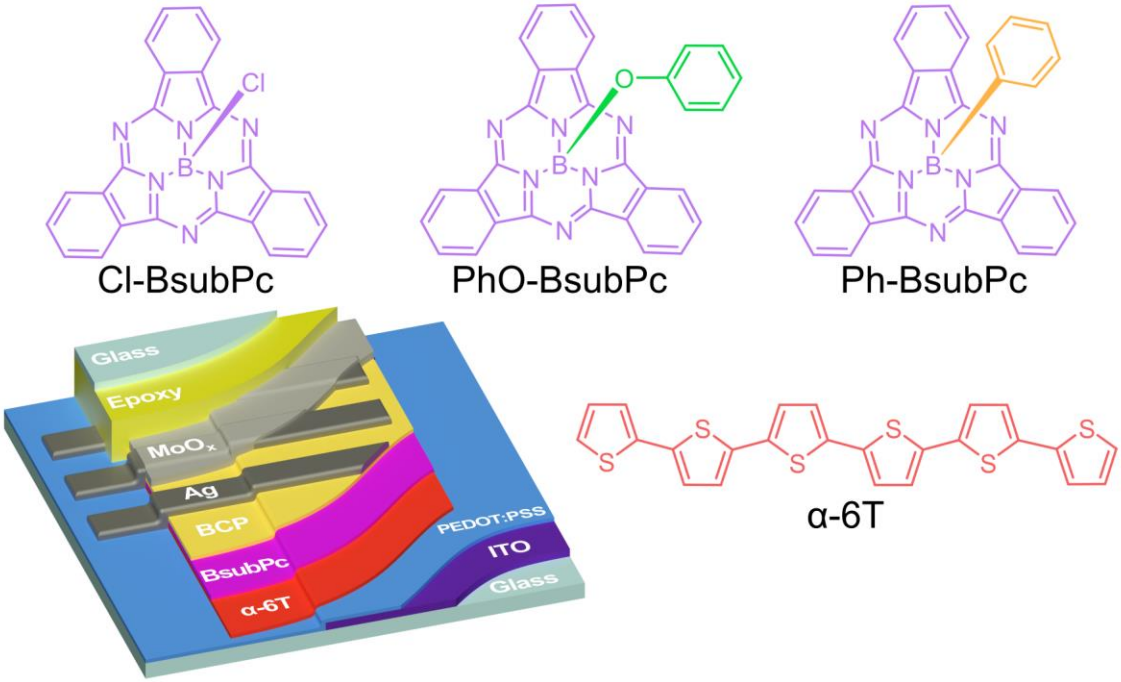

Figure 4.3. Chemical structures of Cl-BsubPc, PhO-BsubPc, Ph-BsubPc, and α-6T. Device schematic illustrating the bilayer architecture and epoxy / glass encapsulation method.

In this section, we present an outdoor lifetime study of PHJ OPVs using a custom-built apparatus to evaluate the performance and stability of Cl-, PhO-, and Ph-BsubPcs in encapsulated, lab-scale OPVs (**Figure 4.3**). Outdoor OPV performance monitored in real time is shown, and total power

production is extrapolated to provide a rough estimate of the true potential of BsubPcs as OPV materials.

Indoor Data. Three BsubPc derivatives were tested in OPVs for outdoor stability: Cl-BsubPc, PhO-BsubPc, and Ph-BsubPc (**Figure 4.3**). As in our previous studies, the active layers consisted of α-6T (electron donor) paired separately with each BsubPc (electron acceptor).[89, 138] Each device was encapsulated using epoxy glue and a glass coverslip to protect the materials from ambient oxygen and moisture (**Figure 4.3**).

On days without precipitation, the OPVs were moved outdoors and monitored under direct sunlight while passively loaded at their time zero resistance at the maximum power point (MPP, R_{MPP}). On these days, current density-voltage (J–V) characterization was performed indoors under artificial solar simulation (**Figure 4.4a** and **Table 4.1**) before moving the OPVs outside. The OPVs were removed from outdoor testing at the end of day and returned to indoor storage at room temperature in the dark. This process was repeated until the Cl-BsubPc OPVs reached "T_{80}" and the PhO- and Ph-BsubPc OPVs reached "T_{50}" (the operation time at which the OPVs reach 80 and 50% of their original PCE, respectively). External quantum efficiency (EQE) measurements taken at T_0, T_{80}, and T_{50}, show the changes in performance throughout the device lifetime (**Figure 4.4b**). Performing both indoor and outdoor characterization satisfies the most advanced level of outdoor testing (ISOS-O3).[39] The frequency of indoor J–V characterization exceeds the minimum ISOS-O3 requirements and provides enough data to monitor each device parameter throughout the OPV degradation closely. This high frequency is especially valuable for measuring changes to the FF and MPP, given the lack of active MPP tracking in the passively loaded outdoor measurements.

Table 4.1. Average device parameters of α-6T / Cl-, PhO-, and Ph-BsubPc OPVs. The standard deviation is indicated in brackets next to each parameter. At least seven devices were used to determine these values.

acceptor	time	Voc[a] (V)	Jsc[b] (mA/cm^2)	FF[c]	PCE[d] (%)
Cl-BsubPc	T_0	1.10 (0.007)	6.04 (0.10)	0.54 (0.02)	3.57 (0.19)
	T_{80}	1.11 (0.014)	5.62 (0.11)	0.46 (0.02)	2.85 (0.18)
PhO-BsubPc	T_0	1.17 (0.019)	4.83 (0.07)	0.49 (0.01)	2.77 (0.09)
	T_{80}	1.18 (0.007)	3.92 (0.10)	0.48 (0.01)	2.20 (0.10)
	T_{50}	1.18 (0.015)	3.22 (0.08)	0.37 (0.01)	1.40 (0.06)
Ph-BsubPc	T_0	1.21 (0.010)	4.40 (0.08)	0.47 (0.01)	2.51 (0.08)
	T_{80}	1.21 (0.005)	3.20 (0.09)	0.51 (0.01)	1.96 (0.05)
	T_{50}	1.21 (0.002)	2.42 (0.08)	0.45 (0.01)	1.30 (0.04)

[a]Open-circuit voltage. [b]Short-circuit current density. [c]Fill factor. [d]Power conversion efficiency.

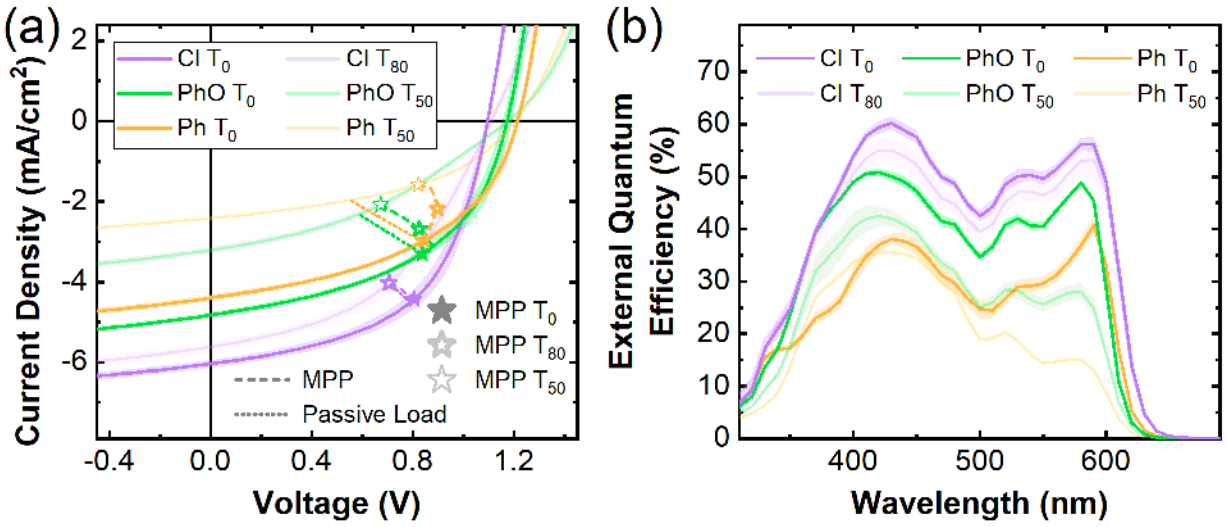

Figure 4.4. (a) J–V characteristics and (b) EQE spectra of α-6T / Cl-, PhO-, and Ph-BsubPc OPVs as measured indoors under AM1.5G solar simulation at time zero (T_0) and after degrading to 80% (T_{80}) and 50% (T_{50}) of their original PCE.

The differences in how the J–V curves degrade over the OPV lifetimes suggest that the stability of the BsubPc derivatives is affected by their structural differences. The degradations in performance are mainly due to losses in J_{SC} and FF, albeit by different amounts for each BsubPc. The V_{OC}

remains mostly unaffected, remaining almost constant over the lifetimes of each OPV. In correlation with the varying degrees of degradation of the J_{SC}s and FFs for different BsubPcs, the MPPs and the corresponding R_{MPP} values also change differently. This difference in change can be seen by comparing the pathways that the MPPs follow over the OPV lifetimes with the corresponding passive load pathways, which is plotted using the time zero R_{MPP}'s. The R_{MPP} values of the Ph-BsubPc OPVs increase the most from T_0 to T_{50}, whereas the R_{MPP}'s of the PhO-BsubPc OPVs only increase by about half of that amount. The R_{MPP} values of the Cl-BsubPc OPVs remain almost constant from T_0 to T_{80}.

Electrically, the BsubPc degradation manifests itself in the differences in MPP pathways. The Cl-BsubPc OPVs maintain a remarkably linear MPP pathway relative to the other two OPVs, with the average R_{MPP} never varying by more than 6%. The MPP pathway of the PhO-BsubPc OPVs deviates from this linear trend, with a rapid initial increase in MPP resistance, followed by a slower but steady increase. The MPP pathway of the Ph-BsubPc OPVs changes similarly to that of PhO-BsubPc but with an even more pronounced deviation from the passive load pathway. Due to this apparent correlation between the MPP pathway and BsubPc degradation, the MPP pathway serves as an interesting tool for future OPV degradation studies. From this study, the linearity of the MPP pathway seems to indicate when active layer degradation or when an imbalance in active layer degradation is occurring.

The EQE measurements show a substantial variation in BsubPc contribution to the photocurrent at the different stages of the OPV lifetime. Comparing the initial and final EQEs measured, the BsubPc peak (~580 nm) in the Cl-BsubPc OPV remains approximately as stable, if not more stable, than the α-6T peak (~430 nm). On the other hand, the PhO-BsubPc contribution drops significantly, and the Ph-BsubPc contribution almost completely disappears (**Figure 4.4b**).

The reduction in EQE contributions is consistent with the J_{SC} losses in the J–V measurements. In the Cl-BsubPc case, the equivalent drops seen in α-6T and BsubPc contributions indicate that either the two materials are degrading at the same rate or that a nonactive layer component of the OPV is the dominant source of degradation. In the cases of PhO- and Ph-BsubPc, the EQE

measurements conclusively show that the BsubPc derivative is the limiting factor in the OPV lifetime.

Outdoor Data. When the OPVs were mounted outside for testing (**Table C.1**), a custom apparatus was used to comply with ISOS outdoor testing protocols for static mounting.[39] The OPVs were passively loaded, and the current output, irradiation, and substrate temperature were continuously monitored (**Figure 4.5**), also by ISOS protocols. These current outputs correspond to the dotted "passive load" from **Figure 4.4** because the OPVs were loaded using a constant resistor but with output variations resulting from the natural variations in sunlight intensities incident on the OPVs.

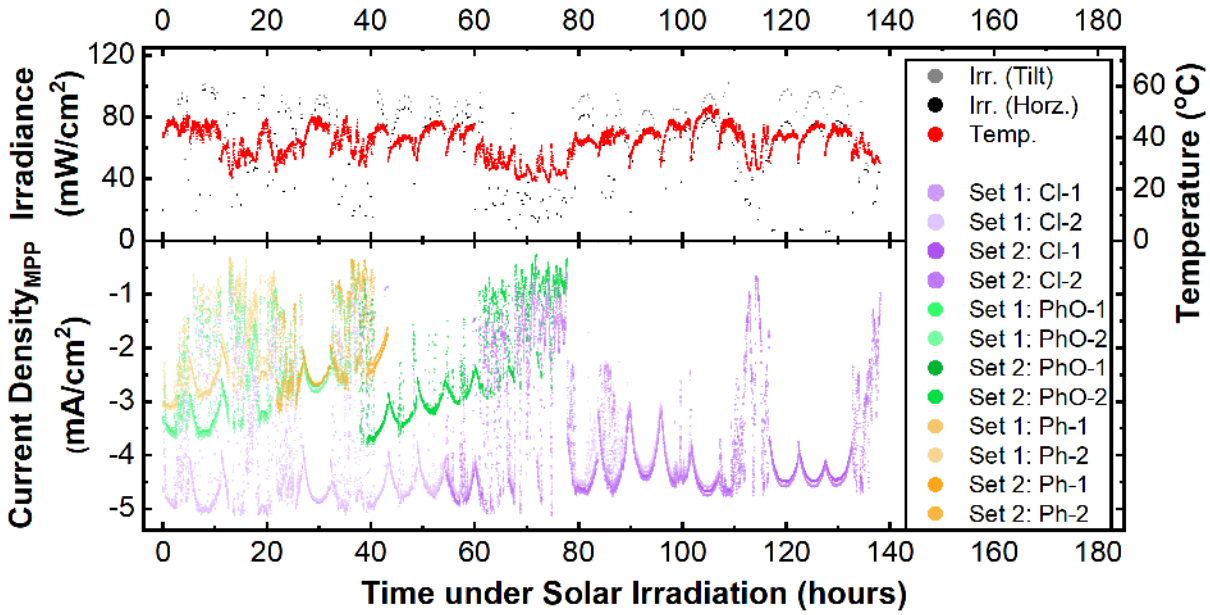

Figure 4.5. Continuous monitoring of current density produced by α-6T / Cl-, PhO-, and Ph-BsubPc OPVs at MPP as tracked under passive load, while mounted on our static outdoor testing apparatus on the roof of the Wallberg Building, University of Toronto, Ontario, Canada. The corresponding horizontal irradiation, calculated incident irradiation (tilted at 43.7°),[171] and substrate temperature are also shown.

The Cl-BsubPc OPVs generated the highest currents under passive load and took far longer to degrade than the other BsubPcs. The T_{80} of the first Cl-BsubPc set was about 24 h longer than that of the second set, at 107 and 83 h of irradiation, respectively. The first set also endured slightly

more intense levels of irradiation than the second set. The two sets of PhO-BsubPc and Ph-BsubPc OPVs generated lower currents and had T_{50}'s of only ~39 and 22 h of irradiation, respectively.

The α-6T / Cl-BsubPc OPVs experience effectively zero degradation on the time scale that it takes the PhO-BsubPc and Ph-BsubPc OPVs to reach T_{50}. The α-6T / Cl-BsubPc OPVs serve as a lower bound for the lifetime of the non-BsubPc layers in the OPV, including the α-6T layer, which is known to degrade faster than Cl-BsubPc.[81] The lifetime of the α-6T / Cl-BsubPc OPVs further demonstrates that the degradation of the PhO- and Ph-BsubPc layers must be exclusively responsible for the significantly reduced lifetimes of their corresponding OPVs. Based on chemical structure, PhO- and Ph-BsubPc are likely more susceptible to hydrolysis than Cl-BsubPc, which may be the primary degradation mechanism if any water is present in the OPV. Additionally, the permeation of protons from the PEDOT:PSS layer through the OPV to the BsubPc layer could be facilitating the hydrolysis, as PEDOT:PSS is also a known cause of OPV degradation.[211-214]

In practical terms, the most industrially relevant metric of OPVs is their actual power generation. Integration of the current output provides the total power output of each cell (**Figure 4.6**). The output from the 0.2 cm^2 devices is extrapolated to kWh/m^2, matching current PV standards in the field.

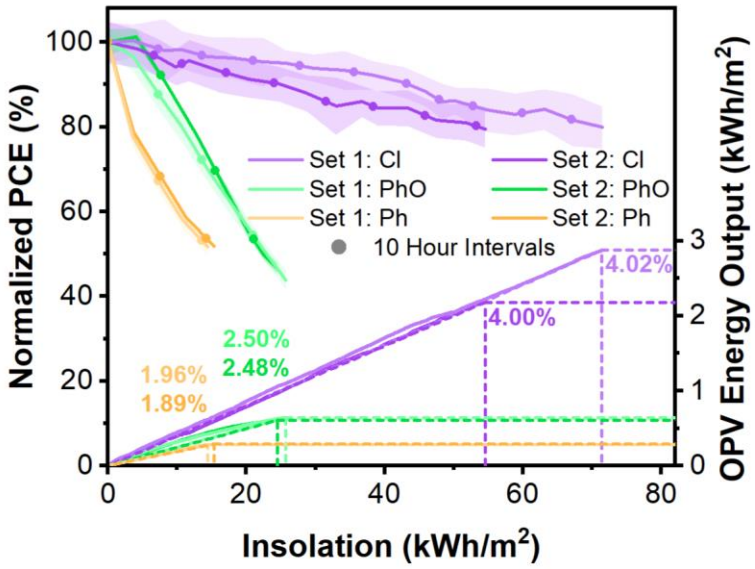

Figure 4.6. Normalized average PCE (left y-axis) and average accumulated energy output from -6T / Cl-, PhO-, and Ph-BsubPc OPV sets (right y-axis) versus the accumulated incident irradiance. Time spent outdoors under solar irradiation is indicated in 10-hour intervals. Overall OPV lifetime efficiency is shown, as calculated from the total energy output and total accumulated irradiance.

The Cl-BsubPc OPVs produce more power for far longer than the other OPVs, converting ~55–71 kWh/m^2 of incident irradiance with an overall PCE of 4.0% before reaching T_{80}. The PhO- and Ph-BsubPc OPVs only endured ~11 and ~22 kWh/m^2 before reaching T_{50}, with overall PCEs of 2.5 and 1.9%, respectively. Despite degrading to 80% of their T_0 PCE throughout testing, the overall outdoor performance of the Cl-BsubPc OPVs exceeds their T_0 PCE (**Table 4.1** and **Figure 4.4**). Compared to indoor simulated light testing, the OPVs encountered lower average incident irradiance and increased device temperature, both of which are known to improve OPV performance. The overall PCEs of the PhO- and Ph-BsubPc OPVs during outdoor testing were lower than their PCEs at T_0, but this also includes a much more extensive degradation.

The evolution of the performance of OPVs with accumulated irradiation is known to have three different regimes: “burn-in” (exponential decay), “long-term” (linear decay), and “failure” (rapid decay).[215] The evolution of the performance of each BsubPc-based OPV studied herein is relatively steady throughout the entire testing period for all sets, and they did not show burn-in, an

effect attributed to fullerene polymerization.[208, 215] The observation of linear decay is potentially supportive of hydrolysis being the degradation mechanism.

Each repeated set almost perfectly duplicates the original sets, apart from the original Cl-BsubPc devices enduring ~16 kWh/m^2 more accumulated irradiance. These discrepancies could be due to a slight difference in the initial performance of the OPVs or due to a difference in environmental conditions endured by the two sets. The FF of the original Cl-BsubPc OPVs was slightly higher than that of the replicate Cl-BsubPc OPVs (0.55 vs 0.53), resulting in a slightly higher initial PCE at T_0. There were generally fewer cloudy days during the testing of the repeated set, which resulted in some days with higher peak temperatures than those incurred by the original set. Despite these discrepancies, the Cl-BsubPc OPVs still perform far better than the other OPVs in the lifetime testing set.

4.2.2 Conclusions

This study demonstrates the significant influence that minor chemical modifications can have on stability. The stability of each BsubPc is shown to be strongly dependent on the functional group substituted at the axial position, with each BsubPc derivative resulting in dramatically different OPV lifetimes. BsubPc stability was shown to influence how the electrical characteristics degrade over time, with the OPV MPPs following different pathways depending on the BsubPc. The functionalization of BsubPcs in the axial position with a chloro group is shown to result in significantly higher outdoor stability compared to BsubPcs functionalized with phenoxy and phenyl groups. To investigate BsubPc derivatives that are potentially more stable than Cl-BsubPc, engineering to specifically address device longevity will have to be undertaken to ensure that the other components in the OPV are at least as stable as the Cl-BsubPc. Considering that none of the OPVs in this study were optimized specifically for device longevity, future optimization could yield significant improvements in lifetime. Future work will also consider additional structural variants of BsubPcs and alternatives to PEDOT:PSS within α-6T PHJ OPVs. This future work will aid in firming the identification of the degradation pathways and mechanism(s) for BsubPcs, and the relative stability of the PHJ OPV device structure.

4.3 Outdoor Stability of Boron Subnaphthalocyanines

In the field of organic photovoltaics (OPVs), outdoor stability research has lagged behind material development and device engineering. Testing protocols established at the International Summit of OPV Stability (ISOS) have stimulated some stability research, but these studies are almost exclusively limited to already-refined devices made with already-commercialized materials. If OPV materials were tested outdoors during small-scale stages, stability issues could be detected earlier in the development cycle. Chloro-(chloro)$_n$ boron subnaphthalocyanine (Cl-Cl$_n$BsubNc) is a material with high OPV performance but has not previously been tested outdoors. An OPV power conversion efficiency of 8.4% has been already demonstrated for a trilayer stack containing α-sexithiophene, Cl-Cl$_n$BsubNc, and chloro-boron subphthalocyanine (Cl-BsubPc). Building on the most advanced ISOS outdoor testing protocols (ISOS-O3), we assess the outdoor stability of small-scale bilayer and trilayer OPVs while establishing an improved stability screening method for future derivatives. The outdoor stability of Cl-Cl$_n$BsubNc is determined to be comparable to that of Cl-BsubPc.

4.3.1 Discussion

Organic photovoltaics (OPVs) are a promising source of renewable energy but have yet to realize their potential on an industrial scale. One significant barrier to large-scale OPV commercialization has been a low priority given to outdoor stability research within the field.[216] There is a significant investment of resources into the development of new materials and the associated optimizing of OPV device structures to achieve high power conversion efficiencies (PCEs),[35, 217-220] but comparatively little research devoted to assessing the ambient environment stability of newly developed OPVs.[180, 216, 221-222]

Stability testing protocols were established in 2011 at the International Summit of OPV Stability (ISOS).[39] The outdoor protocols specify setup requirements (mounting orientation and type of resistive loading), parameters to measure (OPV output, irradiance, J–V characterization, substrate temperature, relative humidity, and wind speed/direction), the frequency of those measurements, and how to report stability studies. The establishment of ISOS protocols has stimulated approximately 23 outdoor OPV stability studies citing the protocol.[170, 183-184, 190, 214, 223-240] OPV

performance losses outdoors and over time can occur due to many factors, such as material instability,[170, 224, 226] change in morphology,[228, 241] introduction of traps,[242] and electrode degradation.[190, 238-239, 243] While the stability benchmarking, device engineering, and encapsulation advances achieved through these outdoor studies have been invaluable, only two of these studies[223-224] (apart from our work[170, 226]) incorporated an organic material that is not yet commercially available. All other ISOS-standardized stability tests of new materials have been limited to laboratory-controlled environments, which are difficult to correlate to the continually changing and geographically dependent environmental conditions outdoors.[225] If outdoor stability testing were conducted earlier in the development cycle of new OPV materials, unstable materials could be filtered out before scale-up and further study.

The use of a planar heterojunction (PHJ) architecture limits the influence of morphology on device performance,[228] making PHJ OPVs an ideal architecture to test material stability. Two similar classes of materials have been demonstrated to perform exceptionally well as electron-accepting fullerene replacements in laboratory-scale, planar heterojunction (PHJ) OPVs: boron subnaphthalocyanines (BsubNcs) and boron subphthalocyanines (BsubPcs).[46, 48, 67-68, 76-77, 79, 89, 138-140] BsubNcs and BsubPcs have many synthetic handles for tuning performance, with established synthetic procedures to achieving many different derivatives.[67, 140, 205, 244-249] We recently determined that BsubNcs actually consist of an alloyed mixture of chlorinated species (Cl_nBsubNc), a mixture that benefits their OPV performance.[67] We also previously conducted small-scale outdoor tests on some BsubPc derivatives, determining that phenoxy and phenyl substituents in the axial position of a BsubPc significantly harm their outdoor stability relative to the prototypical Cl-BsubPc.[170, 226] Cnops et al. demonstrated a record power conversion efficiency of 8.4% for a PHJ OPV by combining chloro-Cl_nBsubNc (Cl-Cl_nBsubNc) and chloro-BsubPc (Cl-BsubPc) with sexithiophene (α-6T).[79] To date, the stability of this device architecture has only been assessed under controlled laboratory conditions.[81]

The ability to visually inspect electroluminescent devices such as OLEDs for inactive regions (dark spots) facilitates degradation analysis. Electroluminescence (EL) is a valuable tool for probing OPV emission spectra and visualizing edge ingress and the formation of nonconductive

spots/regions.[250-256] Cl-BsubPc has a unique EL property of two distinct emission peaks, attributed to monomer and aggregate regions of the solid layer.[43, 257-259] The EL emission spectra can, therefore, indicate the relative monomer/aggregate content within the Cl-BsubPc layer.

In this study, we employ three, high-performance PHJ OPV layer stacks previously reported by Cnops et al. (**Figure 4.7**) and we evaluate their outdoor performance and stability following the highest level of ISOS outdoor testing protocols (ISOS-O3).[79] This study is an expansion of our previous outdoor studies of Cl-BsubPc stability as both electron-accepting and electron-donating materials in a PHJ OPV architecture. We also exploit the EL of Cl-BsubPc[257] and Cl-Cl$_n$BsubNc[260] within PHJ OPV device structures, using EL imaging (ELI) and the spectra to monitor edge ingress and overall device degradation.

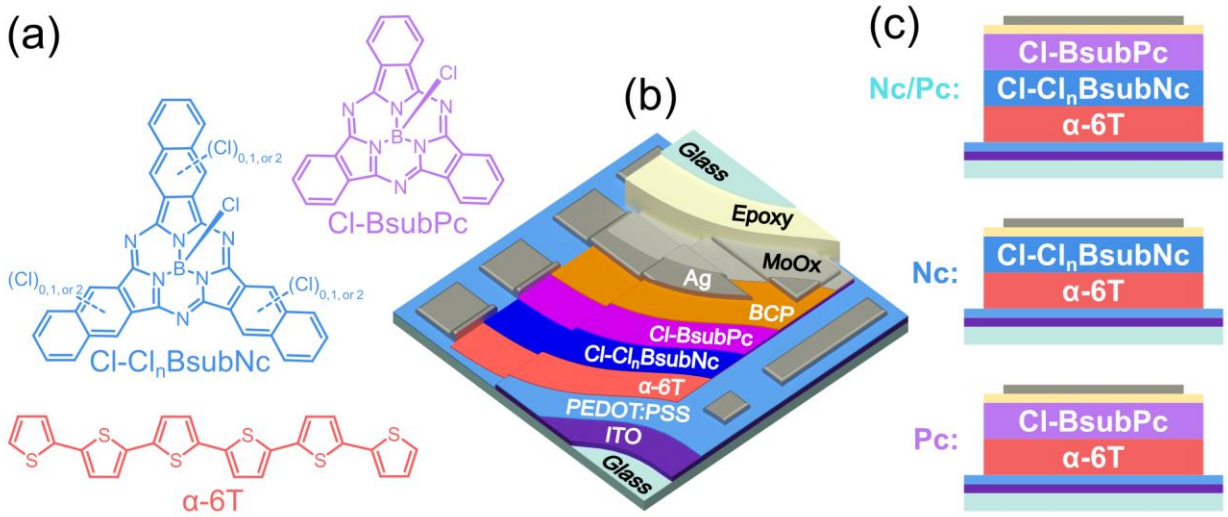

Figure 4.7. (a) Chemical structures of α-6T, Cl-Cl$_n$BsubNc, and Cl-BsubPc; (b) device schematic illustrating the full layer stack, including the encapsulation layers; (c) three different active layer combinations used in this study: "Nc/Pc" = α-6T / Cl-Cl$_n$BsubNc / Cl-BsubPc, "Nc" = α-6T / Cl-Cl$_n$BsubNc, and "Pc" = α-6T / Cl-BsubPc. Layer thicknesses shown are not to scale.

The stability of two high-performance, electron-accepting materials (Cl-BsubPc and Cl-Cl$_n$BsubNc) was examined within PHJ OPV structures while operated in the outdoor environment, following ISOS-O3 protocols. Three different OPV structures were tested, using sexithiophene (α-6T) as the common electron-donating material: α-6T / Cl-Cl$_n$BsubNc / Cl-BsubPc (Nc/Pc), α-6T /

Cl-Cl$_n$BsubNc (Nc), and α-6T / Cl-BsubPc (Pc), referred to as Nc/Pc, Nc, and Pc, respectively, throughout this report. The layer stacks and thicknesses were based on our previous work and those published by Cnops et al.[67, 79, 89] We employed the same electrodes and buffer/injection layers for each structure (ITO / PEDOT:PSS and BCP / Ag). Having already demonstrated the outdoor stability of the Pc device in a previous study,[170] the Pc device serves as a baseline for this study with the reacquisition of associated data.

Following our previous study, outdoor testing was only performed on days without precipitation. On such days (Table D.1) the OPVs were removed from dark storage, characterized with current density-voltage (J–V) sweeps under AM1.5G light, and then moved to our custom outdoor testing apparatus (Figure A.2). The outdoor voltage outputs were converted to current densities and monitored for approximately eight hours (solar noon ± four hours), along with substrate temperature and in-plane irradiance (**Figure 4.8a**). The OPVs were then returned to dark storage indoors at the end of each day. This process was repeated until the OPVs reached T_{80}, characterized as the useful lifetime of an OPV and defined here as the amount of time an OPV spends outdoors until reaching 80% of its peak PCE (**Figure 4.8b**, left *y*-axis). Combining the incident irradiance, the outdoor OPV output and the PCE calculations from the daily indoor J–V characterization (**Figure 4.8b**, right *y*-axis) revealed a direct correlation between OPV degradation and insolation.

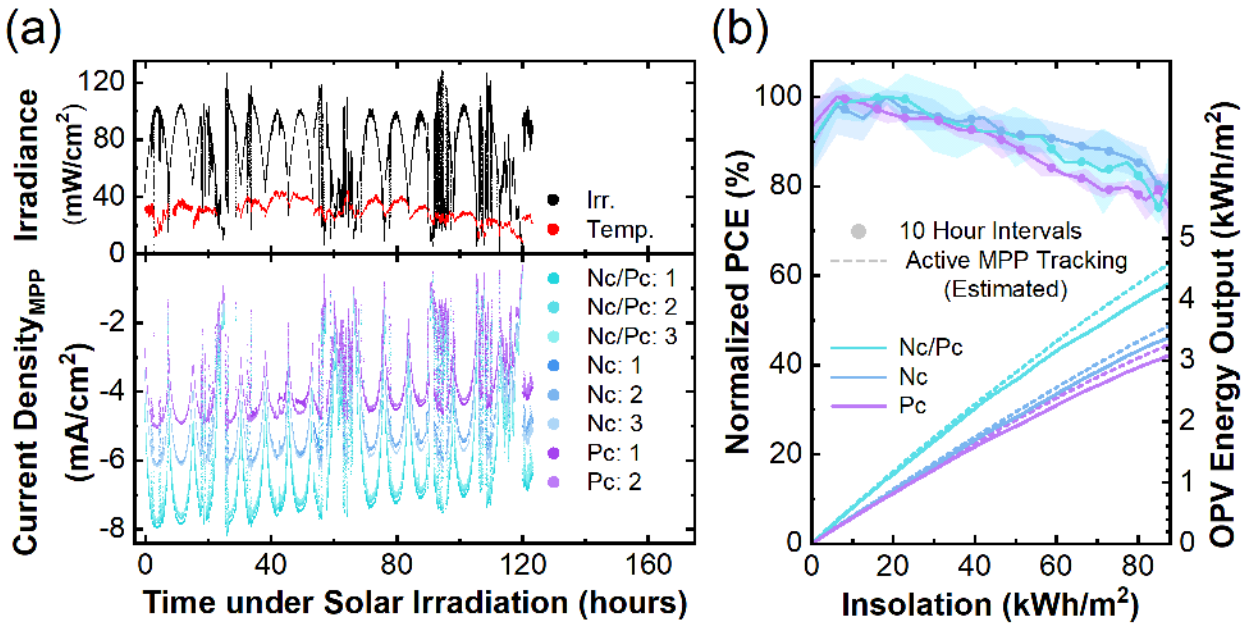

Figure 4.8. (a) In-plane (43.7) irradiation, substrate temperature, and current density produced by Nc/Pc, Nc, and Pc OPVs while passively loaded to their maximum power point (MPP) and mounted on our static outdoor testing apparatus. (b) Normalized average PCE (left y-axis) and average accumulated energy output (right y-axis) from Nc/Pc, Nc, and Pc OPVs versus insolation. Theoretical energy output if active MPP tracking had been employed, indicated with dashed lines. The amount of time spent outdoors is indicated at 10-hour intervals.

The current output from all of the OPVs follow the same trends and have virtually identical T_{80}s, enduring ~123 h over 17 outdoor cycles. The outdoor performance of the OPVs is consistent with initial, indoor performance measurements (Nc/Pc > Nc > Pc). Employing active maximum power point (MPP) tracking could have improved the energy conversion, but our calculations estimate only marginal improvements would have been achieved (dashed lines, **Figure 4.8b**). The estimated energy conversion if actively tracking MPP was calculated using the morning indoor J–V measurements, and by assuming fill factor and open-circuit voltages remain approximately constant for the irradiation intensities incurred (**Equation D.1, Figure D.1**). The analogous OPV lifetimes demonstrate that Cl-Cl$_n$BsubNc and Cl-BsubPc either degrade at very similar rates or degrade at different rates but on much longer time scales than the least stable components in the

device. The longer lifetimes of the α-6T / Cl-BsubPc OPVs in this study is attributed to lower average irradiation intensities and temperatures incurred during this study.

PHJ OPVs share many structural similarities with organic light-emitting diodes (OLEDs). While most OPVs are not optimized for electroluminescence, the pre-established photoluminescence (PL) and EL of Cl-BsubPc and Cl-Cl$_n$BsubNc and favourable energetic alignments with α-6T provide measurable light emission under forward voltage bias. EL spectra (**Figure 4.9a**) of the Pc OPVs were collected throughout the device lifetimes to assess the relative intensities of the monomer and aggregate emissions under various applied current densities (**Figure 4.9b**).

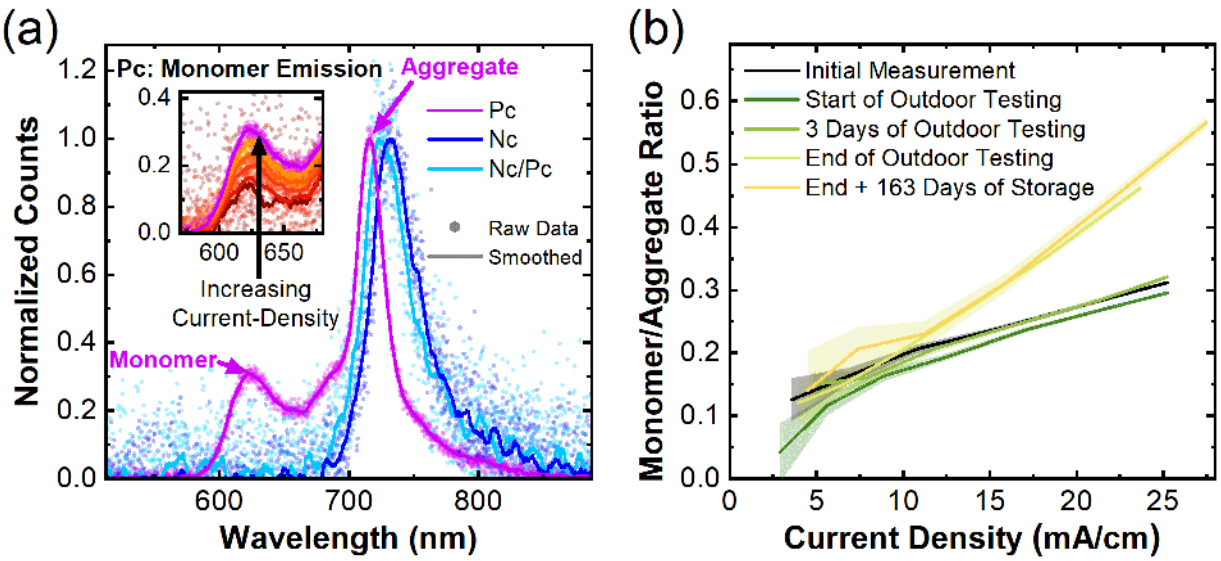

Figure 4.9. (a) Initial electroluminescent spectra measured at a fixed current density (25 mA/cm^2) in forward bias, smoothed using a Savitzky-Golan filter, with inset showing the Pc monomer emission with increasing current density (initial measurement). (b) Pc monomer/aggregate ratio versus current density as it evolves throughout testing and dark storage.

The Pc OPVs exhibit dual emission with peaks at 625 nm (monomer) and 716 nm (aggregate), while the Nc and Nc/Pc OPVs exhibit only a single emission peak. The lack of Cl-BsubPc emission from the Nc/Pc OPVs is attributed to two factors: unfavourable energetic alignment is impeding exciton formation within the Cl-BsubPc layer during operation as an OLED, and rapid transfer of any excitons formed within the Cl-BsubPc layer to Cl-Cl$_n$BsubNc through Förster resonance

energy transfer.[57, 79, 260] The monomer/aggregate emission ratio in the Pc OPVs increases with applied current density, but the amount and rate of increase changes with device degradation. The overall monomer/aggregate ratio decreases during the initial 25 days of dark storage and then increases with each subsequent measurement, particularly after outdoor testing. Disaggregation of emitting aggregate regions seems to be stimulated by outdoor testing, increasing the relative level of monomer emission. It is unclear how a changing number of aggregate sites within the Cl-BsubPc layer might affect OPV performance. Degradation of the OPVs is also directly correlated to the amount of outdoor testing, but the aggregate regions do not appear to participate in photocurrent generation or affect the OPV performance (discussed later).

During EL measurements at the end of outdoor testing, dark regions were observed at the edges of the devices. EL imaging (ELI) was performed immediately to record the extent of the EL area reduction, and further imaging was employed to probe for any continued area reduction while stored in the dark. ELI for a representative sample of OPVs is compared to short-circuit current density (J_{SC}) in **Figure 4.10**. ELI for the entire set of OPVs can be found in **Figure D.2** and **Figure D.3**.

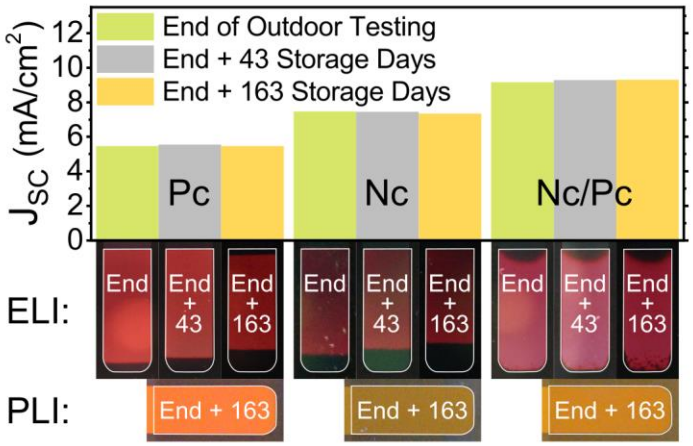

Figure 4.10. Electroluminescent imaging (ELI) and the corresponding short-circuit current density (J_{SC}) of a representative Pc, Nc, and Nc/Pc OPV at the end of outdoor testing, 43 days of dark storage after the end of outdoor testing, and 163 days of dark storage after the end of outdoor testing. Photoluminescent imaging (PLI) of the same OPVs at 163 days of dark storage after the end of outdoor testing.

At the end of outdoor testing, ELI reveals a slight reduction in the EL area from one edge of every OPV. While in dark storage, the EL area shrinkage continued gradually over 163 days. Contrarily, PLI reveals a completely uniform emission across the entire device area. The lack of PL quenching or dark spots indicates that the Cl-BsubPc and Cl-Cl_nBsubNc have not truly degraded. Instead, the EL area shrinkage is likely due to degradation at one of the electrodes with ambient moisture or air slowly diffusing laterally through the hydrophilic PEDOT:PSS layer. The observed ingress generally only reaching the active areas of the devices on the side closest to the encapsulation edge supports this idea. When this ingress occurred from the silver contact side (Nc/Pc images, **Figure 4.10**), a curved shrinkage profile was observed for the devices. This curved profile is consistent with an increased diffusion rate of moisture or air underneath the electrode (**Figure D.4**), which we attribute to elevated temperatures underneath the silver electrode during testing.

The uniform PLI indicates that the active layer materials are relatively stable to the ingress rate likely due to inherent chemical stability, despite the known potential to hydrolyze the B-Cl bond yielding a hydroxyl derivative.[51, 261-262] Unlike EL, PL does not require charge transfer from the electrode. The EL area shrinkage is, therefore, determined to be a result of nonactive layer degradation at one of the electrodes. Increased resistance at regions of the electrode interface is consistent with non-electroluminescent areas, redirecting current away from these regions. Current redirection is more significant for charge injection than charge extraction since charges generated in these regions through photoexcitation can still be collected. While detrimental to operation as an OLED, the OPV parameters were not significantly affected by the continued ingress after outdoor testing. The measured J_{SC} remains essentially constant despite significant EL area shrinkage over 163 days of dark storage. At 163 days after the completion of outdoor testing, J–V measurements that were performed while illuminating only the non-emissive regions of two OPVs revealed only minor reductions in performance relative to the whole OPV (**Figure D.5**).

Performing indoor characterization under simulated AM1.5G every morning enabled OPV device characteristics to be tracked precisely throughout the device lifetime testing (**Figure 4.11a,b**, **Table 4.2**). External quantum efficiencies (EQEs) were measured at the start and end of the outdoor testing days (**Figure 4.11c**, **Table 4.2**).

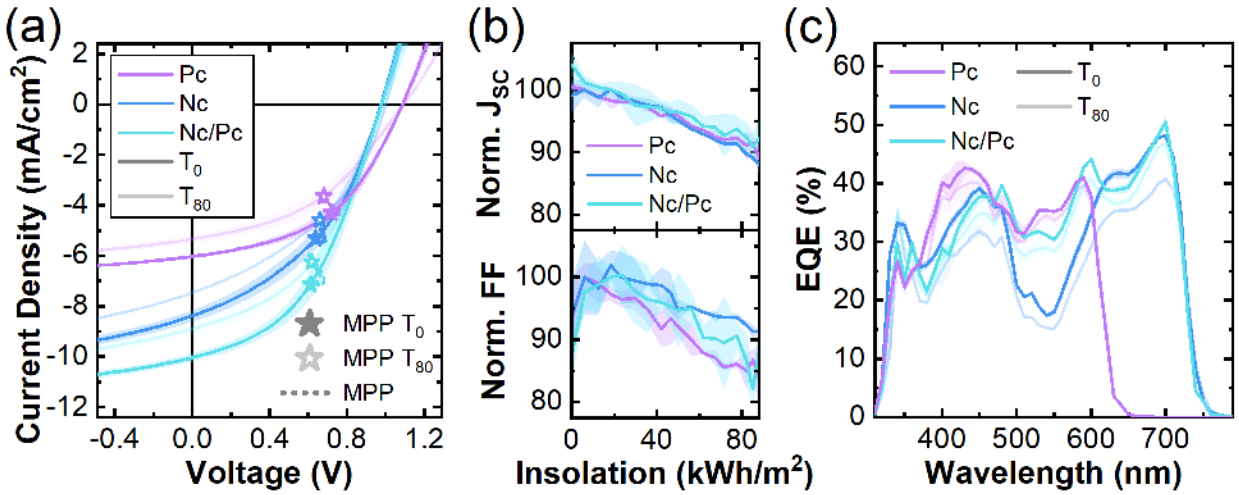

Figure 4.11. (a) J–V characteristics, (b) evolution of the J_{SC} and FF with insolation, and (c) EQE spectra of the Pc, Nc, and Nc/Pc OPVs as measured indoors under simulated AM1.5G spectrum. T_0 = time zero (initial); T_{80} = time after degrading to 80% of the peak PCE.

Table 4.2. Average device parameters and EQE peak contribution ratios of Pc, Nc, and Nc/Pc OPVs.

		J–V Characteristics				EQE Ratios	
acceptor	**time**	**V_{OC}[a]** (V)	**J_{SC}[b]** (mA/cm²)	**FF[c]**	**PCE[d]** (%)	**Pc/α-6T[e]**	**Nc/α-6T[f]**
Pc	T_0	1.09 (0.009)	6.03 (0.04)	0.47 (0.03)	3.10 (0.21)	0.99	
	T_{80}	1.09 (0.012)	5.34 (0.16)	0.42 (0.03)	2.48 (0.27)	0.99	
Nc	T_0	0.98 (0.008)	8.39 (0.23)	0.42 (0.02)	3.41 (0.27)		1.23
	T_{80}	1.00 (0.006)	7.46 (0.01)	0.41 (0.01)	3.03 (0.01)		1.28
Nc/Pc	T_0	0.98 (0.005)	10.03 (0.19)	0.44 (0.02)	4.29 (0.31)	1.13	1.34
	T_{80}	0.99 (0.006)	8.89 (0.29)	0.44 (0.02)	3.89 (0.30)	1.14	1.34

[a]Open-circuit voltage. [b]Short-circuit current density. [c]Fill factor. [d]Power conversion efficiency. [e]Ratio between peak EQE values: Cl-BsubPc (590 nm) / α-6T (450 nm). [f]Ratio between peak EQE values: Cl-Cl_nBsubNc (700 nm) / α-6T (450 nm).

The degradation of OPV PCEs (**Figure 4.8**) during outdoor testing is directly correlated to changes in J_{SC} and fill factor (FF); open-circuit voltage (V_{OC}) remains nearly constant throughout testing (**Table 4.2**, Figure D.6). A downward translation of the EQEs between the beginning and end of testing is consistent with the observed reduction in J_{SC}. The EQE peak contributions from Cl-

BsubPc and Cl-Cl$_n$BsubNc remain comparable and quite stable relative to their respective α-6T contribution (**Table 4.2**). Though overall OPV performance is of minimal consequence to the assessment of OPV stability, we note that our device characteristics, specifically PCE, are lower than those achieved by Cnops et al.[79] despite identical nominal layer thicknesses. We attribute the lower device characteristics obtained by us to differences in layer deposition thickness calibrations between device fabrication systems. Our fabrication system is also not able to perform extensive layer thickness optimization. Our results then do not take into question the results of Cnops et al.[79] Given the relative stability of each active layer component highlighted above with PL and EL measurements, the dominant degradation mechanism in the devices must be occurring within the nonactive layer components. Charge extraction barriers would increase with the degradation of electrodes or charge transport layers, decreasing the extracted current (reduced J_{SC}) and causing charge imbalance within the device (reduced FF). Reductions in J_{SC} and FF are present in all of the OPVs throughout outdoor testing. PEDOT:PSS is known to react with and degrade ITO, especially under elevated temperatures.[263] We infer that this PEDOT:PSS – ITO reaction is the primary OPV degradation mechanism during outdoor testing, which occurs before any ingress of external air or moisture.

A photocurrent contribution from the Cl-BsubPc aggregate is not observed in the EQE of the Pc OPV. Based on the EL aggregate emission peak at 716 nm (**Figure 4.9a**), the anticipated Stokes shift for the Cl-BsubPc aggregate would position the hypothetical absorption in the 680–700 nm region. The lack of Cl-BsubPc aggregate presence in absorption spectra or EQE is consistent with all previous OPV work with Cl-BsubPc, suggesting that the aggregate states are only accessible during the forward bias operation used for OLEDs. While overall OPV degradation does correlate with the observed increases in monomer emission relative to aggregate emission, it does not appear to be a causal relationship. Future work will investigate the OLED properties of neat Cl-BsubPc layers and the influence of aggregates on device performance.

4.3.2 Conclusions

In conclusion, this study establishes the equivalent stability of Cl-Cl$_n$BsubNc compared to Cl-BsubPc when tested in OPVs under ISOS-O3 protocols. Cl-BsubPc and Cl-Cl$_n$BsubNc, placed

alone or together in a PHJ OPV, appear to have negligible degradation on the studied time scales. Despite only passively tracking the maximum power point during testing, the total energy that was converted nearly matches the estimated energy conversion from active tracking. EL analysis methods were employed due to the ability of all three OPV structures to emit light under forward bias. ELI reveals ingress occurring near the encapsulation edge, slightly shrinking the EL area. PLI indicates that the ingress primarily affected nonactive layer components, with the reduction in the EL area caused by increased charge injection/extraction barriers that redirect injected charge from these areas. This ingress is more problematic for EL than OPV operation, as the J_{SC}s remain constant through dark storage despite significant EL area shrinkage. The constant J_{SC} despite visible ingress comes in contrast to research on bulk heterojunction architectures that demonstrate a decreasing J_{SC} with exposure to oxygen and moisture.[242-243] This stable J_{SC} indicates the vacuum-deposited materials within this study, and the PHJ architecture may be more resilient to harmful interactions with oxygen and water. EL spectra enabled the quantification of the relative monomer and aggregate emission changes in the Cl-BsubPc layer, revealing a dependence on current density and stage of degradation. Given the good stability of Cl-BsubPc and Cl-Cl_nBsubNc, the primary source of device degradation is hypothesized to be a degradation of the ITO layer by PEDOT:PSS, consistent with past studies.[263] Eliminating this degradation mechanism and engineering longer-lasting electrode/charge transport layer combinations will be essential for commercial viability. Employing an inverted device structure to eliminate the ITO / PEDOT:PSS interface altogether could result in higher stabilities,[235] which has also been shown to increase the built-in potential to enhance charge extraction.[264] Future studies investigating the ultimate stability of longer-lasting active layer materials such as Cl-BsubPc and Cl-Cl_nBsubNc will require electrode / charge transport layers with better stabilities.

4.4 Influence of Peripheral Chlorines on Outdoor Stability

Peripheral chlorination of boron subphthalocyanines (BsubPcs) has proven to be a valuable method of tuning the frontier molecular orbitals of BsubPcs and the corresponding open-circuit voltage in organic photovoltaics (OPVs). Chloro-BsubPc (Cl-BsubPc) and chloro-hexachloro BsubPc (Cl-Cl_6BsubPc) have demonstrated this tunability in OPVs, but the influence on stability has not previously been investigated. Using our outdoor testing protocols, we test and compare the

outdoor stability of Cl-BsubPc and Cl-Cl_6BsubPc in OPVs. We determine that peripheral chlorination does not affect outdoor stability, and it may even slightly improve the overall stability of BsubPcs.

4.4.1 Discussion

Electronic properties of a BsubPc such as the frontier molecular orbitals can be tuned through peripheral chlorination: chloro-hexachloro BsubPc (Cl-Cl_6BsubPc) and chloro-dodecachloro BsubPc (Cl-Cl_{12}BsubPc).[76] The applications of these peripherally chlorinated BsubPcs have been previously demonstrated for tunings open-circuit voltages (V_{OC}s) and harvesting triplets.[76, 89] Despite the progress towards the development of high-performance OPVs as measured immediately after fabrication (time-zero), relatively little research has assessed the lifetime and stability. The ability to tune electronic properties through peripheral chlorination loses value if the stability of the molecule is adversely affected.

Protocols established at the International Summit on OPV Stability (ISOS) outline methods that should be used to test OPVs outdoors and how to report the data.[39] These protocols ensure comparability between outdoor stability tests, even those performed in different environments and geographical locations. In this study, we adopt the most advanced level of outdoor testing (ISOS-O3) to assess the outdoor stability of Cl-BsubPc and Cl-Cl_6BsubPc as electron acceptors in OPVs (**Figure 4.12**).

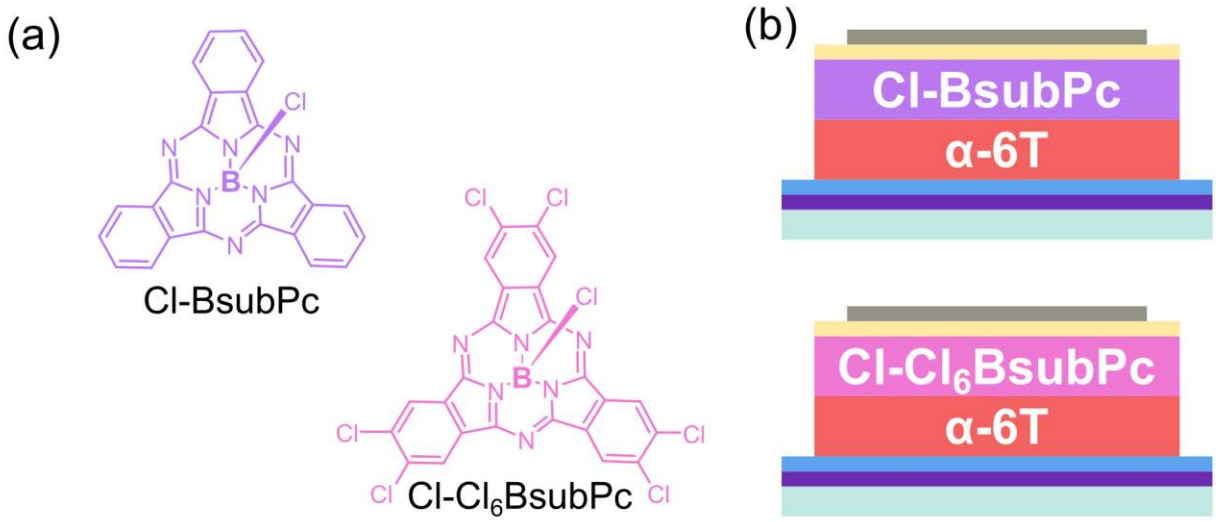

Figure 4.12. (a) Chemical structures of Cl-BsubPc and Cl-Cl_6BsubPc. (b) The two different active layer combinations used in this study: alpha-sexithiophene (α-6T) / Cl-BsubPc and α-6T / Cl-Cl_6BsubPc. Purple, blue, yellow, and grey layers represent indium tin oxide (ITO), poly(3,4-ethylenedioxythiophene)-poly(styrenesulfonate) (PEDOT:PSS), bathocuproine (BCP), and silver (Ag), respectively. Layer thicknesses shown are not to scale.

The stability of Cl-BsubPc and Cl-Cl_6BsubPc was assessed as electron acceptors in planar heterojunction (PHJ) OPVs made by pairing each BsubPc with alpha-sexithiophene (α-6T) as the electron donor in the following layer stack: ITO / PEDOT:PSS / α-6T (50 nm) / BsubPc (20 nm) / BCP (7 nm) / Ag (80 nm) (**Figure 4.12**). These OPVs were tested each morning indoors and then placed outdoors (**Table E.1**). The outdoor current density was produced while passively loaded to MPP. It was tracked according to ISOS protocols while also monitoring solar irradiance and substrate temperature (**Figure 4.13**).

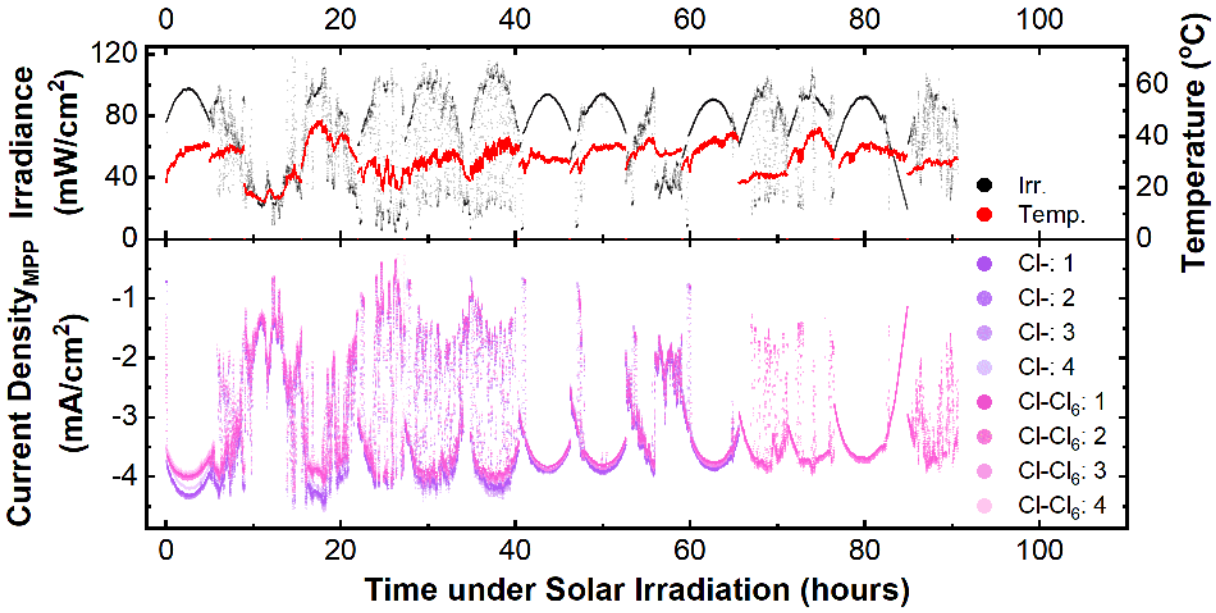

Figure 4.13. Continuous outdoor monitoring of current density produced by α-6T / Cl- and Cl-Cl_6BsubPc OPVs under passive loading to MPP.

The α-6T / Cl-BsubPc and α-6T / Cl-Cl_6BsubPc OPVs generate very similar current densities while outdoors, with their respective outputs following the incoming irradiance intensities and very gradually reducing in efficiency over time. The Cl-Cl_6BsubPc OPVs require an additional four outdoor cycles to reach 80% of their initial PCE (T_{80}) after the Cl-BsubPc OPVs reached their T_{80}.

For a more detailed analysis, the outdoor measurements are combined with the periodic indoor characterization under a constant AM1.5G light source. This combination enables the plotting of standardized indoor measurements (PCE, V_{OC}, J_{SC}, and FF) against the insolation (accumulated irradiation) received by the OPVs outdoors (**Figure 4.14**). Insolation is used as the X-axis instead of time because it provides a more accurate measure of the stress incurred by the OPVs while outdoors. Accumulated OPV output is also shown to represent the amount of energy converted throughout testing.

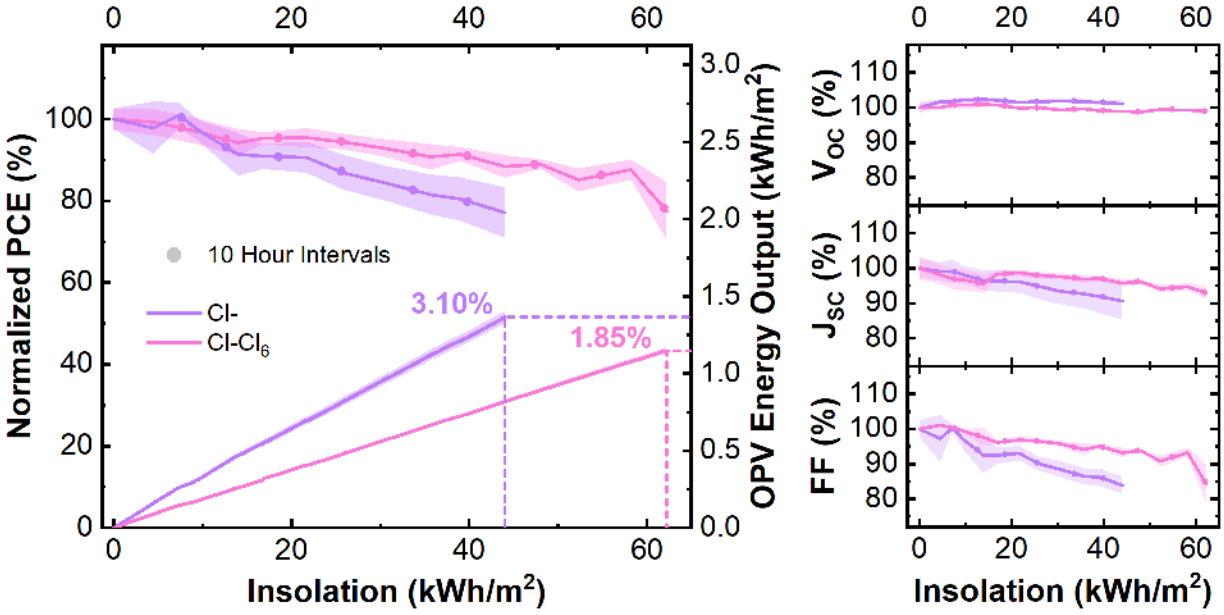

Figure 4.14. Normalized PCE, V_{OC}, J_{SC}, FF, and OPV energy output versus insolation (accumulated irradiance) of α-6T / Cl- and Cl-Cl_6BsubPc OPVs.

The evolution of the V_{OC} and J_{SC} remains approximately equivalent for Cl-BsubPc and Cl-Cl_6BsubPc OPVs. The average PCE of the Cl-BsubPc OPVs is higher than the Cl-Cl_6BsubPc OPVs (3.10% vs 1.85%) due to higher voltage output, resulting in the Cl-BsubPc OPVs converting more overall energy despite spending for fewer days outdoors. However, the difference in PCE can be attributed to a poor match between Cl-Cl_6BsubPc and α-6T; a more suitable electron donor material would likely result in higher PCEs. The FF degradation is the primary difference in the evolution of the two sets of OPVs. This degradation could be due to the additional chlorines providing some resistance to damaging morphological changes. However, data from other outdoor studies (**Section 4.3** and **4.2**) suggests that the stability differences are within the error of α-6T / Cl-BsubPc stability measurements. In any case, the stability of Cl-Cl_6BsubPc is determined to be approximately equivalent if not slightly better than Cl-BsubPc.

4.4.2 Conclusions

In summary, the stabilities of Cl-BsubPc and Cl-Cl_6BsubPc in PHJ OPVs were assessed using the most advanced ISOS protocols for testing outdoors. The stability of the BsubPc with more

peripheral chlorines is determined to be approximately equivalent if not slightly more stable than Cl-BsubPc. Though the PCE of the Cl-Cl_6BsubPc OPVs was lower than the Cl-BsubPc OPVs, a better matching electron donor would likely improve on that deficiency. We conclude that peripherally chlorinated BsubPcs are well-suited for outdoor applications of OPVs.

Chapter 5
Conclusions and Future Work

5.1 Thesis Conclusions

5.1.1 Established Organic Photovoltaic Screening of BsubPcs

Through adopting organic photovoltaic (OPV) architectures first reported by Cnops et al. and Stevens *et al.*,[107] I have established that either P3HT or α-6T can be applied as a baseline electron donor to screen new boron subphthalocyanine (BsubPc) derivatives in planar heterojunction OPVs. A planar architecture minimizes the morphology complexity that can be introduced using bulk heterojunction architectures. Though either P3HT and α-6T are recommended, the higher overall performance made α-6T the preferred option going forward. The baseline architecture also served to highlight a significant performance advantage for BsubPcs as electron acceptors over the more commonly used fullerene (C_{60}). As electron acceptor paired with α-6T, chloro-BsubPc (Cl-BsubPc) and chloro-hexachloro BsubPc (Cl-Cl$_6$BsubPc) achieve significantly higher open-circuit voltages (V_{OC}s) and short-circuit currents (J_{SC}s) than C_{60}. The higher performances are due to the advantages of complementary absorption profiles and reduced recombination rates at the dissociation interface. The full range of V_{OC} tunability through peripheral chlorination of BsubPc was also demonstrated in three steps: 1.10 V with Cl-BsubPc, 0.60 V with Cl-Cl$_6$BsubPc, and 0.35 V with chloro-dodecachloro BsubPc (Cl-Cl$_{12}$BsubPc).

With the effective screening method of pairing BsubPcs with α-6T established, I used this method to assess the performance of many new BsubPcs and boron subnaphthalocyanines (BsubNcs). The composition of chloro-BsubNc (Cl-BsubNc) consists of an alloyed mixture of peripherally chlorinated BsubNc derivatives (Cl-Cl$_n$BsubNc). The OPV performance was dependent on composition, with slight improvements in overall performance achieved when using the newly developed mixture with more chlorinated Cl-Cl$_n$BsubNc species. This surprising result inspired a new study, whereby BsubPc mixtures imitating the compositions of Cl$_n$BsubNc mixtures are developed and examined in OPVs. Three aryl-BsubPc derivatives (phenyl-BsubPc, 4-tolyl-BsubPc, and 4-fluorophenyl-BsubPc) were tested in OPVs, resulting in the discovery of some of the largest reported V_{OC}s for single-junction OPVs (1.16 – 1.25 V). Assessing a group of

fluorinated phenoxy-BsubPcs in OPVs, high V_{OC}s (1.13 – 1.21 V) revealed a correlation between meta-position fluorination and the orbital energy levels. The promising performances of Cl-Cl_nBsubNc and phenoxy-BsubPcs led to an investigation of phenoxy- and pentafluorophenoxy-Cl_nBsubNc. In this case, phenoxylation was determined to be a detriment to Cl_nBsubNc performance in the baseline architecture. Finally, the screening of meta-halogenated phenoxy-BsubPcs led to a more extensive study into the subtle halogen bonding interactions that appear to be influencing OPV performance.

5.1.2 Alloyed Mixtures for Precise Tuning

Investigating the Cl-Cl_nBsubNcs in OPVs revealed a surprising discovery; A mixture containing more derivatives (Cl-Cl_1, Cl-Cl_2, Cl-Cl_3, Cl-Cl_4, and Cl-Cl_5BsubNc) performs better than mixtures with fewer derivatives (Cl-, and Cl-Cl_1BsubNc; Cl-, Cl-Cl_1, Cl-Cl_2, and Cl-Cl_3BsubNc). The evident lack of charge traps implies an electronic alloying effect, where the mixture behaves as one material with averaged properties of the individual derivatives. Inspired by the nature of Cl_nBsubNc alloys, intentional mixtures of peripherally chlorinated BsubPcs were developed to replicate the alloying effect.

A synthetic procedure, using ratios of different phthalonitriles, was developed to produce mixtures of four BsubPcs with varying amounts of peripheral chlorination. Although the exact composition of the mixtures changed at each purification step, the composition could also be measured and tracked at each stage. A set of mixtures with varying degrees of chlorination were synthesized, and the closest mixtures in composition to Cl-BsubPc and Cl-Cl_6BsubPc were assessed in OPVs. Based on OPV performances, the minority derivatives in the mixtures likely do not participate in the electronic alloying; the energy levels are too different at concentrations that are too dilute. However, mixtures can be designed such that the minority derivatives do not act as traps in the chosen application. When mitigating the effects of the minority derivatives, the alloyed majority derivatives have been demonstrated to perform about as well as the nearest compositionally pure BsubPc. Such mixtures can also overcome the V_{OC} tuning limitations of compositionally pure BsubPcs, where the tuning is limited to discrete steps per chlorine added or removed. Having

validated the application of BsubPc mixtures in OPVs, the V_{OC} of OPVs made with BsubPc mixtures can be precisely tuned simply by controlling the ratio of phthalonitriles during synthesis.

5.1.3 Halogen Bonding for Molecular Control

Although halogen bonding can theoretically occur in almost any OPV that contains a material with a halogen, no previous studies investigate the effects of halogen bonding in OPVs. Meta-halogenated phenoxy-BsubPcs (*m*-XPhO-BsubPcs, X = Cl, Br, I) provided the perfect opportunity to isolate and identify the influence of halogen bonds in OPVs. Using tetracene and fullerene to eliminate any potential for interlayer halogen bonds reveals the minimal influence of intralayer halogen bonds in *m*-XPhO-BsubPcs. Potential interlayer halogen bond donors were sequentially introduced to assess their effects on OPV performance. Introducing potential C-X···N or C-X···O interlayer halogen bonding results in noticeably different OPV performance characteristics between each halogen. By controlling for all other sources of performance characteristics variation, it must be concluded that halogen bonding both occurs in OPVs, and it tangibly affects overall performance. The application of halogen bonding in OPVs provides a widely impactful, versatile tool to precisely control molecular orientations in future OPVs.

5.1.4 Stability Testing

Having screened many new BsubPc derivatives in OPVs, five derivatives emerged as promising candidates for stability testing in OPVs: Cl-Cl_6BsubPc, phenyl-BsubPc, phenoxy-BsubPc, and the commercially available derivatives: Cl-BsubPc and Cl-Cl_nBsubNc. These derivatives were separated into three different studies: Cl-BsubPc vs Cl-Cl_6BsubPc, Cl-BsubPc vs Cl-Cl_nBsubNc vs Cl-Cl_nBsubNc / Cl-BsubPc, and Cl-BsubPc vs phenyl-BsubPc (Ph-BsubPc) vs phenoxy-BsubPc (PhO-BsubPc). Cl-BsubPc was repeated each time as a baseline to compare between the different studies. The OPV stabilities of each derivative were tested following the most advanced level of outdoor testing specified by protocols from the International Summit on OPV Stability (ISOS).

The outdoor OPV stability of Cl-Cl_6BsubPc was determined to be approximately equivalent to Cl-BsubPc, if not better. The extrapolation of this result suggests that peripheral chlorination can be

added or removed from a BsubPc in any amounts without negatively impacting the stability. This flexibility in peripheral chlorination is especially significant for mixtures and applications requiring BsubPcs with deep energy levels. The outdoor OPV stabilities of Cl-BsubPc and Cl-Cl_nBsubNc were determined to be approximately equivalent. Electroluminescence and photoluminescence analysis revealed that Cl-BsubPc and Cl-Cl_nBsubNc remained relatively unaffected despite exposure to ambient ingress from the edges of the encapsulation slip. The equivalently strong stabilities of Cl-BsubPc, Cl-Cl_6BsubPc, and Cl-Cl_nBsubNc indicate that at least one of the other components of the OPV is the primary source of degradation. An OPV layer stack with significantly improved stability will be required to explore these longer-lasting derivatives beyond a few weeks. During the outdoor stability testing of Cl-BsubPc, PhO-BsubPc, and Ph-BsubPc stability differences were quickly identified. Despite their promise during initial screening, the OPV performance of Ph-BsubPc and PhO-BsubPc degraded to 50% of their original power conversion efficiencies (PCEs) after only four and seven days, respectively. Hydrolysis of the axial phenoxy and phenyl groups is the most likely explanation for their quick degradation. This study highlights the importance of stability testing, and that promising materials at time-zero will not necessarily translate to a successful material for real-world applications.

5.2 Future Work

5.2.1 Improving the Standard Electron Donors

The commercial supply of α-sexithiophene (α-6T) is a critical and occasionally problematic component of the established method of screening BsubPcs in OPVs. Both Sigma-Aldrich and Luminescence Technology Corporation (Lumtec) have been used at different times as suppliers of α-6T. Initially, α-6T was purchased from Sigma-Aldrich and required purification via train sublimation before use in OPVs. The α-6T supply from Sigma-Aldrich was on back-order in 2016, motivating a search for an alternative that led to Lumtec. The α-6T supply from Lumtec was already sublimation-grade and could be used in OPVs as received. However, an apparent change in material purity resulted in OPV performance issues around the start of 2019, motivating a switch back to the Sigma-Aldrich α-6T. The development of an in-house synthesis process to produce α-6T may alleviate the supply and purity issues that occur as a result of relying on commercial

suppliers. Previously, a novel synthesis method was attempted (with minimal success) to reduce the number of synthetic steps required to produce α-6T. A more traditional synthesis procedure may be a more appropriate starting point to secure a reliable and pure supply of α-6T. Once established, the ability to synthesize α-6T in-house would also provide an opportunity to experiment with chemical modification and tuning of α-6T for OPVs. Slightly longer oligomers such as α-septithiophene and α-octithiophene would be promising thiophenes to attempt, given their slightly broader and red-shifted absorptions.

Screening the BsubPcs by pairing them with α-6T enables rapid assessment of BsubPc derivatives with LUMOs similar to that of Cl-BsubPc. Although BsubPcs with deeper LUMOs may still be assessed, the small energy offset between the HOMO of the electron donor and LUMO of the electron acceptor results in relatively low V_{OC}s and overall performances. Slight performance improvements can be achieved by pairing the deeper BsubPcs with pentacene, but the use of a singlet fission material for screening introduces the complexity of how well the BsubPc harvests triplets. An alternative solution for deep BsubPcs could be to adapt the structure reported by Cnops et al.[46], where electron-accepting BsubPcs are paired with electron-donating Cl-Cl_nBsubNc. This architecture yields relatively high V_{OC}s even for deep BsubPc derivatives: 1.08 V for Cl-$^{\beta}Cl_4$BsubPc, 1.00 V for Cl-$^{\beta}Cl_6$BsubPc, and 0.75 V for Cl-F_{12}BsubPc. An additional benefit of using Cl-Cl_nBsubNc as the electron donor would be the ability to synthesize and tune the derivative in-house, and the ability to quickly introduce any newly developed Cl_nBsubNcs.

5.2.2 Complete Alloys of BsubPc Mixtures

The approach of using intentionally chlorinated BsubPc mixtures in OPVs was validated using a mixture of Cl-, Cl-$^{\beta}Cl_2$, Cl-$^{\beta}Cl_4$, and Cl-$^{\beta}Cl_6$BsubPc. The limiting factor of these initial BsubPc mixtures appears to be the minority derivatives acting as traps rather than participants in the alloy. For the Cl-Cl_nBsubNcs, the mixture containing the most derivatives (Cl-Cl_1, Cl-Cl_2, Cl-Cl_3, Cl-Cl_5BsubNc) achieves the highest OPV performance. The composition of the best Cl-Cl_nBsubNc has chlorination increments of one, with a range of five (Cl-Cl_1 to Cl-Cl_5) in between the derivatives. The composition of the Cl-$^{\beta}Cl_{2n}$BsubPcs has chlorination increments of two, with a range of seven (Cl-Cl_0 to Cl-Cl_6) in between the derivatives. Based on these differences in

composition, the next generation of BsubPc mixtures should be designed more similarly to the Cl-Cl_nBsubNcs, having peripheral chlorination increments of one with a smaller total range.

The synthesis of next-generation BsubPc mixtures will require the development of new phthalonitriles. A BsubPc mixture synthesized with phthalonitrile and 3-chlorophthalonitrile would produce a mixture with peripheral chlorination increment of one and a range four. Although the asymmetry may introduce challenges, the random chlorination of the Cl_nBsubNcs still yields high-performance materials. If a BsubPc mixture with a similar composition as commercial Cl-Cl_nBsubNc could be achieved, the LUMO levels of that BsubPc mixture and Cl-Cl_nBsubNc should match even better than Cl-BsubPc. Therefore, the performance of such a mixture in the α-6T / Cl-Cl_nBsubNc / BsubPc stack could exceed previous results with Cl-BsubPc. Similarly, BsubPc mixtures synthesized with 3-chlorophthalonitrile and 3,6-dichlorophthalonitrile, 4,5-dichlorophthalonitrile and 3,4,5-trichlorophthalonitrile, or 3,4,5-trichlorophthalonitrile and 3,4,5,6-tetrachlorophthalonitrile should each produce mixtures with an increment of one and a range of four.

An interesting application of the theoretical mixture synthesized by mixing 3,4,5-trichlorophthalonitrile and 3,4,5,6-tetrachlorophthalonitrile would be for tuning the deep energy levels of the most chlorinated derivatives. Cl-Cl_{12}BsubPc is a strong triplet harvester from pentacene, but the resulting V_{OC} was quite low. Assuming the successful development of synthetic pathways for 3,4,5-trichlorophthalonitrile, a BsubPc synthesized with 3,4,5-trichlorophthalonitrile and 3,4,5,6-tetrachlorophthalonitrile could provide the ability to optimize the V_{OC} while maintaining the strong triplet harvesting abilities.

Beyond mixtures of differently chlorinated derivatives, the synthesis technique could apply to mixtures of phthalonitriles with any other halogens. BsubPcs mixtures could be synthesized with mixed amounts of peripheral fluorination, mixed amounts of peripheral fluorination and chlorination, or mixed amounts of any amount of halogenation. Although the set of possible mixtures increases rapidly with each additional halogen, the experiments proposed in the next section may provide some guidance for the types and locations of halogens to target around phthalonitriles.

5.2.3 Applied Halogen Bonding

There is strong evidence for the presence and impact of halogen bonding in OPVs (**Section 3.4**). Meta-halogenated phenoxy-BsubPcs (*m*-XPhO-BsubPcs) were used in this study because their properties are virtually identical, other than the type of halogen located at the meta position of the phenoxy moiety. The similarities resulted in the perfect set of materials to study the existence and the influence of halogen bonds in OPVs; all other variables were minimized, enhancing the observed differences when different halogens were present. Intentionally applying halogen bonding to target improved OPV performance requires completely different considerations. Halogen bonding can be applied to target specific molecular orientations. However, the ability to target optimal performance would first require better knowledge about the relationship between orientation and performance.

In general, optimal molecular orientations involve minimizing the distances between the conjugated regions of each molecule. Significant modelling and experimental data, however, will be required to determine the optimal orientations. Intentional application of halogen bonds involves controlling and optimizing the molecular orientations on both ends of the halogen bonds. By locating halogen bond acceptors (halogens) at specific locations around a BsubPc, an ideal molecular design would result in a BsubPc that uses halogen bonds to arrange itself optimally within a layer of identical molecules and to arrange itself optimally with molecules in neighbouring layers. In a similar approach, the locations of the halogen bond donating nitrogens in BsubPc could be used to design halogen bonds with halogen bond acceptors on neighbouring molecules.

The optimal locations for BsubPc halogenation may be specific peripheral locations. Future studies will need to carefully deconvolute the effects of halogen bonding when using different halogens because peripheral halogenation is known to influence the orbital energy levels of the molecule. Additionally, it is implausible that all molecules will adopt the same, halogen-bonded orientation. Halogen bonding increases the statistical probability of that orientation. Increasing the strength of the potential halogen bond may increase that statistical probability even further. Experimentation will be required to determine if chlorine forms sufficiently strong halogen bonds to achieve the desired halogen bonded orientations, or if bromine or iodine would be required.

The development of phthalonitriles for new BsubPc mixtures could simultaneously pair well with halogen bonding design. BsubPcs made with 3-chlorophthalonitrile or 4-chlorophthalonitrile would locate a few chlorines around the exterior of the BsubPc. The surrounding layers in an OPV could be selected such that the halogen bonded orientations would result in placing the conjugated regions of each molecule in close proximity.

Beyond BsubPcs, halogen bonding can occur in almost any OPV material with halogens and halogen bond donors (atoms lone pairs). The imine nitrogens in BsubPc have already demonstrated the ability to form halogen bonds. Therefore, BsubPcs could be applied as the halogen bond donor at interfaces where the neighbouring molecules contain halogens. Although convoluted, halogens could already be playing a significant role in the molecular orientation within OPVs. Understanding the role of halogen bonds and optimizing the corresponding molecular orientations will require many carefully controlled experiments. However, the ability to harness halogen bonding in OPVs could yield powerful results.

5.2.4 Next Steps of Stability Testing

The epoxy used in the stability studies described in this thesis (Ossila: Encapsulation Epoxy for Photovoltaics and OLEDs) is unfortunately no longer commercially available. Finding a suitable replacement has proved challenging. A contributing factor to this problem is our unique position of being one of the few labs actively seeking to test the outdoor stability of small molecule OPVs on small, research-scale substrates. Most commercially available encapsulation epoxies are designed for research groups that use polymer-based OPVs. Organic electronic polymers have negligible solubilities and are, therefore, more amenable to direct encapsulation with epoxy. Attempts to mitigate the solubility issues by using a glass coverslip and sealing only the exterior edges have thus far been unsuccessful.

The non-epoxy alternatives are far from ideal: implementation of a chemical vapour deposition (CVD) system, or stability testing unencapsulated OPVs to assess open-air stability. Developing a CVD system, though requiring significant start-up time and cost, would provide an opportunity to explore a scalable encapsulation technique that is suitable for large, flexible OPVs. The system

designed by Jia *et al*. to deposit parylene-C as an encapsulation layer has been previously considered, but the epoxy challenges may require a reconsideration of this approach.[265] Implementation of this method would enable the ability to synthesize the necessary monomers for CVD of parylene-C, adding another level of control to the supply of required OPV materials, and the flexibility to design improved parylene derivatives.

Moving towards unencapsulated OPVs would likely require the replacement of PEDOT:PSS with an alternative charge transport layer. It may be advantageous to avoid materials containing oxygen atoms which could migrate into adjacent layers, such as oxides like molybdenum oxide (MoO_X). One suitable candidate might be diindenoperylene (DIP), which has resulted in significant performance enhancements when applied as an exciton-blocking hole transport layer in OPVs using Cl_nBsubNc as the electron donor.[46, 68] Beyond replacing PEDOT:PSS, many iterations may be required to achieve layer stack combinations with reasonably long lifetimes. The goal of each iteration would be to identify the least stable material remaining, and then replace or modify that material, depending on the available options. This process can be repeated until improvements are no longer achievable. Silver may end up being the limiting factor in terms of air stability. Though it is perhaps unrealistic to expect an unencapsulated OPV to survive on timescales comparable to encapsulated OPVs, the process of improving stability when fully exposed to air should still also lead to enhanced stability once establishing a working encapsulation method. Some degree of ingress will inevitably occur, regardless of the encapsulation method used. If the functional layers of an OPV are resistant to degradation in the presence of air, the encapsulated OPV will be more resilient to small amounts of ingress. This resilience could mean the difference of requiring a more expensive encapsulation method for commercial applications, potentially saving significant cost.

OPV sizes will need to be scaled up to reach commercial applications. The cost and rigidity of indium tin oxide (ITO) are unlikely to be viable at large scales, particularly for flexible applications. The currently available ITO replacements are high conductivity PEDOT:PSS or silver grids. Graphene is often considered a promising future transparent electrode for OPVs, but significant research is still required. Future OPVs developed should target one of these electrode combinations in preparation for application at larger scales. In terms of the best option for vacuum-

deposited OPVs, the most feasible option is probably a silver grid. Width, spacing, and thickness would need to be optimized for light transmission and charge extraction from the OPVs. Silver is also transparent at low thicknesses, so a full, thin layer of silver could be first deposited to improve charge transport to the grid.

Given the constraints of the fabrication system and material availability, the most realistic, near-term goal for an air-stable device stack that I propose is substrate / silver / DIP / active layer / BCP / silver grid. For building larger OPVs, substrates up to 50 x 50 mm can be accommodated by our fabrication systems. The 50 x 50 mm substrates would enable ~20 cm^2 OPVs to be fabricated, which would far exceed the majority of OPVs reported in the literature. A 20 cm^2 OPV should be large enough to serve as a convincing prototype for future commercialization opportunities.

References

1. IEA *Key World Energy Statistics*; 2017.
2. Kopp, G.; Lean, J. L., A new, lower value of total solar irradiance: Evidence and climate significance. *Geophysical Research Letters* **2011,** *38* (1).
3. Haegel, N. M.; Margolis, R.; Buonassisi, T.; Feldman, D.; Froitzheim, A.; Garabedian, R.; Green, M.; Glunz, S.; Henning, H.-M.; Holder, B.; Kaizuka, I.; Kroposki, B.; Matsubara, K.; Niki, S.; Sakurai, K.; Schindler, R. A.; Tumas, W.; Weber, E. R.; Wilson, G.; Woodhouse, M.; Kurtz, S., Terawatt-scale photovoltaics: Trajectories and challenges. *Science* **2017,** *356* (6334), 141.
4. Aghaei, J.; Alizadeh, M.-I., Demand response in smart electricity grids equipped with renewable energy sources: A review. *Renewable and Sustainable Energy Reviews* **2013,** *18*, 64-72.
5. Lehovec, K., The Photo-Voltaic Effect. *Physical Review* **1948,** *74* (4), 463-471.
6. Schrödinger, E., An Undulatory Theory of the Mechanics of Atoms and Molecules. *Physical Review* **1926,** *28* (6), 1049-1070.
7. Bredas, J.-L., Mind the gap! *Materials Horizons* **2014,** *1* (1), 17-19.
8. Alsema, E. A.; Nieuwlaar, E., Energy viability of photovoltaic systems. *Energy Policy* **2000,** *28* (14), 999-1010.
9. Ramanujam, J.; Singh, U. P., Copper indium gallium selenide based solar cells – a review. *Energy & Environmental Science* **2017,** *10* (6), 1306-1319.
10. El Chaar, L.; lamont, L. A.; El Zein, N., Review of photovoltaic technologies. *Renewable and Sustainable Energy Reviews* **2011,** *15* (5), 2165-2175.
11. Snaith, H. J., Present status and future prospects of perovskite photovoltaics. *Nature Materials* **2018,** *17* (5), 372-376.
12. Slater, J. C., Molecular Energy Levels and Valence Bonds. *Physical Review* **1931,** *38* (6), 1109-1144.
13. Eley, D. D.; Parfitt, G. D.; Perry, M. J.; Taysum, D. H., The semiconductivity of organic substances. Part 1. *Transactions of the Faraday Society* **1953,** *49* (0), 79-86.
14. Willardson, R. K., Transport Properties in Silicon and Gallium Arsenide. *Journal of Applied Physics* **1959,** *30* (8), 1158-1165.
15. Glarum, S. H., Electron mobilities in organic semiconductors. *Journal of Physics and Chemistry of Solids* **1963,** *24* (12), 1577-1583.
16. Gilles, H.; Riadh, H.; Philippe, D., Temperature Dependence of the Field-Effect Mobility of Sexithiophene. Determination of the Density of Traps. *J. Phys. III France* **1995,** *5* (4), 355-371.

17. Bittner, E. R.; Ramon, J. G. S.; Karabunarliev, S., Exciton dissociation dynamics in model donor-acceptor polymer heterojunctions. I. Energetics and spectra. *The Journal of Chemical Physics* **2005,** *122* (21), 214719.

18. Peumans, P.; Forrest, S. R., Separation of geminate charge-pairs at donor–acceptor interfaces in disordered solids. *Chemical Physics Letters* **2004,** *398* (1), 27-31.

19. Rand, B. P.; Burk, D. P.; Forrest, S. R., Offset energies at organic semiconductor heterojunctions and their influence on the open-circuit voltage of thin-film solar cells. *Physical Review B* **2007,** *75* (11), 115327.

20. Savoie, B. M.; Jackson, N. E.; Chen, L. X.; Marks, T. J.; Ratner, M. A., Mesoscopic Features of Charge Generation in Organic Semiconductors. *Accounts of Chemical Research* **2014,** *47* (11), 3385-3394.

21. Heremans, P.; Cheyns, D.; Rand, B. P., Strategies for Increasing the Efficiency of Heterojunction Organic Solar Cells: Material Selection and Device Architecture. *Accounts of Chemical Research* **2009,** *42* (11), 1740-1747.

22. Vogel, M.; Doka, S.; Breyer, C.; Lux-Steiner, M. C.; Fostiropoulos, K., On the function of a bathocuproine buffer layer in organic photovoltaic cells. *Applied Physics Letters* **2006,** *89* (16), 163501.

23. Shrotriya, V.; Li, G.; Yao, Y.; Chu, C.-W.; Yang, Y., Transition metal oxides as the buffer layer for polymer photovoltaic cells. *Applied Physics Letters* **2006,** *88* (7), 073508.

24. Peumans, P.; Bulović, V.; Forrest, S. R., Efficient photon harvesting at high optical intensities in ultrathin organic double-heterostructure photovoltaic diodes. *Applied Physics Letters* **2000,** *76* (19), 2650-2652.

25. Peumans, P.; Forrest, S. R., Very-high-efficiency double-heterostructure copper phthalocyanine/C60 photovoltaic cells. *Applied Physics Letters* **2001,** *79* (1), 126-128.

26. Chiba, T.; Pu, Y.-J.; Sasabe, H.; Kido, J.; Yang, Y., Solution-processed organic light-emitting devices with two polymer light-emitting units connected in series by a charge-generation layer. *Journal of Materials Chemistry* **2012,** *22* (42), 22769-22773.

27. Lee, K. H.; Schwenn, P. E.; Smith, A. R. G.; Cavaye, H.; Shaw, P. E.; James, M.; Krueger, K. B.; Gentle, I. R.; Meredith, P.; Burn, P. L., Morphology of All-Solution-Processed "Bilayer" Organic Solar Cells. *Advanced Materials* **2011,** *23* (6), 766-770.

28. Yu, G.; Heeger, A. J., Charge separation and photovoltaic conversion in polymer composites with internal donor/acceptor heterojunctions. *Journal of Applied Physics* **1995,** *78* (7), 4510-4515.

29. Geens, W.; Aernouts, T.; Poortmans, J.; Hadziioannou, G., Organic co-evaporated films of a PPV-pentamer and C60: model systems for donor/acceptor polymer blends. *Thin Solid Films* **2002,** *403-404*, 438-443.

30. Choy, W. C. H. In *Optical design of organic/polymer solar cells and light emitting devices*, 2011 Numerical Simulation of Optoelectronic Devices, 5-8 Sept. 2011; 2011; pp 1-2.

31. Qi, B.; Wang, J., Fill factor in organic solar cells. *Physical Chemistry Chemical Physics* **2013,** *15* (23), 8972-8982.

32. Tress, W.; Petrich, A.; Hummert, M.; Hein, M.; Leo, K.; Riede, M., Imbalanced mobilities causing S-shaped IV curves in planar heterojunction organic solar cells. *Applied Physics Letters* **2011,** *98* (6), 063301.

33. Zimmermann, E.; Ehrenreich, P.; Pfadler, T.; Dorman, J. A.; Weickert, J.; Schmidt-Mende, L., Erroneous efficiency reports harm organic solar cell research. *Nature Photonics* **2014,** *8*, 669.

34. Dunlop, E. D. In *Lifetime performance of crystalline silicon PV modules*, 3rd World Conference onPhotovoltaic Energy Conversion, 2003. Proceedings of, 11-18 May 2003; 2003; pp 2927-2930 Vol.3.

35. Che, X.; Li, Y.; Qu, Y.; Forrest, S. R., High fabrication yield organic tandem photovoltaics combining vacuum- and solution-processed subcells with 15% efficiency. *Nature Energy* **2018,** *3* (5), 422-427.

36. Meng, L.; Zhang, Y.; Wan, X.; Li, C.; Zhang, X.; Wang, Y.; Ke, X.; Xiao, Z.; Ding, L.; Xia, R.; Yip, H.-L.; Cao, Y.; Chen, Y., Organic and solution-processed tandem solar cells with 17.3% efficiency. *Science* **2018,** *361* (6407), 1094.

37. Yuan, J.; Zhang, Y.; Zhou, L.; Zhang, G.; Yip, H.-L.; Lau, T.-K.; Lu, X.; Zhu, C.; Peng, H.; Johnson, P. A.; Leclerc, M.; Cao, Y.; Ulanski, J.; Li, Y.; Zou, Y., Single-Junction Organic Solar Cell with over 15% Efficiency Using Fused-Ring Acceptor with Electron-Deficient Core. *Joule* **2019,** *3* (4), 1140-1151.

38. Burke, D. J.; Lipomi, D. J., Green chemistry for organic solar cells. *Energy & Environmental Science* **2013,** *6* (7), 2053-2066.

39. Reese, M. O.; Gevorgyan, S. A.; Jørgensen, M.; Bundgaard, E.; Kurtz, S. R.; Ginley, D. S.; Olson, D. C.; Lloyd, M. T.; Morvillo, P.; Katz, E. A.; Elschner, A.; Haillant, O.; Currier, T. R.; Shrotriya, V.; Hermenau, M.; Riede, M.; R. Kirov, K.; Trimmel, G.; Rath, T.; Inganäs, O.; Zhang, F.; Andersson, M.; Tvingstedt, K.; Lira-Cantu, M.; Laird, D.; McGuiness, C.; Gowrisanker, S.; Pannone, M.; Xiao, M.; Hauch, J.; Steim, R.; DeLongchamp, D. M.; Rösch, R.; Hoppe, H.; Espinosa, N.; Urbina, A.; Yaman-Uzunoglu, G.; Bonekamp, J.-B.; van Breemen, A. J. J. M.; Girotto, C.; Voroshazi, E.; Krebs, F. C., Consensus stability testing protocols for organic photovoltaic materials and devices. *Solar Energy Materials and Solar Cells* **2011,** *95* (5), 1253-1267.

40. Josey, D. S.; Ingram, G. L.; Garner, R. K.; Wang, J. M.; Evans, G. J.; Lu, Z.-H.; Bender, T. P., Outdoor Stability of Chloro–(Chloro)n–Boron Subnaphthalocyanine and Chloro–Boron Subphthalocyanine as Electron Acceptors in Bilayer and Trilayer Organic Photovoltaics. *ACS Applied Energy Materials* **2019,** *2* (2), 979-986.

41. Espinosa, N.; Lenzmann, F. O.; Ryley, S.; Angmo, D.; Hösel, M.; Søndergaard, R. R.; Huss, D.; Dafinger, S.; Gritsch, S.; Kroon, J. M.; Jørgensen, M.; Krebs, F. C., OPV for mobile applications: an evaluation of roll-to-roll processed indium and silver free polymer

solar cells through analysis of life cycle, cost and layer quality using inline optical and functional inspection tools. *Journal of Materials Chemistry A* **2013,** *1* (24), 7037-7049.

42. Morse, G. E.; Bender, T. P., Boron Subphthalocyanines as Organic Electronic Materials. *ACS Applied Materials & Interfaces* **2012,** *4* (10), 5055-5068.

43. Morse, G. E.; Castrucci, J. S.; Helander, M. G.; Lu, Z.-H.; Bender, T. P., Phthalimido-boronsubphthalocyanines: New Derivatives of Boronsubphthalocyanine with Bipolar Electrochemistry and Functionality in OLEDs. *ACS Applied Materials & Interfaces* **2011,** *3* (9), 3538-3544.

44. Morse, G. E.; Gantz, J. L.; Steirer, K. X.; Armstrong, N. R.; Bender, T. P., Pentafluorophenoxy Boron Subphthalocyanine (F5BsubPc) as a Multifunctional Material for Organic Photovoltaics. *ACS Applied Materials & Interfaces* **2014,** *6* (3), 1515-1524.

45. Brisson, E. R. L.; Paton, A. S.; Morse, G. E.; Bender, T. P., Boron Subphthalocyanine Dyes: 3-Pentadecylphenol as a Solubilizing Molecular Fragment. *Industrial & Engineering Chemistry Research* **2011,** *50* (19), 10910-10917.

46. Cnops, K.; Zango, G.; Genoe, J.; Heremans, P.; Martinez-Diaz, M. V.; Torres, T.; Cheyns, D., Energy Level Tuning of Non-Fullerene Acceptors in Organic Solar Cells. *Journal of the American Chemical Society* **2015,** *137* (28), 8991-8997.

47. Duan, C.; Zango, G.; García Iglesias, M.; Colberts, F. J. M.; Wienk, M. M.; Martínez-Díaz, M. V.; Janssen, R. A. J.; Torres, T., The Role of the Axial Substituent in Subphthalocyanine Acceptors for Bulk-Heterojunction Solar Cells. *Angewandte Chemie International Edition* **2017,** *56* (1), 148-152.

48. Sullivan, P.; Duraud, A.; Hancox, l.; Beaumont, N.; Mirri, G.; Tucker, J. H. R.; Hatton, R. A.; Shipman, M.; Jones, T. S., Halogenated Boron Subphthalocyanines as Light Harvesting Electron Acceptors in Organic Photovoltaics. *Advanced Energy Materials* **2011,** *1* (3), 352-355.

49. Paton, A. S.; Lough, A. J.; Bender, T. P., A role for π–Br interactions in the solid-state molecular packing of para-halo-phenoxy-boronsubphthalocyanines. *CrystEngComm* **2011,** *13* (11), 3653-3656.

50. Paton, A. S.; Morse, G. E.; Lough, A. J.; Bender, T. P., Observations regarding the crystal structures of non-halogenated phenoxyboronsubphthalocyanines having para substituents on the phenoxy group. *CrystEngComm* **2011,** *13* (3), 914-919.

51. Fulford, M. V.; Jaidka, D.; Paton, A. S.; Morse, G. E.; Brisson, E. R. L.; Lough, A. J.; Bender, T. P., Crystal Structures, Reaction Rates, and Selected Physical Properties of Halo-Boronsubphthalocyanines (Halo = Fluoride, Chloride, and Bromide). *Journal of Chemical & Engineering Data* **2012,** *57* (10), 2756-2765.

52. Fulford, M. V.; Lough, A. J.; Bender, T. P., The first report of the crystal structure of non-solvated [mu]-oxo boron subphthalocyanine and the crystal structures of two solvated forms. *Acta Crystallographica Section B* **2012,** *68* (6), 636-645.

53. Paton, A. S.; Morse, G. E.; Lough, A. J.; Bender, T. P., Utilizing the π-Acidity of Boron Subphthalocyanine To Achieve Novel Solid-State Arrangements. *Crystal Growth & Design* **2013,** *13* (12), 5368-5374.

54. Morse, G. E.; Helander, M. G.; Stanwick, J.; Sauks, J. M.; Paton, A. S.; Lu, Z.-H.; Bender, T. P., Experimentally Validated Model for the Prediction of the HOMO and LUMO Energy Levels of Boronsubphthalocyanines. *The Journal of Physical Chemistry C* **2011,** *115* (23), 11709-11718.

55. Virdo, J. D.; Crandall, L.; Dang, J. D.; Fulford, M. V.; Lough, A. J.; Durfee, W. S.; Bender, T. P., The influence of strong and weak hydrogen bonds on the solid state arrangement of hydroxy-containing boron subphthalocyanines. *CrystEngComm* **2013,** *15* (42), 8578-8586.

56. Endres, J.; Pelczer, I.; Rand, B. P.; Kahn, A., Determination of Energy Level Alignment within an Energy Cascade Organic Solar Cell. *Chemistry of Materials* **2016,** *28* (3), 794-801.

57. Menke, S. M.; Holmes, R. J., Energy-Cascade Organic Photovoltaic Devices Incorporating a Host–Guest Architecture. *ACS Applied Materials & Interfaces* **2015,** *7* (4), 2912-2918.

58. Castrucci, J. S.; Helander, M. G.; Morse, G. E.; Lu, Z.-H.; Yip, C. M.; Bender, T. P., Charge Carrier Mobility in Fluorinated Phenoxy Boron Subphthalocyanines: Role of Solid State Packing. *Crystal Growth & Design* **2012,** *12* (3), 1095-1100.

59. Sullivan, P.; Schumann, S.; Da Campo, R.; Howells, T.; Duraud, A.; Shipman, M.; Hatton, R. A.; Jones, T. S., Ultra-High Voltage Multijunction Organic Solar Cells for Low-Power Electronic Applications. *Advanced Energy Materials* **2013,** *3* (2), 239-244.

60. Grant, T. M.; Josey, D. S.; Sampson, K. L.; Mudigonda, T.; Bender, T. P.; Lessard, B. H., Boron Subphthalocyanines and Silicon Phthalocyanines for Use as Active Materials in Organic Photovoltaics. *The Chemical Record* **2019,** *0* (0).

61. Mutolo, K. L.; Mayo, E. I.; Rand, B. P.; Forrest, S. R.; Thompson, M. E., Enhanced Open-Circuit Voltage in Subphthalocyanine/C60 Organic Photovoltaic Cells. *Journal of the American Chemical Society* **2006,** *128* (25), 8108-8109.

62. Gommans, H. H. P.; Cheyns, D.; Aernouts, T.; Girotto, C.; Poortmans, J.; Heremans, P., Electro-Optical Study of Subphthalocyanine in a Bilayer Organic Solar Cell. *Advanced Functional Materials* **2007,** *17* (15), 2653-2658.

63. Gommans, H.; Verreet, B.; Rand, B. P.; Muller, R.; Poortmans, J.; Heremans, P.; Genoe, J., On the Role of Bathocuproine in Organic Photovoltaic Cells. *Advanced Functional Materials* **2008,** *18* (22), 3686-3691.

64. de la Torre, G.; Bottari, G.; Torres, T., Phthalocyanines and Subphthalocyanines: Perfect Partners for Fullerenes and Carbon Nanotubes in Molecular Photovoltaics. *Advanced Energy Materials* **2017,** *7* (10), 1601700.

65. Gommans, H.; Aernouts, T.; Verreet, B.; Heremans, P.; Medina, A.; Claessens, C. G.; Torres, T., Perfluorinated Subphthalocyanine as a New Acceptor Material in a Small-

Molecule Bilayer Organic Solar Cell. *Advanced Functional Materials* **2009,** *19* (21), 3435-3439.

66. Hancox, I.; New, E.; Jones, T. S., Utilising solution processed zirconium acetylacetonate as an electron extracting layer in both regular and inverted small molecule organic photovoltaic cells. *Organic Electronics* **2015,** *23*, 105-109.

67. Dang, J. D.; Josey, D. S.; Lough, A. J.; Li, Y.; Sifate, A.; Lu, Z.-H.; Bender, T. P., The mixed alloyed chemical composition of chloro-(chloro)n-boron subnaphthalocyanines dictates their physical properties and performance in organic photovoltaic devices. *Journal of Materials Chemistry A* **2016,** *4* (24), 9566-9577.

68. Verreet, B.; Cnops, K.; Cheyns, D.; Heremans, P.; Stesmans, A.; Zango, G.; Claessens, C. G.; Torres, T.; Rand, B. P., Decreased Recombination Through the Use of a Non-Fullerene Acceptor in a 6.4% Efficient Organic Planar Heterojunction Solar Cell. *Advanced Energy Materials* **2014,** *4* (8), 1301413.

69. Chandran, H. T.; Ng, T.-W.; Foo, Y.; Li, H.-W.; Qing, J.; Liu, X.-K.; Chan, C.-Y.; Wong, F.-L.; Zapien, J. A.; Tsang, S.-W.; Lo, M.-F.; Lee, C.-S., Direct Free Carrier Photogeneration in Single Layer and Stacked Organic Photovoltaic Devices. *Advanced Materials* **2017,** *29* (22), 1606909.

70. Rao, A.; Wilson, M. W. B.; Hodgkiss, J. M.; Albert-Seifried, S.; Bässler, H.; Friend, R. H., Exciton Fission and Charge Generation via Triplet Excitons in Pentacene/C60 Bilayers. *Journal of the American Chemical Society* **2010,** *132* (36), 12698-12703.

71. Beaumont, N.; Cho, S. W.; Sullivan, P.; Newby, D.; Smith, K. E.; Jones, T. S., Boron Subphthalocyanine Chloride as an Electron Acceptor for High-Voltage Fullerene-Free Organic Photovoltaics. *Advanced Functional Materials* **2012,** *22* (3), 561-566.

72. Cnops, K.; Rand, B. P.; Cheyns, D.; Heremans, P., Enhanced photocurrent and open-circuit voltage in a 3-layer cascade organic solar cell. *Applied Physics Letters* **2012,** *101* (14), 143301.

73. Smith, M. B.; Michl, J., Singlet Fission. *Chemical Reviews* **2010,** *110* (11), 6891-6936.

74. Wilson, M. W. B.; Rao, A.; Johnson, K.; Gélinas, S.; di Pietro, R.; Clark, J.; Friend, R. H., Temperature-Independent Singlet Exciton Fission in Tetracene. *Journal of the American Chemical Society* **2013,** *135* (44), 16680-16688.

75. Beaumont, N.; Castrucci, J. S.; Sullivan, P.; Morse, G. E.; Paton, A. S.; Lu, Z.-H.; Bender, T. P.; Jones, T. S., Acceptor Properties of Boron Subphthalocyanines in Fullerene Free Photovoltaics. *The Journal of Physical Chemistry C* **2014,** *118* (27), 14813-14823.

76. Castrucci, J. S.; Josey, D. S.; Thibau, E.; Lu, Z.-H.; Bender, T. P., Boron Subphthalocyanines as Triplet Harvesting Materials within Organic Photovoltaics. *The Journal of Physical Chemistry Letters* **2015,** *6* (15), 3121-3125.

77. Lin, Y.; Zhong, J.; Yan, X.; Li, L., Simple planar heterojunction fullerene-free organic photovoltaic cell with high open-circuit voltages above 1.4 V. *Journal of Materials Science: Materials in Electronics* **2017,** *28* (12), 9167-9173.

78. Nikolis, V. C.; Benduhn, J.; Holzmueller, F.; Piersimoni, F.; Lau, M.; Zeika, O.; Neher, D.; Koerner, C.; Spoltore, D.; Vandewal, K., Reducing Voltage Losses in Cascade Organic Solar Cells while Maintaining High External Quantum Efficiencies. *Advanced Energy Materials* **2017,** *7* (21), 1700855.

79. Cnops, K.; Rand, B. P.; Cheyns, D.; Verreet, B.; Empl, M. A.; Heremans, P., 8.4% efficient fullerene-free organic solar cells exploiting long-range exciton energy transfer. *Nature Communications* **2014,** *5*, 3406.

80. Huang, P.-H.; Wang, Y.-H.; Ke, J.-C.; Huang, C.-J., Investigation of Various Active Layers for Their Performance on Organic Solar Cells. *Materials* **2016,** *9* (8).

81. Bormann, L.; Nehm, F.; Weiß, N.; Nikolis, V. C.; Selzer, F.; Eychmüller, A.; Müller-Meskamp, L.; Vandewal, K.; Leo, K., Degradation of Sexithiophene Cascade Organic Solar Cells. *Advanced Energy Materials* **2016,** *6* (9), 1502432.

82. Castrucci, J. S.; Garner, R. K.; Dang, J. D.; Thibau, E.; Lu, Z.-H.; Bender, T. P., Characterization of μ-oxo-(BsubPc)2 in Multiple Organic Photovoltaic Device Architectures: Comparing against and Combining with Cl-BsubPc. *ACS Applied Materials & Interfaces* **2016,** *8* (37), 24712-24721.

83. Takahashi, Y.; Yasuda, T.; Yonezawa, K.; Moritomo, Y., Carrier injection dynamics in heterojunction solar cells with bipolar molecule. *Applied Physics Letters* **2015,** *106* (12), 123902.

84. Morozan, A.; Bourgeteau, T.; Tondelier, D.; Geffroy, B.; Jousselme, B.; Artero, V., Noble metal-free hydrogen-evolving photocathodes based on small molecule organic semiconductors. *Nanotechnology* **2016,** *27* (35), 355401.

85. Barito, A.; Sykes, M. E.; Bilby, D.; Amonoo, J.; Jin, Y.; Morris, S. E.; Green, P. F.; Kim, J.; Shtein, M., Recovering lost excitons in organic photovoltaics using a transparent dissociation layer. *Journal of Applied Physics* **2013,** *113* (20), 203110.

86. Zheng, Y.-q.; Potscavage Jr, W. J.; Zhang, J.; Yasuda, T.; Wei, B.; Adachi, C., Tetraphenyldibenzoperiflanthene as sensitizer for enhancing the performance in dinaphthothienothiophene-based photovoltaics with and without fullerene. *Synthetic Metals* **2015,** *205*, 121-126.

87. Cattin, L.; El Jouad, Z.; Arzel, L.; Neculqueo, G.; Morsli, M.; Martinez, F.; Addou, M.; Bernède, J. C., Comparison of performances of three active layers cascade OPVCs with those obtained from corresponding bi-layers. *Solar Energy* **2018,** *171*, 621-628.

88. Stevens, M. A.; Arango, A. C., Open-circuit voltage exceeding the outermost HOMO-LUMO offset in cascade organic solar cells. *Organic Electronics* **2016,** *37*, 80-84.

89. Josey, D. S.; Castrucci, J. S.; Dang, J. D.; Lessard, B. H.; Bender, T. P., Evaluating Thiophene Electron-Donor Layers for the Rapid Assessment of Boron Subphthalocyanines as Electron Acceptors in Organic Photovoltaics: Solution or Vacuum Deposition? *ChemPhysChem* **2015,** *16* (6), 1245-1250.

90. Goh, C.; Kline, R. J.; McGehee, M. D.; Kadnikova, E. N.; Fréchet, J. M. J., Molecular-weight-dependent mobilities in regioregular poly(3-hexyl-thiophene) diodes. *Applied Physics Letters* **2005,** *86* (12), 122110.

91. Sakai, J.; Taima, T.; Yamanari, T.; Saito, K., Annealing effect in the sexithiophene:C70 small molecule bulk heterojunction organic photovoltaic cells. *Solar Energy Materials and Solar Cells* **2009,** *93* (6), 1149-1153.

92. Paton, A. S.; Lough, A. J.; Bender, T. P., Sulfonate pseudohalides of boron subphthalocyanine. *Acta Crystallographica Section C* **2012,** *68* (11), o459-o464.

93. Paton, A. S.; Lough, A. J.; Bender, T. P., One Well-Placed Methyl Group Increases the Solubility of Phenoxy Boronsubphthalocyanine Two Orders of Magnitude. *Industrial & Engineering Chemistry Research* **2012,** *51* (18), 6290-6296.

94. Virdo, J. D.; Kawar, Y. H.; Lough, A. J.; Bender, T. P., Halogen bonds can direct the solid state arrangement of phenoxy–boron subphthalocyanines. *CrystEngComm* **2013,** *15* (16), 3187-3199.

95. Tong, X.; Lassiter, B. E.; Forrest, S. R., Inverted organic photovoltaic cells with high open-circuit voltage. *Organic Electronics* **2010,** *11* (4), 705-709.

96. Yoo, S.; Domercq, B.; Kippelen, B., Efficient thin-film organic solar cells based on pentacene/C60 heterojunctions. *Applied Physics Letters* **2004,** *85* (22), 5427-5429.

97. Sullivan, P.; Jones, T. S., Pentacene/fullerene (C60) heterojunction solar cells: Device performance and degradation mechanisms. *Organic Electronics* **2008,** *9* (5), 656-660.

98. Anthony, J. E.; Brooks, J. S.; Eaton, D. L.; Parkin, S. R., Functionalized Pentacene: Improved Electronic Properties from Control of Solid-State Order. *Journal of the American Chemical Society* **2001,** *123* (38), 9482-9483.

99. Ehrler, B.; Walker, B. J.; Böhm, M. L.; Wilson, M. W. B.; Vaynzof, Y.; Friend, R. H.; Greenham, N. C., In situ measurement of exciton energy in hybrid singlet-fission solar cells. *Nature Communications* **2012,** *3*, 1019.

100. Jadhav, P. J.; Brown, P. R.; Thompson, N.; Wunsch, B.; Mohanty, A.; Yost, S. R.; Hontz, E.; Van Voorhis, T.; Bawendi, M. G.; Bulović, V.; Baldo, M. A., Triplet Exciton Dissociation in Singlet Exciton Fission Photovoltaics. *Advanced Materials* **2012,** *24* (46), 6169-6174.

101. Dang, M. T.; Hirsch, L.; Wantz, G.; Wuest, J. D., Controlling the Morphology and Performance of Bulk Heterojunctions in Solar Cells. Lessons Learned from the Benchmark Poly(3-hexylthiophene):[6,6]-Phenyl-C61-butyric Acid Methyl Ester System. *Chemical Reviews* **2013,** *113* (5), 3734-3765.

102. Dang, M. T.; Wuest, J. D., Using volatile additives to alter the morphology and performance of active layers in thin-film molecular photovoltaic devices incorporating bulk heterojunctions. *Chemical Society Reviews* **2013,** *42* (23), 9105-9126.

103. Chen, J.; Cao, Y., Development of Novel Conjugated Donor Polymers for High-Efficiency Bulk-Heterojunction Photovoltaic Devices. *Accounts of Chemical Research* **2009,** *42* (11), 1709-1718.

104. Haubner, K.; Gründler, P.; Dunsch, L., Spectro- and thermoelectrochemistry of sexithiophenes in solution. *Journal of Electroanalytical Chemistry* **2012,** *682*, 72-76.

105. Li, G.; Shrotriya, V.; Yao, Y.; Huang, J.; Yang, Y., Manipulating regioregular poly(3-hexylthiophene) : [6,6]-phenyl-C61-butyric acid methyl ester blends—route towards high efficiency polymer solar cells. *Journal of Materials Chemistry* **2007,** *17* (30), 3126-3140.

106. Dang, M. T.; Hirsch, L.; Wantz, G., P3HT:PCBM, Best Seller in Polymer Photovoltaic Research. *Advanced Materials* **2011,** *23* (31), 3597-3602.

107. Stevens, D. M.; Qin, Y.; Hillmyer, M. A.; Frisbie, C. D., Enhancement of the Morphology and Open Circuit Voltage in Bilayer Polymer/Fullerene Solar Cells. *The Journal of Physical Chemistry C* **2009,** *113* (26), 11408-11415.

108. Geiser, A.; Fan, B.; Benmansour, H.; Castro, F.; Heier, J.; Keller, B.; Mayerhofer, K. E.; Nüesch, F.; Hany, R., Poly(3-hexylthiophene)/C60 heterojunction solar cells: Implication of morphology on performance and ambipolar charge collection. *Solar Energy Materials and Solar Cells* **2008,** *92* (4), 464-473.

109. Tong, S. W.; Zhang, C. F.; Jiang, C. Y.; Ling, Q. D.; Kang, E. T.; Chan, D. S. H.; Zhu, C., The use of thermal initiator to make organic bulk heterojunction solar cells with a good percolation path. *Applied Physics Letters* **2008,** *93* (4), 043304.

110. Yang, Y.; Aryal, M.; Mielczarek, K.; Hu, W.; Zakhidov, A., Nanoimprinted P3HT/C60 solar cells optimized by oblique deposition of C60. *Journal of Vacuum Science & Technology B* **2010,** *28* (6), C6M104-C6M107.

111. Servet, B.; Ries, S.; Trotel, M.; Alnot, P.; Horowitz, G.; Garnier, F., X-ray determination of the crystal structure and orientation of vacuum evaporated sexithiophene films. *Advanced Materials* **1993,** *5* (6), 461-464.

112. Sirringhaus, H.; Brown, P. J.; Friend, R. H.; Nielsen, M. M.; Bechgaard, K.; Langeveld-Voss, B. M. W.; Spiering, A. J. H.; Janssen, R. A. J.; Meijer, E. W.; Herwig, P.; de Leeuw, D. M., Two-dimensional charge transport in self-organized, high-mobility conjugated polymers. *Nature* **1999,** *401*, 685.

113. Zhang, G.; Huber, R. C.; Ferreira, A. S.; Boyd, S. D.; Luscombe, C. K.; Tolbert, S. H.; Schwartz, B. J., Crystallinity Effects in Sequentially Processed and Blend-Cast Bulk-Heterojunction Polymer/Fullerene Photovoltaics. *The Journal of Physical Chemistry C* **2014,** *118* (32), 18424-18435.

114. Mihailetchi, V. D.; Xie, H. X.; de Boer, B.; Koster, L. J. A.; Blom, P. W. M., Charge Transport and Photocurrent Generation in Poly(3-hexylthiophene): Methanofullerene Bulk-Heterojunction Solar Cells. *Advanced Functional Materials* **2006,** *16* (5), 699-708.

115. Verreet, B.; Schols, S.; Cheyns, D.; Rand, B. P.; Gommans, H.; Aernouts, T.; Heremans, P.; Genoe, J., The characterization of chloroboron (iii) subnaphthalocyanine thin films and

their application as a donor material for organic solar cells. *Journal of Materials Chemistry* **2009,** *19* (30), 5295-5297.

116. Ma, B.; Woo, C. H.; Miyamoto, Y.; Fréchet, J. M. J., Solution Processing of a Small Molecule, Subnaphthalocyanine, for Efficient Organic Photovoltaic Cells. *Chemistry of Materials* **2009,** *21* (8), 1413-1417.

117. Cheyns, D.; Rand, B. P.; Heremans, P., Organic tandem solar cells with complementary absorbing layers and a high open-circuit voltage. *Applied Physics Letters* **2010,** *97* (3), 033301.

118. Kulshreshtha, C.; Kim, G. W.; Lampande, R.; Huh, D. H.; Chae, M.; Kwon, J. H., New interfacial materials for rapid hole-extraction in organic photovoltaic cells. *Journal of Materials Chemistry A* **2013,** *1* (12), 4077-4082.

119. Chen, G.; Sasabe, H.; Sano, T.; Wang, X.-F.; Hong, Z.; Kido, J.; Yang, Y., Chloroboron (III) subnaphthalocyanine as an electron donor in bulk heterojunction photovoltaic cells. *Nanotechnology* **2013,** *24* (48), 484007.

120. Fleetham, T. B.; Bakkan, N.; Mudrick, J. P.; Myers, J. D.; Cassidy, V. D.; Cui, J.; Xue, J.; Li, J., Enhanced open-circuit voltage in organic photovoltaic cells with partially chlorinated zinc phthalocyanine. *Journal of Materials Science* **2013,** *48* (20), 7104-7114.

121. Fleetham, T. B.; Mudrick, J. P.; Cao, W.; Klimes, K.; Xue, J.; Li, J., Efficient Zinc Phthalocyanine/C60 Heterojunction Photovoltaic Devices Employing Tetracene Anode Interfacial Layers. *ACS Applied Materials & Interfaces* **2014,** *6* (10), 7254-7259.

122. Salzman, R. F.; Xue, J.; Rand, B. P.; Alexander, A.; Thompson, M. E.; Forrest, S. R., The effects of copper phthalocyanine purity on organic solar cell performance. *Organic Electronics* **2005,** *6* (5), 242-246.

123. Pai, D. M.; Yanus, J. F.; Stolka, M., Trap-controlled hopping transport. *The Journal of Physical Chemistry* **1984,** *88* (20), 4714-4717.

124. Street, R. A.; Davies, D.; Khlyabich, P. P.; Burkhart, B.; Thompson, B. C., Origin of the Tunable Open-Circuit Voltage in Ternary Blend Bulk Heterojunction Organic Solar Cells. *Journal of the American Chemical Society* **2013,** *135* (3), 986-989.

125. Street, R. A.; Khlyabich, P. P.; Rudenko, A. E.; Thompson, B. C., Electronic States in Dilute Ternary Blend Organic Bulk Heterojunction Solar Cells. *The Journal of Physical Chemistry C* **2014,** *118* (46), 26569-26576.

126. Cowan, S. R.; Leong, W. L.; Banerji, N.; Dennler, G.; Heeger, A. J., Identifying a Threshold Impurity Level for Organic Solar Cells: Enhanced First-Order Recombination Via Well-Defined PC84BM Traps in Organic Bulk Heterojunction Solar Cells. *Advanced Functional Materials* **2011,** *21* (16), 3083-3092.

127. Nikiforov, M. P.; Lai, B.; Chen, W.; Chen, S.; Schaller, R. D.; Strzalka, J.; Maser, J.; Darling, S. B., Detection and role of trace impurities in high-performance organic solar cells. *Energy & Environmental Science* **2013,** *6* (5), 1513-1520.

128. Hermenau, M.; Riede, M.; Leo, K.; Gevorgyan, S. A.; Krebs, F. C.; Norrman, K., Water and oxygen induced degradation of small molecule organic solar cells. *Solar Energy Materials and Solar Cells* **2011,** *95* (5), 1268-1277.

129. Yang, H. B.; Song, Q. L.; Gong, C.; Li, C. M., The degradation of indium tin oxide/pentacene/fullerene/tris-8-hydroxy-quinolinato aluminum/aluminum heterojunction organic solar cells: By oxygen or moisture? *Solar Energy Materials and Solar Cells* **2010,** *94* (5), 846-849.

130. Volonakis, G.; Tsetseris, L.; Logothetidis, S., Impurity-related degradation in a prototype organic photovoltaic material: A first-principles study. *Organic Electronics* **2013,** *14* (5), 1242-1248.

131. Kaake, L.; Dang, X.-D.; Leong, W. L.; Zhang, Y.; Heeger, A.; Nguyen, T.-Q., Effects of Impurities on Operational Mechanism of Organic Bulk Heterojunction Solar Cells. *Advanced Materials* **2013,** *25* (12), 1706-1712.

132. Manion, J. G.; Gao, D.; Brodersen, P. M.; Seferos, D. S., Insulating polymer additives in small molecule and polymer photovoltaics: how they are tolerated and their use as potential interlayers. *Journal of Materials Chemistry C* **2017,** *5* (13), 3315-3322.

133. Bannock, J. H.; Treat, N. D.; Chabinyc, M.; Stingelin, N.; Heeney, M.; de Mello, J. C., The influence of polymer purification on the efficiency of poly(3-hexylthiophene):fullerene organic solar cells. *Scientific Reports* **2016,** *6*, 23651.

134. Wagner, H. J.; Loutfy, R. O.; Hsiao, C.-K., Purification and characterization of phthalocyanines. *Journal of Materials Science* **1982,** *17* (10), 2781-2791.

135. Tang, C. W.; VanSlyke, S. A.; Chen, C. H., Electroluminescence of doped organic thin films. *Journal of Applied Physics* **1989,** *65* (9), 3610-3616.

136. Rand, B. P.; Schols, S.; Cheyns, D.; Gommans, H.; Girotto, C.; Genoe, J.; Heremans, P.; Poortmans, J., Organic solar cells with sensitized phosphorescent absorbing layers. *Organic Electronics* **2009,** *10* (5), 1015-1019.

137. Zyskowski, C. D.; Kennedy, V. O., Compounds in the series from boron subphthalocyanine to boron subnaphthalocyanine. *Journal of Porphyrins and Phthalocyanines* **2000,** *4* (8), 707-712.

138. Bonnier, C.; Josey, D. S.; Bender, T. P., Aryl-Substituted Boron Subphthalocyanines and their Application in Organic Photovoltaics. *Australian Journal of Chemistry* **2015,** *68* (11), 1750-1758.

139. Sampson, K. L.; Josey, D. S.; Li, Y.; Virdo, J. D.; Lu, Z.-H.; Bender, T. P., Ability To Fine-Tune the Electronic Properties and Open-Circuit Voltage of Phenoxy-Boron Subphthalocyanines through Meta-Fluorination of the Axial Substituent. *The Journal of Physical Chemistry C* **2018,** *122* (2), 1091-1102.

140. Dang, J. D.; Josey, D. S.; Dang, M. T.; Bender, T. P., Phenoxy-(Chloro)n-Boron Subnaphthalocyanines: Alloyed Mixture, Electron-Accepting Functionality, and Enhanced

Solubility for Bulk Heterojunction Organic Photovoltaics. *ACS Omega* **2018,** *3* (2), 2093-2103.

141. Menke, S. M.; Holmes, R. J., Exciton diffusion in organic photovoltaic cells. *Energy & Environmental Science* **2014,** *7* (2), 499-512.

142. Chen, S.; Tsang, S.-W.; Lai, T.-H.; Reynolds, J. R.; So, F., Dielectric Effect on the Photovoltage Loss in Organic Photovoltaic Cells. *Advanced Materials* **2014,** *26* (35), 6125-6131.

143. Deibel, C.; Strobel, T.; Dyakonov, V., Role of the Charge Transfer State in Organic Donor–Acceptor Solar Cells. *Advanced Materials* **2010,** *22* (37), 4097-4111.

144. Shoaee, S.; Clarke, T. M.; Huang, C.; Barlow, S.; Marder, S. R.; Heeney, M.; McCulloch, I.; Durrant, J. R., Acceptor Energy Level Control of Charge Photogeneration in Organic Donor/Acceptor Blends. *Journal of the American Chemical Society* **2010,** *132* (37), 12919-12926.

145. Chen, H.-Y.; Hou, J.; Zhang, S.; Liang, Y.; Yang, G.; Yang, Y.; Yu, L.; Wu, Y.; Li, G., Polymer solar cells with enhanced open-circuit voltage and efficiency. *Nature Photonics* **2009,** *3*, 649.

146. Scharber, M. C.; Mühlbacher, D.; Koppe, M.; Denk, P.; Waldauf, C.; Heeger, A. J.; Brabec, C. J., Design Rules for Donors in Bulk-Heterojunction Solar Cells—Towards 10 % Energy-Conversion Efficiency. *Advanced Materials* **2006,** *18* (6), 789-794.

147. Elumalai, N. K.; Uddin, A., Open circuit voltage of organic solar cells: an in-depth review. *Energy & Environmental Science* **2016,** *9* (2), 391-410.

148. Bartynski, A. N.; Grob, S.; Linderl, T.; Gruber, M.; Brütting, W.; Thompson, M. E., Organic Solar Cells with Open Circuit Voltage over 1.25 V Employing Tetraphenyldibenzoperiflanthene as the Acceptor. *The Journal of Physical Chemistry C* **2016,** *120* (34), 19027-19034.

149. Shin, J.; Kim, M.; Lee, J.; Kim, H. G.; Hwang, H.; Cho, K., Positional effects of fluorination in conjugated side chains on photovoltaic properties of donor–acceptor copolymers. *Chemical Communications* **2017,** *53* (6), 1176-1179.

150. Xu, X.; Li, Z.; Bäcke, O.; Bini, K.; James, D. I.; Olsson, E.; Andersson, M. R.; Wang, E., Effects of side chain isomerism on the physical and photovoltaic properties of indacenodithieno[3,2-b]thiophene–quinoxaline copolymers: toward a side chain design for enhanced photovoltaic performance. *Journal of Materials Chemistry A* **2014,** *2* (44), 18988-18997.

151. Liu, P.; Zhang, K.; Liu, F.; Jin, Y.; Liu, S.; Russell, T. P.; Yip, H.-L.; Huang, F.; Cao, Y., Effect of Fluorine Content in Thienothiophene-Benzodithiophene Copolymers on the Morphology and Performance of Polymer Solar Cells. *Chemistry of Materials* **2014,** *26* (9), 3009-3017.

152. Lessard, B. H.; Grant, T. M.; White, R.; Thibau, E.; Lu, Z.-H.; Bender, T. P., The position and frequency of fluorine atoms changes the electron donor/acceptor properties of

fluorophenoxy silicon phthalocyanines within organic photovoltaic devices. *Journal of Materials Chemistry A* **2015,** *3* (48), 24512-24524.

153. Lessard, B. H.; White, R. T.; Al-Amar, M.; Plint, T.; Castrucci, J. S.; Josey, D. S.; Lu, Z.-H.; Bender, T. P., Assessing the Potential Roles of Silicon and Germanium Phthalocyanines in Planar Heterojunction Organic Photovoltaic Devices and How Pentafluoro Phenoxylation Can Enhance π–π Interactions and Device Performance. *ACS Applied Materials & Interfaces* **2015,** *7* (9), 5076-5088.

154. Lessard, B. H.; Dang, J. D.; Grant, T. M.; Gao, D.; Seferos, D. S.; Bender, T. P., Bis(tri-n-hexylsilyl oxide) Silicon Phthalocyanine: A Unique Additive in Ternary Bulk Heterojunction Organic Photovoltaic Devices. *ACS Applied Materials & Interfaces* **2014,** *6* (17), 15040-15051.

155. Graham, K. R.; Erwin, P.; Nordlund, D.; Vandewal, K.; Li, R.; Ngongang Ndjawa, G. O.; Hoke, E. T.; Salleo, A.; Thompson, M. E.; McGehee, M. D.; Amassian, A., Re-evaluating the Role of Sterics and Electronic Coupling in Determining the Open-Circuit Voltage of Organic Solar Cells. *Advanced Materials* **2013,** *25* (42), 6076-6082.

156. Erwin, P.; Thompson, M. E., Elucidating the interplay between dark current coupling and open circuit voltage in organic photovoltaics. *Applied Physics Letters* **2011,** *98* (22), 223305.

157. Lam, S. L.; Liu, X.; Zhao, F.; Lee, C.-L. K.; Kwan, W. L., Manipulating open-circuit voltage in an organic photovoltaic device via a phenylalkyl side chain. *Chemical Communications* **2013,** *49* (40), 4543-4545.

158. Raboui, H.; Al-Amar, M.; Abdelrahman, A. I.; Bender, T. P., Axially phenoxylated aluminum phthalocyanines and their application in organic photovoltaic cells. *RSC Advances* **2015,** *5* (57), 45731-45739.

159. Yang, L.; Zhou, H.; You, W., Quantitatively Analyzing the Influence of Side Chains on Photovoltaic Properties of Polymer−Fullerene Solar Cells. *The Journal of Physical Chemistry C* **2010,** *114* (39), 16793-16800.

160. Bassani, D. M.; Jonusauskaite, L.; Lavie-Cambot, A.; McClenaghan, N. D.; Pozzo, J.-L.; Ray, D.; Vives, G., Harnessing supramolecular interactions in organic solid-state devices: Current status and future potential. *Coordination Chemistry Reviews* **2010,** *254* (19), 2429-2445.

161. Rim, S.-B.; Fink, R. F.; Schöneboom, J. C.; Erk, P.; Peumans, P., Effect of molecular packing on the exciton diffusion length in organic solar cells. *Applied Physics Letters* **2007,** *91* (17), 173504.

162. Venkataraman, D.; Yurt, S.; Venkatraman, B. H.; Gavvalapalli, N., Role of Molecular Architecture in Organic Photovoltaic Cells. *The Journal of Physical Chemistry Letters* **2010,** *1* (6), 947-958.

163. Botiz, I.; Stingelin, N., Influence of Molecular Conformations and Microstructure on the Optoelectronic Properties of Conjugated Polymers. *Materials* **2014,** *7* (3).

164. Mukherjee, A.; Tothadi, S.; Desiraju, G. R., Halogen Bonds in Crystal Engineering: Like Hydrogen Bonds yet Different. *Accounts of Chemical Research* **2014,** *47* (8), 2514-2524.

165. Desiraju, G. R.; Ho, P. S.; Kloo, L.; Legon, A. C.; Marquardt, R.; Metrangolo, P.; Politzer, P.; Resnati, G.; Rissanen, K., Definition of the halogen bond (IUPAC Recommendations 2013). In *Pure and Applied Chemistry*, 2013; Vol. 85, p 1711.

166. Simon, S. J. C.; Parlane, F. G. L.; Swords, W. B.; Kellett, C. W.; Du, C.; Lam, B.; Dean, R. K.; Hu, K.; Meyer, G. J.; Berlinguette, C. P., Halogen Bonding Promotes Higher Dye-Sensitized Solar Cell Photovoltages. *Journal of the American Chemical Society* **2016,** *138* (33), 10406-10409.

167. Parlane, F. G. L.; Mustoe, C.; Kellett, C. W.; Simon, S. J.; Swords, W. B.; Meyer, G. J.; Kennepohl, P.; Berlinguette, C. P., Spectroscopic detection of halogen bonding resolves dye regeneration in the dye-sensitized solar cell. *Nature Communications* **2017,** *8* (1), 1761.

168. Abate, A.; Saliba, M.; Hollman, D. J.; Stranks, S. D.; Wojciechowski, K.; Avolio, R.; Grancini, G.; Petrozza, A.; Snaith, H. J., Supramolecular Halogen Bond Passivation of Organic–Inorganic Halide Perovskite Solar Cells. *Nano Letters* **2014,** *14* (6), 3247-3254.

169. Castrucci, J. S.; Dang, J. D.; Kamino, B. A.; Campbell, A.; Pitts, D.; Lu, Z.-H.; Bender, T. P., Considerations for the physical vapor deposition of high molar mass organic compounds. *Vacuum* **2014,** *109*, 26-33.

170. Josey, D. S.; Nyikos, S. R.; Garner, R. K.; Dovijarski, A.; Castrucci, J. S.; Wang, J. M.; Evans, G. J.; Bender, T. P., Outdoor Performance and Stability of Boron Subphthalocyanines Applied as Electron Acceptors in Fullerene-Free Organic Photovoltaics. *ACS Energy Letters* **2017,** *2* (3), 726-732.

171. Erbs, D. G.; Klein, S. A.; Duffie, J. A., Estimation of the diffuse radiation fraction for hourly, daily and monthly-average global radiation. *Solar Energy* **1982,** *28* (4), 293-302.

172. Mishra, A.; Bäuerle, P., Small Molecule Organic Semiconductors on the Move: Promises for Future Solar Energy Technology. *Angewandte Chemie International Edition* **2012,** *51* (9), 2020-2067.

173. Brabec, C. J.; Gowrisanker, S.; Halls, J. J. M.; Laird, D.; Jia, S.; Williams, S. P., Polymer–Fullerene Bulk-Heterojunction Solar Cells. *Advanced Materials* **2010,** *22* (34), 3839-3856.

174. Dou, L.; You, J.; Hong, Z.; Xu, Z.; Li, G.; Street, R. A.; Yang, Y., 25th Anniversary Article: A Decade of Organic/Polymeric Photovoltaic Research. *Advanced Materials* **2013,** *25* (46), 6642-6671.

175. Søndergaard, R. R.; Hösel, M.; Krebs, F. C., Roll-to-Roll fabrication of large area functional organic materials. *Journal of Polymer Science Part B: Polymer Physics* **2013,** *51* (1), 16-34.

176. Mazzio, K. A.; Luscombe, C. K., The future of organic photovoltaics. *Chemical Society Reviews* **2015,** *44* (1), 78-90.

177. Cheng, Y.-J.; Yang, S.-H.; Hsu, C.-S., Synthesis of Conjugated Polymers for Organic Solar Cell Applications. *Chemical Reviews* **2009,** *109* (11), 5868-5923.

178. Chen, Y.-H.; Lin, L.-Y.; Lu, C.-W.; Lin, F.; Huang, Z.-Y.; Lin, H.-W.; Wang, P.-H.; Liu, Y.-H.; Wong, K.-T.; Wen, J.; Miller, D. J.; Darling, S. B., Vacuum-Deposited Small-Molecule Organic Solar Cells with High Power Conversion Efficiencies by Judicious Molecular Design and Device Optimization. *Journal of the American Chemical Society* **2012,** *134* (33), 13616-13623.

179. Haillant, O., Accelerated weathering testing principles to estimate the service life of organic PV modules. *Solar Energy Materials and Solar Cells* **2011,** *95* (5), 1284-1292.

180. Gevorgyan, S. A.; Madsen, M. V.; Roth, B.; Corazza, M.; Hösel, M.; Søndergaard, R. R.; Jørgensen, M.; Krebs, F. C., Lifetime of Organic Photovoltaics: Status and Predictions. *Advanced Energy Materials* **2016,** *6* (2), 1501208.

181. Seethamraju, S.; Ramamurthy, P. C.; Madras, G., Reactive interlayer based ultra-low moisture permeable membranes for organic photovoltaic encapsulation. *Physical Chemistry Chemical Physics* **2015,** *17* (35), 23165-23172.

182. Seethamraju, S.; Kumar, S.; B, K. B.; Madras, G.; Raghavan, S.; Ramamurthy, P. C., Million-Fold Decrease in Polymer Moisture Permeability by a Graphene Monolayer. *ACS Nano* **2016,** *10* (7), 6501-6509.

183. Weerasinghe, H. C.; Vak, D.; Robotham, B.; Fell, C. J.; Jones, D.; Scully, A. D., New barrier encapsulation and lifetime assessment of printed organic photovoltaic modules. *Solar Energy Materials and Solar Cells* **2016,** *155*, 108-116.

184. Corazza, M.; Krebs, F. C.; Gevorgyan, S. A., Lifetime of organic photovoltaics: Linking outdoor and indoor tests. *Solar Energy Materials and Solar Cells* **2015,** *143*, 467-472.

185. Espinosa, N.; Laurent, A.; dos Reis Benatto, G. A.; Hösel, M.; Krebs, F. C., Which Electrode Materials to Select for More Environmentally Friendly Organic Photovoltaics? *Advanced Engineering Materials* **2016,** *18* (4), 490-495.

186. Roth, B.; A. dos Reis Benatto, G.; Corazza, M.; Carlé, J. E.; Helgesen, M.; Gevorgyan, S. A.; Jørgensen, M.; Søndergaard, R. R.; Krebs, F. C., Improving the Operational Stability of PBDTTTz-4 Polymer Solar Cells Modules by Electrode Modification. *Advanced Engineering Materials* **2016,** *18* (4), 511-517.

187. dos Reis Benatto, G. A.; Roth, B.; Corazza, M.; Søndergaard, R. R.; Gevorgyan, S. A.; Jørgensen, M.; Krebs, F. C., Roll-to-roll printed silver nanowires for increased stability of flexible ITO-free organic solar cell modules. *Nanoscale* **2016,** *8* (1), 318-326.

188. Espinosa, N.; Zimmermann, Y.-S.; dos Reis Benatto, G. A.; Lenz, M.; Krebs, F. C., Outdoor fate and environmental impact of polymer solar cells through leaching and emission to rainwater and soil. *Energy & Environmental Science* **2016,** *9* (5), 1674-1680.

189. Beliatis, M. J.; Helgesen, M.; García-Valverde, R.; Corazza, M.; Roth, B.; Carlé, J. E.; Jørgensen, M.; Krebs, F. C.; Gevorgyan, S. A., Slot-Die-Coated V2O5 as Hole Transport

Layer for Flexible Organic Solar Cells and Optoelectronic Devices *Advanced Engineering Materials* **2016,** *18* (8), 1494-1503.

190. Lima, F. A. S.; Beliatis, M. J.; Roth, B.; Andersen, T. R.; Bortoti, A.; Reyna, Y.; Castro, E.; Vasconcelos, I. F.; Gevorgyan, S. A.; Krebs, F. C.; Lira-Cantu, M., Flexible ITO-free organic solar cells applying aqueous solution-processed V2O5 hole transport layer: An outdoor stability study. *APL Materials* **2016,** *4* (2), 026104.

191. Kumar, P.; Bilen, C.; Vaughan, B.; Zhou, X.; Dastoor, P. C.; Belcher, W. J., Comparing the degradation of organic photovoltaic devices under ISOS testing protocols. *Solar Energy Materials and Solar Cells* **2016,** *149*, 179-186.

192. Martinez, F.; Neculqueo, G.; Bernède, J. C.; Cattin, L.; Makha, M., Influence of the presence of Ca in the cathode buffer layer on the performance and stability of organic photovoltaic cells using a branched sexithienylenevinylene oligomer as electron donor. *physica status solidi (a)* **2015,** *212* (8), 1767-1773.

193. Tan, K.-S.; Chuang, M.-K.; Chen, F.-C.; Hsu, C.-S., Solution-Processed Nanocomposites Containing Molybdenum Oxide and Gold Nanoparticles as Anode Buffer Layers in Plasmonic-Enhanced Organic Photovoltaic Devices. *ACS Applied Materials & Interfaces* **2013,** *5* (23), 12419-12424.

194. Jin, F.; Chu, B.; Li, W.; Su, Z.; Zhao, B.; Yan, X.; Zhang, F.; Fan, D.; Zhang, T.; Gao, Y.; Lee, C. S.; Wang, J., Improvement in power conversion efficiency and long-term lifetime of organic photovoltaic cells by using bathophenanthroline/molybdenum oxide as compound cathode buffer layer. *Solar Energy Materials and Solar Cells* **2013,** *117*, 189-193.

195. Dong, W. J.; Jung, G. H.; Lee, J.-L., Solution-processed-MoO3 hole extraction layer on oxygen plasma-treated indium tin oxide in organic photovoltaics. *Solar Energy Materials and Solar Cells* **2013,** *116*, 94-101.

196. Kwon, K. C.; Dong, W. J.; Jung, G. H.; Ham, J.; Lee, J.-L.; Kim, S. Y., Extension of stability in organic photovoltaic cells using UV/ozone-treated graphene sheets. *Solar Energy Materials and Solar Cells* **2013,** *109*, 148-154.

197. Kettle, J.; Waters, H.; Horie, M.; Chang, S. W., Effect of hole transporting layers on the performance of PCPDTBT : PCBM organic solar cells. *Journal of Physics D: Applied Physics* **2012,** *45* (12), 125102.

198. Ding, Z.; Kettle, J.; Horie, M.; Chang, S. W.; Smith, G. C.; Shames, A. I.; Katz, E. A., Efficient solar cells are more stable: the impact of polymer molecular weight on performance of organic photovoltaics. *Journal of Materials Chemistry A* **2016,** *4* (19), 7274-7280.

199. Turkovic, V.; Engmann, S.; Tsierkezos, N.; Hoppe, H.; Madsen, M.; Rubahn, H.-G.; Ritter, U.; Gobsch, G., Long-term stabilization of organic solar cells using hydroperoxide decomposers as additives. *Applied Physics A* **2016,** *122* (3), 255.

200. Waters, H.; Bristow, N.; Moudam, O.; Chang, S.-W.; Su, C.-J.; Wu, W.-R.; Jeng, U. S.; Horie, M.; Kettle, J., Effect of processing additive 1,8-octanedithiol on the lifetime of PCPDTBT based Organic Photovoltaics. *Organic Electronics* **2014,** *15* (10), 2433-2438.

201. Carlé, J. E.; Helgesen, M.; Zawacka, N. K.; Madsen, M. V.; Bundgaard, E.; Krebs, F. C., A comparative study of fluorine substituents for enhanced stability of flexible and ITO-free high-performance polymer solar cells. *Journal of Polymer Science Part B: Polymer Physics* **2014,** *52* (13), 893-899.

202. Livi, F.; Zawacka, N. K.; Angmo, D.; Jørgensen, M.; Krebs, F. C.; Bundgaard, E., Influence of Side Chain Position on the Electrical Properties of Organic Solar Cells Based on Dithienylbenzothiadiazole-alt-phenylene Conjugated Polymers. *Macromolecules* **2015,** *48* (11), 3481-3492.

203. Zawacka, N. K.; Andersen, T. R.; Andreasen, J. W.; Rossander, L. H.; Dam, H. F.; Jørgensen, M.; Krebs, F. C., The influence of additives on the morphology and stability of roll-to-roll processed polymer solar cells studied through ex situ and in situ X-ray scattering. *Journal of Materials Chemistry A* **2014,** *2* (43), 18644-18654.

204. Kim, M.-S.; Kim, B.-G.; Kim, J., Effective Variables To Control the Fill Factor of Organic Photovoltaic Cells. *ACS Applied Materials & Interfaces* **2009,** *1* (6), 1264-1269.

205. Claessens, C. G.; González-Rodríguez, D.; Rodríguez-Morgade, M. S.; Medina, A.; Torres, T., Subphthalocyanines, Subporphyrazines, and Subporphyrins: Singular Nonplanar Aromatic Systems. *Chemical Reviews* **2014,** *114* (4), 2192-2277.

206. Ebenhoch, B.; Prasetya, N. B. A.; Rotello, V. M.; Cooke, G.; Samuel, I. D. W., Solution-processed boron subphthalocyanine derivatives as acceptors for organic bulk-heterojunction solar cells. *Journal of Materials Chemistry A* **2015,** *3* (14), 7345-7352.

207. Sfyri, G.; Kumar, C. V.; Sabapathi, G.; Giribabu, L.; Andrikopoulos, K. S.; Stathatos, E.; Lianos, P., Subphthalocyanine as hole transporting material for perovskite solar cells. *RSC Advances* **2015,** *5* (85), 69813-69818.

208. Wang, N.; Tong, X.; Burlingame, Q.; Yu, J.; Forrest, S. R., Photodegradation of small-molecule organic photovoltaics. *Solar Energy Materials and Solar Cells* **2014,** *125*, 170-175.

209. Tong, X.; Wang, N.; Slootsky, M.; Yu, J.; Forrest, S. R., Intrinsic burn-in efficiency loss of small-molecule organic photovoltaic cells due to exciton-induced trap formation. *Solar Energy Materials and Solar Cells* **2013,** *118*, 116-123.

210. Gadisa, A.; Svensson, M.; Andersson, M. R.; Inganäs, O., Correlation between oxidation potential and open-circuit voltage of composite solar cells based on blends of polythiophenes/ fullerene derivative. *Applied Physics Letters* **2004,** *84* (9), 1609-1611.

211. Drakonakis, V. M.; Savva, A.; Kokonou, M.; Choulis, S. A., Investigating electrodes degradation in organic photovoltaics through reverse engineering under accelerated humidity lifetime conditions. *Solar Energy Materials and Solar Cells* **2014,** *130*, 544-550.

212. Girotto, C.; Voroshazi, E.; Cheyns, D.; Heremans, P.; Rand, B. P., Solution-Processed MoO3 Thin Films As a Hole-Injection Layer for Organic Solar Cells. *ACS Applied Materials & Interfaces* **2011,** *3* (9), 3244-3247.

213. Voroshazi, E.; Verreet, B.; Buri, A.; Müller, R.; Di Nuzzo, D.; Heremans, P., Influence of cathode oxidation via the hole extraction layer in polymer:fullerene solar cells. *Organic Electronics* **2011,** *12* (5), 736-744.

214. Angmo, D.; Sommeling, P. M.; Gupta, R.; Hösel, M.; Gevorgyan, S. A.; Kroon, J. M.; Kulkarni, G. U.; Krebs, F. C., Outdoor Operational Stability of Indium-Free Flexible Polymer Solar Modules Over 1 Year Studied in India, Holland, and Denmark. *Advanced Engineering Materials* **2014,** *16* (8), 976-987.

215. Mateker, W. R.; McGehee, M. D., Progress in Understanding Degradation Mechanisms and Improving Stability in Organic Photovoltaics. *Advanced Materials* **2017,** *29* (10), 1603940.

216. Zhang, Y.; Samuel, I. D. W.; Wang, T.; Lidzey, D. G., Current Status of Outdoor Lifetime Testing of Organic Photovoltaics. *Advanced Science* **2018,** *5* (8), 1800434.

217. Zhao, W.; Li, S.; Yao, H.; Zhang, S.; Zhang, Y.; Yang, B.; Hou, J., Molecular Optimization Enables over 13% Efficiency in Organic Solar Cells. *Journal of the American Chemical Society* **2017,** *139* (21), 7148-7151.

218. Li, G.; Chang, W.-H.; Yang, Y., Low-bandgap conjugated polymers enabling solution-processable tandem solar cells. *Nature Reviews Materials* **2017,** *2*, 17043.

219. Gao, L.; Zhang, Z.-G.; Bin, H.; Xue, L.; Yang, Y.; Wang, C.; Liu, F.; Russell, T. P.; Li, Y., High-Efficiency Nonfullerene Polymer Solar Cells with Medium Bandgap Polymer Donor and Narrow Bandgap Organic Semiconductor Acceptor. *Advanced Materials* **2016,** *28* (37), 8288-8295.

220. Li, S.; Ye, L.; Zhao, W.; Zhang, S.; Mukherjee, S.; Ade, H.; Hou, J., Energy-Level Modulation of Small-Molecule Electron Acceptors to Achieve over 12% Efficiency in Polymer Solar Cells. *Advanced Materials* **2016,** *28* (42), 9423-9429.

221. Jørgensen, M.; Norrman, K.; Gevorgyan, S. A.; Tromholt, T.; Andreasen, B.; Krebs, F. C., Stability of Polymer Solar Cells. *Advanced Materials* **2012,** *24* (5), 580-612.

222. Gevorgyan, S. A.; Heckler, I. M.; Bundgaard, E.; Corazza, M.; Hosel, M.; Soendergaard, R. R.; Benatto, G. A. d. R.; Joergensen, M.; Krebs, F. C., Improving, characterizing and predicting the lifetime of organic photovoltaics. *J. Phys. D: Appl. Phys.* **2017,** *50* (10), 103001/1-103001/35.

223. Zhang, Y.; Yi, H.; Iraqi, A.; Kingsley, J.; Buckley, A.; Wang, T.; Lidzey, D. G., Comparative indoor and outdoor stability measurements of polymer based solar cells. *Scientific Reports* **2017,** *7* (1), 1305.

224. Unay, H.; dos Reis Benatto, G. A.; Beliatis, M. J.; Gevorgyan, S. A.; Kavak, P.; Memiş, S.; Cirpan, A.; Toppare, L.; Parlak, E. A.; Krebs, F. C., High stability of benzotriazole and

benzodithiophene containing medium band-gap polymer solar cell. *Solar Energy Materials and Solar Cells* **2018,** *174*, 433-444.

225. Kettle, J.; Stoichkov, V.; Kumar, D.; Corazza, M.; Gevorgyan, S. A.; Krebs, F. C., Using ISOS consensus test protocols for development of quantitative life test models in ageing of organic solar cells. *Solar Energy Materials and Solar Cells* **2017,** *167*, 53-59.

226. Garner, R. K.; Josey, D. S.; Nyikos, S. R.; Dovijarski, A.; Wang, J. M.; Evans, G. J.; Bender, T. P., Boron subphthalocyanines as electron donors in outdoor lifetime monitored organic photovoltaic cells. *Solar Energy Materials and Solar Cells* **2018,** *176*, 331-335.

227. Bristow, N.; Kettle, J., Outdoor organic photovoltaic module characteristics: Benchmarking against other PV technologies for performance, calculation of Ross coefficient and outdoor stability monitoring. *Solar Energy Materials and Solar Cells* **2018,** *175*, 52-59.

228. Zhang, S.; Ye, L.; Hou, J., Breaking the 10% Efficiency Barrier in Organic Photovoltaics: Morphology and Device Optimization of Well-Known PBDTTT Polymers. *Advanced Energy Materials* **2016,** *6* (11), 1502529.

229. Owens, C.; Ferguson, M. G.; Hermenau, M.; Voroshazi, E.; Galagan, Y.; Zimmermann, B.; Rösch, R.; Angmo, D.; Teran-Escobar, G.; Uhrich, C.; Andriessen, R.; Hoppe, H.; Würfel, U.; Lira-Cantu, M.; Krebs, C. F.; Tanenbaum, M. D., Comparative Indoor and Outdoor Degradation of Organic Photovoltaic Cells via Inter-laboratory Collaboration. *Polymers* **2016,** *8* (1).

230. Angmo, D.; Krebs, F. C., Over 2 Years of Outdoor Operational and Storage Stability of ITO-Free, Fully Roll-to-Roll Fabricated Polymer Solar Cell Modules. *Energy Technology* **2015,** *3* (7), 774-783.

231. Bristow, N.; Kettle, J., Outdoor performance of organic photovoltaics: Diurnal analysis, dependence on temperature, irradiance, and degradation. *Journal of Renewable and Sustainable Energy* **2015,** *7* (1), 013111.

232. Madsen, M. V.; Gevorgyan, S. A.; Pacios, R.; Ajuria, J.; Etxebarria, I.; Kettle, J.; Bristow, N. D.; Neophytou, M.; Choulis, S. A.; Stolz Roman, L.; Yohannes, T.; Cester, A.; Cheng, P.; Zhan, X.; Wu, J.; Xie, Z.; Tu, W.-C.; He, J.-H.; Fell, C. J.; Anderson, K.; Hermenau, M.; Bartesaghi, D.; Jan Anton Koster, L.; Machui, F.; González-Valls, I.; Lira-Cantu, M.; Khlyabich, P. P.; Thompson, B. C.; Gupta, R.; Shanmugam, K.; Kulkarni, G. U.; Galagan, Y.; Urbina, A.; Abad, J.; Roesch, R.; Hoppe, H.; Morvillo, P.; Bobeico, E.; Panaitescu, E.; Menon, L.; Luo, Q.; Wu, Z.; Ma, C.; Hambarian, A.; Melikyan, V.; Hambsch, M.; Burn, P. L.; Meredith, P.; Rath, T.; Dunst, S.; Trimmel, G.; Bardizza, G.; Müllejans, H.; Goryachev, A. E.; Misra, R. K.; Katz, E. A.; Takagi, K.; Magaino, S.; Saito, H.; Aoki, D.; Sommeling, P. M.; Kroon, J. M.; Vangerven, T.; Manca, J.; Kesters, J.; Maes, W.; Bobkova, O. D.; Trukhanov, V. A.; Paraschuk, D. Y.; Castro, F. A.; Blakesley, J.; Tuladhar, S. M.; Alexander Röhr, J.; Nelson, J.; Xia, J.; Parlak, E. A.; Tumay, T. A.; Egelhaaf, H.-J.; Tanenbaum, D. M.; Mae Ferguson, G.; Carpenter, R.; Chen, H.; Zimmermann, B.; Hirsch, L.; Wantz, G.; Sun, Z.; Singh, P.; Bapat, C.; Offermans, T.;

Krebs, F. C., Worldwide outdoor round robin study of organic photovoltaic devices and modules. *Solar Energy Materials and Solar Cells* **2014,** *130*, 281-290.

233. Gevorgyan, S. A.; Madsen, M. V.; Dam, H. F.; Jørgensen, M.; Fell, C. J.; Anderson, K. F.; Duck, B. C.; Mescheloff, A.; Katz, E. A.; Elschner, A.; Roesch, R.; Hoppe, H.; Hermenau, M.; Riede, M.; Krebs, F. C., Interlaboratory outdoor stability studies of flexible roll-to-roll coated organic photovoltaic modules: Stability over 10,000h. *Solar Energy Materials and Solar Cells* **2013,** *116*, 187-196.

234. Pereira, M. S.; Lima, F. A. S.; Ribeiro, T. S.; da Silva, M. R.; Almeida, R. Q.; Barros, E. B.; Vasconcelos, I. F., Application of Fe-doped SnO2 nanoparticles in organic solar cells with enhanced stability. *Optical Materials* **2017,** *64*, 548-556.

235. Chander, N.; Singh, S.; Iyer, S. S. K., Stability and reliability of P3HT:PC61BM inverted organic solar cells. *Solar Energy Materials and Solar Cells* **2017,** *161*, 407-415.

236. Emmott, C. J. M.; Moia, D.; Sandwell, P.; Ekins-Daukes, N.; Hösel, M.; Lukoschek, L.; Amarasinghe, C.; Krebs, F. C.; Nelson, J., In-situ, long-term operational stability of organic photovoltaics for off-grid applications in Africa. *Solar Energy Materials and Solar Cells* **2016,** *149*, 284-293.

237. Kettle, J.; Bristow, N.; Gethin, D. T.; Tehrani, Z.; Moudam, O.; Li, B.; Katz, E. A.; dos Reis Benatto, G. A.; Krebs, F. C., Printable luminescent down shifter for enhancing efficiency and stability of organic photovoltaics. *Solar Energy Materials and Solar Cells* **2016,** *144*, 481-487.

238. Roth, B.; dos Reis Benatto, G. A.; Corazza, M.; Søndergaard, R. R.; Gevorgyan, S. A.; Jørgensen, M.; Krebs, F. C., The Critical Choice of PEDOT:PSS Additives for Long Term Stability of Roll-to-Roll Processed OPVs. *Advanced Energy Materials* **2015,** *5* (9), 1401912.

239. Terán-Escobar, G.; Pampel, J.; Caicedo, J. M.; Lira-Cantú, M., Low-temperature, solution-processed, layered V2O5 hydrate as the hole-transport layer for stable organic solar cells. *Energy & Environmental Science* **2013,** *6* (10), 3088-3098.

240. Angmo, D.; Gevorgyan, S. A.; Larsen-Olsen, T. T.; Søndergaard, R. R.; Hösel, M.; Jørgensen, M.; Gupta, R.; Kulkarni, G. U.; Krebs, F. C., Scalability and stability of very thin, roll-to-roll processed, large area, indium-tin-oxide free polymer solar cell modules. *Organic Electronics* **2013,** *14* (3), 984-994.

241. Carlé, J. E.; Andreasen, B.; Tromholt, T.; Madsen, M. V.; Norrman, K.; Jørgensen, M.; Krebs, F. C., Comparative studies of photochemical cross-linking methods for stabilizing the bulk hetero-junction morphology in polymer solar cells. *Journal of Materials Chemistry* **2012,** *22* (46), 24417-24423.

242. Chellappan, V.; Ng, G. M.; Tan, M. J.; Goh, W.-P.; Zhu, F., Imbalanced charge mobility in oxygen treated polythiophene/fullerene based bulk heterojunction solar cells. *Applied Physics Letters* **2009,** *95* (26), 263305.

243. Wang, X.; Xinxin Zhao, C.; Xu, G.; Chen, Z.-K.; Zhu, F., Degradation mechanisms in organic solar cells: Localized moisture encroachment and cathode reaction. *Solar Energy Materials and Solar Cells* **2012,** *104*, 1-6.

244. Claessens, C. G.; González-Rodríguez, D.; Torres, T., Subphthalocyanines: Singular Nonplanar Aromatic CompoundsSynthesis, Reactivity, and Physical Properties. *Chemical Reviews* **2002,** *102* (3), 835-854.

245. González-Rodríguez, D.; Torres, T.; Guldi, D. M.; Rivera, J.; Herranz, M. Á.; Echegoyen, L., Subphthalocyanines: Tuneable Molecular Scaffolds for Intramolecular Electron and Energy Transfer Processes. *Journal of the American Chemical Society* **2004,** *126* (20), 6301-6313.

246. Claessens, Christian G.; González-Rodríguez, D.; del Rey, B.; Torres, T.; Mark, G.; Schuchmann, H.-P.; von Sonntag, C.; MacDonald, J. G.; Nohr, Ronald S., Highly Efficient Synthesis of Chloro- and Phenoxy-Substituted Subphthalocyanines. *European Journal of Organic Chemistry* **2003,** *2003* (14), 2547-2551.

247. Díaz, D. D.; Bolink, H. J.; Cappelli, L.; Claessens, C. G.; Coronado, E.; Torres, T., Subphthalocyanines as narrow band red-light emitting materials. *Tetrahedron Letters* **2007,** *48* (27), 4657-4660.

248. Rodríguez-Morgade, M. S.; Claessens, C. G.; Medina, A.; González-Rodríguez, D.; Gutiérrez-Puebla, E.; Monge, A.; Alkorta, I.; Elguero, J.; Torres, T., Synthesis, Characterization, Molecular Structure and Theoretical Studies of Axially Fluoro-Substituted Subazaporphyrins. *Chemistry – A European Journal* **2008,** *14* (4), 1342-1350.

249. Morse, G. E.; Paton, A. S.; Lough, A.; Bender, T. P., Chloro boron subphthalocyanine and its derivatives: dyes, pigments or somewhere in between? *Dalton Transactions* **2010,** *39* (16), 3915-3922.

250. Seeland, M.; Rösch, R.; Hoppe, H., Luminescence imaging of polymer solar cells: Visualization of progressing degradation. *Journal of Applied Physics* **2011,** *109* (6), 064513.

251. Klumbies, H.; Karl, M.; Hermenau, M.; Rösch, R.; Seeland, M.; Hoppe, H.; Müller-Meskamp, L.; Leo, K., Water ingress into and climate dependent lifetime of organic photovoltaic cells investigated by calcium corrosion tests. *Solar Energy Materials and Solar Cells* **2014,** *120*, 685-690.

252. Rösch, R.; Tanenbaum, D. M.; Jørgensen, M.; Seeland, M.; Bärenklau, M.; Hermenau, M.; Voroshazi, E.; Lloyd, M. T.; Galagan, Y.; Zimmermann, B.; Würfel, U.; Hösel, M.; Dam, H. F.; Gevorgyan, S. A.; Kudret, S.; Maes, W.; Lutsen, L.; Vanderzande, D.; Andriessen, R.; Teran-Escobar, G.; Lira-Cantu, M.; Rivaton, A.; Uzunoğlu, G. Y.; Germack, D.; Andreasen, B.; Madsen, M. V.; Norrman, K.; Hoppe, H.; Krebs, F. C., Investigation of the degradation mechanisms of a variety of organic photovoltaic devices by combination of imaging techniques—the ISOS-3 inter-laboratory collaboration. *Energy & Environmental Science* **2012,** *5* (4), 6521-6540.

253. Tanenbaum, D. M.; Hermenau, M.; Voroshazi, E.; Lloyd, M. T.; Galagan, Y.; Zimmermann, B.; Hösel, M.; Dam, H. F.; Jørgensen, M.; Gevorgyan, S.; Kudret, S.; Maes, W.; Lutsen, L.; Vanderzande, D.; Würfel, U.; Andriessen, R.; Rösch, R.; Hoppe, H.; Lira-Cantu, M.; Teran-Escobar, G.; Dupuis, A.; Bussière, P.-O.; Rivaton, A.; Uzunoglu, G. Y.; Germack, D.; Andreasen, B.; Madsen, M. V.; Norrman, K.; Bundgaard, E.; Krebs, F. C., *Stability and degradation of organic photovoltaics fabricated, aged, and characterized by the ISOS 3 inter-laboratory collaboration*. SPIE: 2012; Vol. 8477, p 9.

254. Seeland, M.; Rösch, R.; Hoppe, H., Quantitative analysis of electroluminescence images from polymer solar cells. *Journal of Applied Physics* **2012,** *111* (2), 024505.

255. Hoyer, U.; Pinna, L.; Swonke, T.; Auer, R.; Brabec, C. J.; Stubhan, T.; Li, N., Comparison of Electroluminescence Intensity and Photocurrent of Polymer Based Solar Cells. *Advanced Energy Materials* **2011,** *1* (6), 1097-1100.

256. Seeland, M.; Rösch, R.; Muhsin, B.; Gobsch, G.; Hoppe, H., Electroluminescence as Characterization Tool for Polymer Solar Cells and Modules. *Energy Procedia* **2012,** *31*, 167-172.

257. Helander, M. G.; Morse, G. E.; Qiu, J.; Castrucci, J. S.; Bender, T. P.; Lu, Z.-H., Pentafluorophenoxy Boron Subphthalocyanine As a Fluorescent Dopant Emitter in Organic Light Emitting Diodes. *ACS Applied Materials & Interfaces* **2010,** *2* (11), 3147-3152.

258. Gommans, H.; Schols, S.; Kadashchuk, A.; Heremans, P.; Meskers, S. C. J., Exciton Diffusion Length and Lifetime in Subphthalocyanine Films. *The Journal of Physical Chemistry C* **2009,** *113* (7), 2974-2979.

259. Morse, G. E.; Helander, M. G.; Maka, J. F.; Lu, Z.-H.; Bender, T. P., Fluorinated Phenoxy Boron Subphthalocyanines in Organic Light-Emitting Diodes. *ACS Applied Materials & Interfaces* **2010,** *2* (7), 1934-1944.

260. Plint, T. G.; Lessard, B. H.; Bender, T. P., Doping chloro boron subnaphthalocyanines and chloro boron subphthalocyanine in simple OLED architectures yields warm white incandescent-like emissions. *Optical Materials* **2018,** *75*, 710-718.

261. Yamasaki, Y.; Mori, T., μ-Oxo-Bridged Subphthalocyanine Dimers: Preparation and Characterization by X-ray Structure Analysis. *Bulletin of the Chemical Society of Japan* **2011,** *84* (11), 1208-1214.

262. Guilleme, J.; González-Rodríguez, D.; Torres, T., Triflate-Subphthalocyanines: Versatile, Reactive Intermediates for Axial Functionalization at the Boron Atom. *Angewandte Chemie International Edition* **2011,** *50* (15), 3506-3509.

263. de Jong, M. P.; van Ijzendoorn, L. J.; de Voigt, M. J. A., Stability of the interface between indium-tin-oxide and poly(3,4-ethylenedioxythiophene)/poly(styrenesulfonate) in polymer light-emitting diodes. *Applied Physics Letters* **2000,** *77* (14), 2255-2257.

264. Wang, Y.; Wu, B.; Wu, Z.; Lan, Z.; Li, Y.; Zhang, M.; Zhu, F., Origin of Efficient Inverted Nonfullerene Organic Solar Cells: Enhancement of Charge Extraction and Suppression of

Bimolecular Recombination Enabled by Augmented Internal Electric Field. *The Journal of Physical Chemistry Letters* **2017,** *8* (21), 5264-5271.

265. Jia, Z.; Lee, V. W.; Hsu, Y.-J.; Kymissis, I., Laboratory pentacene and parylene evaporation systems for fabricating organic thin film devices. *Journal of Vacuum Science & Technology B* **2011,** *29* (2), 022401.

266. Morse, G. E.; Bender, T. P., Aluminum Chloride Activation of Chloro-Boronsubphthalocyanine: a Rapid and Flexible Method for Axial Functionalization with an Expanded Set of Nucleophiles. *Inorganic Chemistry* **2012,** *51* (12), 6460-6467.

267. Nonell, S.; Rubio, N.; del Rey, B.; Torres, T., Synthesis, optical absorption and photophysical properties of cone-shaped subnaphthalocyanine*Journal of the Chemical Society, Perkin Transactions 2* **2000,** (6), 1091-1094.

Appendix A
Experimental Details

A.1 Materials

The following materials were synthesized and purified at least once by train sublimation[134] before use, according to the cited synthesis methods:

- Cl-BsubPc[137]
- Cl-Cl_6BsubPc[54]
- Cl-Cl_{12}BsubPc[266]
- literature-Cl-Cl_nBsubNc[267]
- *p*-cymene-Cl-Cl_nBsubNc[67]
- nitrobenzene-Cl-Cl_nBsubNc[67]
- Ph-BsubPc[138]
- FPh-BsubPc[138]
- MePh-BsubPc[138]
- PhO-BsubPc[139]
- 246F_3PhO-BsubPc[139]
- 35F_2PhO-BsubPc[139]
- F_5-BsubPc[139]
- PhO-Cl_nBsubNc[140]
- F_5-Cl_nBsubNc[140]
- *m*-ClPhO-BsubPc[94]
- *m*-BrPhO-BsubPc[94]
- *m*-IPhO-BsubPc[94]

The following materials were purchased and purified once by train sublimation before use:

- alpha-sexithiophene (α-6T, Sigma-Aldrich)
- C_{60} fullerene (SES Research, 99.5%)

Ag (R.D. Mathis), α-6T (Sigma-Aldrich), and BCP (Sigma-Aldrich) were used in **Section 2.1**, **2.2**, **3.1**, **3.2**, **3.3**, and **4.2**. Ag (Angstrom), α-6T (Lumtec), and BCP (Lumtec) were used in **Section 2.3**, **3.4**, **4.2**, and **4.3**.

The following materials were purchased and used as received:

- poly(3,4-ethylenedioxythiophene)-poly(styrenesulfonate) (PEDOT:PSS, Heraeus: Clevios™ P VP AI 4083)
- regioregular poly(3-hexylthiophene-2,5-diyl) (P3HT, Rieke Metals: RMI-001EE MW: 69K)
- alpha-sexithiophene (α-6T, Lumtec: LT-S969, >99%)
- tetracene (Tc, Lumtec: LT-S940, >99%)
- chloro-(chloro)$_n$ boron subnaphthalocyanine (Cl-Cl$_n$BsubNc, Lumtec: LT-S947, >99%)
- bathocuproine (BCP, Sigma-Aldrich, 99.6%)
- bathocuproine (BCP, Lumtec: LT-E304, >99%)
- silver (Ag, R.D. Mathis, 99.999%)
- silver (Ag, Angstrom, 99.99%)
- molybdenum oxide (MoO_X, Lumtec: LT-E003, >99.998%)
- epoxy (Ossila: Encapsulation Epoxy for Photovoltaics and OLEDs)
- silver paint (Ted Pella, Inc: PELCO® Conductive Silver Paint)
- all solvents (Sigma-Aldrich)

A.2 Substrates and Cleaning

OPV devices were fabricated on 25 mm by 25 mm glass substrates coated with pre-patterned, indium-tin oxide (ITO) having a sheet resistance of 15 Ω per square (Thin Film Devices, Inc.). Four different ITO patterns were used throughout this thesis: original OPV pattern, multi-size OPV pattern, standard OPV pattern, and large-area pattern, all illustrated in **Figure A.1**. The original OPV pattern was used in **Section 2.1**, **2.2**, **3.1**, **3.2**, **3.3**. The multi-size OPV pattern was only used in **Section 4.2**. The standard OPV pattern was used in **Section 2.3**, **3.4**, **4.2**, **4.3**, and **5.2.1**. The large-area pattern was only used to collect preliminary data in **Section 5.2.3** of Future Work.

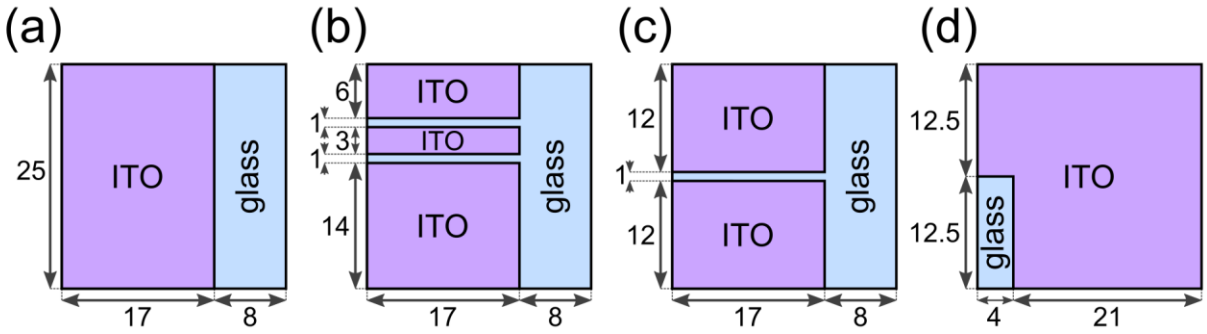

Figure A.1. ITO-coated glass substrates with (a) original OPV pattern, (b) multi-size OPV pattern, (c) standard OPV pattern, and (d) large-area pattern. All dimensions are in millimetres.

Device substrates were cleaned with an Alconox solution, then placed in a Wash-N-Dry coverslip rack (Sigma-Aldrich) for successive sonication processes in the Alconox solution, DI water, acetone, and methanol (5 min each). The substrates were then dried under a stream of nitrogen gas and treated with atmospheric plasma for 5 min.

Glass slides for vacuum-deposited tooling (calibration) films were cut to 25 mm by ~ 55 mm by scoring 25 mm by 75 mm glass slides with a diamond tip pen. The tooling slides were cleaned by wiping with a methanol soaked Kimwipe and dried under a stream of nitrogen gas.

A.3 Solution Deposition

PEDOT:PSS was spin-coated onto the substrates at 500 rpm for 10 s, followed by 4000 rpm for 30 s. Substrates were baked on a hot plate at 110°C for at least 10 min, and then transferred into a nitrogen atmosphere glove box (O_2 < 10 ppm, H_2O < 10 ppm). After spin-coating PEDOT:PSS, the substrates were removed from atmospheric conditions for the remainder of fabrication and characterization by transferring to a nitrogen atmosphere glove box attached to a custom vacuum deposition chamber. The PEDOT:PSS layers were further dried overnight at room temperature in a nitrogen atmosphere.

P3HT films were spin-coated using a modified procedure from Lee *et al.*[27] Using a 15 mg/mL solution in dichlorobenzene (DCB), P3HT was spin-coated onto the substrates at 1000 rpm for 18

s followed by 2000 rpm for 40 s. P3HT film thicknesses were measured using a KLA-Tencor P16+ surface profilometer.

A.4 Vacuum Deposition

All small molecules were thermally evaporated at ~1.0 A/s, a 30 cm throw distance, and a working pressure of ~1 x 10^{-7} Torr. MoO_X and Ag were thermally evaporated at ~1.0 A/s, a 30 cm throw distance, and a working pressure of ~1 x 10^{-7} Torr for MoO_X and ~1 x 10^{-6} Torr for Ag. MoOx and organics were evaporated through a large, rectangular shadow mask, defining an area that covers most of the substrate. Silver electrodes were evaporated to a thickness of 80 nm through a shadow mask, defining 0.2 cm^2 or 0.4 cm^2 as the active area for each device. A transfer back to the glove box was required between the organic and Ag layers to change the shadow masks.

The layer thicknesses and deposition rates of evaporated films were monitored using a quartz crystal microbalance calibrated against films deposited on glass and measured with a KLA-Tencor P16+ surface profilometer. To enhance the electrical contact for testing, silver paint or evaporated silver was applied to the ITO and metal electrode contact points. Silver paint was left to dry for 20 min before testing.

A.5 J–V and EQE Characterization

In **Chapter 2** and **Chapter 3**, all devices remained in a nitrogen-filled glove box throughout testing. Voltage sweeps of OPVs were performed under the illumination of a 300 W Xe arc lamp (Newport: 6258) in a research arc lamp housing (Newport: 67005) with an AM 1.5G filter, through an in-line monochromator (Newport: Cornerstone 260 1/4 m). The corresponding OPV currents were measured with a low voltage sourcemeter (Keithley 2401). In **Section 2.1**, **2.2**, **3.1**, **3.2**, and **3.3**, light intensity was calibrated to one sun with reference to a silicon photodetector (Newport: 71675_71580). In **Section 2.3** and **3.4**, light intensity was calibrated to one sun using a certified silicon photodetector (Newport: 818-SL/DB) with a KG5 filter (Newport: FSR-KG5).

In **Chapter 4**, all devices were encapsulated and removed from the glove box after fabrication. Voltage sweeps of OPVs were performed under full illumination by a 100 W Xe lamp in a small

area solar simulator (Newport: LCS-100) with an AM 1.5G filter. The corresponding OPV currents were measured with a low voltage sourcemeter (Keithley: 2401). Light intensity was calibrated to one sun with reference to a calibrated reference cell and meter (Newport: 91150V). Currents were converted to current densities by dividing by the OPV active area, defined by the overlap between the ITO and Ag electrodes. OPV active areas were 0.2 cm^2 in **Section 2.1**, **2.2**, **3.1**, **3.2**, **3.3**, and **4.2**, and 0.4 cm^2 in **Section 2.3**, **3.4**, **4.2**, and **4.3**.

All wavelengths scans were performed at 10 nm intervals using an in-line Cornerstone 260 1/4 m Monochromator, and the corresponding currents were measured using a Newport Optical Power Meter 2936-R. External quantum efficiencies were calculated using the measured currents and a reference wavelength scan of a calibrated silicon photodetector.

A.6 Stability Testing

All OPVs undergoing stability testing were first encapsulated with epoxy. For encapsulation, a 100 nm layer of MoOx was thermally evaporated over the devices to serve as a physical barrier between the organic / metal layers and the epoxy. Next, a drop of epoxy was applied to a glass coverslip, which was then placed onto the substrate and cured under a lamp for 20 min. Silver paint was applied to the contact points to enhance electrical contact.

The protocols for outdoor stability testing were based on the consensus protocols from the international summit on OPV stability (ISOS) for advanced outdoor testing (ISOS-O3). On days without precipitation, the OPVs were taken outside and placed in direct sunlight from ~3-4 hours before solar noon until ~3-4 hours after solar noon. Devices were mounted on a static, custom-built apparatus (**Figure A.2**) on a rooftop in Toronto, Canada (latitude = 43.7°, longitude = -79.4°) with the front side oriented towards the equator, tilted at ~43.7°. While outdoors, resistors were used to passively load some devices with resistances corresponding to the MPP calculated from the initial voltage sweeps at T_0. The voltage output from each passively-loaded device was continuously monitored at 2 Hz while outdoors using a voltage input module (NI: 9205) connected to a CompactDAQ Chassis (NI: cDAQ-9171).

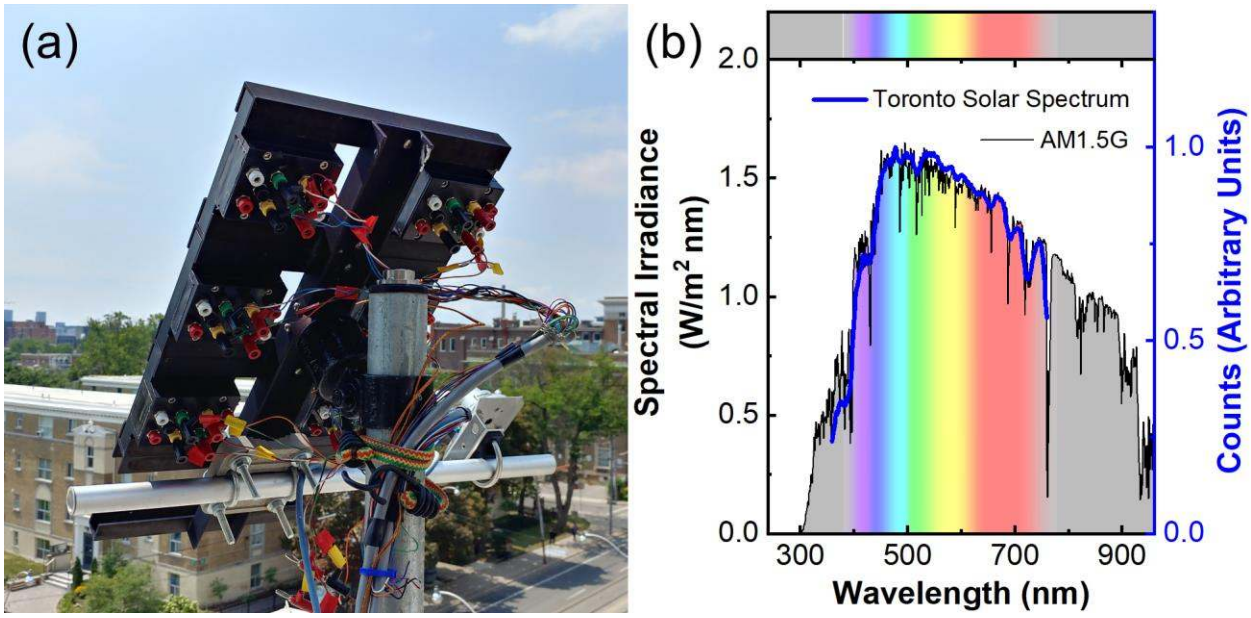

Figure A.2. (a) Custom outdoor testing apparatus for mounting OPVs, tilted at ~43.7° with the front side oriented towards the equator, located at latitude = 43.7°, longitude = -79.4°. (b) AM1.5G spectrum compared to a Toronto outdoor solar spectrum as measured next to the outdoor testing apparatus using a handheld spectrophotometer (MK350 LED Meter, UPRtek). Spectrum measurement was made on a cloudless day (July 23rd, 2019) ~10:45am while the solar irradiance was ~711 W/m^2. This irradiance was measured using a pyranometer attached to the outdoor testing apparatus, tilted at 43.7°.

Substrate temperatures were measured on the backside of a representative device and continuously monitored at 1 Hz while outdoors. Irradiance was monitored with an in-plane pyranometer (Hukseflux: LP02). Air temperature, relative humidity, wind speed, and wind direction were monitored within ~6 m of the testing apparatus (**Figure E.1**, **Figure D.7**, **Figure C.1**).

Aside from the exceptions listed below, all protocols followed for these studies conform to the ISOS-O3 advanced level of outdoor testing. For all outdoor studies, the location of the wind speed monitoring (optional for ISOS-O1 and ISOS-O2) was not quite within the recommended proximity to the testing apparatus for ISOS-O3 (~6 m instead of 1.2 m) but is still reported. In **Section 4.2**, the MPP loading for the PhO-BsubPc and Ph-BsubPc devices only meets the requirements of the basic level of testing (ISOS-O1) as the resistance at MPP deviated by more than 10% and the

resistors were not adjusted. EQE monitoring of PhO-BsubPc and Ph-BsubPc only meets the intermediate level (ISOS-O2) as their EQEs were only measured at T_0 and T_{50}, not T_{80}.

A.7 Design of Substrate Holders, Modules

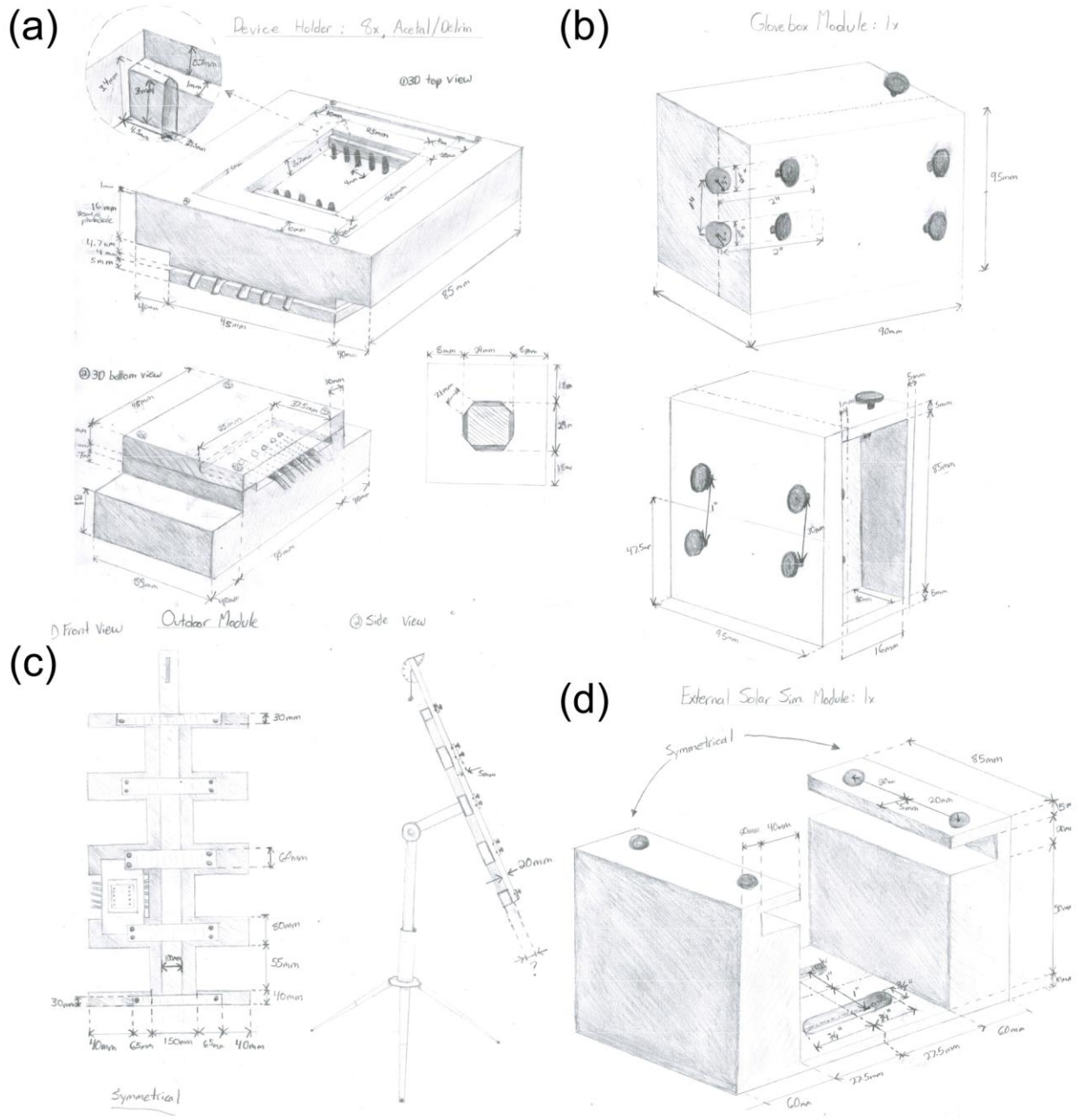

Figure A.3. Original sketches of (a) substrate holder and mounting modules for (b) glove box, (c) outdoor, and (d) indoor testing.

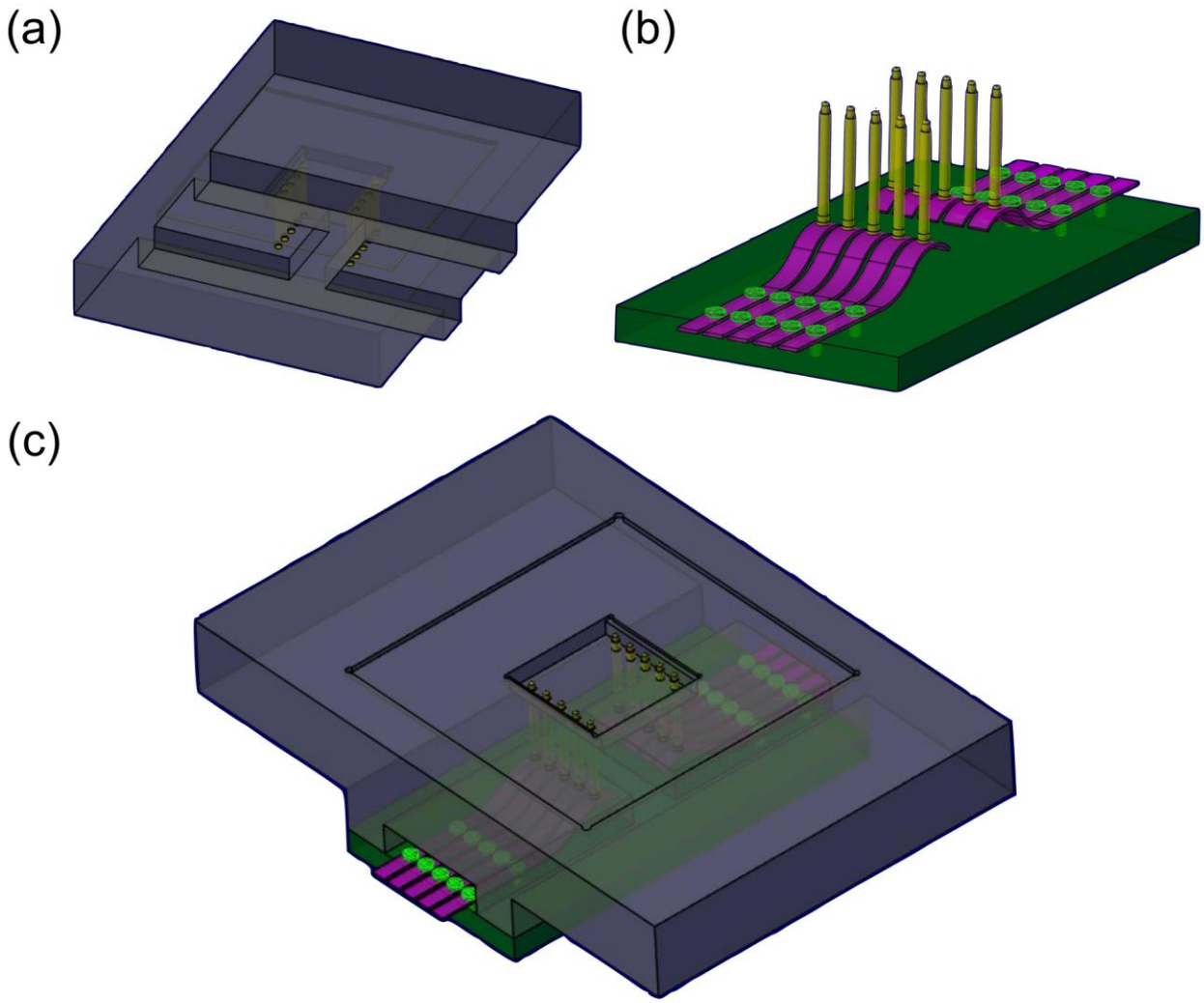

Figure A.4. (a) CAD render of the top of the substrate holder (grey, view from bottom), showing the bottom of the spring-loaded gold-coated pins (gold) that penetrate through the holder to contact the substrate. (b) CAD render of the bottom of the substrate holder (green, view from top), showing the metal contacts (magenta). (c) A combined CAD render of the top and bottom of the sample holder (top view).

The substrate rests on two ledges within the top, middle square (**Figure A.4c**). A metal mask with small metal clamps (not shown) apply a downward pressure to the corners of the substrate, compressing the spring-loaded gold-coated pins onto the electrode contact regions on the substrate. Friction keeps the pins from sliding into the holder, but pressure is also maintained on the back of

the pins as a result of the bend in the metal contacts (**Figure A.4b**). The pressure ensuring the pins remain in place and eliminates the need for soldering. The absence of soldering at this contact means the top and bottom of the sample holder can be easily separated by removing 4 screws (not shown), facilitating any repair or service. The metal contacts are wired to banana plugs on the bottom of the sample holder (not shown), enabling rapid connections and disconnections for electrical testing.

Appendix B
Supplemental Information for Section 2.3

Table B.1. An exhaustive list of every possible chlorinated phthalonitrile (available or theoretical) and the proposed abbreviation for the resulting BsubPc. The proposed abbreviations of BsubPc mixtures synthesized by mixing two phthalonitriles are also listed, where n = 0, 1, 2, and 3. *Appears in this thesis.

Abbreviation	Phthalonitrile #1	Phthalonitrile #2 (mixtures)
*Cl-BsubPc	phthalonitrile	
Cl-$^{3/6}$Cl$_3$BsubPc	3-chlorophthalonitrile	
Cl-$^{4/5}$Cl$_3$BsubPc	4-chlorophthalonitrile	
Cl-$^{(3,4)/(5,6)}$Cl$_6$BsubPc	3,4-dichlorophthalonitrile	
Cl-$^{(3,5)/(4,6)}$Cl$_6$BsubPc	3,5-dichlorophthalonitrile	
Cl-$^{\alpha}$Cl$_6$BsubPc	3,6-dichlorophthalonitrile	
*Cl-$^{\beta}$Cl$_6$BsubPc	4,5-dichlorophthalonitrile	
Cl-$^{\beta,3/6}$Cl$_9$BsubPc	3,4,5-trichlorophthalonitrile	
Cl-$^{\alpha,4/5}$Cl$_9$BsubPc	3,4,6-trichlorophthalonitrile	
*Cl-Cl$_{12}$BsubPc	3,4,5,6-tetrachlorophthalonitrile	
Cl-$^{3/6}$Cl$_n$BsubPc	phthalonitrile	3-chlorophthalonitrile
Cl-$^{4/5}$Cl$_n$BsubPc	phthalonitrile	4-chlorophthalonitrile
Cl-$^{(3,4)/(5,6)}$Cl$_{2n}$BsubPc	phthalonitrile	3,4-dichlorophthalonitrile
Cl-$^{(3,5)/(4,6)}$Cl$_{2n}$BsubPc	phthalonitrile	3,5-dichlorophthalonitrile
Cl-$^{\alpha}$Cl$_{2n}$BsubPc	phthalonitrile	3,6-dichlorophthalonitrile
*Cl-$^{\beta}$Cl$_{2n}$BsubPc	phthalonitrile	4,5-dichlorophthalonitrile
Cl-$^{\beta,3/6}$Cl$_{3n}$BsubPc	phthalonitrile	3,4,5-trichlorophthalonitrile
Cl-$^{\alpha,4/5}$Cl$_{3n}$BsubPc	phthalonitrile	3,4,6-trichlorophthalonitrile
*Cl-Cl$_{4n}$BsubPc	phthalonitrile	3,4,5,6-tetrachlorophthalonitrile
Cl-$^{3/6}$Cl$_n$$^{4/5}Cl_{3-n}$BsubPc	3-chlorophthalonitrile	4-chlorophthalonitrile
Cl-$^{3/6}$Cl$_n$$^{(3,4)/(5,6)}Cl_{6-2n}$BsubPc	3-chlorophthalonitrile	3,4-dichlorophthalonitrile
Cl-$^{3/6}$Cl$_n$$^{(3,5)/(4,6)}Cl_{6-2n}$BsubPc	3-chlorophthalonitrile	3,5-dichlorophthalonitrile
Cl-$^{3/6}$Cl$_n$$^{\alpha}Cl_{6-2n}$BsubPc	3-chlorophthalonitrile	3,6-dichlorophthalonitrile
Cl-$^{3/6}$Cl$_n$$^{\beta}Cl_{6-2n}$BsubPc	3-chlorophthalonitrile	4,5-dichlorophthalonitrile
Cl-$^{3/6}$Cl$_n$$^{\beta,3/6}Cl_{9-3n}$BsubPc	3-chlorophthalonitrile	3,4,5-trichlorophthalonitrile
Cl-$^{3/6}$Cl$_n$$^{\alpha,4/5}Cl_{9-3n}$BsubPc	3-chlorophthalonitrile	3,4,6-trichlorophthalonitrile
Cl-$^{3/6}$Cl$_n$Cl$_{12-4n}$BsubPc	3-chlorophthalonitrile	3,4,5,6-tetrachlorophthalonitrile
Cl-$^{4/5}$Cl$_n$$^{(3,4)/(5,6)}Cl_{6-2n}$BsubPc	4-chlorophthalonitrile	3,4-dichlorophthalonitrile
Cl-$^{4/5}$Cl$_n$$^{(3,5)/(4,6)}Cl_{6-2n}$BsubPc	4-chlorophthalonitrile	3,5-dichlorophthalonitrile
Cl-$^{4/5}$Cl$_n$$^{\alpha}Cl_{6-2n}$BsubPc	4-chlorophthalonitrile	3,6-dichlorophthalonitrile
Cl-$^{4/5}$Cl$_n$$^{\beta}Cl_{6-2n}$BsubPc	4-chlorophthalonitrile	4,5-dichlorophthalonitrile

Cl-$^{4/5}$Cl$_n$$^{\beta,3/6}Cl_{9-3n}$BsubPc	4-chlorophthalonitrile	3,4,5-trichlorophthalonitrile
Cl-$^{4/5}$Cl$_n$$^{\alpha,4/5}Cl_{9-3n}$BsubPc	4-chlorophthalonitrile	3,4,6-trichlorophthalonitrile
Cl-$^{4/5}$Cl$_n$Cl$_{12-4n}$BsubPc	4-chlorophthalonitrile	3,4,5,6-tetrachlorophthalonitrile
Cl-$^{(3,4)/(5,6)}$Cl$_{2n}$$^{(3,5)/(4,6)}Cl_{6-2n}$BsubPc	3,4-dichlorophthalonitrile	3,5-dichlorophthalonitrile
Cl-$^{(3,4)/(5,6)}$Cl$_{2n}$ $^{\alpha}$Cl$_{6-2n}$BsubPc	3,4-dichlorophthalonitrile	3,6-dichlorophthalonitrile
Cl-$^{(3,4)/(5,6)}$Cl$_{2n}$ $^{\beta}$Cl$_{6-2n}$BsubPc	3,4-dichlorophthalonitrile	4,5-dichlorophthalonitrile
Cl-$^{(3,4)/(5,6)}$Cl$_{2n}$$^{\beta,3/6}Cl_{9-3n}$BsubPc	3,4-dichlorophthalonitrile	3,4,5-trichlorophthalonitrile
Cl-$^{(3,4)/(5,6)}$Cl$_{2n}$$^{\alpha,4/5}Cl_{9-3n}$BsubPc	3,4-dichlorophthalonitrile	3,4,6-trichlorophthalonitrile
Cl-$^{(3,4)/(5,6)}$Cl$_{2n}$Cl$_{12-4n}$BsubPc	3,4-dichlorophthalonitrile	3,4,5,6-tetrachlorophthalonitrile
Cl-$^{(3,5)/(4,6)}$Cl$_{2n}$ $^{\alpha}$Cl$_{6-2n}$BsubPc	3,5-dichlorophthalonitrile	3,6-dichlorophthalonitrile
Cl-$^{(3,5)/(4,6)}$Cl$_{2n}$ $^{\beta}$Cl$_{6-2n}$BsubPc	3,5-dichlorophthalonitrile	4,5-dichlorophthalonitrile
Cl-$^{(3,5)/(4,6)}$Cl$_{2n}$$^{\beta,3/6}Cl_{9-3n}$BsubPc	3,5-dichlorophthalonitrile	3,4,5-trichlorophthalonitrile
Cl-$^{(3,5)/(4,6)}$Cl$_{2n}$$^{\alpha,4/5}Cl_{9-3n}$BsubPc	3,5-dichlorophthalonitrile	3,4,6-trichlorophthalonitrile
Cl-$^{(3,5)/(4,6)}$Cl$_{2n}$Cl$_{12-4n}$BsubPc	3,5-dichlorophthalonitrile	3,4,5,6-tetrachlorophthalonitrile
Cl-$^{\alpha}$Cl$_{2n}$$^{\beta}Cl_{6-2n}$BsubPc	3,6-dichlorophthalonitrile	4,5-dichlorophthalonitrile
Cl-$^{\alpha}$Cl$_{2n}$$^{\beta,3/6}Cl_{9-3n}$BsubPc	3,6-dichlorophthalonitrile	3,4,5-trichlorophthalonitrile
Cl-$^{\alpha}$Cl$_6$$^{4/5}Cl_n$BsubPc	3,6-dichlorophthalonitrile	3,4,6-trichlorophthalonitrile
Cl-$^{\alpha}$Cl$_6$$^{\beta}Cl_{2n}$BsubPc	3,6-dichlorophthalonitrile	3,4,5,6-tetrachlorophthalonitrile
Cl-$^{\beta}$Cl$_6$$^{3/6}Cl_n$BsubPc	4,5-dichlorophthalonitrile	3,4,5-trichlorophthalonitrile
Cl-$^{\beta}$Cl$_{2n}$$^{\alpha,4/5}Cl_{9-3n}$BsubPc	4,5-dichlorophthalonitrile	3,4,6-trichlorophthalonitrile
*Cl-$^{\beta}$Cl$_6$$^{\alpha}Cl_{2n}$BsubPc	4,5-dichlorophthalonitrile	3,4,5,6-tetrachlorophthalonitrile
Cl-$^{\beta,3/6}$Cl$_{3n}$$^{\alpha,4/5}Cl_{9-3n}$BsubPc	3,4,5-trichlorophthalonitrile	3,4,6-trichlorophthalonitrile
Cl-$^{\beta,3/6}$Cl$_{3n}$Cl$_{12-4n}$BsubPc	3,4,5-trichlorophthalonitrile	3,4,5,6-tetrachlorophthalonitrile
Cl-$^{\alpha,4/5}$Cl$_{3n}$Cl$_{12-4n}$BsubPc	3,4,6-trichlorophthalonitrile	3,4,5,6-tetrachlorophthalonitrile

Appendix C
Supplemental Information for Section 4.2

Table C.1. Days in 2015 that each set of OPVs was tested outdoors, typically for ~6 hours centred around solar noon.

Date	Set 1: Cl	Set 2: Cl	Set 1: PhO	Set 2: PhO	Set 1: Ph	Set 2: Ph
July 29th	✓	×	✓	×	✓	×
July 30th	✓	×	✓	×	✓	×
Aug 4th	✓	×	✓	×	✓	×
Aug 5th	✓	×	✓	×	✓	×
Aug 6th	✓	×	✓	×	×	✓
Aug 7th	✓	×	✓	×	×	✓
Aug 11th	✓	×	✓	×	×	✓
Aug 12th	✓	×	×	✓	×	✓
Aug 13th	✓	×	×	✓	×	×
Aug 17th	✓	×	×	✓	×	×
Aug 19th	✓	✓	×	✓	×	×
Aug 24th	✓	✓	×	✓	×	×
Aug 25th	✓	✓	×	✓	×	×
Aug 27th	✓	✓	×	✓	×	×
Aug 28th	✓	✓	×	×	×	×
Aug 31st	✓	✓	×	×	×	×
Sep 1st	✓	✓	×	×	×	×
Sep 2nd	✓	✓	×	×	×	×
Sep 4th	✓	✓	×	×	×	×
Sep 10th	×	✓	×	×	×	×
Sep 11th	×	✓	×	×	×	×
Sep 15th	×	✓	×	×	×	×
Sep 16th	×	✓	×	×	×	×
Sep 17th	×	✓	×	×	×	×
Sep 18th	×	✓	×	×	×	×

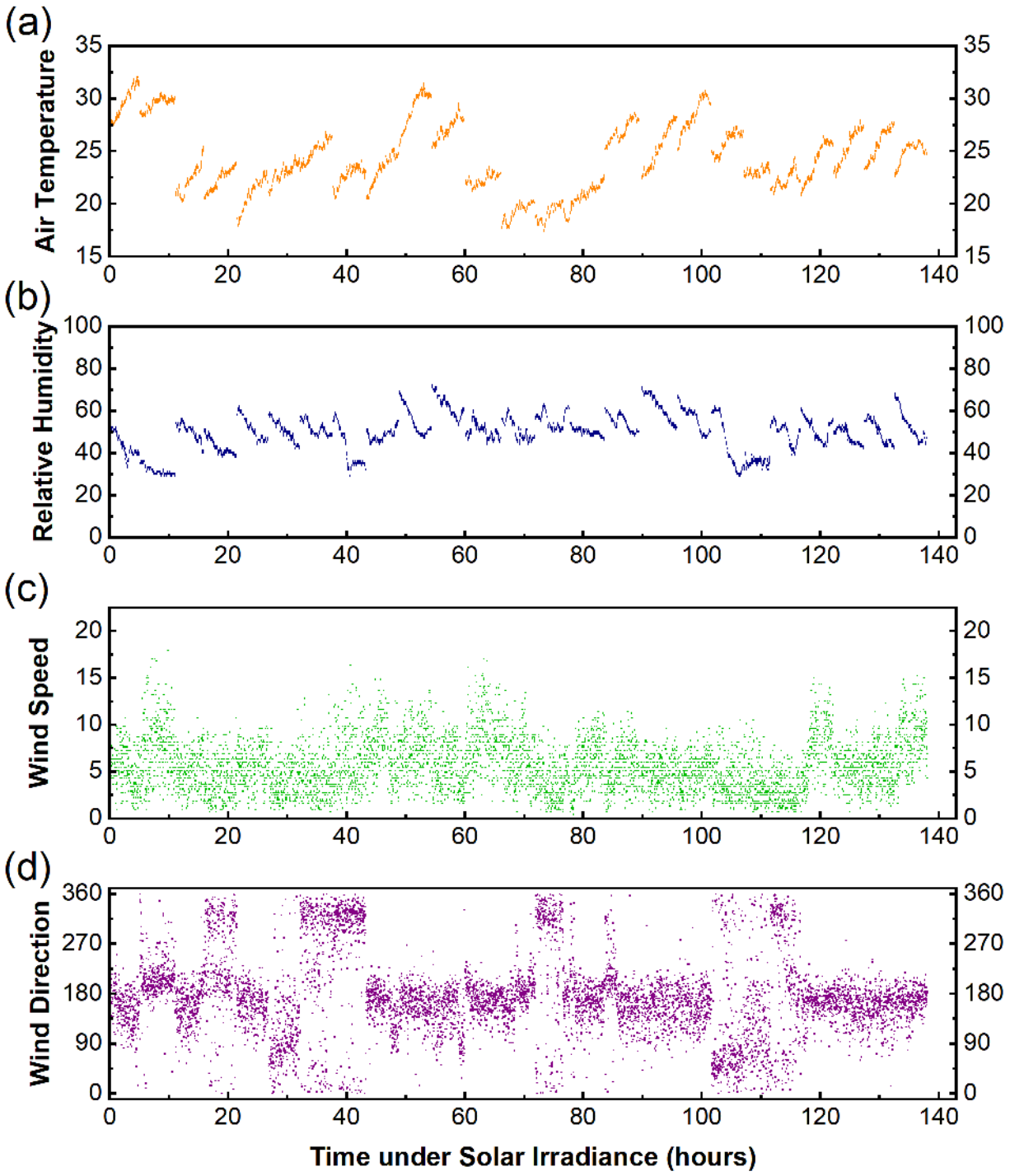

Figure C.1. (a) Air temperature (°C), (b) relative humidity (%), (c) wind speed (m/s), and (d) wind direction during 2015 outdoor testing. Wind direction is shown according to the following: 0° & 360° = from the north, 180° = from the south, 90° = from the east, and 270° = from the west.

Appendix D
Supplemental Information for Section 4.3

Table D.1. Days in 2016 that each set of OPVs was tested outdoors, typically for ~6 hours centred around solar noon.

Date	Nc/Pc	Nc	Pc
Sep 9th	✓	✓	✓
Sep 12th	✓	✓	✓
Sep 13th	✓	✓	✓
Sep 14th	✓	✓	✓
Sep 15th	✓	✓	✓
Sep 16th	✓	✓	✓
Sep 19th	✓	✓	✓
Sep 27th	✓	✓	✓
Sep 28th	✓	✓	✓
Oct 5th	✓	✓	✓
Oct 6th	✓	✓	✓
Oct 12th	✓	✓	✓
Oct 13th	✓	✓	✓
Oct 14th	✓	✓	✓
Oct 25th	✓	✓	✓
Oct 26th	✓	✓	✓
Oct 28th	✓	✓	✓

Equation D.1. Estimating generated power if active MPP tracking were employed

$$J_{outdoor}\left(V_{outdoor}(day,t)\right) = \frac{V_{outdoor}(day,t)}{R_{resistor} \times A}$$

$$J_{indoor-intrpl.}(V,day,t) = J_{indoor}(V,day) + \left(J_{indoor}(V,day+1) - J_{indoor}(V,day)\right) \times \left(\frac{Q(day,t)}{Q(day,t=end)}\right)$$

$$J_{outdoor-fit}(V,day,t) = J_{indoor-intrpl.}(V,day,t) \times \left(\frac{J_{outdoor}\left(V_{outdoor}(day,t)\right)}{J_{indoor-intrpl.}\left(V_{outdoor}(day,t),day,t\right)}\right)$$

$$P_{max-fit}(day,t) = V_{MPP} \times J_{outdoor-fit}(V_{MPP},day,t)$$

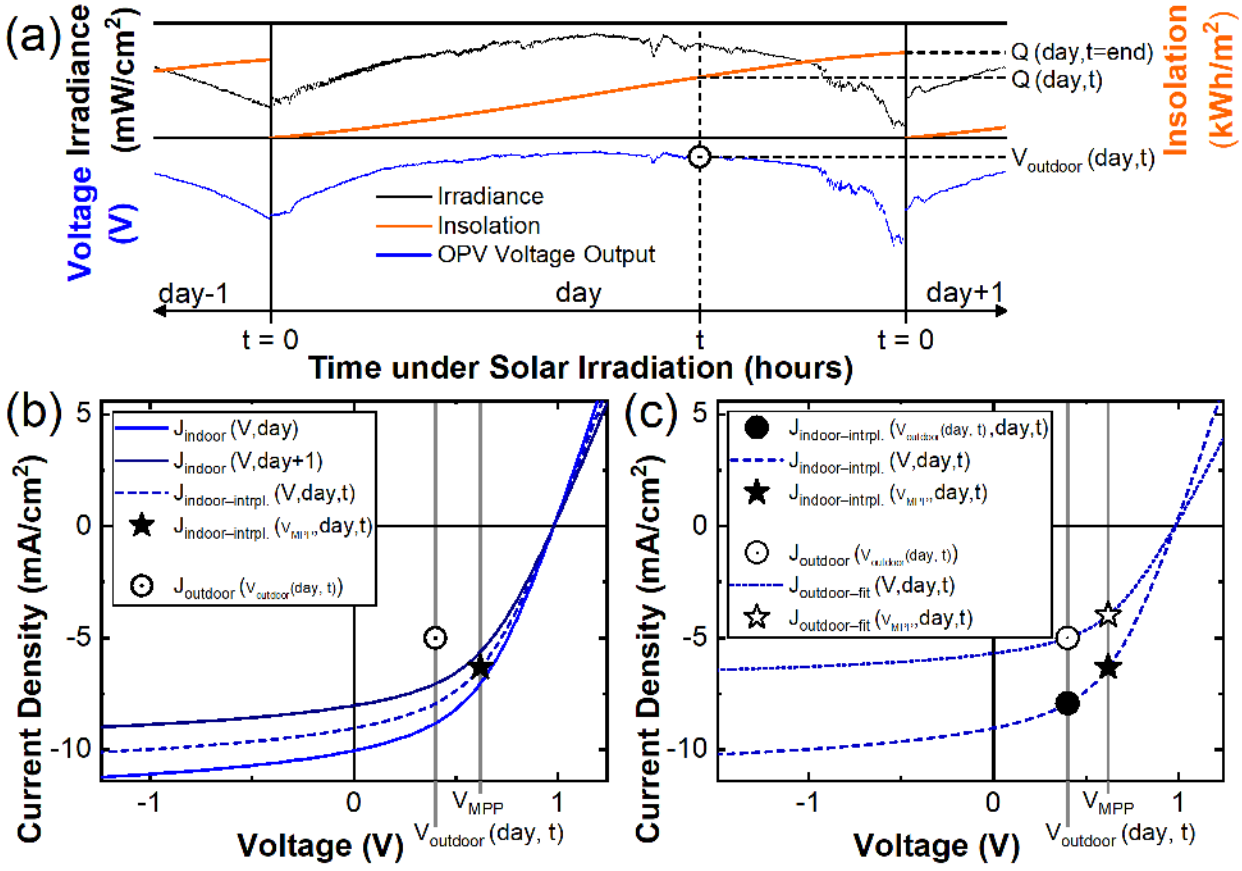

Figure D.1. Graphical illustration of the parameters in **Equation D.1**. (a) A sample day of the irradiance, insolation, and corresponding voltage outputs from an OPV. (b) Interpolating indoor JV measurements (using $\boldsymbol{Q(day,t)}$ and $\boldsymbol{Q(day,t=end)}$) to generate an AM1.5G JV curve for the OPV at each point (time = $\boldsymbol{t}$) during the day, accounting for degradation incurred since the morning, indoor measurement. (c) Fitting an interpolated JV curve to its corresponding outdoor measurement by adjusting only the current density (to account for fluctuating irradiation intensities). That fitted JV curve is used to find the estimated maximum power point (MPP).

Where V is voltage, R is resistance, A is the device active area (0.4 cm^2 for all OPVs), J is current-density, I is irradiance, Q is insolation (accumulated irradiance), Q_{daily} is the total insolation received by the device on a given day, and P is power. day and t represent the day and time of day, respectively, that the values were measured. Subscripts "outdoor" and "indoor" indicate whether the values were measured outdoors or indoors.

The voltage outputs of the OPVs were continuously measured across a resistor during outdoor testing. Current densities are calculated using Ohm's law and the device areas:

$$J_{outdoor}\big(V_{outdoor}(day,t)\big) = \frac{V_{outdoor}(day,t)}{R_{resistor} \times 0.4\ cm^2}$$

The JV curves from the morning of outdoor testing and the following morning are interpolated to each outdoor measurement based on the insolation received by the device to account for degradation incurred by the devices each day:

$$J_{indoor-intrpl.}(V,day,t) = J_{indoor}(V,day) + \big(J_{indoor}(V,day+1) - J_{indoor}(V,day)\big) \times \left(\frac{Q(day,t)}{Q(day,t=end)}\right)$$

$Q(day,t=end)$ represents the total insolation received by the device each day, which is also the total insolation received by the device between each indoor J–V measurement. $Q(day,t=end)$ is used with $Q(day,t)$ for interpolation. $J_{indoor-intrpl}(V,day,t)$ represents an estimation of the J–V curves that would be produced if a voltage sweep was performed under 1 sun of irradiation at each moment that an outdoor voltage measurement was made. Inputting the outdoor voltage measurements, $V_{outdoor}(day,t)$, into $J_{indoor-intrpl}(V,day,t)$ provides an estimation of the theoretical "1 sun" current-density at each outdoor voltage.

Assuming FF and V_{OC} remain approximately constant under the variable irradiance intensities of outdoor testing, the difference between the theoretical "1 sun" current-densities and the actual outdoor current-densities can be used to fit the interpolated J–V curves, $J_{indoor-intrpl}(V,day,t)$, to the outdoor measurements:

$$J_{outdoor-fit}(V,day,t) = J_{indoor-intrpl.}(V,day,t) \times \left(\frac{J_{outdoor}\big(V_{outdoor}(day,t)\big)}{J_{indoor-intrpl.}(V_{outdoor}(day,t),day,t)}\right)$$

$J_{outdoor-fit}(V, day, t)$ represents the theoretical JV curve of the OPV at each moment spent outdoors, accounting for the state of OPV degradation and as measured under the instantaneous irradiance and temperature conditions. The current-density at the maximum power point of this JV curve can be calculated by inserting V_{MPP} into $J_{outdoor-fit}(V, day, t)$, and multiplying those together provides the power that would have been generated if actively tracking the maximum power point of the OPV while outdoors:

$$P_{max-fit}(day, t) = V_{MPP} \times J_{outdoor-fit}(V_{MPP}, day, t)$$

Finally, $P_{max-fit}(day, t)$ represents the estimated power output from the OPV for each outdoor measurement if active maximum power point tracking were employed.

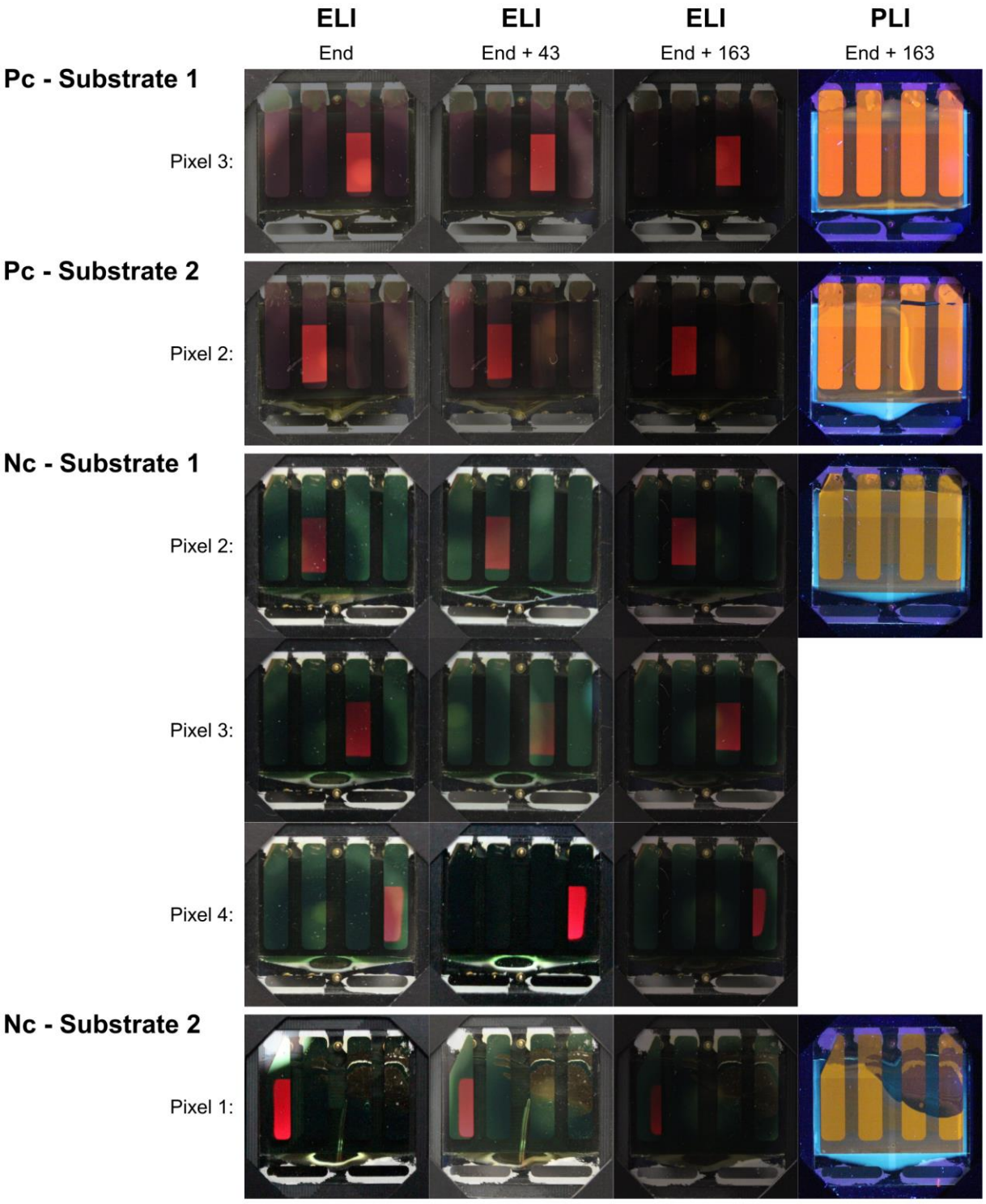

Figure D.2. Electroluminescence imaging (ELI) of Pc and Nc OPVs: immediately after and 43 days after outdoor testing. ELI, photoluminescence imaging (PLI) 163 days after outdoor testing.

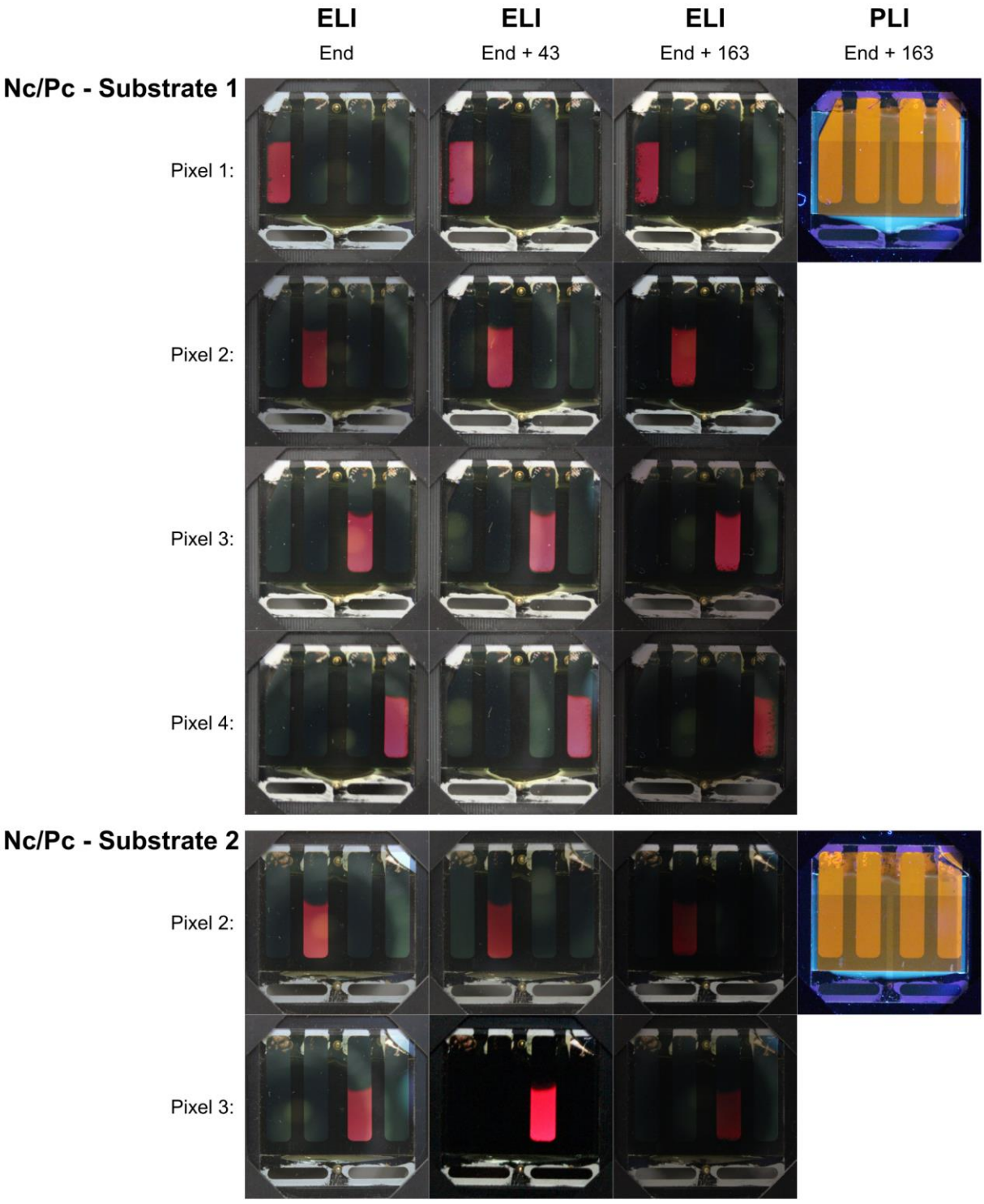

Figure D.3. Electroluminescence imaging (ELI) of Nc/Pc OPVs: immediately after and 43 days after outdoor testing. ELI, photoluminescence imaging (PLI) 163 days after outdoor testing.

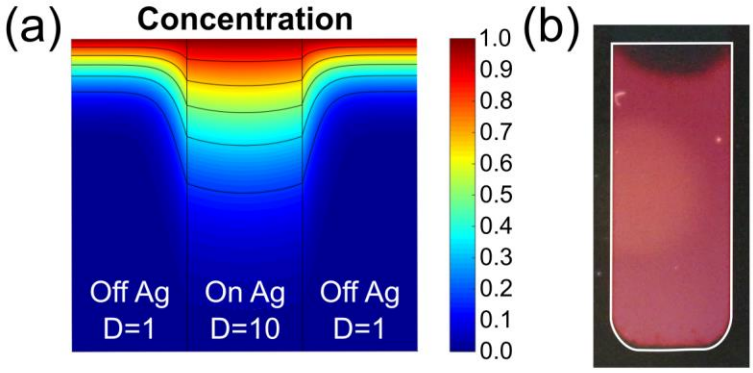

Figure D.4. (a) Simulation of contaminant diffusion with varying diffusivity (D) on and off the Ag electrode. (b) ELI of an Nc/Pc OPV (substrate 1, pixel 3) after outdoor testing ended, demonstrating a curved boundary between bright and dark EL.

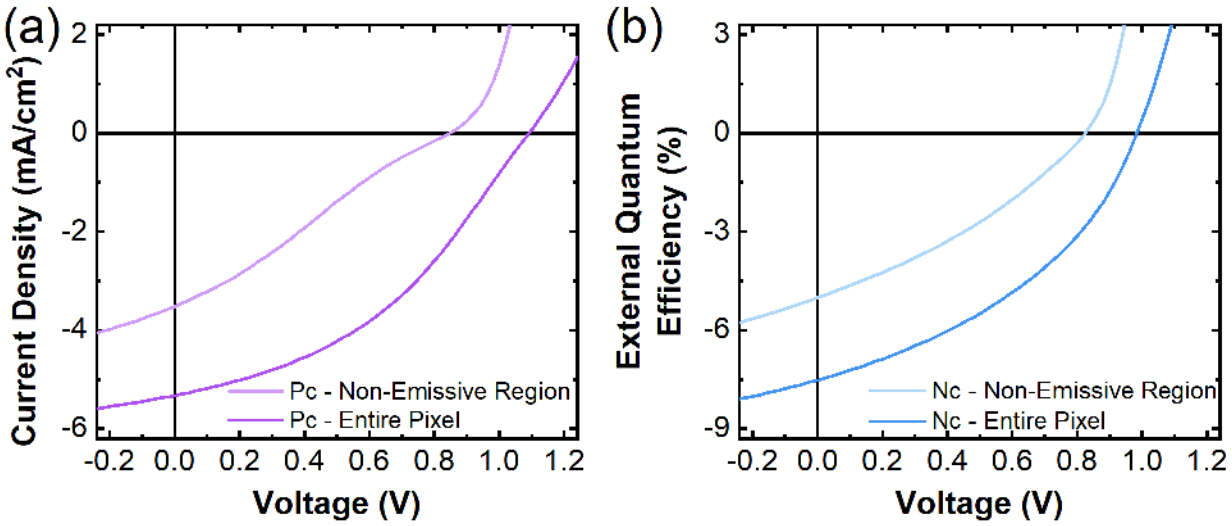

Figure D.5. J–V characteristics of (a) a Pc OPV (substrate 2, pixel 2) and (b) an Nc OPV (substrate 1, pixel 3), measured by illuminating the entire pixel with AM1.5G, and then by illuminating only the non-emissive regions with AM1.5G. Areas were estimated using image analysis to calculate the current densities.

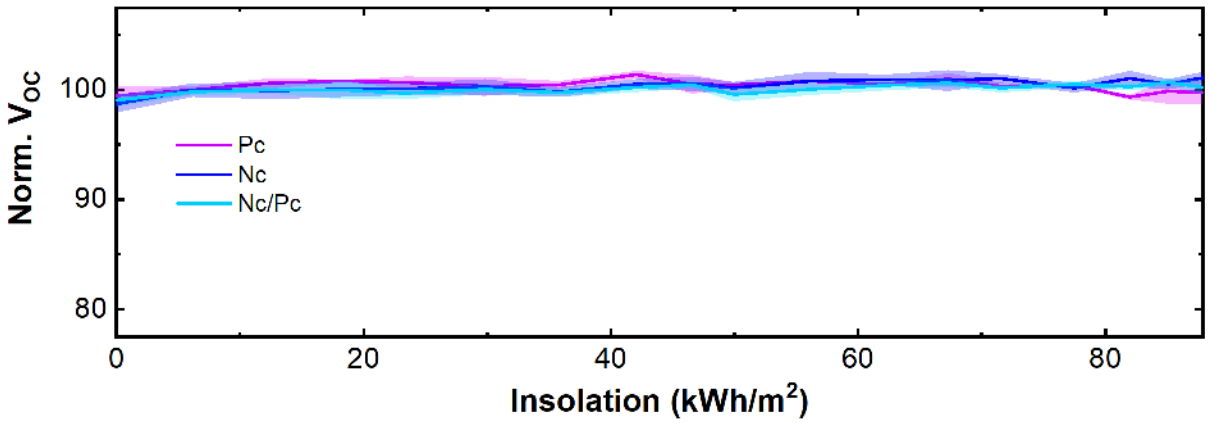

Figure D.6. Evolution of the V_{OC} with insolation, as measured indoors under simulated AM1.5G spectrum

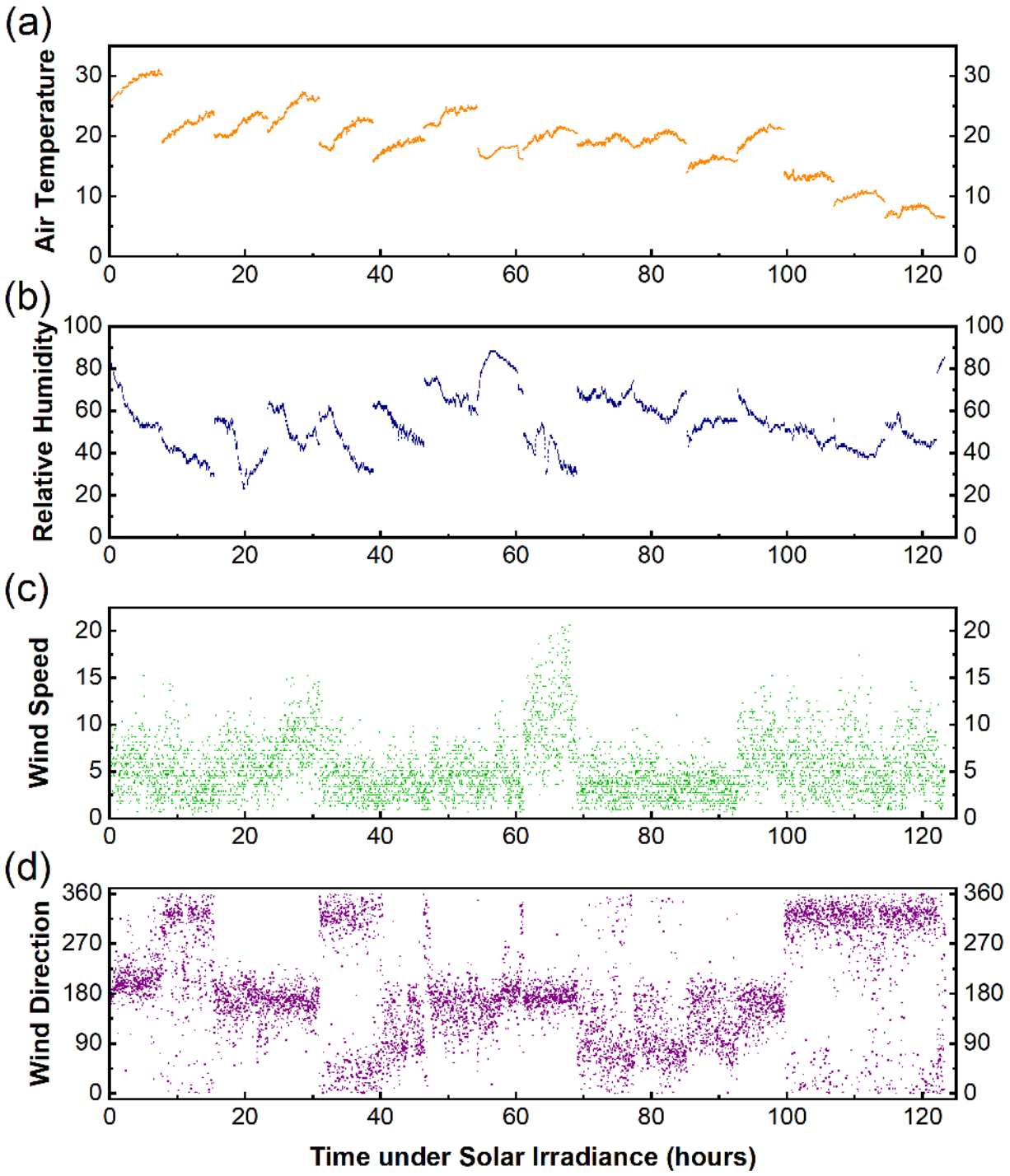

Figure D.7. (a) Air temperature (°C), (b) relative humidity (%), (c) wind speed (m/s), and (d) wind direction during 2016 outdoor testing. Wind direction is shown according to the following: 0° & 360° = from the north, 180° = from the south, 90° = from the east, and 270° = from the west.

Appendix E
Supplemental Information for Section 4.4

Table E.1. Days in 2017 that each set of OPVs was tested outdoors, typically for ~6 hours centred around solar noon.

Date	α-6T / Cl-BsubPc	α-6T / Cl-Cl_6BsubPc
May 15th	✓	✓
May 17th	✓	✓
May 19th	✓	✓
May 24th	✓	✓
May 31st	✓	✓
June 1st	✓	✓
June 2nd	✓	✓
June 7th	✓	✓
June 8th	✓	✓
June 12th	✓	✓
June 14th	✓	✓
June 28th	×	✓
July 4th	×	✓
July 5th	×	✓
July 6th	×	✓

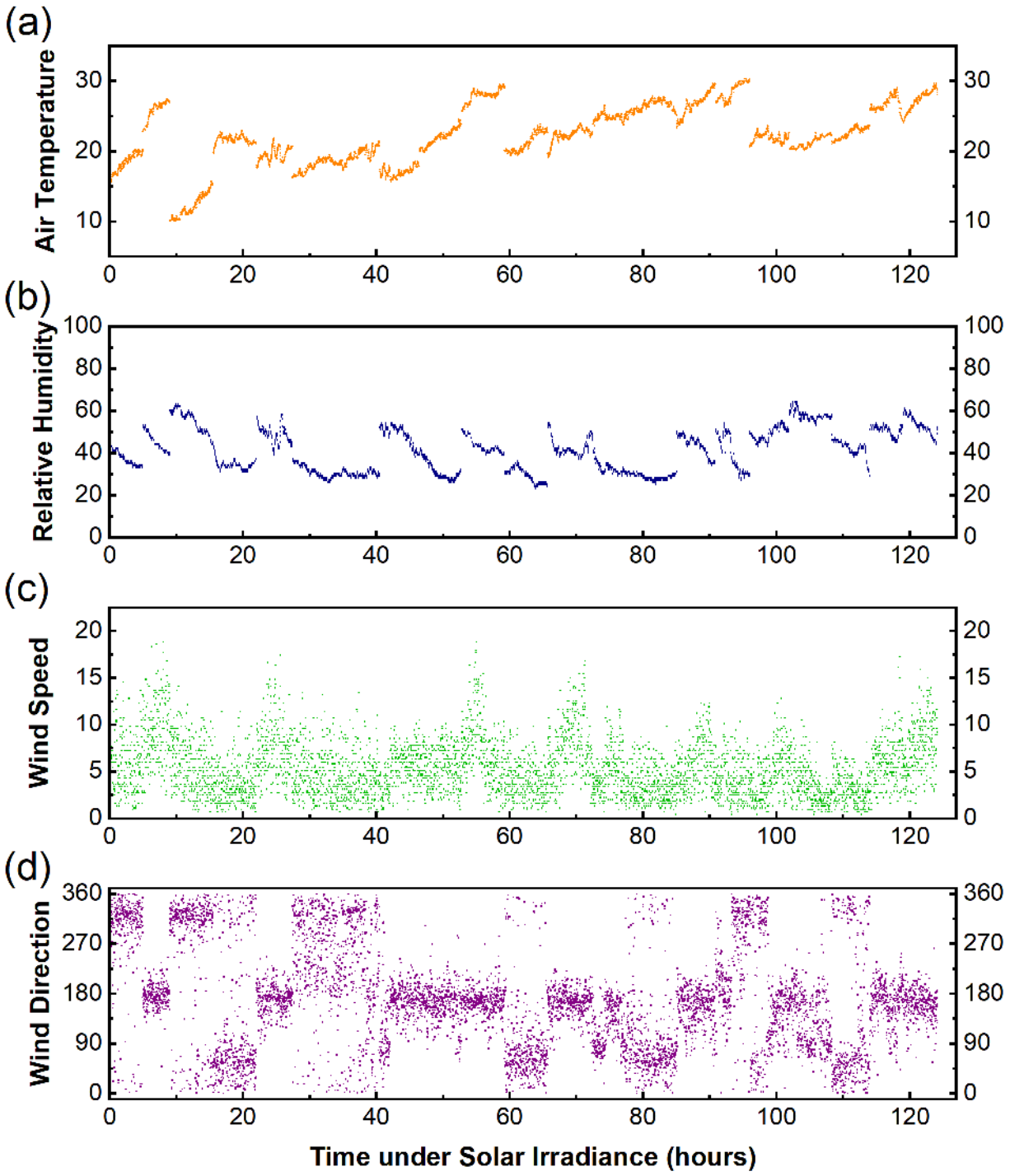

Figure E.1. (a) Air temperature (°C), (b) relative humidity (%), (c) wind speed (m/s), and (d) wind direction during 2017 outdoor testing. Wind direction is shown according to the following: 0° & 360° = from the north, 180° = from the south, 90° = from the east, and 270° = from the west.